UNCLASSIFIED

AD NUMBER
AD378773
CLASSIFICATION CHANGES
TO: **UNCLASSIFIED**
FROM: **CONFIDENTIAL**
LIMITATION CHANGES
TO: **Approved for public release; distribution is unlimited.**
FROM: **Distribution authorized to U.S. Gov't. agencies and their contractors; Administrative/Operational Use; DEC 1965. Other requests shall be referred to Air Force Rocket Propulsion Lab., Edwards AFB, CA.**
AUTHORITY
AFRPL ltr 7 May 1973 ; AFRPL ltr 7 May 1973

THIS PAGE IS UNCLASSIFIED

SECURITY MARKING

The classified or limited status of this report applies to each page, unless otherwise marked.
Separate page printouts MUST be marked accordingly.

THIS DOCUMENT CONTAINS INFORMATION AFFECTING THE NATIONAL DEFENSE OF THE UNITED STATES WITHIN THE MEANING OF THE ESPIONAGE LAWS, TITLE 18, U.S.C., SECTIONS 793 AND 794. THE TRANSMISSION OR THE REVELATION OF ITS CONTENTS IN ANY MANNER TO AN UNAUTHORIZED PERSON IS PROHIBITED BY LAW.

NOTICE: When government or other drawings, specifications or other data are used for any purpose other than in connection with a definitely related government procurement operation, the U. S. Government thereby incurs no responsibility, nor any obligation whatsoever; and the fact that the Government may have formulated, furnished, or in any way supplied the said drawings, specifications, or other data is not to be regarded by implication or otherwise as in any manner licensing the holder or any other person or corporation, or conveying any rights or permission to manufacture, use or sell any patented invention that may in any way be related thereto.

CONFIDENTIAL

378273

AFRPL-TR-66-294

(Unclassified Title)

FINAL REPORT, PHYSICO-CHEMICAL CHARACTERIZATION OF HIGH-ENERGY STORABLE PROPELLANTS

December 1966

Air Force Rocket Propulsion Laboratory
Research and Technology Division
Air Force Systems Command
Edwards Air Force Base, California

Air Force Program Structure No. 750G
AFSC Project No. 3148

Prepared Under Contract AF04(611)-10544

By
Chemistry Section
Research Division of Rocketdyne
A Division of North American Aviation, Inc.
6633 Canoga Avenue, Canoga Park, California

In addition to security requirements which must be met, this document is subject to special export controls and each transmittal to foreign governments or foreign nationals may be made only with prior approval of AFRPL(RPPR-STINFO), Edwards, California 93523.

Group 4
Downgraded at 3-Year Intervals
Declassified After 12 Years

THIS MATERIAL CONTAINS INFORMATION AFFECTING THE NATIONAL DEFENSE OF THE UNITED STATES WITHIN THE MEANING OF THE ESPIONAGE LAWS, TITLE 18 U.S.C., SECTIONS 793 AND 794, THE TRANSMISSION OR REVELATION OF WHICH IN ANY MANNER TO AN UNAUTHORIZED PERSON IS PROHIBITED BY LAW.

CONFIDENTIAL

When U.S. Government drawings, specifications, or other data are used for any purpose other than a definitely related Government procurement operation, the Government thereby incurs no responsibility nor any obligation whatsoever, and the fact that the Government may have formulated, furnished, or in any way supplied the said drawings, specifications, or other data is not to be regarded by implication or otherwise, or in any manner licensing the holder or any other person or corporation, or conveying any rights or permission to manufacture, use, or sell any patented invention that may in any way be related thereto.

AFRPL-TR-66-294

(Unclassified Title)

FINAL REPORT, PHYSICO-CHEMICAL CHARACTERIZATION OF HIGH-ENERGY STORABLE PROPELLANTS

December 1966

Air Force Rocket Propulsion Laboratory
Research and Technology Division
Air Force Systems Command
Edwards Air Force Base, California

Air Force Program Structure No. 750G
AFSC Project No. 3148

Prepared Under Contract AF04(611)-10544

By
Chemistry Section
Research Division of Rocketdyne,
A Division of North American Aviation, Inc.
6633 Canoga Avenue, Canoga Park, California

In addition to security requirements which must be met, this document is subject to special export controls and each transmittal to foreign governments or foreign nationals may be made only with prior approval of AFRPL(RPPR-STINFO), Edwards, California 93523.

Group 4
Downgraded at 3-Year Intervals
Declassified After 12 Years

THIS MATERIAL CONTAINS INFORMATION AFFECTING THE NATIONAL DEFENSE OF THE UNITED STATES WITHIN THE MEANING OF THE ESPIONAGE LAWS, TITLE 18 U.S.C., SECTIONS 793 AND 794, THE TRANSMISSION OR REVELATION OF WHICH IN ANY MANNER TO AN UNAUTHORIZED PERSON IS PROHIBITED BY LAW.

FOREWORD

The research reported herein was sponsored by the Air Force Rocket Propulsion Laboratory, Research and Technology Division, Edwards Air Force Base, California, under Contract AF04(611)-10544.

This program was conducted in the Chemical Research Section of the Rocketdyne Research Division. Dr. J. Silverman was the Program Manager and Dr. E. F. C. Cain was the Project Scientist. The principal areas of study involved and the corresponding Responsible Scientists and contributors are as follows:

1. Homogeneous Oxidizers: Dr. N. Ogimachi, Mr. D. Sheehan, and Mr. G. Rowley
2. Desensitization of Oxidizers: Dr. A. Axworthy, Mr. J. M. Sullivan.
3. Heterogeneous Fuel Systems:
   (a) Conventional Gelled Propellants: Dr. J. Farrar, Dr. M. Kirsch, Dr. A. Tarsey, Mr. R. Melvold, and Dr. W. R. Yates
   (b) Mechanisms of Heterogeneous Propellant Incompatibility: Dr. A. Axworthy, Dr. M. Ladacki, Dr. W. Givens, and Mr. J. M. Sullivan
   (c) Advanced Heterogeneous Propellants: Dr. F. Gunderloy, Jr., and Dr. C. Fujikawa
4. Engineering Characterization of Propellants: Dr. J. E. Sinor, Mr. C. Younts, and Mr. R. Rice

Analytical Chemical support for the various tasks was provided by the following contributors: Dr. H. Schultz, Mr. B. C. Neale, and Mr. R. Rushworth.

This report has been assigned the Rocketdyne Report No. R-6737.

This technical report has been reviewed and is approved.

W. H. EBELKE, Colonel, USAF
Chief, Propellant Division

ABSTRACT AFRPL-TR-66-294

Homogeneous oxidizer mixtures based on Compounds R and T were studied and found to be intractable. The kinetics of the decomposition of CNF oxidizers were studied and the results indicated that the additive approach to inhibition did not seem promising. Heterogeneous fuels based on Be/N_2H_4, Be-BeH_2/MMH were formulated and evaluated during small motor firings. A monopropellant containing a Be + BeH_2/H_2O-HN was also prepared and evaluated in a small rocket motor. The mechanisms of gas forming reactions of such heterogeneous propellants were studied. A new family of stable heterogeneous fuels based upon the use of various alane- and borane-terminated beryllium hydride liquids was conceived and studied. A stable gel was formulated. The effect of the addition of up to 25 w/o of a fluorine to the oxidizer in the Be-N_2H_4/H_2O_2 was studied in a small rocket engine system.

(Confidential Abstract)

CONTENTS

Foreword ii

Abstract iii

Introduction 1

Summary 3

Task 1: Homogeneous Oxidizer Mixtures 7

Introduction 7

Discussion and Results 9

Theoretical Performance 9

Vapor Pressure Studies 27

Compatibility Studies 40

Kinetic Studies 45

Experimental 55

Vapor Pressure Studies 55

Compatibility Studies 55

Solubility of XeF_4 and XeF_2 in ClF_5 56

Conclusions 59

Task 2: Desensitization of Oxidizers 63

Introduction 63

Discussion and Results 67

Pyrolysis of Compound T at Elevated Temperatures 67

Pyrolysis of PFG 69

Relationship of PFG Pyrolysis Results to Compound T Decomposition Mechanism 97

Relationship of PFG Decomposition Mechanism to the Detonation Sensitivity of Compound T 104

Inhibition of the Heterogeneous Decomposition of PFG 105

Pyrolysis of PFF 106

Relationship of PFF Pyrolysis Results to Mechanism 112

Pyrolysis of Compound T in Static Reactors 114

Experimental Technique 117

Flow Reactors 117

Static Reactors 117

Product Analysis 118
Conclusions 119
Task 3: Heterogeneous Propellants 121
Conventional Gelled Propellants 121
Introduction 121
Discussion and Results 123
Experimental 161
Conclusions 173
Mechanism of Heterogeneous Propellant Incompatibility 177
Introduction 177
Discussion and Results 177
Experimental 193
Conclusions 197
Advanced Heterogeneous Propellants 199
Introduction 199
Discussion and Results 201
Experimental. 207
Conclusions 213
Task 4: Engineering Characterization of Propellants 215
Introduction 215
Discussion and Results 217
Propellant Sensitivity Measurements 217
Heterogeneous Propellant Flow and Performance Evaluation . . 260
Analysis of Propellant Evaluation Data 306
Conclusions 329
Propellant Sensitivity Measurements 329
Heterogeneous Propellant Performance Evaluation 331
References 333
Appendix A
Purity and Purification of PFG A-1
Appendix B
Design of B-3 Formulation Experiments B-1
Appendix C
Toxic Chemicals Laboratories Safety Standing Operating Procedure (SSOP) C-1

Appendix D

Theoretical Analysis of Wenograd Thermal Sensitivity Apparatus . . D-1

References D-15

Appendix E

Air and Water Pollution Control E-1

Appendix F

Removal of Dissolved Beryllium From Solution F-1

Appendix G

Beryllium Analyses G-1

ILLUSTRATIONS

1. Performance vs Oxidizer Composition of ClF_5-TNM-T With B_5H_9 10
2. Performance vs Oxidizer Composition of ClF_5-TNM-T With N_2H_4 11
3. Performance vs Oxidizer Composition of ClF_5-TNM-T With MMH 12
4. Performance vs Oxidizer Composition of N_2F_4-TNM-T With B_5H_9 13
5. Performance vs Oxidizer Composition of N_2F_4-TNM-T With N_2H_4 14
6. Performance vs Oxidizer Composition of N_2F_4-$C(NF_2)_4$-$C(NO_2)_4$ With MMH 15
7. Performance vs Oxidizer Composition of N_2F_4-ClF_5-$C(NF_2)_4$ With MMH 16
8. Performance vs Oxidizer Composition of N_2F_4-ClF_5-T With N_2H_4 17
9. Performance vs Oxidizer Composition of N_2F_4-ClF_5-$C(NF_2)_4$ With B_5H_9 18
10. Performance, Combustion Temperature, and Percent Condensed Phase Curves for NF_3O-N_2O_4 With Be-N_2H_4 22
11. Performance, Combustion Temperature, and Percent Condensed Phase Curves for NF_3O-H_2O_2 With Be-N_2H_4 23
12. Performance, Combustion Temperature, and Percent Condensed Phase Curves for N_2O_4-FNO_2 With Be-N_2H_4 24
13. Boundary Curves for High-Density Propellant Systems . . . 26
14. Vapor Pressure of ClF_5-$C(NF_2)_4$ 30
15. Vapor Pressure of N_2F_4-$C(NF_2)_4$ 33
16. Solubility of XeF_4 in ClF_5 37
17. Solubility of XeF_2 in ClF_5 39
18. First-Order Plot for Compound A at 293 C 46
19. Influence of Temperature on Principal Intermediates (Initial Partial Pressure of Oxidizer 11.4 mm Hg) 65

20. Thermal Decomposition of Compound T at 340 C 68
21. Thermal Stability of PFG Compared With Compound T 76
22. First-Order Plot of PFG Pyrolysis at 413 C 82
23. Arrhenius Plot for High- and Low-Temperature Pyrolysis of PFG 83
24. Products of PFG Pyrolysis at 252 C 85
25. Products of PFG Pyrolysis at 252 C 86
26. Products of Pyrolysis of 91-Percent Purity PFG at 272 C . . 87
27. Products of Pyrolysis of 91-Percent Purity PFG at 272 C . . 88
28. Product Distribution From PFG Homogeneous Pyrolysis at 416 C 89
29. Pyrolysis of PFG at 528 C (initial pressure PFG = 3.08 millimeters) 91
30. Pyrolysis of Compound T at 528 C (initial pressure Compound T = 3.77 millimeters) 92
31. Comparison of Pyrolysis Rates 100
32. First-Order Plot for the Pyrolysis of PFF at 428 C 108
33. Arrhenius Plot for Thermal Decomposition of PFF 110
34. Product Distribution From PFF at 426 C 111
35. Dependence of Hydrazine Apparent Viscosity on Kelzan Concentration at 24 C Measured With Brookfield Spindle T-A at 10 rpm 126
36. Light Scattered by Kelzan Solutions 128
37. Effect of Particle Size of Beryllium Metal on Apparent Viscosity of Hydrazine Gels 130
38. Rheogram of Typical Normal R-2 Gel 137
39. Performance of Be-N_2H_4/H_2O_2 System at Various Loadings . . . 138
40. Rheogram of R-3 Gel 147
41. Gas Evolution From R-3 Gel 148
42. Be and BeH_2/Hydrazine Nitrate in H_2O, Specific Impulse and Temperature vs Volume Percent Solids 155
43. Be and BeH_2/Hydrazine Nitrate in H_2O, Weight Percent Be and BeH_2 vs Volume Percent Solids 156

44. Thermal Stability of R-5 Gel 160
45. Gel Mixing Facility 162
46. Arrhenius Plot of Hydrazine Vapor Decomposition in Flow Reactors 180
47. Comparison of Arrhenius Plots for Decomposition of Hydrazine Vapor 182
48. Ultraviolet Spectra in Hydrazine 189
49. Ultraviolet Spectra in Cyclohexane 191
50. Sample Holders 195
51. Vacuum Apparatus 196
52. Theoretical Performance Comparison of BeH_2-Beryllium Hydride Liquid Gelled Fuels and BeH_2-MMH Gelled Fuels With 98-Percent H_2O_2 200
53. Glass Thermal Stability Apparatus 204
54. Simplified U-Tube Schematic 217
55. Schematic of U-Tube Section 218
56. Schematic Diagram of U-Tube Adiabatic Compression Sensitivity Tester 221
57. Empirical Correction Factor for Nonideal Behavior of N_2F_4 at 0 C 223
58. U-Tube Sensitivity of Compound R With Pure, Dry Air . . . 231
59. U-Tube Sensitivity of Compound R-N_2O_4 234
60. Sensitivity of Compound T-N_2O_4 Mixtures 236
61. Results of U-Tube Sensitivity Test on Compound R-N_2F_4-TNM System 238
62. Experimental Circuit 242
63. Time Delay as a Function of Temperature at Detonation . . . 244
64. Wenograd Test Results for Various Oxidizers 245
65. Wenograd Test Results for Mixtures of TNM and Compound T . . 247
66. Sensitivity of Mixtures of T and TNM 248
67. Explosion of Compound T in Hypodermic Tubing 249
68. Tubing Fragment 250
69. Propagation Velocity Measurements 252
70. Wenograd Test Results for Mixtures of Hydrazine Nitrate in Hydrazine 255

71. Wenograd Test Results for Mixtures of Hydrazine Nitrate in Hydrazine 256
72. Heterogeneous Fuel Flow Characterization System 261
73. Gel Expulsion Tank 262
74. Scrubber System 263
75. Exhaust Scrubber System 264
76. Motor Connection to Scrubber 265
77. Thrust Stand and Propellant Tanks 267
78. Throat Deposits 270
79. Eroded Throat 273
80. Test Data Showing Nozzle Throat Erosion 274
81. Injector Performance Data 276
82. Tripropellant Injector 278
83. Water-Cooled Nozzle Assembly 279
84. Water-Cooled Nozzle Assembly 280
85. Thrust Chamber Trace Showing Throat Plugging 282
86. Thrust Chamber Trace Showing Throat Plugging 283
87. Tripropellant Test Data 285
88. Be-N_2H_4-H_2O_2 System Test Data 287
89. Be-N_2H_4-N_2O_4 System Test Data 289
90. Be-BeH_2-MMH-H_2O_2 System Test Data 291
91. Hot-Core Tripropellant Injector 293
92. Hot-Core Injector Test Data 294
93. Performance of Gelled and Ungelled N_2H_4 With H_2O_2 297
94. Expendable Monopropellant Test Stand 298
95. Chamber Pressure vs Time 300
96. Chamber Pressure vs Time for Test No. 60 301
97. Chamber Pressure vs Time for Test No. 61 302
98. Fuel System Pressure Drops 304
99. Fuel Injector Pressure Drops 305
100. Characteristic Velocity Efficiency (Runs No. 13 through 20) 310

101. Delivered Specific Impulse With Be-N_2H_4-H_2O_2 System . . . 312
102. Performance vs Mixture Ratio of 98-Percent H_2O_2/R-2 . . . 314
103. Performance vs Mixture Ratio of N_2O_4/R-2 316
104. Specific Impulse, Percent Condensed Phase, and Chamber Temperature vs Composition of H_2O_2/ClF_5/29-Percent Be in N_2H_4 318
105. Thrust Chamber Performance With Tripropellant (No. 3) Injector 319
106. Injector Comparison With Be-N_2H_4-H_2O_2-ClF_5 System . . . 321
107. Performance vs Mixture Ratio of R-3/H_2O_2 System 323
108. Performance of R-5 Monopropellant 326

TABLES

1. Ternary Oxidizers and Maximum Specific Impulse With Monomethylhydrazine Within 500-psig Limitation 20
2. Theoretical Performance of XeF_4, BrF_5, and ClF_5 With Hydrazine 25
3. Vapor Pressure of the ClF_5-$C(NF_2)_4$ System 28
4. Vapor Pressure of the N_2F_4-$C(NF_2)_4$ System 31
5. Vapor Pressure of the N_2F_4-$C(NF_2)_4$-$C(NO_2)_4$ System 35
6. Solubility of XeF_4 in ClF_5 36
7. Solubility of XeF_2 in ClF_5 38
8. Kinetic Data for the Pyrolysis of ClF_5 48
9. Reaction Between ClF_5 and NF_2 Radicals 50
10. Reaction Between ClF_5 and NF_2 Radicals 52
11. Summary of Homogeneous Ternary Oxidizer Mixtures 60
12. Apparent First-Order Rate Constants for the Pyrolysis of PFG 71
13. Order of PFG Decomposition at 235 C 75
14. Low-Temperature Pyrolysis of 91-Percent Purity PFG in a Well-Passivated Stirred Flow Reactor 78
15. Low-Temperature Pyrolysis of 79-Percent Purity PFG in a Well-Passivated Stirred Flow Reactor 79
16. High-Temperature Pyrolysis of 79-Percent Purity PFG in a Well-Passivated Stirred Flow Reactor 81
17. Effect of Additives Upon the Rate of the Low-Temperature Pyrolysis of PFG 94
18. Effect of Additives Upon the Rate of the High-Temperature Pyrolysis of PFG 95
19. Effect of N_2F_4 on the Rate of Pyrolysis of PFG 96
20. Influence of Additives Upon the Stable Product Formation From PFG at High Temperature 98
21. Formation of PFG From Compound T as a Function of Temperature 102

22. Maximum Concentration of PFG From Compound T as a Function of Temperature 103
23. First-Order Rate Constants for the Pyrolysis of PFF (at 7.8 mm Hg of PFF) 109
24. Heterogeneous Propellants Selected for Study 122
25. Apparent Viscosity of Kelzan Solutions in Hydrazine and Water 125
26. Preparation and Qualities of R-2 Gels 131
27. Composition of Regular R-2 133
28. Swelling Rate of Loaded and Unloaded Hydrazine Gels . . . 134
29. Composition of Highly Loaded R-2HL 139
30. Properties of R-3 Mixtures 142
31. Summary of R-3 Formulations 143
32. Composition of R-3 145
33. Gas Evolution From N_2H_4-H_2O-$N_2H_5NO_3$ (38-24-38) 149
34. Behavior of H_2O-N_2H_4-$N_2H_5NO_3$ Gels on Heating and Cooling . . 151
35. Preparation of R-4 Gels 153
36. Composition of R-5 Gel 161
37. Composition and Size Distribution of Beryllium Powders . . 167
38. Composition and Characteristics of Beane 168
39. Pyrolysis of Hydrazine Vapor 179
40. Gas Evolution During Room-Temperature Storage 184
41. Thermal Decomposition of Liquid Hydrazine at 71 C 185
42. Gas Evolution From Be/N_2H_4 System 186
43. Gas Evolution From Neat Hydrazine at 71 C 187
44. Influence of Oxygen Upon the Rate of Hydrazine Decomposition at 71 C 188
45. Thermal Stability of Boron- and Aluminum-Terminated Beryllium Hydride Liquids 205
46. Effect of Gellant Candidates on Pyrophoric Liquids . . . 207
47. Results of Scale-up Preparation of ATBH Liquids 210
48. Vapor-Liquid Equilibrium Concentration Determinations at 0 C for the Ternary System (TNM-N_2F_4-R) 224
49. U-Tube Sensitivity Calibration Data 226

50. U-Tube Sensitivity Data for Compound R With No Additional Gas Space Pressurant 228
51. U-Tube Sensitivity Data for Pure Compound R With Dry Air as a Gas Space Pressurant 230
52. Compound T Test Data 232
53. U-Tube Sensitivity for Compound R-N_2O_4 Mixtures 233
54. Results of U-Tube Sensitivity Tests on Mixtures of Compound T-N_2O_4 235
55. Summary of U-Tube Sensitivity Test Results With R-N_2F_4-TNM Mixtures 237
56. Results of U-Tube Sensitivity Tests on Compound T-N_2F_4 . . 240
57. Velocity of Propagation 253
58. Compositions of R-5 Monopropellant Gel Formulations . . . 258
59. Results of Detonation Propagation Tests on R-5 Gels . . . 259
60. Timer Sequence Chart 268
61. Thrust Chamber Tests, Al-N_2H_4-H_2O_2 System 271
62. Thrust Chamber Tests, Be-N_2H_4-H_2O_2 System 275
63. Thrust Chamber Tests, Be-N_2H_4-H_2O_2-ClF_5 System 284
64. Thrust Chamber Tests, Be-N_2H_4-H_2O_2 System (Tripropellant Injector) 284
65. Thrust Chamber Performance, Be-N_2H_4-H_2O_2 System (308-Inch L*) 286
66. Thrust Chamber Performance, Be-N_2H_4-N_2O_4 System 288
67. Thrust Chamber Performance, Be-BeH_2-MMH-H_2O_2 System . . . 290
68. Thrust Chamber Performance, Be-N_2H_4-H_2O_2-ClF_5 System (Hot-Core Injector) 292
69. Thrust Chamber Performance, H_2O_2-N_2H_4 System 296
70. Thrust Chamber Performance Data 307
71. Be-N_2H_4-H_2O_2 System 311
72. Summary of Propellant Sensitivity Measurements 330

INTRODUCTION

The work reported herein comprises the final report on a program concerned with the preparation, stabilization, and physico-chemical characterization of homogeneous and heterogeneous earth-storable oxidizers and fuels that will exceed a target specific impulse of 315 seconds. For convenience, the program was originally divided into four areas of study, reflecting both the most promising approaches and the technical areas where the severest problems were anticipated. On the basis of technical results obtained during this program, additional tasks were established.

The first area of study involved the utilization of energetic oxidizer ingredients such as ClF_5, N_2F_4, $C(NF_2)_4$, and $C(NO_2)_4$ to achieve new and useful earth-storable propellants. The formulated oxidizer must have a storage pressure of less than 500 psig at 160 F, acceptable stability, and a theoretical specific impulse of at least 315 seconds with known fuels.

The second area of study involved studying the high-energy CNF oxidizers, Compounds T and R, with respect to their detonation sensitivity. The objectives of this area of study were to determine the kinetics and mechanisms for the gas phase decomposition of Compounds T and R, to correlate the rate and mechanism results with detonation sensitivity, and to propose test additives or other methods that will desensitize these compounds.

The third area of study involved the preparation and characterization of certain heterogeneous propellants composed of energetic metals and/or metal hydrides suspended in a suitable liquid vehicle. Sufficient quantities were prepared for engineering characterization and small-scale motor firings. Much of the effort was directed toward facilitating scale-up of the propellants and clarifying those factors which affect their flow characteristics. During the program, two new tasks were added to this area of study. The first involved a basic study of the mechanism of heterogeneous incompatibility. The second involved the development of a new family of high-energy heterogeneous fuels based on beryllium hydride suspended in various borane- and alane-terminated beryllium hydride liquids.

The fourth area of study was to determine the engineering characteristics of both homogeneous oxidizer and heterogeneous fuel mixtures. The most promising mixtures were evaluated as to detonation sensitivity, thermal stability, and handling hazards. Flow characterization and performance evaluation tests of various heterogeneous propellants which were developed during this program were conducted in a propellant handling facility and a small engine system.

Theoretical performance calculations for the three ternary oxidizer mixtures, N_2F_4-$C(NF_2)_4$-$C(NO_2)_4$, ClF_5-$C(NF_2)_4$-$C(NO_2)_4$, and ClF_5-N_2F_4-$C(NF_2)_4$ with monomethylhydrazine, hydrazine, and pentaborane are presented as constant impulse contours on oxidizer composition triangles. Calculations were also performed on XeF_4-ClF_5 mixtures with hydrazine and hydrazine with additives. The data are presented in graphical form showing impulse and density impulse relationships.

Determination of vapor pressures for the N_2F_4-$C(NF_2)_4$, ClF_5-$C(NF_2)_4$, and ClF_5-N_2F_4-$C(NF_2)_4$ systems at 0.0, 45.0, and 71.0 C have been accomplished. Compatibility tests on the binary mixtures, N_2F_4-$C(NF_2)_4$ and $C(NF_2)_4$-$C(NO_2)_4$, and the ternary mixtures, N_2F_4-$C(NF_2)_4$-$C(NO_2)_4$ and ClF_5-$C(NF_2)_4$-$C(NO_2)_4$ have been completed. Kinetic studies and compatibility tests were carried out the N_2F_4-ClF_5 binary mixture. The results indicate that this mixture will not meet the storability requirements of this contract and that the mixture is inherently unstable because of the reaction between components.

The solubilities of XeF_4 and XeF_2 in ClF_5 have been determined in the temperature range 0.0 to 45.5 C. The solubilities were too low to take advantage of the theoretically increased density impulse of such mixtures.

Three binary oxidizer systems, NF_3O-N_2O_4, NF_3O-H_2O_2, and FNO_2-N_2O_4 were investigated for use with a Be-N_2H_4 gel. All three oxidizer systems were found to be incompatible at elevated storage temperatures and were eliminated from further consideration.

The study of the kinetics of decomposition of the CNF oxidizers was continued with a goal of obtaining leads to methods of reducing their detonation sensitivity. The investigation of the pyrolysis of Compound T was extended up to 528 C. At higher temperatures, the initial products were almost exclusively PFG, NF_3, and N_2F_4. It was definitely established that PFG is a direct intermediate in the decomposition of Compound T.

The kinetics of PFG pyrolysis were studied from 210 to 455 C. The reaction was found to be heterogeneous at lower temperatures and homogeneous and first order at temperatures above 400 C. The activation energy for the reaction at the surface was less than 15 kcal/mole while that of the homogeneous reaction was 52.9 kcal/mole. The homogeneous and heterogeneous decompositions of PFG gave the same product distribution (N_2>CF_3NF_2>CF_4>NF_3>N_2F_4>PFF>PFM) suggesting a similar mechanism. Additives had only a slight effect on the pyrolysis rate but did markedly affect the product distribution.

The pyrolysis of PFF was found to be first order and homogeneous between 400 and 477 C with an activation energy of 49.3 kcal/mole. PFF is slightly more stable than PFG in this temperature range. The products of PFF pyrolysis are N_2, CF_3NF_2, CF_4, and PFM. Additives markedly affect the product distribution. It was established that the initial step is not the rupture of a C-N bond in the PFF molecule.

PFG was found to decompose as readily on a Teflon surface as on a Monel surface. Compound T was found to give the same reaction rates in a static reactor as in the flow reactor.

The results of this study indicate that the initial step in the pyrolysis of Compound T is a unimolecular bond rupture which is not reversible. The initial step in the subsequent pyrolyses of the direct intermediate PFG is apparently not a C-N bond rupture, but again does not appear to be reversible. Because neither of these reactions appear to involve chain reaction or autocatalysis, the additive approach to inhibition does not seem promising. No further kinetic studies were carried out.

Four mechanically stable conventional gelled propellants were formulated, and three were prepared in quantities sufficient for engine firing tests. The gels were cohesive and nonadhesive, and their apparent viscosities decreased with increasing shear.

The preferred gellant for beryllium-hydrazine gels was a mixture of Kelzan and aluminum octanoate. Swelling of these gels could apparently be reduced by washing the beryllium powder with water before incorporating it into a gel.

Optimum conditions and the best gelling agent for formulating a mixture of beryllium and beryllium hydride in MMH were selected from the results of a statistically designed experiment involving eight mixing variables and seven gellant candidates. The preferred gelling agent is SeaTex HCB cross-linked with boric acid. Swelling and gassing of this gel was rapid for the first few hours, but slowed down to acceptable rates thereafter.

A monopropellant, which exhibits a theoretical specific impulse of approximately 315 seconds, was formulated from a mixture of beryllium and beryllium hydride suspended in 50/50 water/hydrazinium nitrate solution. Drop weight, thermal sensitivity, and detonation propagation tests showed that this propellant formulation was tractable.

An investigation of the mechanisms of the gas-forming reactions which occur during the storage of heterogeneous propellants was undertaken midway in the contract period. The kinetics of the heterogeneous decomposition of hydrazine vapor was studied in flow and static reactors from 200 to 340 C. The rate was found to be faster on a Pyrex surface than on aluminum. The results of the vapor-phase study were extrapolated to storage (ullage) conditions. Liquid-phase decomposition studies were conducted at 71 C. The rate of decomposition of liquid hydrazine was accelerated when the liquid was placed in contact with beryllium powder. The presence of beryllium powder in the ullage space of the reactor did not increase the decomposition rate when precautions were taken to prevent the condensation of a liquid film on the surface of the metal powder. Pretreatment of hydrazine by bubbling oxygen through it increases the rate of decomposition. A species which strongly absorbs ultraviolet light was observed to form during the heating of liquid hydrazine. The noncondensable products from

the decomposition of MMH at 71 C were found to consist of nitrogen and methane with virtually no hydrogen. The products were the same when liquid MMH was decomposed in the presence of BeH_2 powder, beryllium powder, or aluminum powder.

A new high performance heterogeneous fuel system based on beryllium hydride suspended in various borane- and alane-terminated beryllium hydride liquids was studied. The thermal stability and chemical compatibility of an available alane-terminated liquid with beryllium hydride was demonstrated to be excellent. A stable gel was prepared.

The sensitivity of a number of homogeneous oxidizer components and mixtures was determined by means of the U-tube adiabatic compression test and the Wenograd thermal sensitivity test. Compounds R and T proved to be the most sensitive materials tested on either apparatus. Addition of small amounts of oxygen-containing compounds, i.e., N_2O_4 and TNM, to compounds R and T did not provide any significant desensitization and in some cases the mixture appeared to be actually more sensitive than the pure compounds. The addition of low concentrations of N_2F_4 to both compounds R and T does produce a desensitization effect.

Small scale thrust chamber performance evaluation tests were conducted at the 500-pound thrust level and 1000-psia chamber pressure for combinations of R-2 gel with 98-percent H_2O_2, R-2 with N_2O_4, R-2 with H_2O_2 and ClF_5, R-3 with H_2O_2, N_2H_4 with H_2O_2, and for the R-5 monopropellant formulation. Analysis of the data from these tests indicates that the percent beryllium burned varied from 20 percent for the R-2/H_2O_2, R-2/H_2O_2/ClF_5 and R-5 systems to approximately 50 percent for the R-2/N_2O_4, and R-3/H_2O_2 systems. Tripropellant tests with the R-2/H_2O_2/ClF_5 system were conducted with two different injectors. One injector produced a uniform distribution of ClF_5 in the oxidizer and the other "hot-core" injector introduced all the ClF_5 at the center of the injector face. No significant difference in performance was noted between the two methods of injecting ClF_5.

TASK 1: HOMOGENEOUS OXIDIZER MIXTURES

INTRODUCTION

Efforts in this area of study have consisted essentially of a continuation of the program identified as the second area of study in Contract AF04(611)-9380 (Ref. 1) with the same basic objectives, i.e., the preparation and characterization of homogeneous liquid oxidizer mixtures with high theoretical specific impulse and earth storability characteristics. The formulated oxidizer must have a storage pressure of less than 500 psig at 160 F, a freezing point below -65 F, acceptable thermal and shock stability, and a theoretical specific impulse of at least 315 seconds with known liquid fuels. This continuation effort was oriented toward detailed studies of the more promising oxidizer mixtures formulated during the initial program. Specifically, this included the completion of feasibility demonstrations for $C(NF_2)_4$ (Compound T or Δ) as a higher performance replacement for $FC(NF_2)_3$ (Compound R) in formulated oxidizer mixtures, as well as detailed studies of preferred (based on sensitivity and liquidus range) binary and ternary mixtures of ClF_5, N_2F_4, $C(NO_2)_4$ (TNM), $FC(NF_2)_3$, and NF_3O with one another and other conventional oxidizers.

Further study in this area of research was terminated during the third quarter because of the extremely unfavorable results obtained from shock sensitivity and detonation propagation experiments on mixtures containing Compound T. Studies on the compatibility problem of N_2F_4-ClF_5 were continued with particular emphasis being placed on a kinetic study of the direct gas-phase reaction between ClF_5 and $\cdot NF_2$ radicals.

A subsidiary effort was directed toward laboratory feasibility experiments on the use of xenon fluorides as oxidizer ingredients.

During the latter part of this program, the theoretical emphasis for Task I was shifted from mixed oxidizers for use with pure fuels to mixtures for use with heterogeneous fuels. The selected heterogeneous fuel was beryllium dispersed in hydrazine (designated R-2). The three binary oxidizer mixtures selected for initial investigation were: N_2O_4-NF_3O, N_2O_4-FNO_2, and H_2O_2-NF_3O. In each case it was hoped that the fluorine-containing component would increase the combustion efficiency with R-2.

DISCUSSION AND RESULTS

THEORETICAL PERFORMANCE

Theoretical performance calculations were carried out on binary and ternary mixed oxidizer systems containing $C(NF_2)_4$ to aid the direction of laboratory study. On the basis of the discussion on the selection of oxidizer ingredients presented during the earlier program (Ref. 1) and the performance calculations in which $FC(NF_2)_3$ was a component, three ingredients were considered for inclusion in mixtures with $C(NF_2)_4$; these were ClF_5, N_2F_4, and $C(NO_2)_4$. Combining these ingredients into ternary systems containing $C(NF_2)_4$ gives three distinctive oxidizer mixtures, ClF_5-$C(NF_2)_4$-$C(NO_2)_4$, N_2F_4-$C(NF_2)_4$-$C(NO_2)_4$, and ClF_5-N_2F_4-$C(NF_2)_4$. Calculations have been completed for these ternary oxidizers with pentaborane, hydrazine, and monomethylhydrazine. The data are presented as constant impulse contours on oxidizer triangles (Fig. 1 through 9). Mixture ratio, which is not shown, has been optimized for maximum impulse in all cases. The binary oxidizer systems have not been presented separately because they are special cases of the ternary systems.

Ideal 500-psig isobars are shown on the triangles containing N_2F_4 so that the compositions of interest appear as areas bounded by the isobars and the 315-second constant impulse curves. The estimated experimental 500-psig isobar (from binary vapor pressure data) is also shown for comparative purposes. These triangles have proven extremely valuable in guiding the laboratory evaluation of oxidizer mixtures. For example, in Fig. 2 it can be seen that a composition of 25 w/o $C(NF_2)_4$ - 72 w/o ClF_5 - 3 w/o $C(NO_2)_4$ can meet the 315-second performance goal with hydrazine. This composition has a minimum of the high-freezing component, $C(NO_2)_4$. It also has the minimum amount of the high-performing, but shock-sensitive component, $C(NF_2)_4$. The diagram also shows that oxidizer performance can be increased by utilizing more $C(NF_2)_4$ in the mixture while keeping the amount of $C(NO_2)_4$ relatively constant.

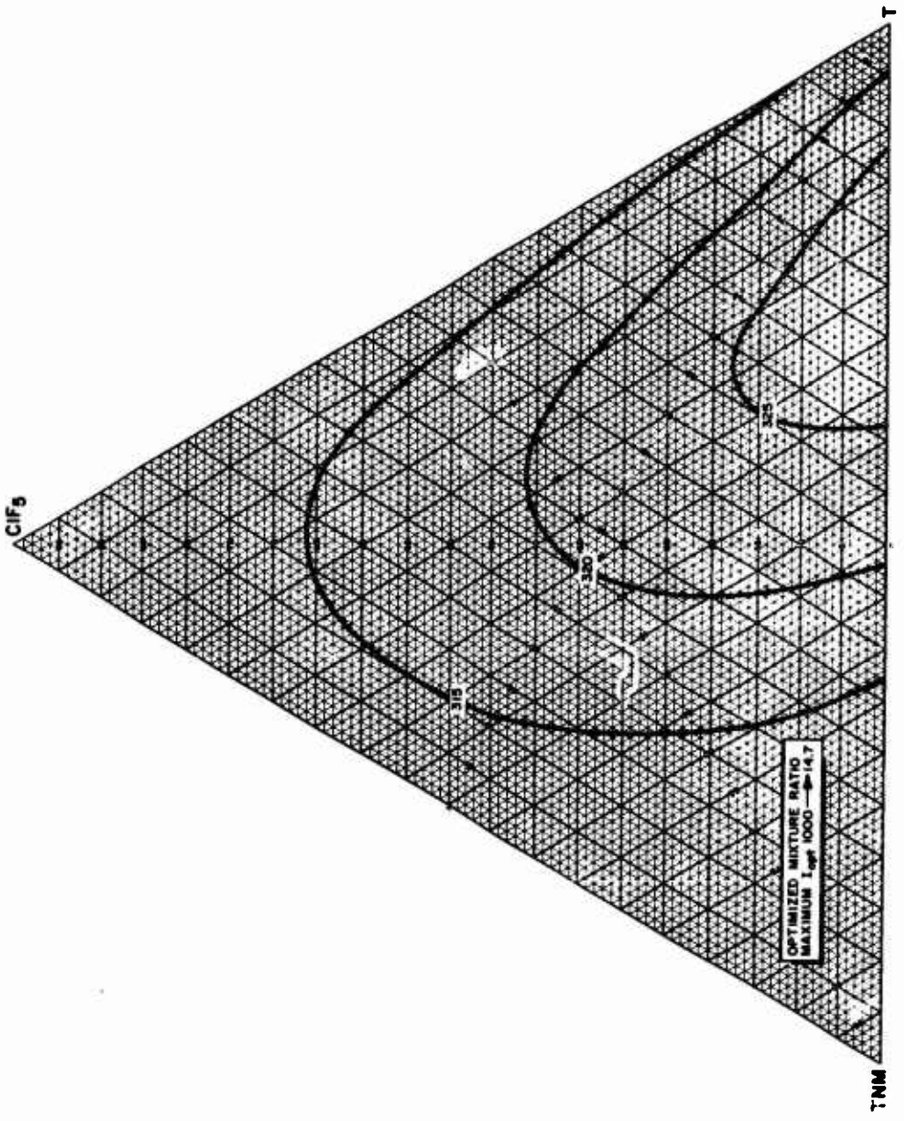


Figure 1. Performance vs Oxidizer Composition of ClF_5-TNM-T With B_5H_9

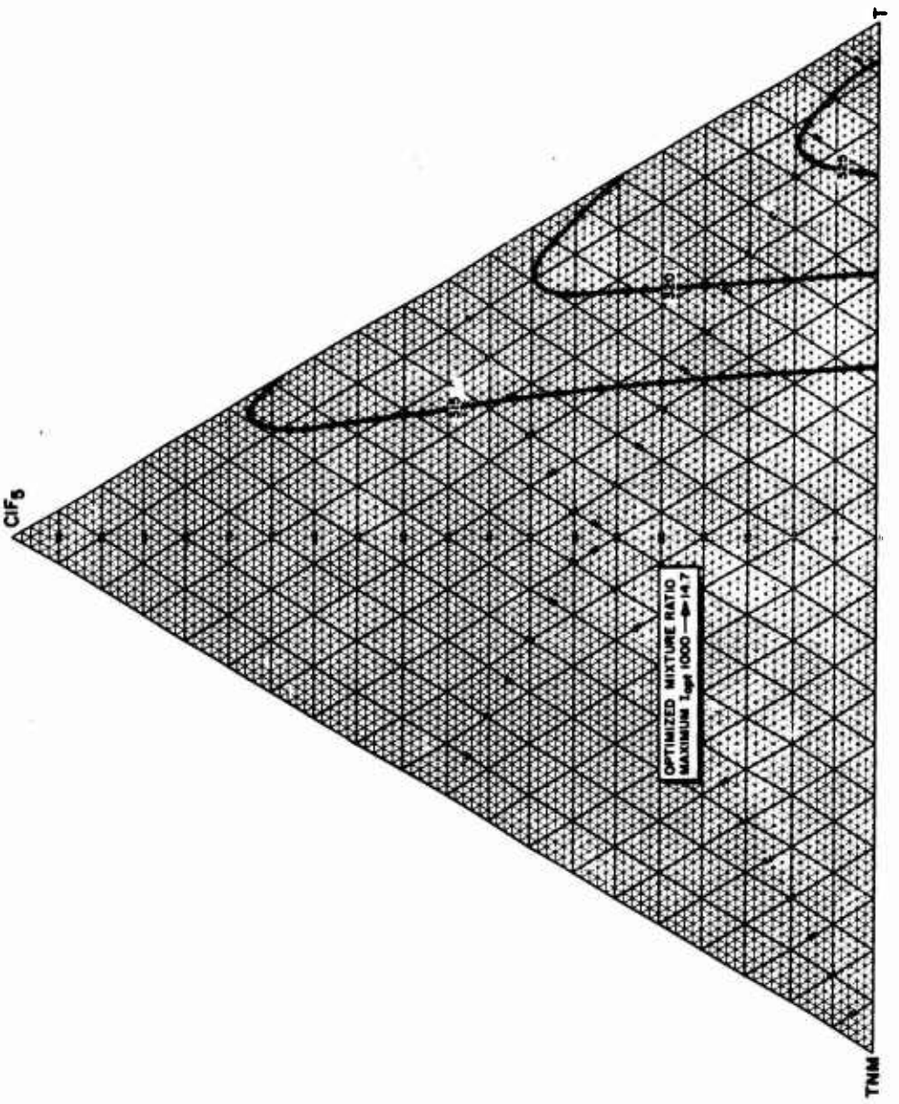


Figure 2. Performance vs Oxidizer Composition of ClF_5-TNM-T with N_2H_4

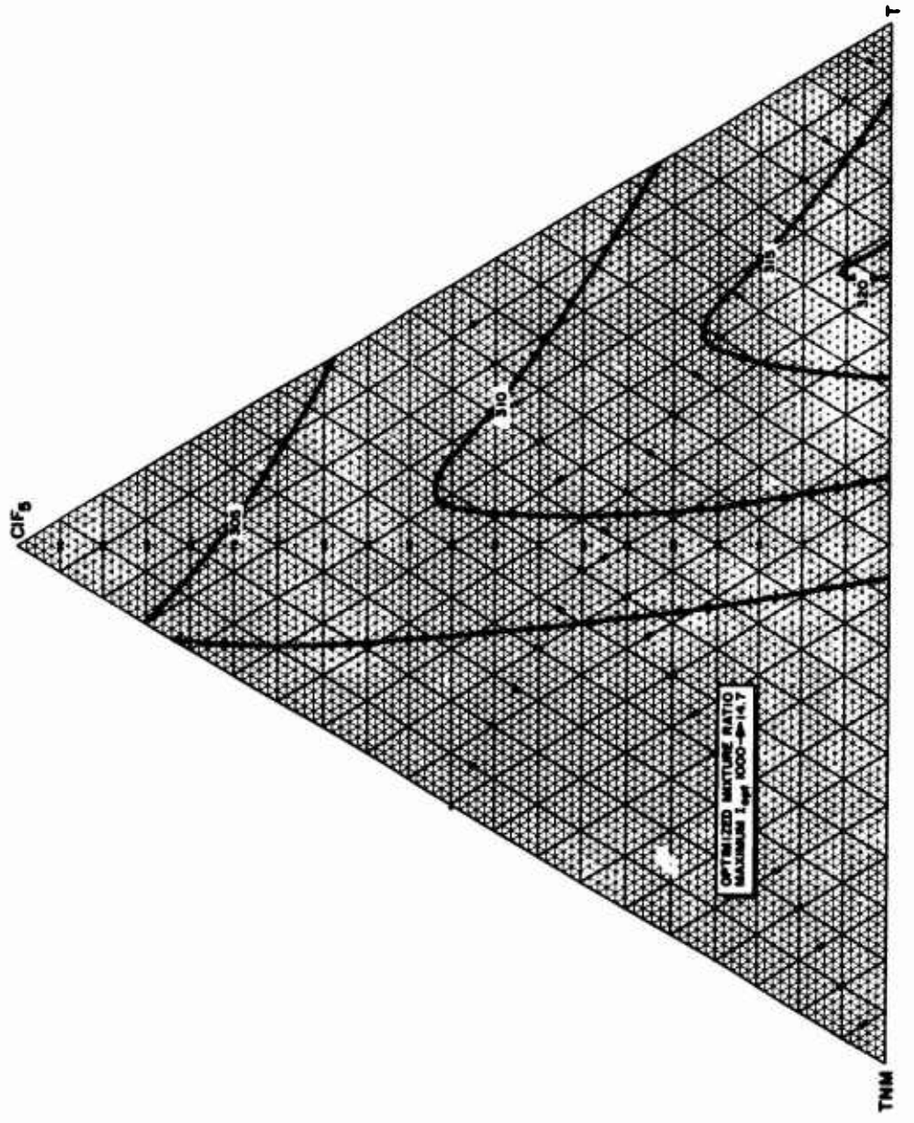


Figure 3. Performance vs Oxidizer Composition of ClF_5-TNM-T With MMH

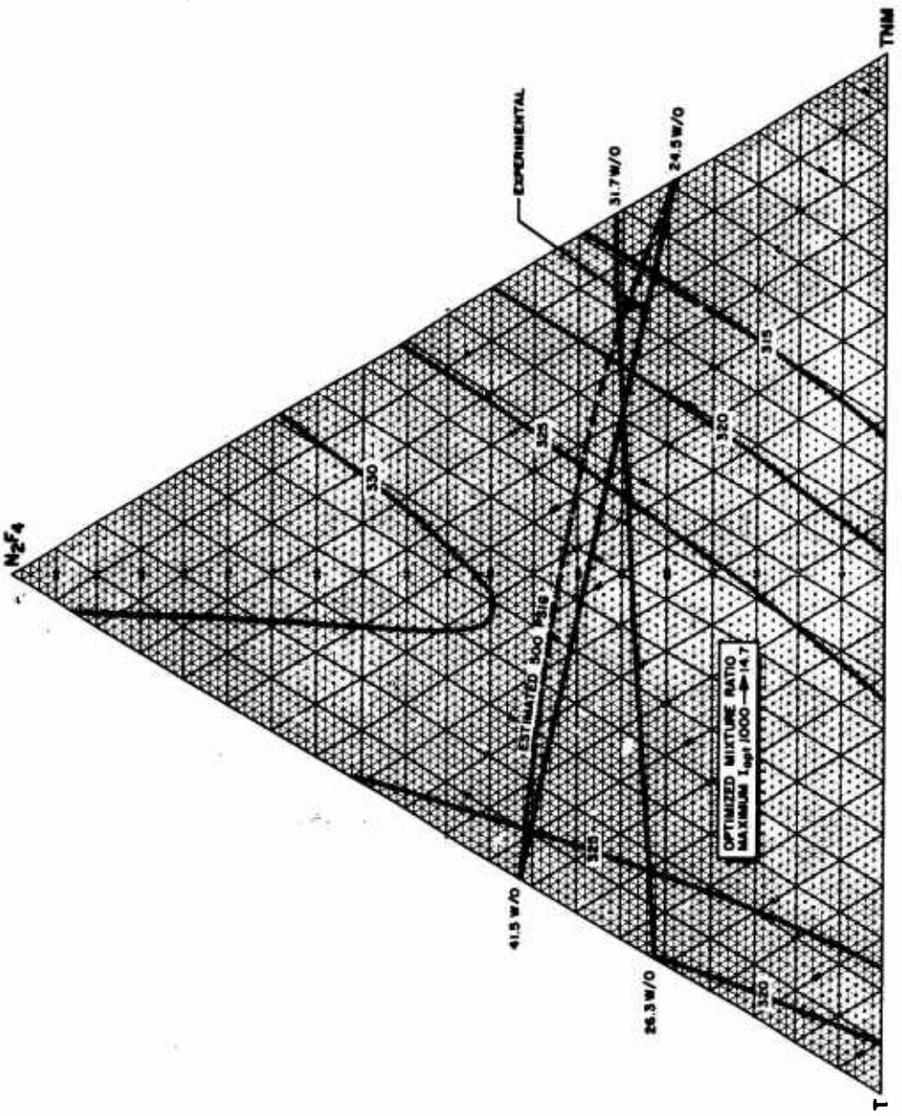


Figure 4. Performance vs Oxidizer Composition of N_2F_4-TNM-T with B_5H_9

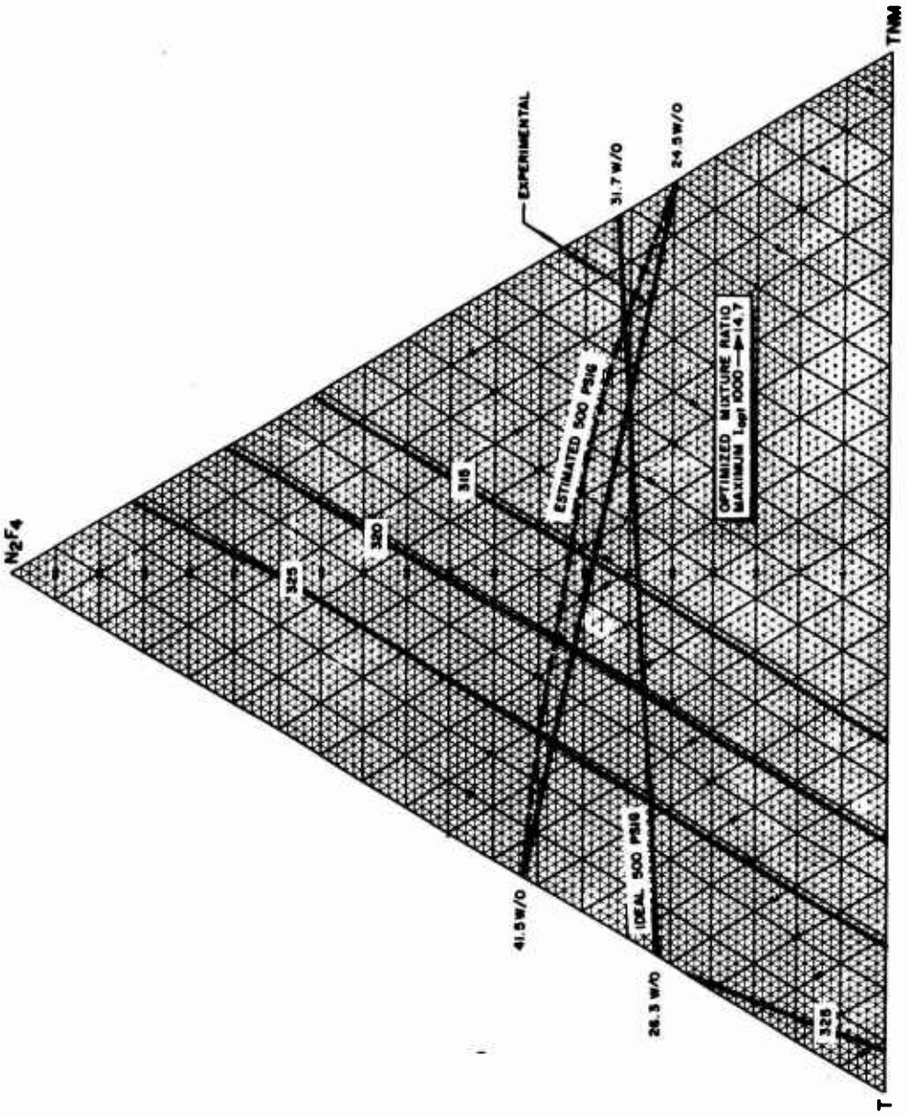


Figure 5. Performance vs Oxidizer Composition of N_2F_4-TNM-T with N_2H_4

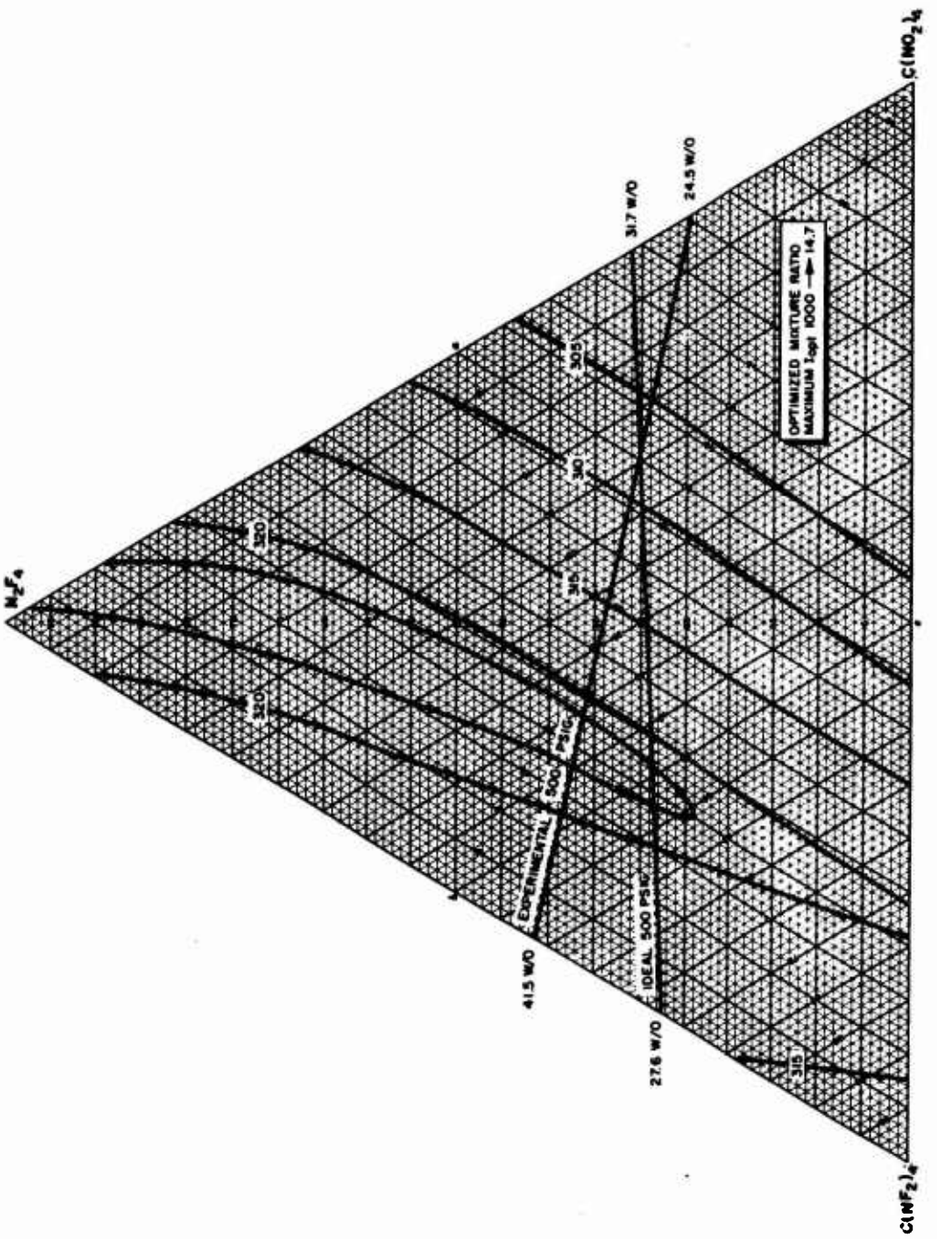


Figure 6. Performance vs Oxidizer Composition of N_2F_4-$C(NF_2)_4$-$C(NO_2)_4$ With MMH

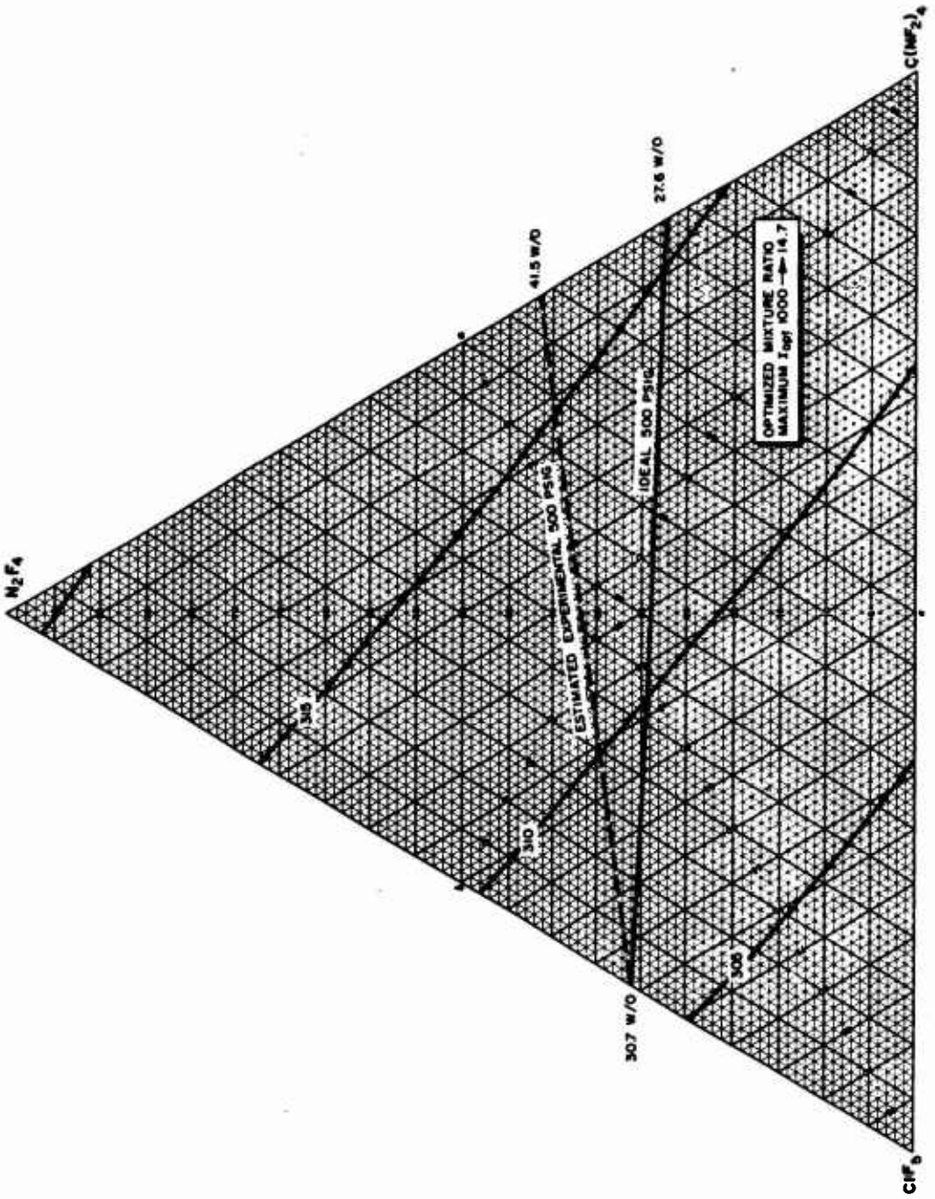


Figure 7. Performance vs Oxidizer Composition of N_2F_4-ClF_5-$C(NF_2)_4$ With MMH

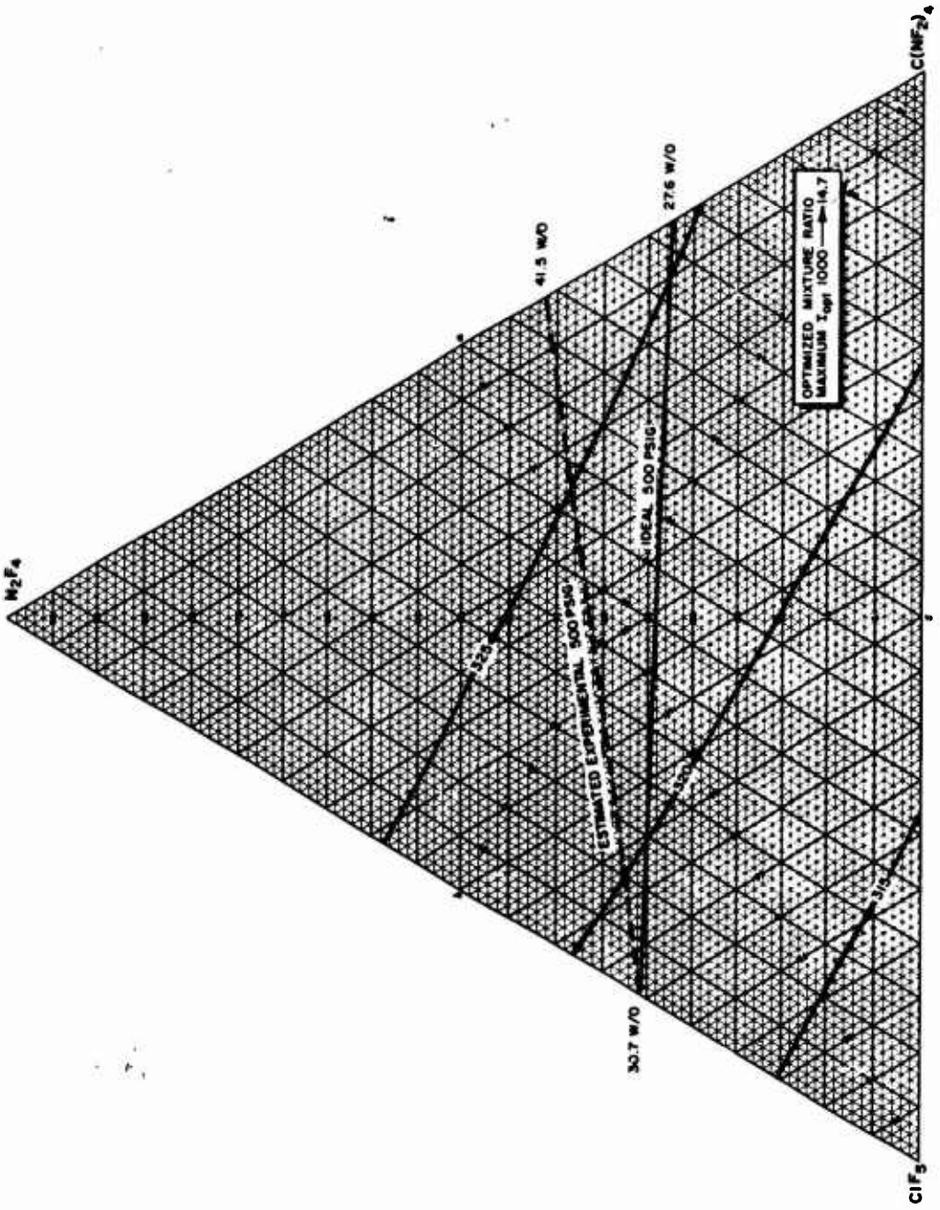


Figure 8. Performance vs Oxidizer Composition of N_2F_4-ClF_5-T With N_2H_4

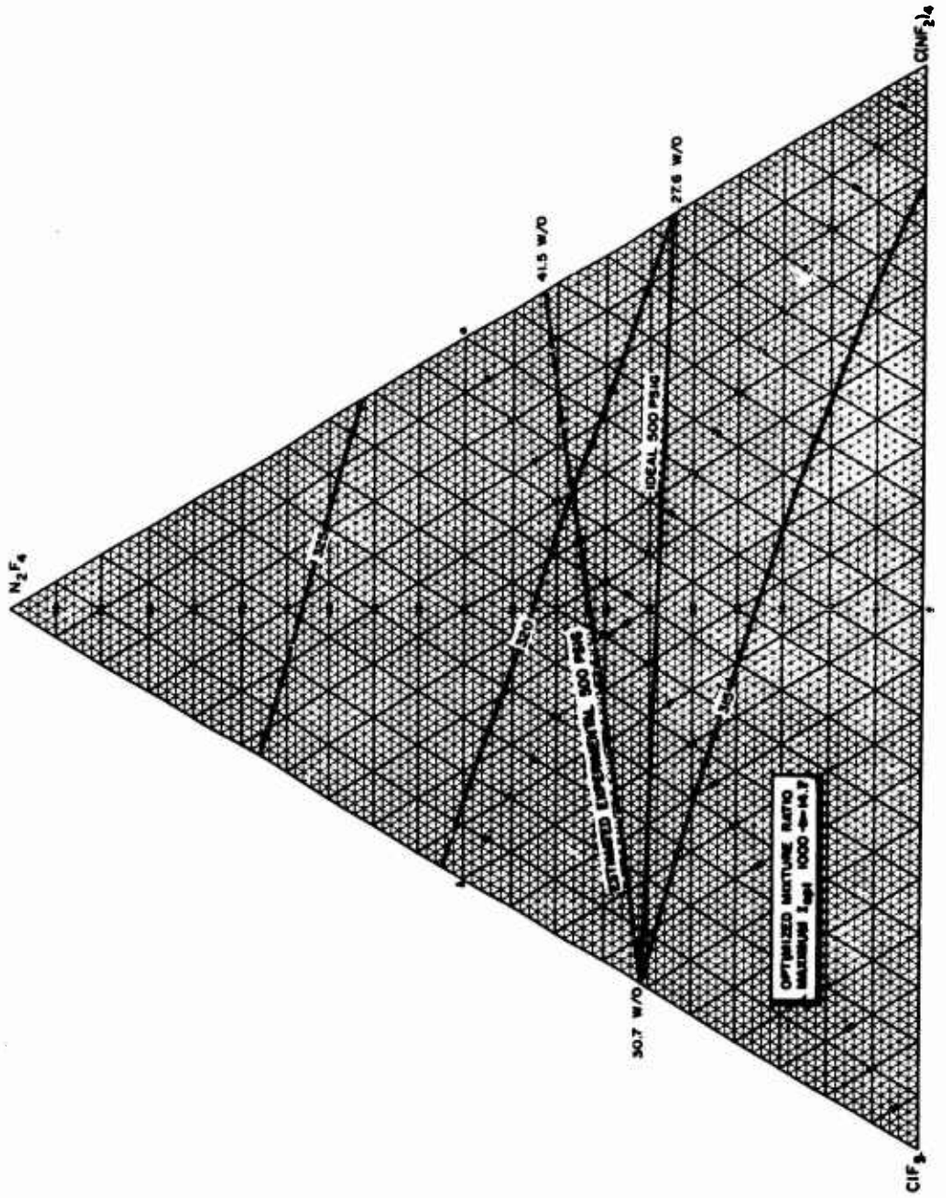


Figure 9. Performance vs Oxidizer Composition of N_2F_4-ClF_5-$C(NF_2)_4$ with B_5H_9

In Fig. 7 through 9, the triangles show that the 315-second performance goal can be met by the ClF_5-N_2F_4-$C(NF_2)_4$ mixture with all three fuels: monomethylhydrazine, hydrazine, and pentaborane. A minimum (5 w/o) of the shock-sensitive compound $C(NF_2)_4$ is necessary to reach performance goals with hydrazine and pentaborane, but at least 49 w/o $C(NF_2)_4$ is required to reach performance goals with monomethylhydrazine. Performances above 325 seconds can be obtained with hydrazine if the ternary mixture contains at least 43 w/o $C(NF_2)_4$.

The determination of the maximum amount of $C(NF_2)_4$ which could be used safely was undertaken through shock-sensitivity studies performed under another task of this program. Here again, the diagrams were useful for selecting mixture compositions for shock-sensitivity testing.

The four ternary oxidizers from the components, N_2F_4, ClF_5, $C(NO_2)_4$, and $C(NF_2)_4$, are listed in Table 1 with their highest impulse with monomethylhydrazine commensurate with the 500-psig vapor pressure limitation. Also presented are some of their characteristics and the amount of $C(NF_2)_4$ necessary to reach the maximum impulse. In considering the 500-psig vapor pressure limitation for the N_2F_4-$C(NF_2)_4$-$C(NO_2)_4$ system, an allowance was made for the negative vapor pressure deviation from ideality of the N_2F_4-$C(NF_2)_4$ system to be described in the following section on vapor pressure.

Table 1 reveals that the two ternary oxidizer mixtures, N_2F_4-$C(NF_2)_4$-$C(NO_2)_4$ and ClF_5-$C(NF_2)_4$-$C(NO_2)_4$, give the highest specific impulse with monomethylhydrazine. The ClF_5-$C(NF_2)_4$-N_2F_4 ternary mixture is somewhat inferior in performance and has the possible problems of shock sensitivity and ClF_5-N_2F_4 compatibility as compared with only the shock-sensitivity problem of the previous two oxidizer mixtures. The remaining mixture of ClF_5-N_2F_4-$C(NO_2)_4$ will not meet the performance goal of 315 seconds with monomethylhydrazine although it can do so with hydrazine and pentaborane.

During the latter part of the program, the emphasis of the homogeneous oxidizer study was changed to evaluating oxidizer mixtures which would be applicable for use with heterogeneous fuels. The shift from pure fuels

TABLE 1

TERNARY OXIDIZERS AND MAXIMUM SPECIFIC IMPULSE WITH MONOMETHYLHYDRAZINE WITHIN 500-PSIG LIMITATION

Ternary Oxidizer	Maximum Specific Impulse, seconds	Weight Percent of $C(NF_2)_4$	Characteristics	Possible Problems
N_2F_4-$C(NF_2)_4$-$C(NO_2)_4$	323	40	Highest specific impulse; high vapor pressure	Shock sensitive
ClF_5-$C(NF_2)_4$-$C(NO_2)_4$	320	77	High specific impulse; low vapor pressure	Shock sensitive
ClF_5-$C(NF_2)_4$-N_2F_4	317	58	High vapor pressure	Shock sensitive; ClF_5-N_2F_4 compatibility
ClF_5-N_2F_4-$C(NO_2)_4$	310	0	Does not meet specific impulse goals; insensitive to shock; high vapor pressure	ClF_5-N_2F_4 compatibility

to a heterogeneous fuel (R-2, beryllium dispersed in N_2H_4) did not change the program requirements with respect to the physical properties of the oxidizers. The basic theoretical 315-second specific impulse requirement of a proposed propellant system was increased to 325 seconds. This increase in specific impulse was considered essential if a heterogeneous fuel was to be employed. The reasoning behind the concept was based on the belief that small quantities (less than 25 w/o) of a fluorine-containing component would increase the combustion efficiency of the basic beryllium-containing propellant system by increasing theoretical chamber temperature and reducing the percentage of condensed BeO in the combustion products. The three binary oxidizer mixtures initially selected were N_2O_4-NF_3O, N_2O_4-FNO_2, and H_2O_2-NF_3O. Theoretical studies indicated that in the case of N_2O_4-NF_3O, both of these advantages would occur on addition of NF_3O (Fig. 10). The same double advantage was calculated for the H_2O_2-NF_3O system (Fig. 11). The N_2O_4-FNO_2 system theoretically has the advantage that the percent condensed BeO in the products diminishes with addition of FNO_2, but this may be entirely offset by the fact that the combustion temperature diminishes with the same addition of FNO_2 (Fig. 12).

Xenon Fluoride Systems

The xenon fluorides appeared to have potentially significant propellant applications. Because of the high atomic weight of xenon, 131.3, and the fact that the fluorides contain only 22.4 to 46.5 w/o fluorine, high specific impulses were not expected. However, unusually high density impulses would be expected for systems using these compounds. Calculations were made for a system using xenon tetrafluoride, which has a density of approximately 4.1 gm/cc. For example, comparing the density and density impulse of XeF_4 to the high values for BrF_5 and ClF_5 with hydrazine as the fuel, both quantities are higher for XeF_4. The parameters of interest are presented in Table 2.

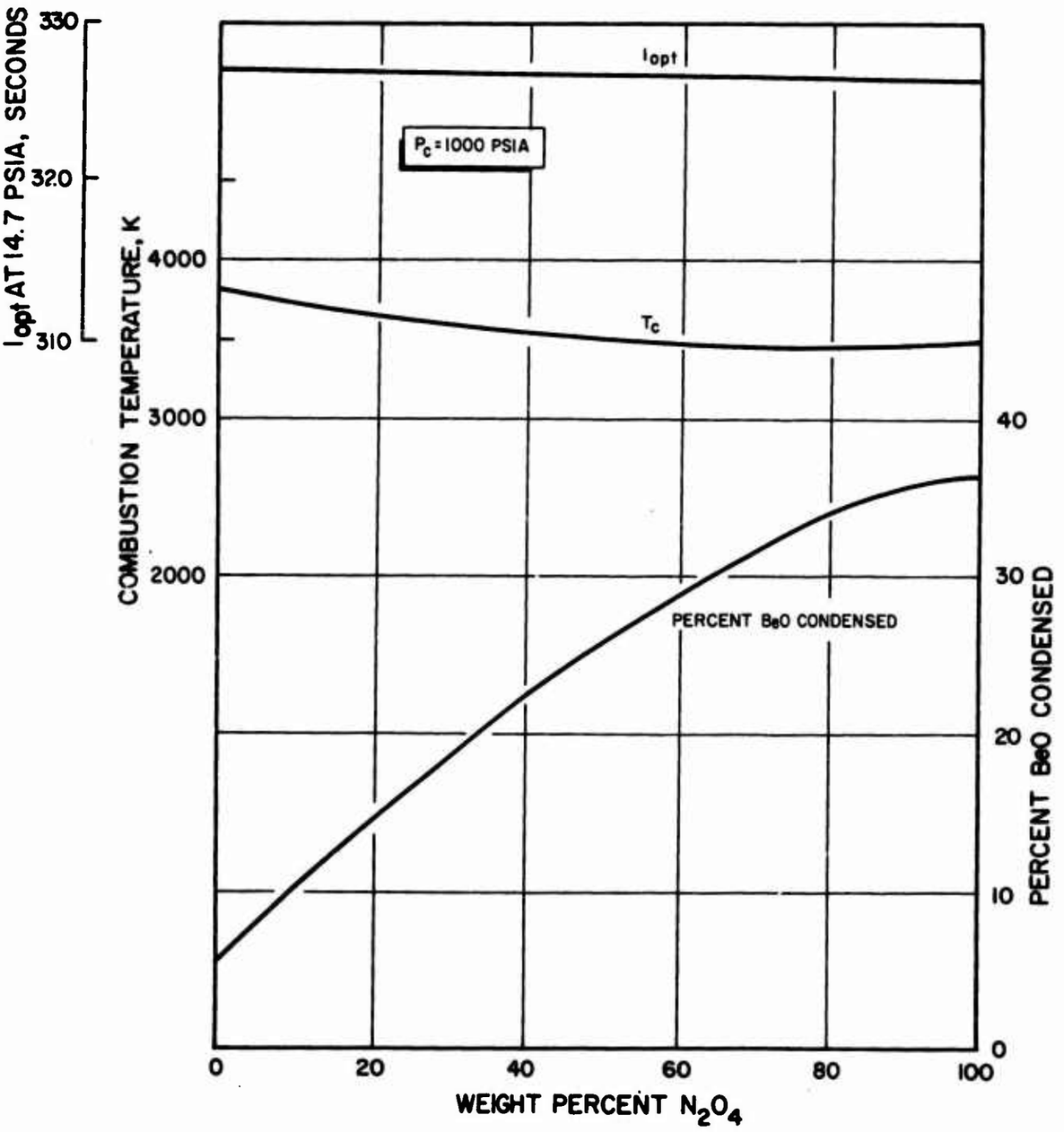


Figure 10. Performance, Combustion Temperature, and Percent Condensed Phase Curves for NF_3O–N_2O_4 With Be–N_2H_4

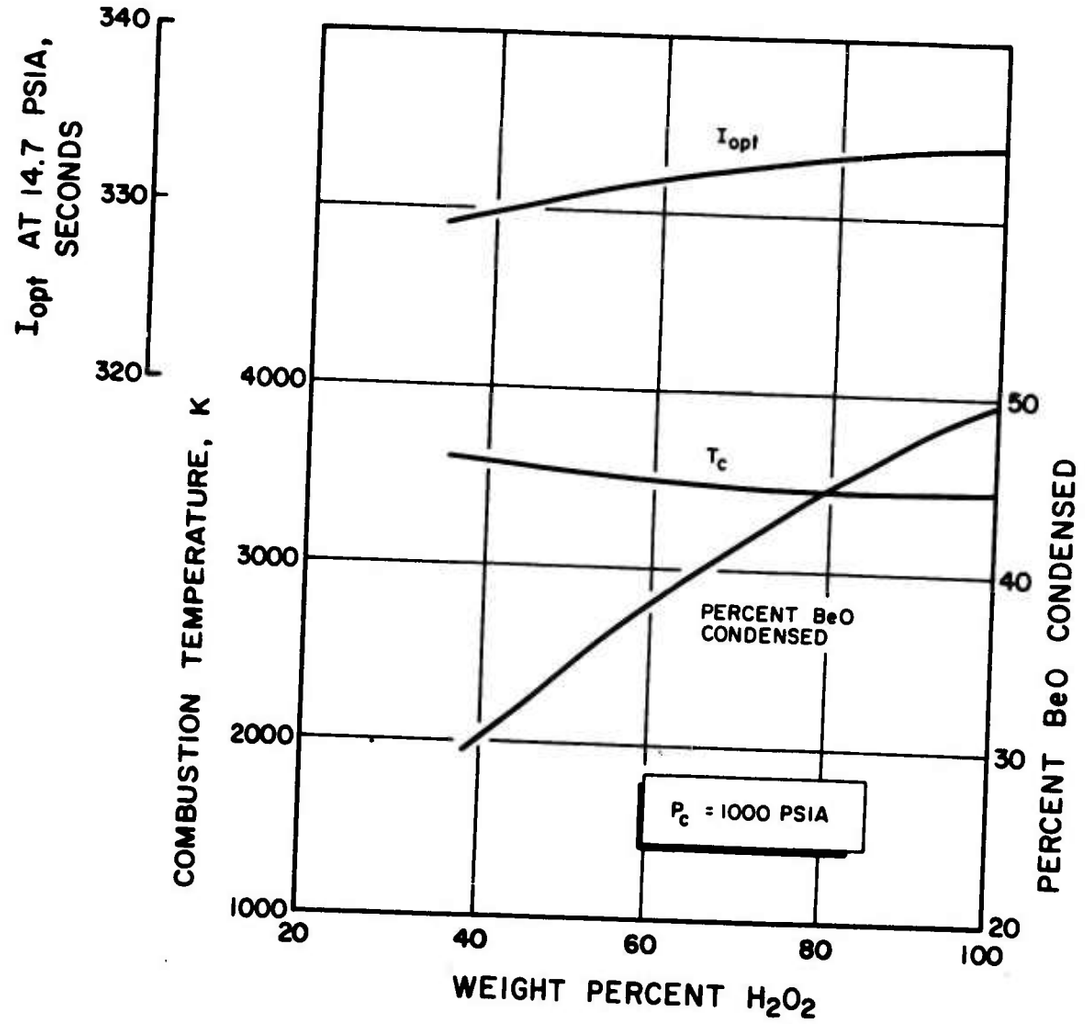


Figure 11. Performance, Combustion Temperature, and Percent Condensed Phase Curves for NF_3O–H_2O_2 With Be–N_2H_4

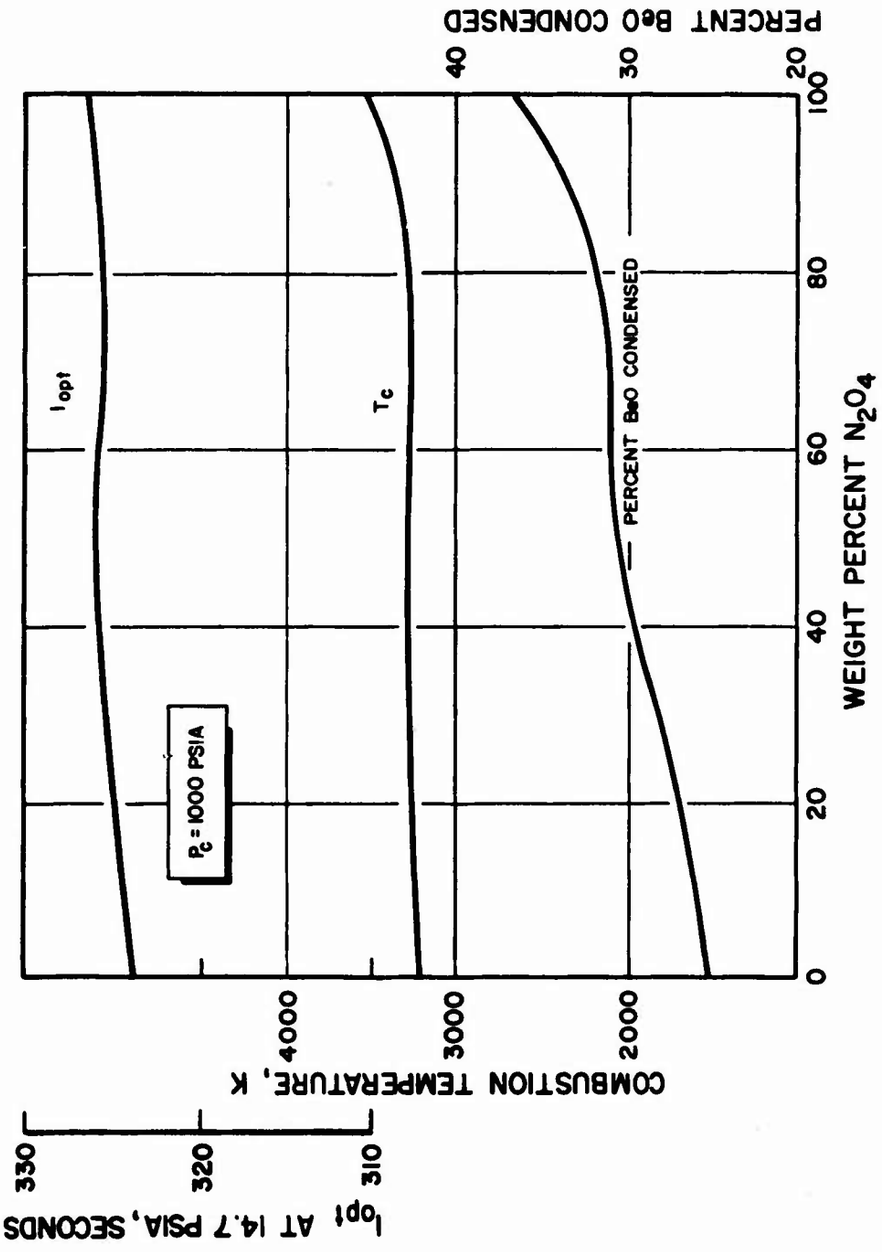


Figure 12. Performance, Combustion Temperature, and Percent Condensed Phase Curves for N_2O_4–FNO_2 With Be–N_2H_4

TABLE 2

THEORETICAL PERFORMANCE OF XeF_4, BrF_5, AND ClF_5 WITH HYDRAZINE

Compound	Density, gm/cc	Heat of Formation, kcal/mole	I_s x d (maximum)*
XeF_4	4.1	-60	670
BrF_5	2.46	-131.2	456
ClF_5	1.75	-60	454
*$(I_s)_{opt}$, 1000 ⟶ 14.7 psia			

It should be emphasized that the heats of formation of XeF_4 and BrF_5, and the density of XeF_4 are not well established, but the accepted values were used. It was not expected that new values would be appreciably different.

Xenon tetrafluoride was considered for use in liquid oxidizer systems as a solution in chlorine pentafluoride because it seemed likely that the two compounds would be compatible; they are both perfluoro compounds of comparable oxidizing tendency. A high degree of solubility was expected because both compounds are nonpolar and should have similar solubility parameters.

Maximum impulse vs density data for high-density liquid propellant systems are presented in Fig. 13. Each system is based upon ClF_5-N_2H_4 and contains one of the following additives: BrF_5, B, Be, XeF_4, XeF_4 and B, or XeF_4 and Be. The curves for the last two systems represent varying oxidizer composition with constant fuel compositions, 20-percent Be in N_2H_4 and 30-percent B in N_2H_4, respectively. These are approximately the optimum fuel compositions required to maximize the density impulse over the entire range of oxidizer compositions.

It can be noted from Fig. 13 that fairly high concentrations of XeF_4 in ClF_5 are necessary to produce large improvements in density impulse. For example, 75 percent is required to raise the density impulse of ClF_5-N_2H_4

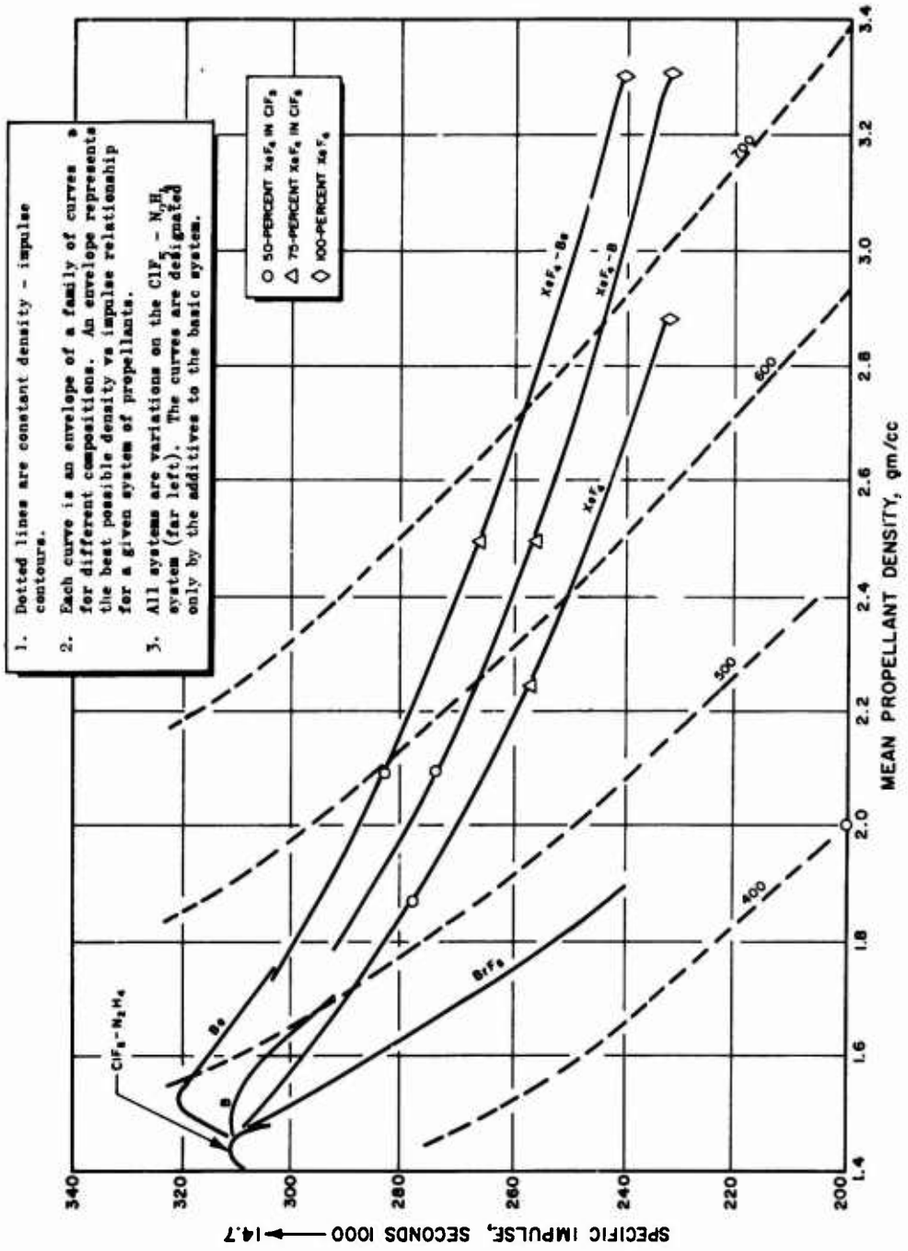


Figure 13. Boundary Curves for High-Density Propellant Systems

from 454 to 585 seconds (maximum with 100-percent XeF_4 is 680). If such high concentrations are not obtainable, it may be possible to achieve high xenon concentrations by including the difluoride and hexafluoride, as well as the tetrafluoride. It is expected that the density impulse of such mixtures may be close to those for the tetrafluoride.

VAPOR PRESSURE STUDIES

Studies were conducted on the vapor pressures of binary and ternary oxidizer mixtures that met the theoretical performance requirement and had a vapor pressure of less than 500 psig at 160 F (71 C). During this report period, vapor pressure determinations were conducted on the binary mixtures ClF_5-$C(NF_2)_4$ and N_2F_4-$C(NF_2)_4$, as well as the ternary N_2F_4-$C(NF_2)_4$-$C(NO_2)_4$. All liquid compositions presented with vapor pressure data have been corrected for material lost to the vapor phase as explained in the Experimental Section of this task. A further correction for deviation of the N_2F_4 vapor from ideal gas law behavior was applied to the two systems using N_2F_4.

ClF_5-$C(NF_2)_4$ Binary System

The low-volume vapor pressure apparatus described previously (Ref. 1) was used to study this system at 0.0, 45.0, and 71.0 C. The vapor pressure data are presented in Table 3 and are graphically depicted in Fig. 14. The system showed slight positive deviation at all three temperatures investigated.

N_2F_4-$C(NF_2)_4$ Binary System

The low-volume vapor pressure apparatus was also used to study this system at 0.0, 45.0, and 71.0 C. The vapor pressure data are presented in Table 4 and are graphically represented in Fig. 15. The system exhibited ideal

TABLE 3

VAPOR PRESSURE OF THE ClF_5-$C(NF_2)_4$ SYSTEM

Mixture Number	Total Composition, percent		Temperature, F	Liquid Composition				Ideal Vapor Pressure, psia	Experimental Vapor Pressure, psia
				Mole Percent		Weight Percent			
	ClF_5	$C(NF_2)_4$		ClF_5	$C(NF_2)_4$	ClF_5	$C(NF_2)_4$		
1	12.8	87.2							
			0.0	8.7	91.3	4.4	95.6	3.2	5.7
			45.0	6.1	93.9	3.7	96.3	22.3	21.5
			71.0	5.3	94.7	3.2	96.8	44.8	40.2
2	16.0	84.0							
			0.0	13.7	86.3	8.6	91.4	6.1	8.4
			45.0	11.4	88.6	7.1	92.9	26.9	28.8
			71.0	10.2	89.8	6.3	93.7	52.3	47.6
3	22.3	77.7							
			0.0	19.6	80.4	12.6	87.4	7.4	10.6
			45.0	16.4	83.6	10.4	89.6	19.5	34.1
			71.0	14.4	85.6	9.1	90.9	58.7	58.0
4	36.4	63.6							
			0.0	33.5	66.5	23.0	77.0	10.6	14.6
			45.0	28.9	71.1	19.4	80.6	42.0	48.1
			71.0	25.7	74.3	17.0	83.0	75.9	81.4
5	53.4	46.6							
			0.0	51.0	49.0	38.1	61.9	14.5	20.2
			45.0	46.5	53.5	34.0	66.0	57.1	69.4

AFRPL-TR-66-294

TABLE 3
(Concluded)

Mixture Number	Total Composition, percent		Temperature, C	Liquid Composition				Ideal Vapor Pressure, psia	Experimental Vapor Pressure, psia
				Mole Percent		Weight Percent			
	ClF_5	$C(NF_2)_4$		ClF_5	$C(NF_2)_4$	ClF_5	$C(NF_2)_4$		
6	50.0	50.0							
			0.0	46.3	53.7	33.8	66.2	13.4	20.5
			45.0	40.1	59.9	28.4	71.6	51.6	65.8
			71.0	36.5	63.5	25.4	74.6	92.4	100.6
7	75.0	25.0							
			0.0	73.7	26.3	62.4	37.6	19.6	28.2
			45.0	71.3	28.7	59.5	40.5	78.4	92.1
8	85.7	14.3							
			0.0	85.3	14.7	77.5	22.5	22.2	29.4
			45.0	84.4	15.6	76.3	23.7	89.8	104.3
			71.0	83.6	16.4	75.2	24.8	164.3	182.4

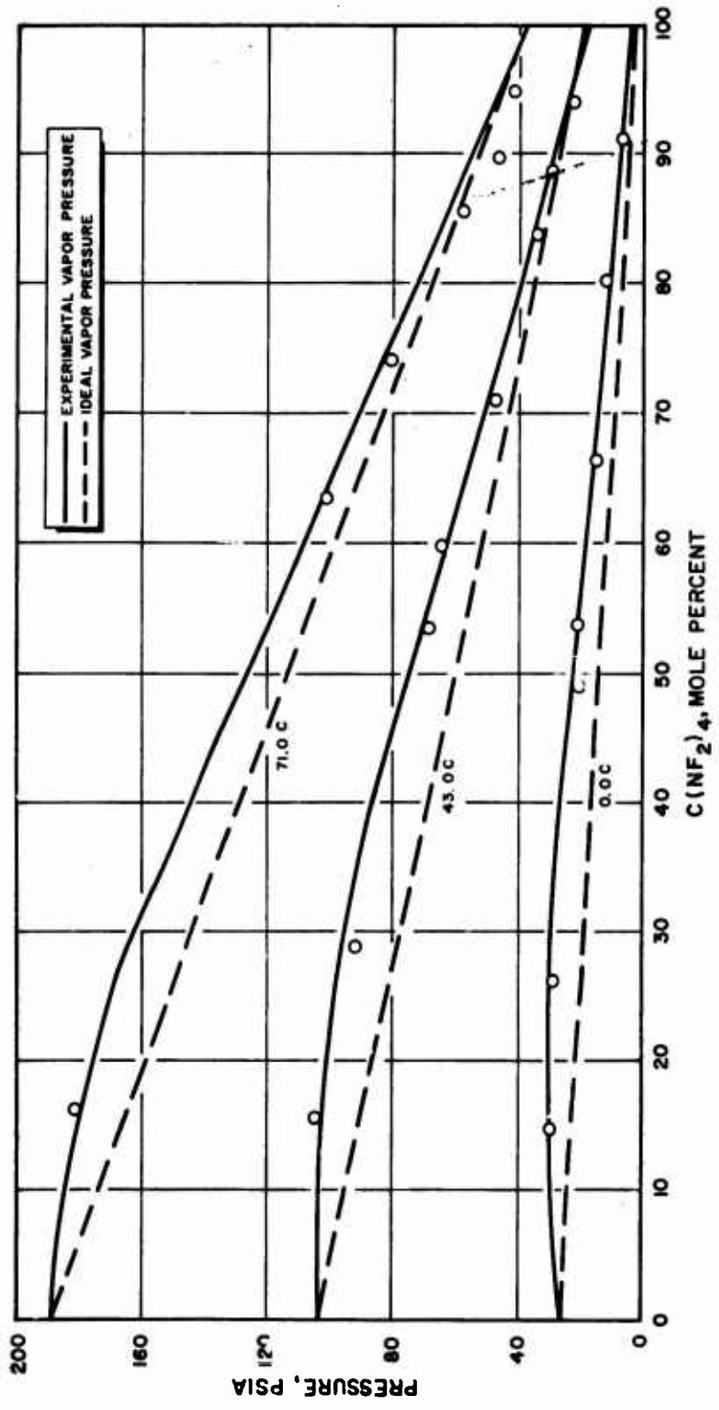


Figure 14. Vapor Pressure of ClF_5-$C(NF_2)_4$

TABLE 4

VAPOR PRESSURE OF THE N_2F_4-$C(NF_2)_4$ SYSTEM

Mixture Number	Total Composition, percent		Temperature, C	Liquid Composition				Ideal Vapor Pressure, psia	Experimental Vapor Pressure, psia
				Mole Percent		Weight Percent			
	N_2F_4	$C(NF_2)_4$		N_2F_4	$C(NF_2)_4$	N_2F_4	$C(NF_2)_4$		
1	16.7	83.3							
			0	4.2	95.8	2.0	98.0	13.1	14.1
			45	1.9	98.1	0.9	99.1	29.8	32.1
			71	1.4	98.6	0.7	99.3	51.8	54.5
2	28.6	71.4							
			0	9.0	91.0	4.5	95.5	24.7	23.7
			45	4.2	95.8	2.0	98.0	45.2	44.9
			71	3.1	96.9	1.5	98.5	69.4	66.5
3	44.5	55.5							
			0	15.6	84.4	8.1	91.9	40.6	45.7
			45	8.6	91.4	4.2	95.8	74.0	73.2
			71	6.0	94.0	2.9	97.1	100.3	97.9
4	61.6	38.4							
			0	33.7	66.3	19.3	80.7	83.8	77.9
			45	17.3	82.7	9.0	91.0	132.3	124.0
			71	11.8	88.2	6.0	94.0	162.9	152.8
5	70.6	29.4							
			0	45.6	54.4	28.4	71.6	112.6	108.0
			45	25.2	74.8	13.8	86.2	184.8	171.2
			71	17.3	82.7	9.0	91.0	221.0	207.0
6	90.6	9.4							
			0	86.8	13.2	75.7	24.3	211.4	208.9
			45	75.7	24.3	59.6	40.4	520.2	456.5
			71	67.7	32.3	49.7	50.3	757.7	568.7

TABLE 4

(Concluded)

Mixture Number	Total Composition, percent		Temperature, C	Liquid Composition				Ideal Vapor Pressure, psia	Experimental Vapor Pressure, psia
				Mole Percent		Weight Percent			
	N_2F_4	$C(NF_2)_4$		N_2F_4	$C(NF_2)_4$	N_2F_4	$C(NF_2)_4$		
7	95.0	5.0							
			0	94.1	5.9	88.3	11.7	229.0	237.9
			45	91.5	8.5	83.6	16.4	625.3	603.5
			71	87.3	12.7	76.5	23.5	967.3	833.6
8	97.2	2.8							
			0	97.0	3.0	93.9	6.1	235.9	238.8
			45*						
			7'*						
9	95.4	4.6							
			0	94.7	5.3	89.4	10.6	230.3	226.6
			45	92.8	7.2	85.9	14.1	633.8	613.8
			71	89.2	10.8	79.6	20.4	987.4	883.2
10	90.7	9.3							
			0	86.8	13.2	75.7	24.3	211.5	215.5
			45	76.2	23.7	60.3	39.7	523.6	471.7
			71	65.0	35.0	46.7	53.3	729.2	586.1
11	86.0	14.0							
			0	76.7	23.3	60.9	39.1	187.3	191.6
			45	54.5	45.5	36.1	63.9	379.1	356.9
			71	46.7	53.3	29.2	70.8	533.9	424.8

*Exceeds critical temperature of the mixture

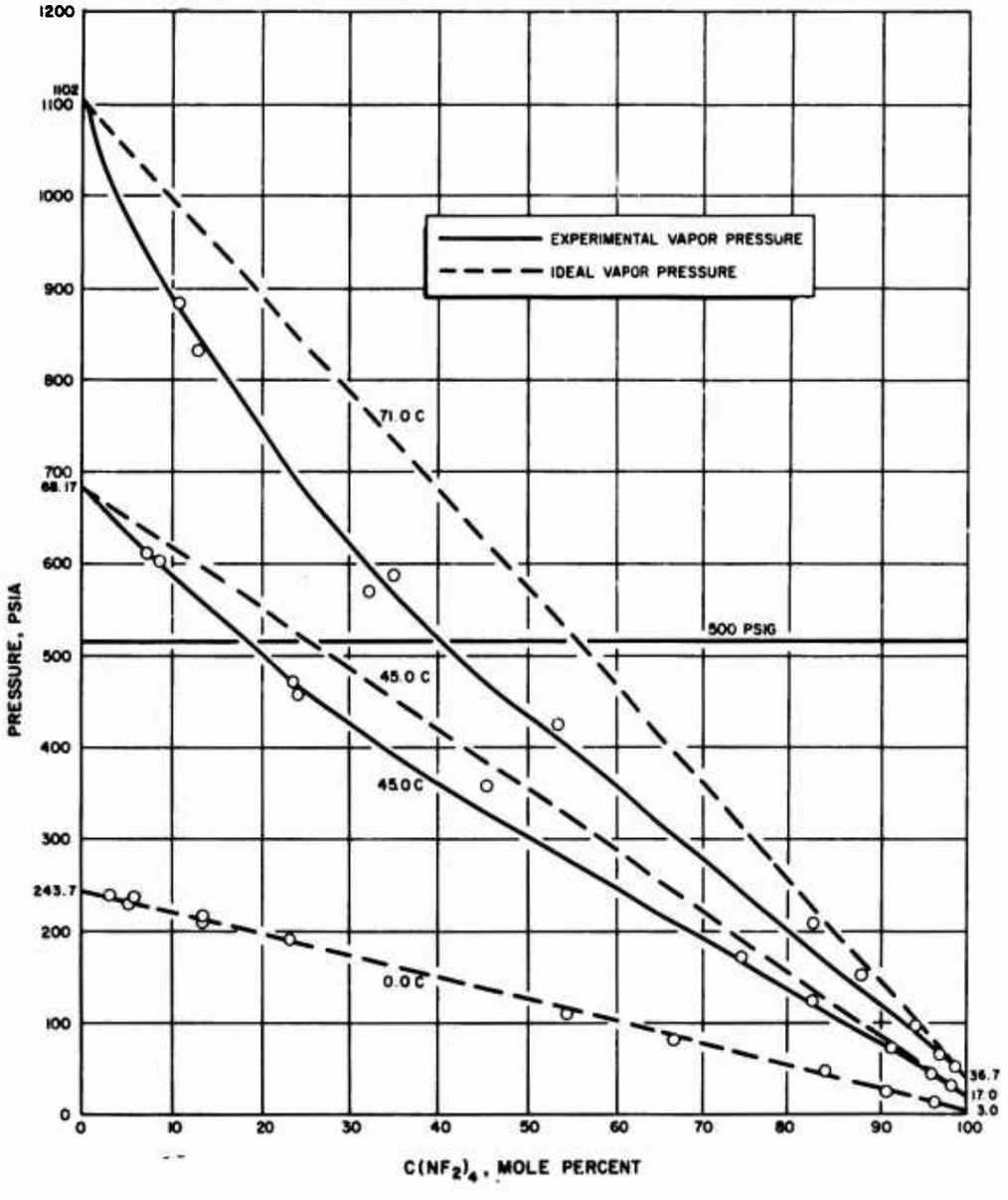


Figure 15. Vapor Pressure of N_2F_4-$C(NF_2)_4$

solution behavior at 0.0 C but at 45 C a slight negative deviation from ideality was apparent. This became even more negative at 71.0 C. These observations are in accordance with the negative deviation found for the vapor pressure of 47.6 w/o N_2F_4- 52.4 w/o $C(NF_2)_4$ mixture at 60 C (Ref. 2).

N_2F_4-$C(NF_2)_4$-$C(NO_2)_4$ System

The low-volume vapor pressure apparatus was used to study this system at 0.0, 45.0, and 71.0 C. The experimentally derived 500-psig isobar at 71.0 C (Fig. 6) was found to be a straight line between the 500-psig points of the N_2F_4-$C(NF_2)_4$ and N_2F_4-$C(NO_2)_4$ binary systems. The data (Table 5) indicated that this system behaved similar to the N_2F_4-$FC(NF_2)_3$-$C(NO_2)_4$ system. Mixtures rich in $C(NO_2)_4$ were found to have a positive deviation from vapor pressure expected for an ideal solution, whereas mixtures with less than 49 w/o $C(NO_2)_4$ were found to have only negative deviations. The area of compositions which displayed negative deviations increased with increasing temperature similar to the behavior of the N_2F_4-$FC(NF_2)_3$-$C(NO_2)_4$ system (Ref. 1).

NF_3O-N_2O_4 System

The low-volume vapor pressure apparatus was used to study this system at 71 C. In view of the fact that NF_3O has a critical temperature of 29 C, a calculation was made to determine how much N_2O_4 would be required to obtain a binary mixture with a critical temperature above 71 C. The results indicated that a 65 m/o N_2O_4-35 m/o NF_3O mixture had a critical temperature below 71 C, while a 78 m/o N_2O_4-22 m/o NF_3O mixture had a critical temperature above 71 C. Further effort was not conducted in refining this system because of the complexity of the $N_2O_4 \rightleftharpoons 2NO_2$ equilibrium which is both pressure and temperature sensitive. There was also a compatibility problem between NF_3O and N_2O_4.

TABLE 5

VAPOR PRESSURE OF THE N_2F_4-$C(NF_2)_4$-$C(NO_2)_4$ SYSTEM

Temperature, C	Liquid Composition						Ideal Vapor Pressure, psia	Experimental Vapor Pressure, psia	Deviation, percent
	Weight Percent			Mole Percent					
	N_2F_4	$C(NF_2)_4$	$C(NO_2)_4$	N_2F_4	$C(NF_2)_4$	$C(NO_2)_4$			
0.0	15.8	16.3	67.9	26.6	12.9	60.5	65.1	109.7	68.5
	21.5	15.3	63.2	34.6	9.3	53.8	84.5	133.6	58.1
	20.9	20.6	58.5	33.8	15.8	50.4	82.7	126.7	53.2
	34.3	17.2	48.5	50.3	11.9	37.8	122.7	161.7	31.8
	53.5	12.2	34.3	69.1	7.4	23.5	168.1	194.0	15.4
	48.5	21.3	30.2	65.0	13.5	21.5	158.5	175.1	10.5
	52.0	19.8	28.2	68.1	12.3	19.6	165.9	180.1	8.6
45.0	12.9	16.6	70.5	22.2	13.5	64.3	153.8	167.9	9.2
	16.1	16.0	67.9	27.0	12.6	60.4	186.0	219.5	18.0
	15.6	21.5	62.9	26.3	17.3	56.4	182.4	215.6	18.2
	27.1	18.8	54.1	41.8	13.7	44.4	287.8	315.6	9.7
	47.0	13.7	39.3	63.2	8.8	28.0	432.4	463.0	7.1
	44.0	23.0	33.0	60.8	15.0	24.2	417.0	383.7	-8.0
	47.5	21.6	30.9	64.1	13.8	22.1	439.5	416.4	-5.3
71.0	8.6	16.6	74.8	15.2	14.0	70.8	173.2	195.3	12.8
	11.3	16.2	72.5	19.7	13.3	67.0	221.6	256.3	15.7
	11.3	21.9	66.8	19.8	18.1	62.1	225.3	251.4	11.6
	19.5	20.1	60.4	31.9	15.5	52.6	357.3	375.2	5.0
	35.0	16.4	48.6	51.0	11.3	37.7	566.5	593.7	4.8
	35.1	26.3	38.6	51.6	18.3	30.1	575.6	537.3	-6.7
	38.9	24.8	36.3	55.7	16.8	27.5	619.9	576.5	-7.0

SOLUBILITY OF XeF_4 AND XeF_2 IN ClF_5

The solubility of XeF_4 in ClF_5 was investigated as part of the laboratory feasibility experiments on the utilization of the xenon fluorides as oxidizer ingredients. The first attempts to measure the solubility were made using the principle of vapor pressure lowering of a solvent by a solute. The vapor pressure lowering of a XeF_4 saturated solution of ClF_5 was measured at 0 C. However, reproducibility of the vapor pressure lowering was poor and the method was replaced by direct visual observation of solubility.

The solubility data are summarized in Table 6 and in Fig. 16, where the log of the solubility is plotted against the reciprocal of the absolute temperature. The differential heat of solution estimate from the line drawn in Fig. 16 is 4.3 kcal/mole. For comparative purposes, 6.7 kcal/mole has been reported for the heat of solution of XeF_4 in anhydrous HF (Ref. 3). The solubility of XeF_4 in ClF_5 is too small to take advantage of the increase in density impulse which XeF_4 would provide as described in the section on theoretical performance.

TABLE 6

SOLUBILITY OF XeF_4 IN ClF_5

Temperature, C	Solubility, moles/1000 grams ClF_5	Solubility, grams/100 grams ClF_5
4.5	0.141	2.92
7.0	0.150	3.10
27.5	0.266	5.52
33.0	0.300	6.22
33.0	0.298	6.19
35.5	0.307	6.36
45.5	0.382	7.92

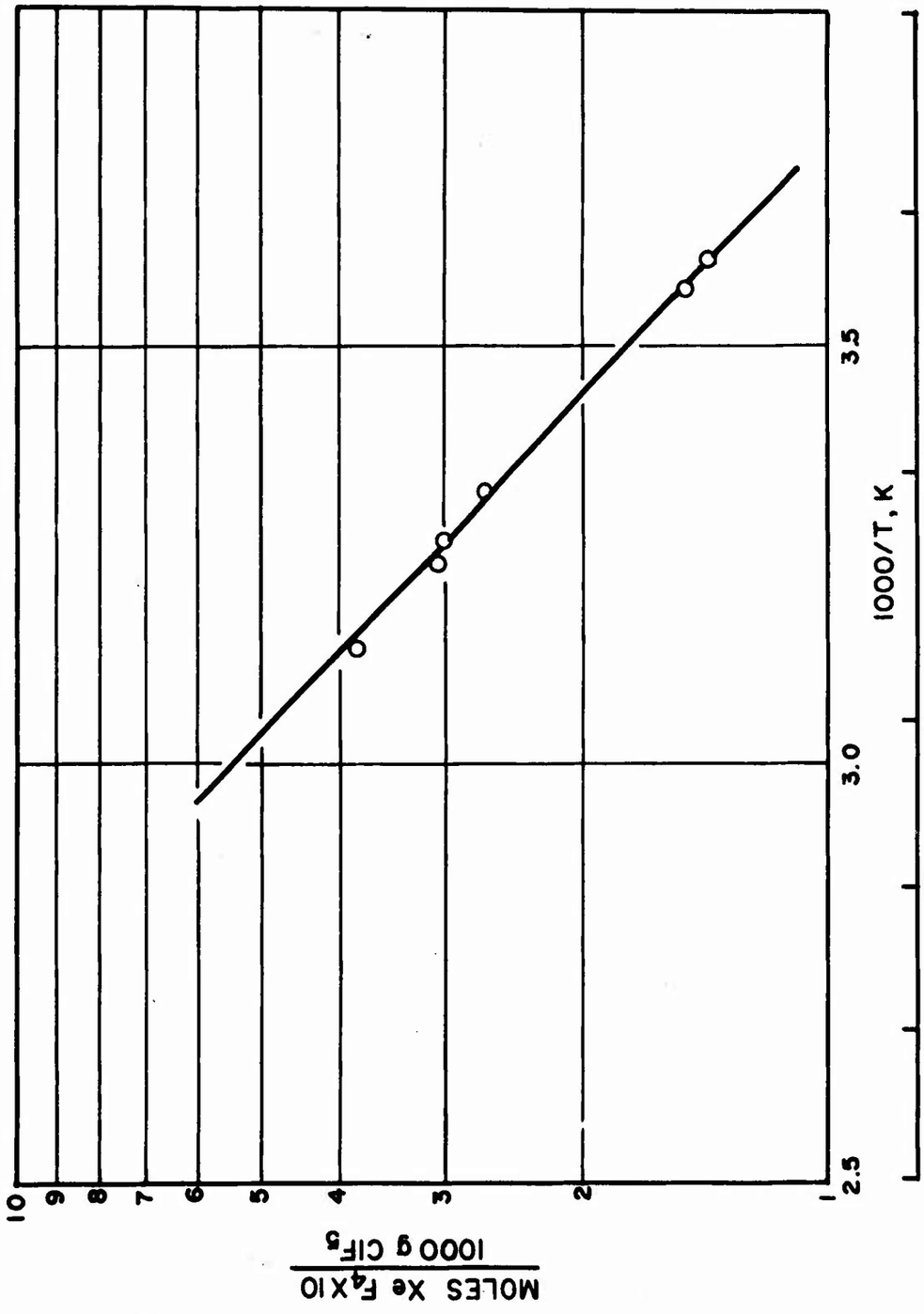


Figure 16. Solubility of XeF_4 in ClF_5

The solubility of XeF_6 in ClF_5 was also investigated because of the possibility that XeF_2 and XeF_6 would be compatible and more soluble in ClF_5. Solubility measurements of XeF_2, XeF_4, and XeF_6 in anhydrous HF show XeF_2 and XeF_6 to have 30 to 50 times greater solubility in HF than XeF_4 (Ref. 3). Solubility data for XeF_2 in ClF_5 are summarized in Table 7 and Fig. 17. Some scatter may be noted in Fig. 17 but additional efforts to redefine some of the data points were thought to be unjustified in view of the low solubilities observed. An estimate of the differential heat of solutions from the line drawn in Fig. 17 gave 4.2 kcal/mole. For comparative purposes, 2.5 kcal/mole has been reported for the heat of solution of XeF_2 in anhydrous HF (Ref. 3).

The solubility of XeF_2 in ClF_5 is approximately twice that of XeF_4, but is still too small to take advantage of the increase in density impulse which the xenon fluorides could provide as described in the theoretical section. Further experiments to measure the solubility of XeF_6 in ClF_5 were not undertaken because of the low solubilities of XeF_2 and XeF_4 in ClF_5.

TABLE 7

SOLUBILITY OF XeF_2 IN ClF_5

Temperature, C	Solubility, moles/1000 g ClF_5	Solubility, grams/100 g ClF_5
0.1	0.285	4.82
6.8	0.335	4.68
16.1	0.372	6.30
21.3	0.382	6.47
33.6	0.548	9.27
41.2	0.784	13.27

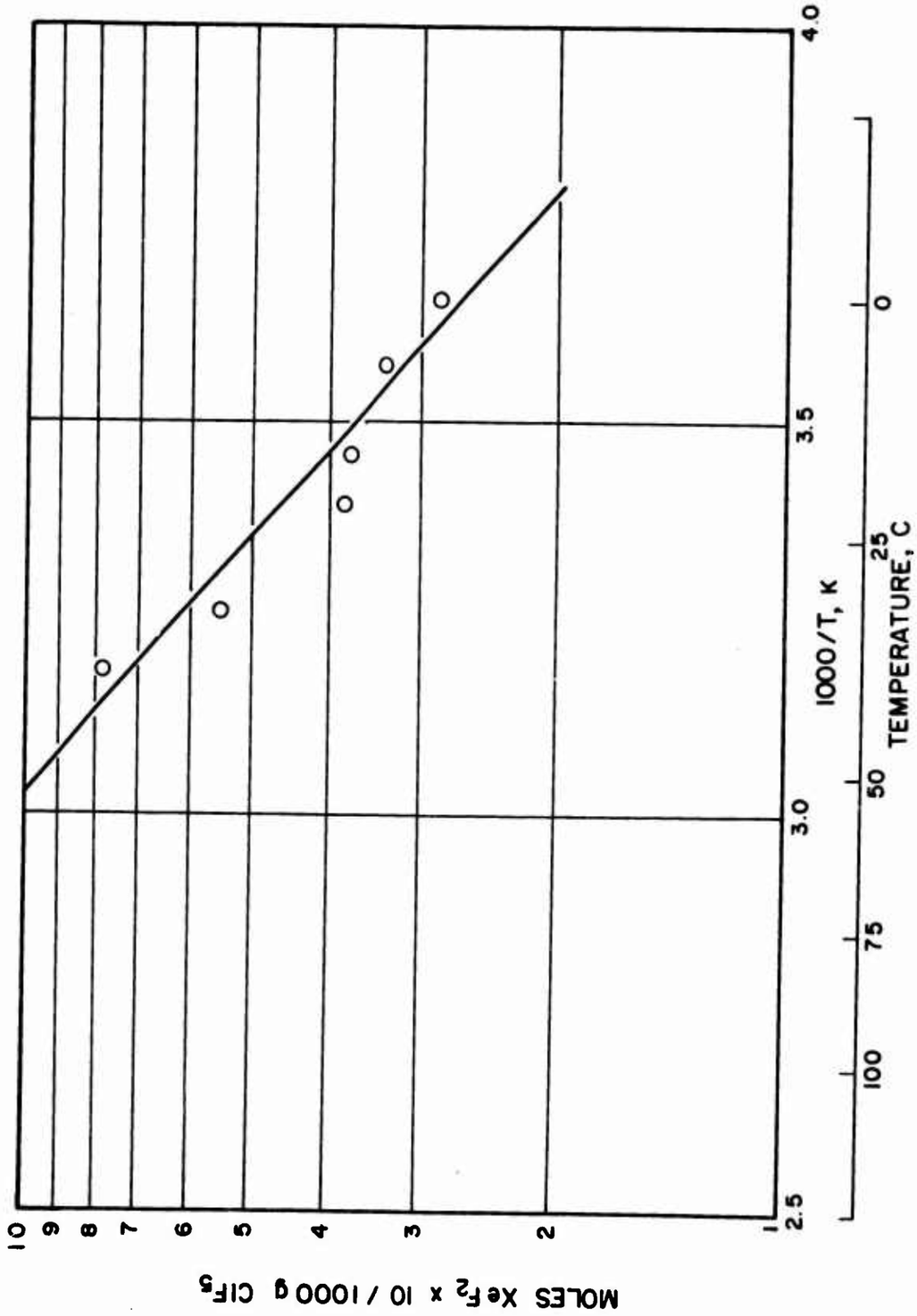


Figure 17. Solubility of XeF_2 in ClF_5

COMPATIBILITY STUDIES

A test period of 5 days or 120 hours was standardized for all compatibility tests.

Compatibility studies were carried out on binary and ternary mixtures of $C(NF_2)_4$ with ClF_5, N_2F_4, and $C(NO_2)_4$ as part of the feasibility demonstration to use $C(NF_2)_4$ as a higher-performance replacement for $FC(NF_2)_3$ in formulated oxidizer mixtures. The ternary system ClF_5-$C(NF_2)_4$-$C(NO_2)_4$ caused some concern until the cause of the slight decomposition observed was traced to faulty valves on the containers. The ternary system N_2F_4-$C(NO_2)_4$-$C(NF_2)_4$ was found to be compatible, while the ClF_5-N_2F_4-$C(NF_2)_4$ system was not investigated because of the unresolved incompatibility of the ClF_5-N_2F_4 binary, which is a component of this mixture. Further investigation of the ClF_5 reaction with N_2F_4 was initiated to gain additional evidence that would suggest a possible mechanism for the reaction and perhaps some means for inhibition of the reaction.

ClF_5-$C(NF_2)_4$ System

The binary mixture 84.6 w/o ClF_5 in $C(NF_2)_4$ was previously reported to be compatible for 24 hours at 71 C in Type 304 stainless-steel containers (Ref. 1). Two additional mixtures were tested during this report period at 71 C for the standardized test period of 5 days. Mixtures of 79.6 and 78.4 w/o ClF_5 in $C(NF_2)_4$, held in nickel containers with Hastelloy-C valves, remained unchanged after the heating period. Infrared spectra of the mixture showed the presence of only the pure starting components. Nickel bombs were used during this study because bombs of stainless steel were not available.

$C(NO_2)_4$-$C(NF_2)_4$ System

The compatibility of the $C(NO_2)_4$-$C(NF_2)_4$ mixture was examined in Type 304 stainless steel at 71 C. Two mixtures of 35.0 and 36.3 w/o $C(NF_2)_4$ in $C(NO_2)_4$ were recovered unchanged after being heated for 5 days.

N_2F_4-$C(NF_2)_4$ System

Mixtures of 29.8 and 31.6 w/o $C(NF_2)_4$ in N_2F_4 were heated for 5 days at 71 C. One of the mixtures was in a nickel container while the other was in a Monel container. Again the choice of the use of these containers was a matter of convenience and does not reflect a test on the effects of metals. Both mixtures remained unchanged as only the two components were recovered from the containers. No other compounds were observed.

N_2F_4-$C(NO_2)_4$-$C(NF_2)_4$ System

The compatibility of the ternary system N_2F_4-$C(NO_2)_4$-$C(NF_2)_4$ was examined in Type 304 stainless steel at 71 C. The $C(NO_2)_4$-$C(NF_2)_4$ binary mixtures, previously tested, were converted to the ternary mixture by the addition of N_2F_4. The mixtures 42.7-36.5-20.8 and 41.7-20.4-37.9 w/o N_2F_4-$C(NO_2)_4$-$C(NF_2)_4$ both remained unchanged after 5 days of heating. No other compounds were observed in the infrared spectra of the mixture.

ClF_5-$C(NF_2)_4$-$C(NO_2)_4$ System

The compatibility of the ternary system ClF_5-$C(NF_2)_4$-$C(NO_2)_4$ was examined in Type 304 stainless steel at 71 C. Two mixtures, 68.5-5.7-25.8 and 68.9-7.5-23.6 w/o ClF_5-$C(NF_2)_4$-$C(NO_2)_4$, remained unchanged after 5 days of heating. No other compounds were observed in the infrared spectra of the mixtures. Two other mixtures of approximately the same composition were found to have suffered slight decomposition, as small amounts of ClF_3, NF_3, CF_4, and $FClO_2$ were detected. However, the containers for both these mixtures were found to have defective valves, which could have been the source of oxygenated impurities that initiated the reaction.

$NF_3O/C(NO_2)_4$ System

Compatibility tests on 41.8 and 54.0 w/o NF_3O in $C(NO_2)_4$ mixtures were carried out at 160 F for 120 hours in Type 304 stainless-steel containers. No incompatibility was found because the components were recovered unchanged.

$C(NF_2)_4$-N_2O_4 System

The compatibility of the $C(NF_2)_4$-N_2O_4 mixture was examined in Type 304 stainless steel at 71 C. The mixture 11.0 w/o $C(NF_2)_4$ in N_2O_4 was recovered unchanged after being heated for 120 hours.

NF_3O-N_2O_4 System

Four mixtures of NF_3O-N_2O_4, approximately 50/50 w/o, were tested at 71 C for 120 hours. Three were tested in Type 304 stainless steel and the end products were NOF, NO_2F, N_2, and unused N_2O_4; there was no NF_3O recovered. The fourth test was conducted in a nickel bomb with a Monel valve and the end products included some NF_3O as well as the previously mentioned products. For control purposes, tests were conducted with just NF_3O alone in both Type 304 stainless steel and Monel. In neither case was decomposition observed after 120 hours at 71 C.

FNO_2-N_2O_4 System

Compatibility testing of the FNO_2-N_2O_4 mixture was initiated in Type 304 stainless-steel and nickel containers which had been previously passivated with ClF_5 and with FNO_2. A 20 w/o FNO_2 mixture in N_2O_4 held in Type 304 stainless steel showed slight reaction after 120 hours at 71 C. The reaction products, FNO and noncondensable gases, are believed to have

arisen from the reaction of the mixture with the container walls. A control test of FNO_2 alone under the same conditions also resulted in small amounts of noncondensable gases as well as N_2O_4. The reaction found for the FNO_2-N_2O_4 mixture is believed to be caused by incomplete passivation of the container surface and not by incompatibility of FNO_2 with N_2O_4. The tests conducted in the nickel container produced the same results for both a FNO_2-N_2O_4 mixture and a FNO_2 control. These results indicated that FNO_2-N_2O_4 mixtures are compatible if the container has been completely passivated.

NF_3O-H_2O_2 System

A brief investigation was conducted of the compatibility of the binary system NF_3O-H_2O_2. A 10-milliliter aluminum cylinder/aluminum valve container was employed which had been cleaned successively with trichloroethylene, diluted nitric acid, and distilled water. It was filled with 30-percent H_2O_2 and left standing at ambient temperature for 4 hours and then was filled with 92-percent H_2O_2 and left for 3 additional hours before being employed. Two tests were conducted using 92-percent H_2O_2 and NF_3O. The mixtures were 67/33 and 50/50 m/o and were held at 71 C for 66 and 20 hours, respectively. In both cases, the products were mainly noncondensable gases and a trace of N_2O_4 and NF_3O. After the second test, the container was opened and found to be heavily coated with a white solid which slowly gave off brown fumes of N_2O_4. An attempt to determine the solubility of NF_3O in 92-percent H_2O_2, based on Henry's Law Principle, was unsuccessful.

ClF_5-N_2F_4 System

Four additional static compatibility tests were conducted on the ClF_5-N_2F_4 binary mixture. Two mixtures were checked for ambient temperature stability. One mixture, 46.2 m/o ClF_5-53.8 m/o N_2F_4, was placed in a Type 304 stainless-steel container with a Type 304 stainless-steel valve; and the other,

47.5 m/o ClF_5-52.5 m/o N_2F_4, was placed in a nickel bomb with a Monel valve. No reaction was observed in either mixture after 42 days. However, after 115 days, small amounts of NF_3 and ClF_3 were detected. Analysis of the mixtures by gas chromatography revealed that 0.9 m/o NF_3 and 1.5 m/o NF_3 respectively, were formed in the containers. These results indicate a slow but definite reaction at ambient temperatures for the ClF_5-N_2F_4 mixture in the presence of these metals. The third mixture, completely gaseous 59.2 m/o ClF_5-40.8 m/o N_2F_4, was contained in a 175-milliliter Kel-F ampoule fitted with a "Mace" Teflon valve. The total pressure was approximately 1 atmosphere and the mixture was heated at 71 C for 5 days and then analyzed; 2.1 m/o NF_3 was found. A fourth gaseous mixture, 57.6 m/o ClF_5-42.4 m/o N_2F_4, run in the same manner as the third mixture, revealed 1.2 m/o NF_3 to have formed. The occurrence of the NF_3 product in a completely nonmetallic container strengthens the hypothesis that the ClF_5-N reaction may be at least partially homogeneous. However, earlier studi in metal containers indicated the reaction to be at least partially heterogeneous. Tests in Type 304 stainless steel to determine the stoichiometry of the reaction indicated the following:

$$ClF_5 + N_2F_4 \longrightarrow ClF_3 + 2NF_3$$

ClF_5-N_2F_4-ClF_3 System

The compatibility of the ternary system, 42.0 m/o ClF_5-49.7 m/o N_2F_4-8.3 m/o ClF_3, was examined in a Type 304 stainless-steel container at 71 C for 120 hours. Analysis at the end of the test revealed the products to be only ClF_5, N_2F_4, ClF_3, and NF_3. While no quantitative recovery of the NF_3 was made, it did appear that more NF_3 was formed than during tests of ClF_5 and N_2F_4 without ClF_3.

KINETIC STUDIES

ClF_5-N_2F_4 System

In an effort to gain a further insight into the mechanism of the ClF_5-N_2F_4 reaction, it was postulated that the reaction might proceed as follows:

$$ClF_5 \underset{}{\overset{k_1}{\rightleftharpoons}} ClF_3 + F_2 \qquad (1)$$

$$1/2\ F_2 + \cdot NF_2 \longrightarrow NF_3 \qquad (2)$$

It was found that F_2 and N_2F_4 do react at an appreciable rate at 70 C to produce NF_3. It therefore seemed appropriate to investigate the thermal decomposition of ClF_5 into ClF_3 and F_2 (Eq. 1). The velocity of this reaction would dictate whether or not Eq. 1 and 2 occur at 70 C.

An investigation of the pyrolysis of ClF_5 was conducted over the temperature range 252 to 307 C. This study utilized a 92-ml nickel stirred-flow reactor as discussed previously for Compounds T, R, and H (Ref. 1). The rate of ClF_5 disappearance was followed by measuring the change in its infrared absorption spectrum at 12.5 microns. The concentration of ClF_5 was 30 millimeters at a helium carrier gas pressure of approximately 1 atmosphere.

A plot of $(\alpha^o-\alpha)/\alpha$ at 293 C is presented in Fig. 18

where

α^o = absorbance at 12.5 microns of ClF_5 entering the reactor

α = absorbance at 12.5 microns of ClF_5 leaving the reactor

τ = residence time in seconds

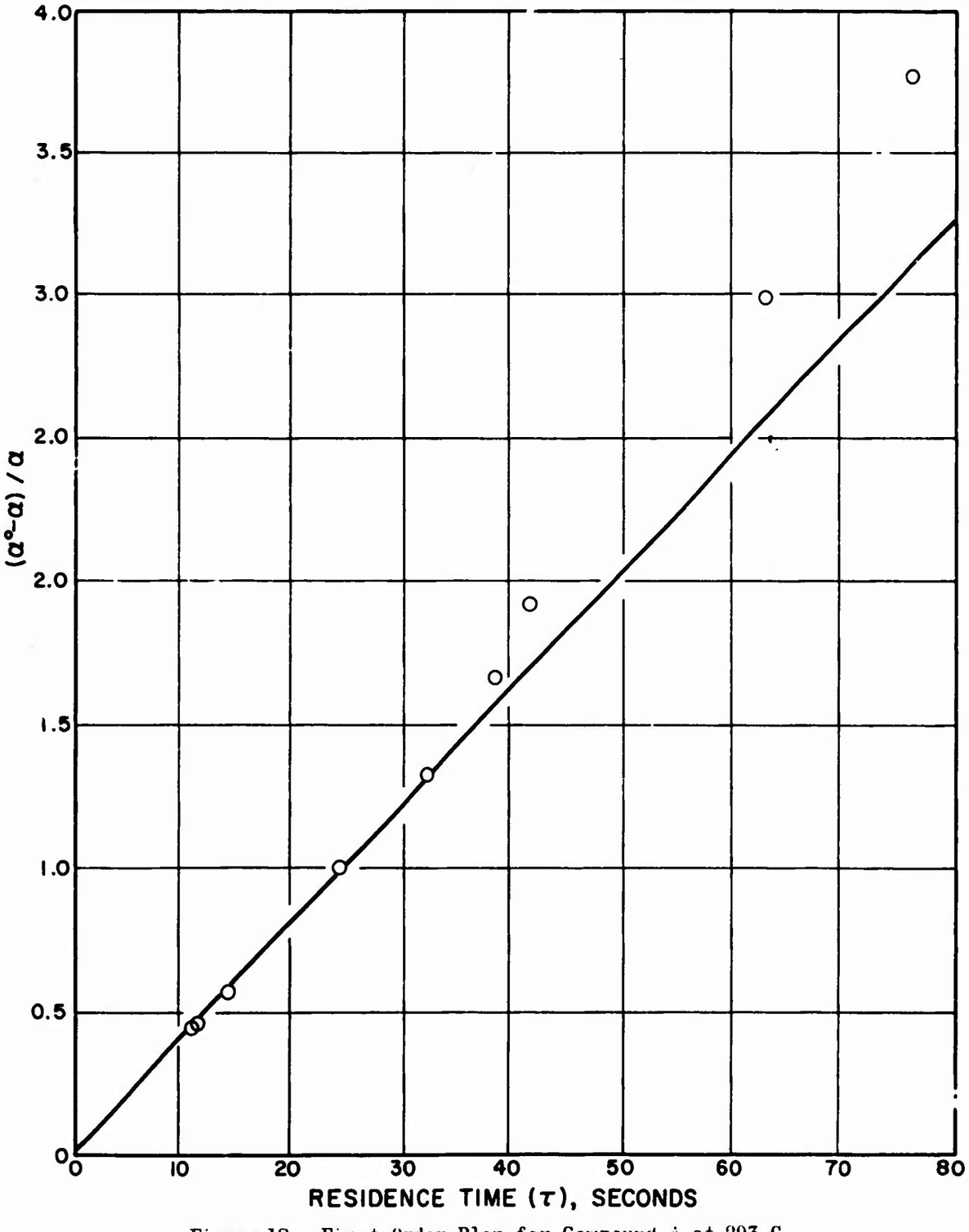


Figure 18. First-Order Plot for Compound A at 293 C

This plot should give a straight line through the origin for a first-order decomposition and the reaction follows first-order kinetics up to approximately 57-percent decomposition.

The first-order rate constants obtained over the temperature range of 252 to 307 C are presented in Table 8. These rate constants are expressed by the Arrhenius equation:

$$K_1 = 10^{15.20} \exp(-43{,}034/RT) \text{ sec}^{-1} \qquad (3)$$

Extrapolation of the data presented in Table 8, using Eq. 3, indicates that the decomposition of ClF_5 into ClF_3 and F_2 would be negligibly slow at 70 C. For example, at 70 C, the first-order rate constant for the decomposition of ClF_5 would be 10^{-12} sec^{-1}. Therefore, it appears that the proposed mechanism as outlined in Eq. 1 and 2 is not responsible for the incompatibility of ClF_5 and N_2F_4 in the gas phase, although it should also be noted that the data do not eliminate the possibility of a direct homogeneous reaction. With this in mind, the direct gas-phase reaction between ClF_5 and $\cdot NF_2$ radicals has been investigated over the temperature range of 189 to 250 C.

This investigation was hampered by the lack of a suitable analytical technique for following the simultaneous disappearance of N_2F_4 and ClF_5. The disappearance of ClF_5 was followed by measuring the change in its infrared absorption spectrum at 12.5 microns using a flow-through infrared cell. The change in N_2F_4 concentration was followed by gas chromatography. Product identification by both procedures suggests that the reaction proceeds according to the following stoichiometry:

$$ClF_5 + 2 \cdot NF_2 \longrightarrow ClF_3 + 2NF_3 \qquad (4)$$

TABLE 8

KINETIC DATA FOR THE PYROLYSIS OF ClF_5

Temperature, C	Flowrate, ml/sec	Residence Time (τ), seconds	α° *	α **	k_1, sec^{-1} ***
252.2	0.208	449	0.421	0.200	0.00246
268.5	0.[illegible]	197	0.423	0.164	0.00803
279.4	0.[illegible]2	115	0.412	0.146	0.0158
279.4	2.591	36.2		0.255	0.0170
288.0	3.36	27.9	0.368	0.176	0.0391
288.2	2.32	40.4	0.363	0.136	0.0413
287.4	3.84	24.4		0.194	0.0357
287.4	2.21	42.4		0.135	0.0398
287.6	1.70	55.0		0.103	0.0459
288.0	9.87	9.50		0.288	0.0374
291.5	3.89	24.1	0.439	0.220	0.0413
293.5	2.25	41.7		0.150	0.0462
293.3	2.91	32.4		0.189	0.0408
293.0	2.44	38.4		0.165	0.0432
293.0	1.49	62.8		0.110	0.0476
293.0	6.44	14.6		0.279	0.0394
291.8	7.86	11.9		0.302	0.0380
293.0	8.09	11.6		0.302	0.0391
294.0	1.15	81.3		0.092	0.0464
307.5	7.27	12.9	0.432	0.1800	0.109
307.5	11.79	7.96		0.245	0.0959

* α° = absorbance at 12.5 μ of unreacted mixture

** α = absorbance at 12.5 μ of reacted mixture

*** $k_1 = \frac{1}{\tau} \left(\frac{\alpha^{\circ}-\alpha}{\alpha}\right)$

If this reaction proceeds via a direct bimolecular process (this point has not been established), then the second-order rate constants, k_2, would be given by the stirred-flow equation:

$$k_2 = \frac{1}{\tau} \frac{\alpha^0 - \alpha}{\alpha B} \tag{5}$$

where

α^0 = absorbance at 12.5 microns of ClF_5 entering the reactor

α = absorbance at 12.5 microns of ClF_5 leaving the reactor

B = concentration of NF_2 radicals in the reactor at steady state

τ = residence time in seconds

The kinetic data derived by this procedure are presented in Table 8. The second-order rate constants can be expressed by the equation.

$$k_2 = 10^{12.20} \exp(-25{,}760/RT) \cdot \frac{\text{liter}}{\text{mole sec}} \tag{6}$$

where

$$\frac{d(ClF_5)}{dt} = -k_2(ClF_5)(\cdot NF_2) \tag{7}$$

Although the rate constants obtained from Eq. 5 are fairly consistent, Table 8 indicates some rather high deviations in the moles of $\cdot NF_2$ reacting per mole of ClF_5 consumed. The ratio $\Delta \cdot NF_2 / \Delta ClF_5$ should be 2.0 in all cases. Although there are several outstanding discrepancies (Table 9), the average value is 1.9.

If Eq. 6 does express the temperature dependence of the second-order rate constants, then extrapolation to 71 C gives $k_2 = 6.7 \times 10^{-5}$ liter/mole sec. Thus, the half-life for a mixture containing 1 atmosphere of N_2F_4 and 1 atmosphere of ClF_5 would be approximately 225 days. These results would

suggest that ClF_5 and N_2F_4 may be inherently incompatible at 71 C. However, it should be emphasized that the reaction may be heterogeneous. For this reason, further experiments were conducted.

Rate in Tubular Reactor

Using an improved gas chromatographic technique (discussed below), the reaction of gaseous ClF_5 and NF_2 radicals was investigated further in a Monel tubular reactor which has a surface-to-volume ratio eight times that of the previously used stirred-flow reactor. The results are presented in Table 10. At 200 C, the rate of reaction in the tubular reactor was found to be approximately 25 times greater than in the stirred-flow reactor. Again, the measured stoichiometry showed considerable variation, but in this case most of the experiments indicated 3 moles of NF_2 reacted per mole of ClF_5. Furthermore, gas chromatographic analysis showed the presence of two unidentified components in addition to the usual species NF_3, ClF_3, N_2F_4, and ClF_5. If one of the unidentified species was ClF (gas chromatographic data indicated that this hypothesis was reasonable), it would indicate that the ClF_3 may be partially reacting with N_2F_4 under these conditions and this would be in agreement with the observed stoichiometry.

The preceding results suggest that the gaseous reaction between N_2F_4 and ClF_5 is not of a simple nature, but probably involves both homogeneous and heterogeneous components, and also secondary reactions after the initial rate-determining process.

Relationship of Kinetic Results to Storage Stability

The objective of the kinetic study was to obtain rate data from which the maximum rate of a direct homogeneous reaction between N_2F_4 and Compound A at 71 C could be estimated. If it could be shown that the homogeneous reaction was slow, further studies to find ways of reducing reaction at the container wall would be warranted.

TABLE 10

REACTION BETWEEN ClF_5 AND NF_2 RADICALS

Temperature, C	τ, seconds	$ClF_5^0 \times 10^5$, $\frac{\text{mole}}{\text{liter}}$	$ClF_5 \times 10^5$, $\frac{\text{mole}}{\text{liter}}$	$NF_2^0 \times 10^5$, $\frac{\text{mole}}{\text{liter}}$	$NF_2 \times 10^5$, $\frac{\text{mole}}{\text{liter}}$	$\frac{\Delta NF_2}{\Delta ClF_5}$	k_2, $\frac{\text{liter}}{\text{mole sec}}$
198	8.63	25.5	9.01	114.0	64.6	2.99	145
(Tubular Reactor)	5.36	37.9	24.6	86.5	47.0	2.97	122
	7.87	24.0	7.87	117.3	76.1	2.55	192
	6.27	38.1	22.0	86.0	39.6	2.88	132
	5.48	36.4	20.7	89.6	44.8	2.86	121
207	160	36.5	29.0	82.8	56.7	3.48	2.85
(Stirred-Flow Reactor)	208	34.6	23.8	82.1	50.0	2.98	4.36

At the elevated temperatures and pressures employed during the gas-phase study, all of the N_2F_4 was dissociated into NF_2 radicals. Because a heterogeneous reaction was observed, the slowest rate data (obtained in the stirred-flow reactor) were used to estimate a maximum rate of homogeneous reaction between Compound A and NF_2, although this is probably greater than the actual maximum rate.

If it is assumed that the rate constant of the reaction between Compound A and NF_2 radicals is the same in solution as in the gas phase, the following calculations can be made. The second-order rate constant at 25 C is 2×10^{-7} l/mole-sec. The concentration of NF_2 radicals in liquid N_2F_4 at 25 C has been reported (Ref. 4) as 1.2×10^{-7} moles/liter.

These data give a predicted reaction rate at 25 C of 1 mole percent per month. However, at 71 C the concentration of radicals is increased by a factor of 8.5 and the rate constant is increased by a factor of 310. Therefore, if the reaction which is occurring has an activation on the order of 35 kcal/mole, the difference in rate between 25 and 71 C should be a factor of approximately 3000.

The available data indicate that there is a marked effect of temperature on the rate of the liquid phase reaction but it does not appear to be this large. No kinetic data have been obtained on the possible homogeneous reaction between N_2F_4 molecules and Compound A, because the N_2F_4 dissociates in the gas-phase reactor. It is expected, however, that this reaction would also have an appreciable activation energy. It can be seen that establishing the activation energy of the liquid-phase reaction would give an indication whether the observed reaction during storage is homogeneous or heterogeneous.

Improved Analytical Technique

Considerable effort has been devoted to developing a new gas chromatographic column system to separate ClF_5 and ClF_3. The standby "Gel Column,"

50-percent Halocarbon Oil 11-14, which is the low viscosity distillation fraction of low molecular weight polymers of chlorotrifluoroethylene, proved successful in the separation of ClF_5 and ClF_3. A 22-foot, 1/4-inch-diameter column of 50-percent Halocarbon Oil 11-A on Kel-F (30 to 40 mesh) gave sufficient separation for quantitative measurements.

EXPERIMENTAL

VAPOR PRESSURE STUDIES

The low-volume vapor pressure apparatus (Ref. 1) was used to study the binary systems, N_2F_4-$C(NF_2)_4$, ClF_5-$C(NF_2)_4$, NF_3O-N_2O_4, as well as the ternary system N_2F_4-$C(NF_2)_4$-$C(NO_2)_4$. Calibration and loading of the apparatus was carried out essentially in the manner previously reported (Ref. 1). The total amount of mixture used in the N_2F_4-$C(NF_2)_4$ and ClF_5-$C(NF_2)_4$ systems was approximately 100 mmoles, while in the ternary system the total mixture was approximately 55 mmoles. The N_2F_4 was research grade material (99.9-percent purity) purchased from Air Products and Chemical Corporation. The $C(NF_2)_4$ was provided by the American Cyanamid Company in accordance with Advanced Research Projects Agency (ARPA) and Air Force instructions. The $C(NF_2)_4$ was fractionally distilled before use to remove $FC(NF_2)_3$ and noncondensable gases which were found in the delivered product. The ClF_5 was manufactured at Rocketdyne, and was fractionally distilled to remove traces of chlorine. The NF_3O was provided by the Allied Chemical Corporation in accordance with ARPA and Air Force instructions and showed purity of better than 99.9 percent. The N_2O_4 and $C(NO_2)_4$ were standard reagent chemicals. The purity of all the compounds was checked by infrared analysis and all but the $C(NO_2)_4$ were further checked by vapor pressure measurements.

The liquid compositions were determined with the computer program which was developed to calculate the molar distribution of the constituents between the vapor and liquid phases (Ref. 1). The empirical correction factor, C, where PV = CnRT, determined earlier (Ref. 1), for nonideal behavior of N_2F_4 vapor at 71.0 C, was employed.

COMPATIBILITY STUDIES

The compatibility studies were carried out in 10-milliliter cylinders of the metals mentioned. The $C(NF_2)_4$ and ClF_5 were purified by fractional

distillation to remove the impurities noted previously in the vapor pressure section. The N_2F_4 and $C(NO_2)_4$ (Hummel Chemical Company) were used without further purification. The NF_3O and FNO_2 were fractionally distilled to remove any impurities, especially N_2O_4. The $C(NO_2)_4$ was measured by weighing, and the $C(NF_2)_4$, ClF_5, N_2F_4, NF_3O, and FNO_2 were measured by gas volumes. Heating at 71 C was carried out in a Fisher Isotemp Oven (Junior Model).

SOLUBILITY OF XeF_4 AND XeF_2 IN ClF_5

Xenon tetrafluoride was prepared according to the procedure of H. H. Claassen, John G. Malm, and H. Selig with slight modification (Ref. 5). Xenon (1200 cc) and fluorine (3000 cc) were introduced into a 200-cc Monel bomb. This was heated for 2 hours at 450 C and cooled to -196 C, and the unreacted fluorine was removed by pumping. No unreacted xenon was recovered. Purity of the XeF_4 was ascertained by infrared spectrophotometric methods. No absorptions as a result of XeF_2 were detected.

The solubility of XeF_4 in ClF_5 was determined visually by use of a Kel-F ampoule approximately 3/8-inch OD by 8 inches long. The Kel-F ampoule was connected to a Hoke 328 valve through AN fittings. A 6-inch-long, thin iron rod coated with shrinkable Teflon tubing was placed inside the Kel-F ampoule to allow stirring by use of a solenoid placed around the ampoule. The XeF_4 was loaded into the ampoule in a dry box and weighed.

The ClF_5 was measured out volumetrically in a vacuum line and condensed into the ampoule. The temperature at which the last crystal disappeared was then observed. Repeated freezing and thawing of the same sample did not affect the observed temperature. Heating of the ampoule was carried out with a water bath, and the temperature was measured with a copper-constantan thermocouple. After the solubility measurements were completed, the XeF_4 and ClF_5 were separated, and their purity was checked by their infrared spectra. No changes as a result of reaction were found.

Xenon difluoride was prepared by both glow discharge and ultraviolet irradiation methods. Passage of a 1:1 Xe:F_2 gas mixture through a glow discharge gave a fairly rapid method for preparing XeF_2 in better than 99 percent purity (Ref. 6). A simpler but slower method of preparing XeF_2 is the irradiation of a 1:1 Xe:F_2 gas mixture in a Pyrex bulb by a Hanovia ultraviolet lamp (Ref. 7). After 3 days of irradiation, large crystals of XeF_2 were deposited on the sides of the bulb. The XeF_2 was sublimed out of the bulb after removal of the unreacted Xe and F_2. The XeF_2 was analyzed by reaction with Hg and recovery of the Xe liberated, which gave a purity of better than 99 percent.

The solubility of XeF_2 in ClF_5 was measured in the same manner as was XeF_4. After the solubility measurements were completed, the XeF_2 and ClF_5 were separated and analyzed. No changes were found as a result of reaction.

CONCLUSIONS

The ternary systems considered in the theoretical section of the previous program, (Ref. 1) as well as those proposed in the theoretical section of this Task are summarized in Table 11. The theoretical performance calculations indicate that these seven homogeneous oxidizer mixtures will yield 315-second specific impulse or better with fuels noted in Table 11. Theoretical and experimental data for both vapor pressure and freezing points have established ranges of mixtures for each system that meet the requirements of not exceeding 500 psig at 160 F and a single-phase liquid at -65 F. In systems IV, V, and VI it is estimated that there are mixtures in each system that will meet the freezing point requirement with the desired performance and vapor pressure. These theoretical estimates are based on experience obtained in measuring freezing point ranges of the other ternary systems.

All seven systems listed in Table 11 have been eliminated from further consideration based on either compatibility or shock-sensitivity problems. Systems III, VI, and VII containing both N_2F_4 and ClF_5 were eliminated because of the apparent inherent incompatibility of N_2F_4 and ClF_5. Based on sensitivity studies, subsequently discussed in detail in Tasks 3 and 4, systems IV, V and VI containing $C(NF_2)_4$ are too shock sensitive to be used. In systems I and II, the high percentage of $FC(NF_2)_3$ (47 to 55 percent), required to meet the 315-second specific impulse, eliminates these two oxidizer mixtures because of the shock sensitivity of $FC(NF_2)_3$.

The three binary oxidizer systems proposed for use with the heterogeneous fuel R-2 were all eliminated from further consideration. Both the NF_3O-N_2O_4 and NF_3O-H_2O_2 binary systems were found to be incompatible. The FNO_2-N_2O_4 system showed a theoretical lowering of the combustion temperature upon raising the percentage of FNO_2 in the mixture.

TABLE 11

SUMMARY OF HOMOGENEOUS TERNARY OXIDIZER MIXTURES

System	Oxidizer Mixtures Which Meet 315-Second Performance Requirement[a]	Fuel	Reason for Elimination[b]
I	$FC(NF_2)_3$ $-N_2F_4$ $-C(NO_2)_4$	N_2H_4 B_5H_9	Useful compositions too shock sensitive
II	$FC(NF_2)_3$ $-ClF_5$ $-C(NO_2)_4$	B_5H_9	Useful compositions too shock sensitive
III	$FC(NF_2)_3$ $-N_2F_4$ $-ClF_5$	N_2H_4 B_5H_9	N_2F_4-ClF_5 incompatibility
IV[c]	$C(NF_2)_4$ $-ClF_5$ $-C(NO_2)_4$	N_2H_4 B_5H_9	Useful compositions too shock sensitive
V[c]	$C(NF_2)_4$ $-N_2F_4$ $-C(NO_2)_4$	N_2H_4 B_5H_9	Useful compositions too shock sensitive
VI[c]	$C(NF_2)_4$ $-N_2F_4$ $-ClF_5$	MMH N_2H_4 B_5H_9	Useful compositions too shock sensitive; N_2F_4-ClF_5 incompatibility
VII	ClF_5 $-N_2F_4$ $-C(NO_2)_4$	N_2H_4 B_5H_9	N_2F_4-ClF_5 incompatibility

(a) Vapor pressure: 500 psig at 160 F, single-phase liquid at -65 F

(b) Based on either compatibility or sensitivity or both

(c) It is theoretically probable that the freezing point requirement can be obtained in these systems although no freezing points were experimentally obtained on mixtures containing $C(NF_2)_4$.

Kinetic studies on the gaseous N_2F_4-ClF_5 mixture suggest that the reaction is not of a simple nature, but probably involves both homogeneous and heterogeneous components, and may also involve secondary reactions after the initial rate-determining process. In view of these studies, further effort on the ClF_5-N_2F_4 reaction was suspended and there is little hope for inhibition of the reaction. A modified "Gel" gas chromatographic column has been developed to separate ClF_5 from ClF_3.

Theoretical performance calculations on the use of xenon fluorides as oxidizer ingredients showed them to have promise in yielding high-density impulse propellants. However, solubility studies of XeF_2 and XeF_4, in ClF_5 show the solubilities to be too small to take advantage of the increased density impulse these xenon fluorides would provide to the ClF_5-N_2H_4 propellant system.

TASK 2: DESENSITIZATION OF OXIDIZERS

INTRODUCTION

The high-energy CNF oxidizers, Compounds R and T, are unusable as propellants because of their detonation sensitivity. The objectives of this area of study were to: (1) determine the kinetics and mechanisms for the gas-phase decomposition of Compounds R and T, (2) correlate the rate and mechanism results with detonation sensitivity, and (3) propose additives or other methods that will desensitize these compounds.

Under the previous contract, AF04(611)-9380, the rates of pyrolysis of compounds T, R, and H were studied in some detail (Ref. 1). The thermal stabilities of these oxidizers, studied over the temperature range of 190 to 460 C, were found to decrease markedly in the order H > R > T. This is precisely the order of increasing detonation sensitivity for this series.

It should not be inferred however, that thermal stability is the only parameter which governs the detonation sensitivity in this series of compounds. The sensitivities undoubtedly are dependent also on the heats of pyrolysis, and on the thermal conductivities and heat capacities of the products and intermediates formed.

All experimental evidence obtained in the previous study indicates that the decomposition of these species proceeds via a nonchain, radical mechanism (Ref. 1); and that the initial and rate-determining step under the conditions studied is, in each case, the rupture of a C-N bond to give an $\cdot NF_2$ radical. Following the initial C-N bond rupture, the mechanisms of the subsequent reactions leading to the observed products and intermediates are less certain. The importance of the observed intermediates in the formation of the stable products had not been established at the start of this contract period, i.e., whether the products are formed by a direct path or result from decomposition of

the principal intermediates (PFG and PFF arising from compounds T and R, respectively). It was apparent that an independent investigation of the pyrolyses of these C-N double-bond-containing intermediates was required for an understanding of the pyrolysis mechanisms of Compounds T and R and of the relationship of these mechanisms to detonation sensitivity.

Results obtained under the previous contract (Ref. 1) have shown that the maximum observed concentrations of the principal intermediates are strongly temperature dependent. These results are presented in Fig. 19. The concentrations are greater at the hig'er temperatures, and the percent reactions at which the maxima occur are greater at the higher temperatures. The similarity of the results obtained with the two oxidizers is interesting considering they were obtained over quite different temperature ranges. The results presented in Fig. 19 suggest that, at even higher temperatures, it might be possible to convert more of the oxidizer to the principal intermediate as the mixture passes through the reactor.

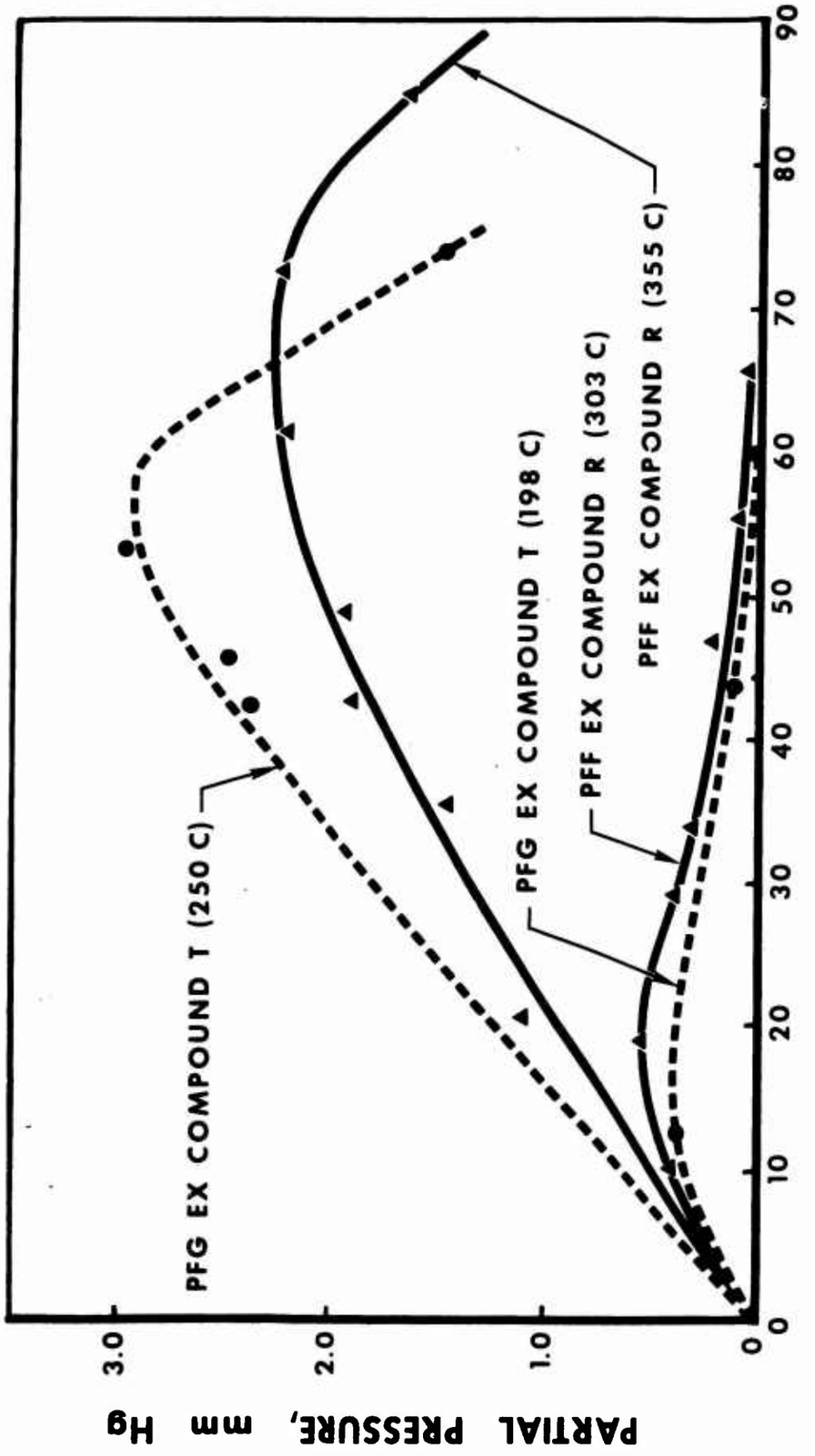


Figure 19. Influence of Temperature on Principal Intermediates (Initial Partial Pressure of Oxidizer 11.4 mm Hg)

DISCUSSION AND RESULTS

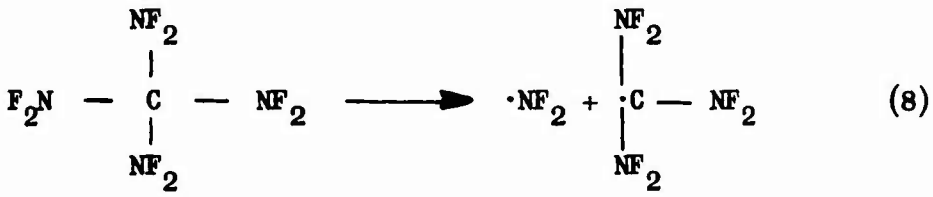
PYROLYSIS OF COMPOUND T AT ELEVATED TEMPERATURES

For reasons discussed in the previous paragraph, it appeared of interest to investigate the pyrolysis of Compound T at much higher temperatures than those obtainable with this compound in the 90-milliliter stirred-flow reactor. For this purpose, a tubular reactor of 2.4-milliliter volume was constructed from 1/8-inch copper tubing. This small reactor permitted the attainment of very short residence times and, therefore, much higher temperatures.

The results of a series of experiments conducted at 340 C and residence times ranging from 7 to 190 milliseconds are presented in Fig. 20. Compound T is seen to be more than 99 percent decomposed at residence times greater than approximately 50 milliseconds. The principal products under these conditions are PFG, NF_3, and N_2F_4. The concentration of PFG reaches approximately 85 percent of the initial Compound T concentration and then begins to decompose slowly at longer residence times.

It would appear from Fig. 20 that the species present at the second highest concentration is NF_3. It should be noted, however, that N_2F_4 is completely dissociated into NF_2 radicals at this temperature and partial pressure. Thus, the concentrations of NF_2 radicals in the reactor are actually greater than those of NF_3. Lower concentrations of PFF, PFM, CF_3NF_2, CF_4, and N_2 also are formed.

The experimental results presented in Fig. 20 give very strong evidence that the pyrolysis of Compound T occurs via the cleavage of a C-N bond:



(8)

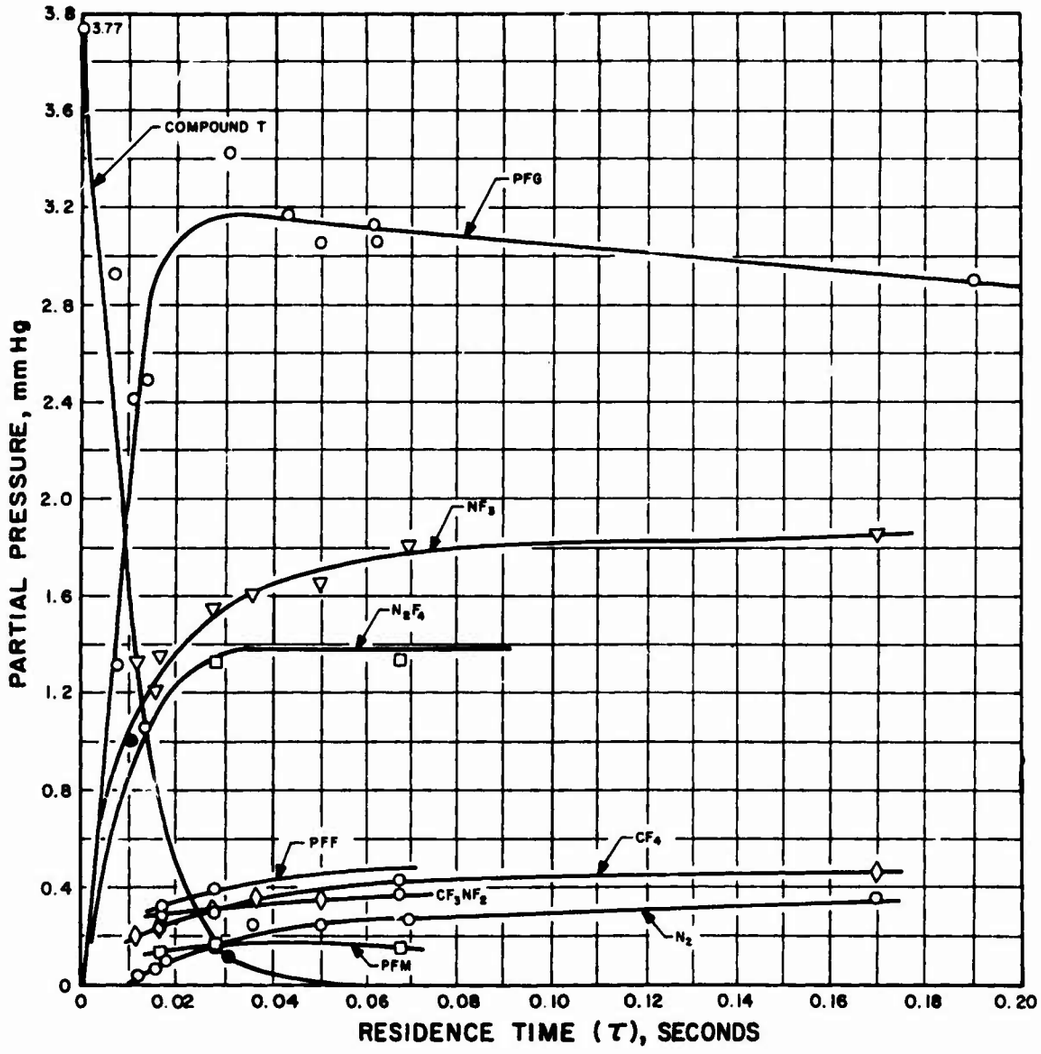
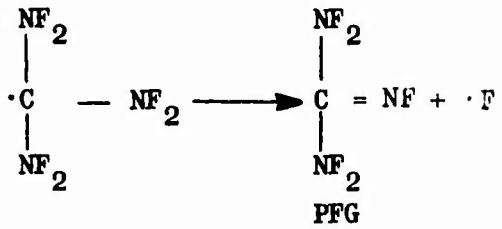
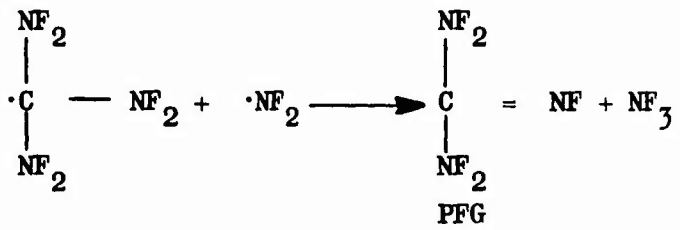


Figure 20. Thermal Decomposition of Compound T at 340 C

followed by the first or both of the following processes:

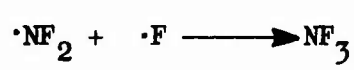


(9)



(10)

The fact that the concentration of NF_3 is not equal to that of PFG indicates that Reaction 10 is not the predominant process. Reaction 9 is apparently so rapid that no other competing process can occur. Much of the NF_3 may form by reaction of NF_2 radicals with fluorine atoms generated in Reaction 9.



(11)

PYROLYSIS OF PFG

The data presented in Fig. 20 indicate that PFG is indeed a true reaction intermediate in the pyrolysis of Compound T. That is, all of the Compound T is converted to PFG which, in turn, decomposes (or reacts) to form the observed stable products and other intermediates. To test this hypothesis further, an investigation of the pyrolysis of a sample of PFG was undertaken.

Kinetics of PFG Pyrolysis

Preliminary analyses by gas chromatography showed the sample of PFG to be low purity (approximately 79 percent PFG; Appendix A). The rate of thermal decomposition of the "as received" PFG was investigated over the temperature range of 210 to 324 C in a Monel stirred-flow reactor that had been used previously, in a new Monel stirred-flow reactor, and in a Monel tubular reactor. The results shown are presented in Table 12 Here, the results are presented as first-order rate constants for later comparison. It is recognized that the pyrolysis of PFG is definitely not first order under these conditions. However, because the initial PFG concentrations were about the same during each experiment, this should give a qualitative comparison of the reaction rates and activation energies. Table 13 shows that the data at 235 C are best correlated by assuming half-order kinetics. In this table, the rate constants are calculated for zero-, half-, first-, and second-order reactions. However, all of the pyrolysis data did not give as good a half-order f. and the results, in general, were quite erratic and nonreproducible.

Figure 21 shows a plot of log k vs 1/T for the apparent first-order rate constants for the thermal decomposition of PFG. The previously obtained Arrhenius plot for Compound T (Ref.1) is included for comparison. These results indicate that the decomposition of PFG proceeds with a much lower activation energy than that of Compound T. The apparent first-order rate constant for PFG obtained from Fig. 21 is

$$k_1 = 10^{3.5} \exp(-12,560/RT) \text{ sec}^{-1} \qquad (12)$$

The low activation energy and the scatter of the results suggest that the decomposition of PFG is predominantly heterogeneous. However, Table 12 and Fig. 21 show that the rate constants obtained using a 60-milliliter, tubular Monel reactor are slightly lower than those obtained using the 90-milliliter, stirred-flow reactors even though the surface-to-volume ratio of the former is eight times that of the latter.

TABLE 12

APPARENT FIRST-ORDER RATE CONSTANTS
FOR THE PYROLYSIS OF PFG

Temperature, C	τ, seconds	Initial Partial Pressure PFG, mm Hg	A^{**}_{ave}, cm^2	A, cm^2	k_1, $^{**}sec^{-1}$	k_1 ave, sec^{-1}
235.8	8.79	8.8	279	150	0.0979	0.0738
236.2	13.6			136	0.0775	
236.4	13.7			150	.0626	
236.4	14.0			155	.0574	
210.5	141.4	8.8	265	71	.0193	0.0122
210.5	36.3			195	0.00990	
210.5	36.4			198	0.00929	
210.7	67.3			155	.0105	
225.0	17.7	8.8	269	219	0.0129	0.0148
225.5	24.2			200	0.0143	
225.5	44.3			153	0.0171	
235.4	12.8	8.8	290	232	0.0195	0.0231
235.6	15.2			220	0.0209	
234.2	19.0			215	0.0184	
234.2	19.1			214	0.0186	
234.8	19.2			209	0.0202	
235.0	25.4			192	0.0201	

*A = Chromatogram peak area

$^{**}k_1 = \frac{1}{\tau}\left(\frac{A^{\circ} - A}{A}\right)$

TABLE 12
(Continued)

Temperature, C	τ, seconds	Initial Partial Pressure PFG, mm Hg	A°_{ave}, cm^2	A, cm^2	k_1, sec^{-1}	k_1 ave, sec^{-1}
235.8	48.9	8.8	290	128	0.0259	0.0231
235.2	51.6			126	0.0252	
235.2	71.6			93	0.0296	
235.8	77.0			83	0.0324	
253.5	5.12	8.8	272	250	0.0172	0.0252
253.5	15.6			195	0.0253	
254.0	24.2			162	0.0281	
254.2	22.8			169	0.0270	
254.5	23.0			164	0.0286	
276.2	7.56	8.8	268	217	0.0311	0.0374
276.8	17.2			156	0.0418	
277.0	15.7			166	0.0392	
302.4	5.01	8.8	268	208	0.0575	0.0654
302.6	6.70			187	0.0647	
303.0	6.76			182	0.0699	
303.0	6.80			182	0.0695	
309.6	11.1	8.8	263	139	0.0821	0.0849
309.6	10.9			138	0.0828	

TABLE 12

(Continued)

Temperature, C	τ, seconds	Initial Partial Pressure PFG, mm Hg	A°_{ave}, cm^2	A, cm^2	k_1, sec^{-1}	k_1 ave, sec^{-1}
309.8	16.8	8.8	263	105	0.0896	0.0849
310.5	5.61		268	186	0.0785	
310.7	30.1		253	62	0.102	
309.4	3.34		276	221	0.0745	
323.7	5.14	8.8	281	181	0.107	0.100
323.7	5.23			184	0.101	
323.7	5.97			178	0.0969	
		New stirred-flow reactor				
281.8	39.2	8.8	220	89	0.0376	0.0321
282.0	37.2			105	0.0294	
282.2	37.3			101	0.0316	
282.7	37.3			104	0.0299	
281.5	27.4	8.8	251	152	0.0238	0.0251
281.5	21.3			180	0.0185	
281.0	21.7			175	0.0200	
281.2	15.6			198	0.0171	
280.8	31.4			147	0.0238	
280.6	35.4			138	0.0232	

TABLE 12

(Concluded)

Temperature C	τ, seconds	Initial Partial Pressure PFG, mm Hg	A°_{ave}, cm^2	A, cm^2	k_1, sec^{-1}	$k_{1\ ave}$, sec^{-1}
280.3	55.1	8.8	251	96	0.0312	0.0251
280.3	102.3			46	0.0435	
			Tubular reactor			
281.3	5.54	8.8	256	247	0.0127	0.0162
281.4	5.56			247	0.0126	
281.4	13.6		265	217	0.0146	
281.5	21.6		285	200	0.0164	
281.5	21.8			198	0.0167	
281.5	24.8			192	0.0160	
281.5	49.5			115	0.0183	
281.5	83.3			57	0.0193	
281.5	11.2			231	0.0188	
312.5	5.74	8.8	292	250	0.0273	0.0228
312.7	8.29		290	236	0.0250	
312.8	15.81		287	188	0.0278	
312.8	19.4		285	193	0.0200	
313.0	23.2		282	186	0.0180	
312.8	66.2		279	76	0.0197	

TABLE 13

ORDER OF PFG DECOMPOSITION AT 235 C

Temperature, C	Residence Time, seconds	Percent Reaction	k_o*	$k_{1/2}$*	k_1	k_2*
235.4	12.83	20	4.52	0.297	0.0195	0.0000840
235.6	15.25	24	4.59	0.310	0.0209	0.0000950
234.2	19.00	26	3.96	0.270	0.0184	0.0000855
234.2	19.06	26	3.98	0.292	0.0186	0.0000870
234.8	19.20	28	4.22	0.278	0.0202	0.0000967
235.0	25.40	34	3.86	0.293	0.0201	0.000105
235.8	48.9	55	3.32	0.284	0.0259	0.000202
235.2	51.6	57	3.18	0.285	0.0252	0.000200
235.2	71.6	68	2.76	0.296	0.0296	0.000318
235.8	77.0	71	2.68	0.295	0.0324	0.000395

*These are not true rate constants because they include the calibration factor for converting chromatographic peak areas to concentrations. They were calculated from the stirred flow equation:

$$k_n = \frac{U}{V} \frac{A^o - A}{A^n}$$

where:

n = order of reaction
A = peak area
U = volume flowrate
V = volume of reactor

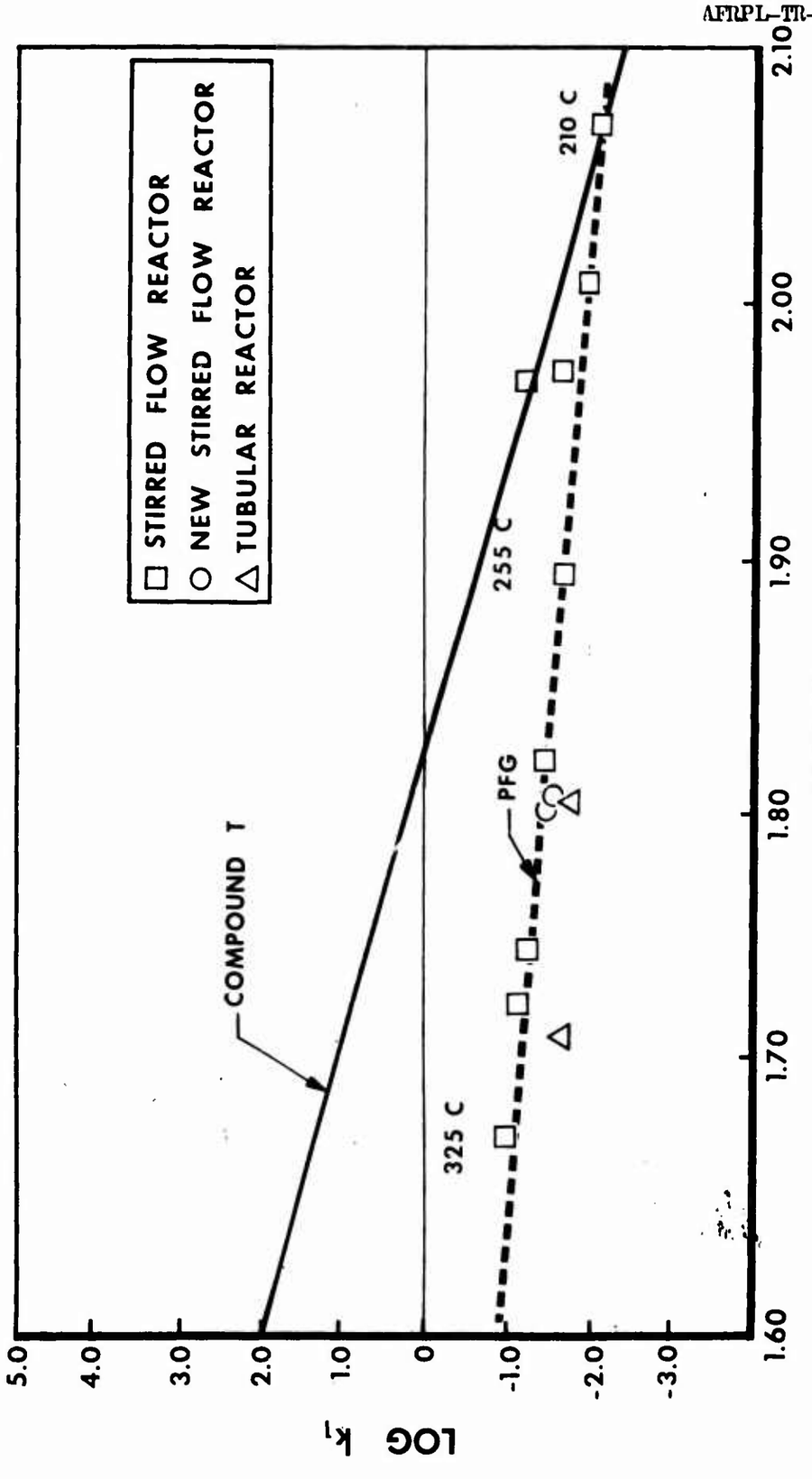


Figure 21. Thermal Stability of PFG Compared With Compound T

Further experiments using a similar Monel, stirred-flow reactor that had been subjected to a prolonged passivation with Compound A and N_2F_4 gave results which were more amenable to first-order kinetics, the first-order rate constants for PFG pyrolysis being approximately an order-of-magnitude lower than those predicted from Eq. 12. These results are presented in Table 14. These first-order rate constants are given approximately by:

$$k_1 = 10^{3.68} \exp(-15{,}100/RT) \text{ sec}^{-1} \quad (13)$$

The PFG sample used to obtain the results presented in Table 13 had a purity of approximately 79 percent (used as received), whereas the sample used to obtain the data in Table 14 had been partially purified (to 91 percent purity) by the procedure described in Appendix A. It is, therefore, possible that the large difference in observed rate was the result of changing the purity of the sample rather than of changing to another reactor (i.e., two parameters were changed at once). Experiments were then conducted with the lower purity material in the well-passivated, stirred-flow reactor to resolve this point. The results are given in Table 15. Interestingly, the lower purity sample gave the same first-order rate constant in this reactor as that obtained from the higher purity sample.

The conclusion that the low-temperature pyrolysis of PFG is heterogeneous is based on the observations that (1) the rates are extremely sensitive to the nature of the reactor surface, (2) low-activation energies on the order of 12 to 15 kcal/mole are obtained, and (3) the pre-exponential factor is lower than that normally obtained for a first-order homogeneous reaction. It was observed that changing the surface-to-volume ratio by a factor of approximately eight did not affect the rate of the low-temperature pyrolysis. This is consistent with the conclusion that the reaction is heterogeneous if it is assumed that the surface of the tubular reactor (eightfold greater surface) had a specific activity (per unit area) approximately equal to that of the well-passivated, stirred-flow reactor used to obtain the data in Tables 14 and 15. Coincidentally,

TABLE 14

LOW-TEMPERATURE PYROLYSIS OF 91-PERCENT PURITY PFG
IN A WELL-PASSIVATED STIRRED FLOW REACTOR

Temperature, C	τ, seconds	Initial Partial Pressure PFG, mm Hg	Final Partial Pressure PFG, mm Hg	k_1, sec^{-1}
270.0	204	16.7	8.4	0.0048
270.0	206	16.7	8.4	0.0048
287.8	77.6	16.7	12.4	0.0045
287.8	78.6	16.7	11.9	0.0051
320.5	40.5	16.7	11.6	0.0108
321.0	77.0	16.7	8.3	0.0132
321.0	26.4	16.7	12.4	0.0131
321.0	90.2	16.7	7.3	0.0144
321.2	58.0	16.7	9.8	0.0120
332.5	38.2	16.7	11.0	0.0135
332.2	39.8	16.7	10.8	0.0135
352.8	17.4	16.7	10.2	0.036
353.2	10.8	16.7	11.3	0.043
354.0	27.2	16.7	7.9	0.041
353.2	20.8	5.1	2.7	0.042
353.2	20.0	5.1	2.9	0.037

TABLE 15

LOW-TEMPERATURE PYROLYSIS OF 79-PERCENT PURITY PFG IN A WELL-PASSIVATED STIRRED FLOW REACTOR

Temperature, C	τ, seconds	Initial Partial Pressure PFG, mm Hg	Final Partial Pressure PFG, mm Hg	k_1, sec^{-1}
268.0	126	4.1	2.8	0.0037
269.5	130	4.1	2.7	0.0040

two of the reactors (the Monel, tubular reactor and the well-passivated, Monel, stirred-flow reactor) gave approximately the same specific rate, whereas the other reactors (the two Monel, stirred-flow reactors in Table 12) gave a specific rate that was approximately 10 times faster.

Even though the rates of PFG pyrolysis in the well-passivated reactor were nearly an order-of-magnitude lower than those obtained previously, the small temperature dependence of these rates suggested that the observed decomposition was still essentially heterogeneous at these low temperatures. To investigate the homogeneous mode of decomposition, it was necessary to go to higher temperatures and, consequently, to shorter residence times in the stirred-flow reactor. Under these conditions, a process (presumably homogeneous) with a much higher activation energy was found to predominate. Because the purity of the PFG sample did not appear to affect the pyrolysis rate at low temperatures (over the purity range investigated, 79 to 91 percent), the "as received" material was used in the high-temperature experiments.

The first-order rate constants obtained for the high-temperature (372 to 455 C) decomposition of PFG are given in Table 16. The first-order nature of the decomposition at 413 C is shown in Fig. 22, where a plot of $(A^\circ - A)/A$ vs τ gives a straight line which passes through the origin as predicted from stirred-flow theory. Here, A° is the initial gas chromotographic peak area for PFG entering the reactor, A is the peak area for PFG leaving the reactor, and τ is the residence time in seconds. (The percent decomposition was varied from 25 to 80 percent at 413 C.)

Figure 23 gives the Arrhenius plot for both the high- and low-temperature rate constants obtained using the well-passivated reactor (Tables 14 and 16). The data give a curved plot which becomes linear at temperatures above 400 C (approximately). Graphical analysis of the high-temperature data (> 400 C) indicates that the first-order rate constants may be expressed by the Arrhenius equation:

$$K_1 = 10^{16.80} \exp(-52{,}900/RT) \text{ sec}^{-1} \qquad (14)$$

TABLE 16

HIGH-TEMPERATURE PYROLYSIS OF 79-PERCENT PURITY PFG IN A WELL-PASSIVATED STIRRED FLOW REACTOR

Temperature, C	τ, seconds	Initial Partial Pressure PFG, mm Hg	Initial PFG, A^o, (Chromatograph Peak Area, cm^2)	Final PFG, A, (Chromatograph Peak Area, cm^2)	k_1, sec
372.0	5.43	4.6	234	145	0.113
372.2	12.04		236	108	0.0984
401.0	2.96	4.6	236	102	0.444
403.6	2.98		235	98	0.468
406.2	1.01		235	143	0.635
412.8	3.77	4.6	253	53	1.00
413.2	2.10		242	82	0.988
413.2	1.11		242	120	0.919
414.6	0.823		242	136	0.947
414.2	0.509		242	160	1.01
412.8	0.357		242	180	0.065
412.0	0.370		242	172	1.10
420.2	0.320	4.6	241	143	1.32
421.5	0.544		241	131	1.54
451.2	0.330	4.6	243	73	7.06
454.6	0.262		243	82	7.50

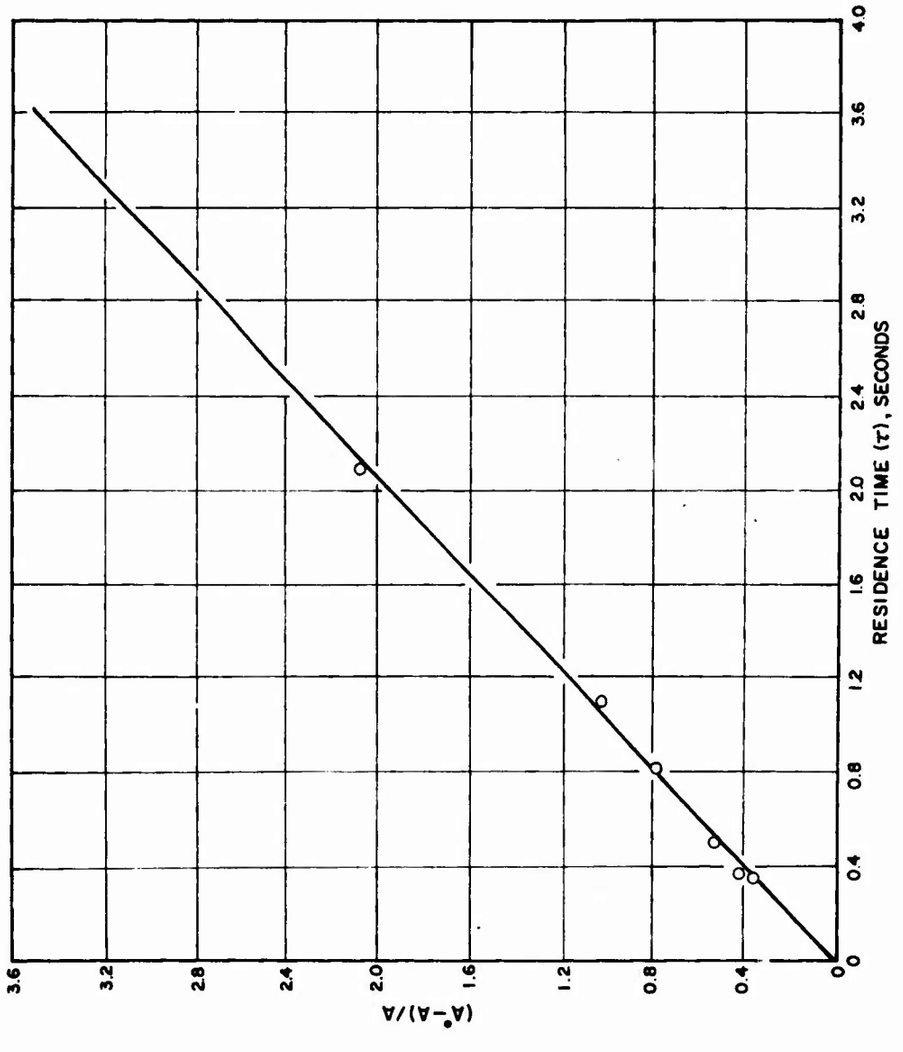


Figure 22. First-Order Plot of PFG Pyrolysis at 413 C

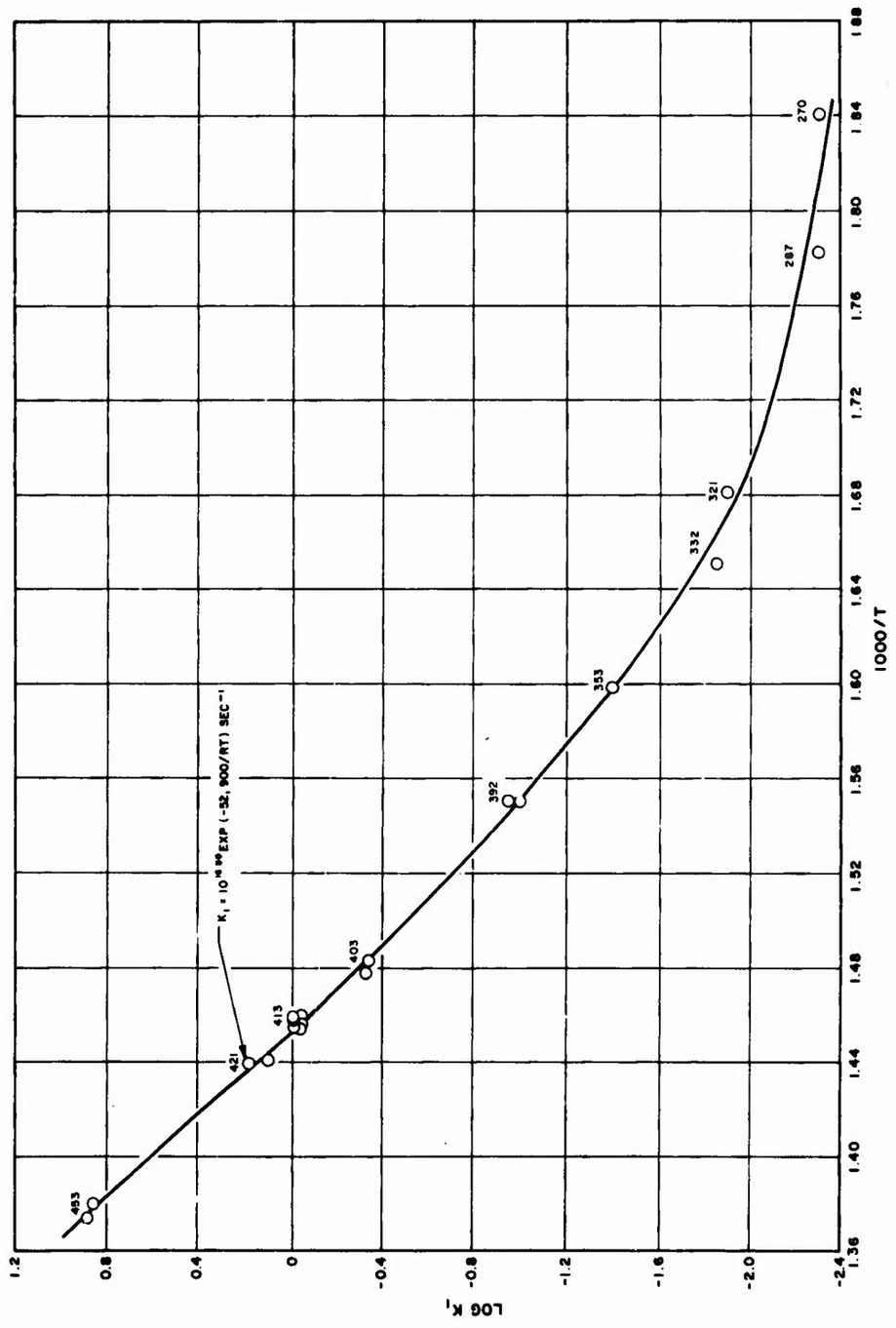


Figure 23. Arrhenius Plot for High- and Low-Temperature Pyrolysis of PFG

Figure 23 indicates that the activation energy for the low-temperature reaction may be even less than 15 kcal/mole in this reactor.

Products of PFG Pyrolysis

Products at Low Temperature. The major stable products obtained from the heterogeneous pyrolysis of PFG at 252 C in the first Monel, stirred-flow reactor are N_2 and CF_4 along with a much lower concentration of NF_3. These results are shown in Fig. 24. The low kinetic order of the PFG decomposition is illustrated by the linearity of the PFG decomposition curve. Figure 25 gives a plot of chromatogram peak area vs residence time for all of the species involved in the decomposition of PFG. It is very significant that all the products of Compound T decomposition are formed during the pyrolysis of PFG.

The product distribution from the low-temperature pyrolysis of PFG in the well-passivated reactor is similar to that obtained previously from the initial reactor. A plot of the partial pressure of the major stable products N_2, CF_4, and NF_3 as a function of residence time (τ) in the reactor at 272 C is presented in Fig. 26. A similar plot for the remaining species, N_2F_4, PFF, PFM, and CF_3NF_2, is presented in Fig. 27. The results in Fig. 27 are presented in terms of the gas chromatogram peak areas, as the calibration factors were not obtained for each species in this series of experiments.

Products at High Temperature. Figure 28 shows a plot of partial pressure vs residence time in the stirred-flow reactor for the species involved in the homogeneous decomposition of PFG at 416 C. The products of the homogeneous pyrolysis of PFG are quite similar to those of the heterogeneous pyrolysis (compare Fig. 28 with Fig 26 and 27). This suggests that a similar mechanism prevails in each case, except that the rate-determining step occurs homogeneously in one case and on the reactor surface in the other.

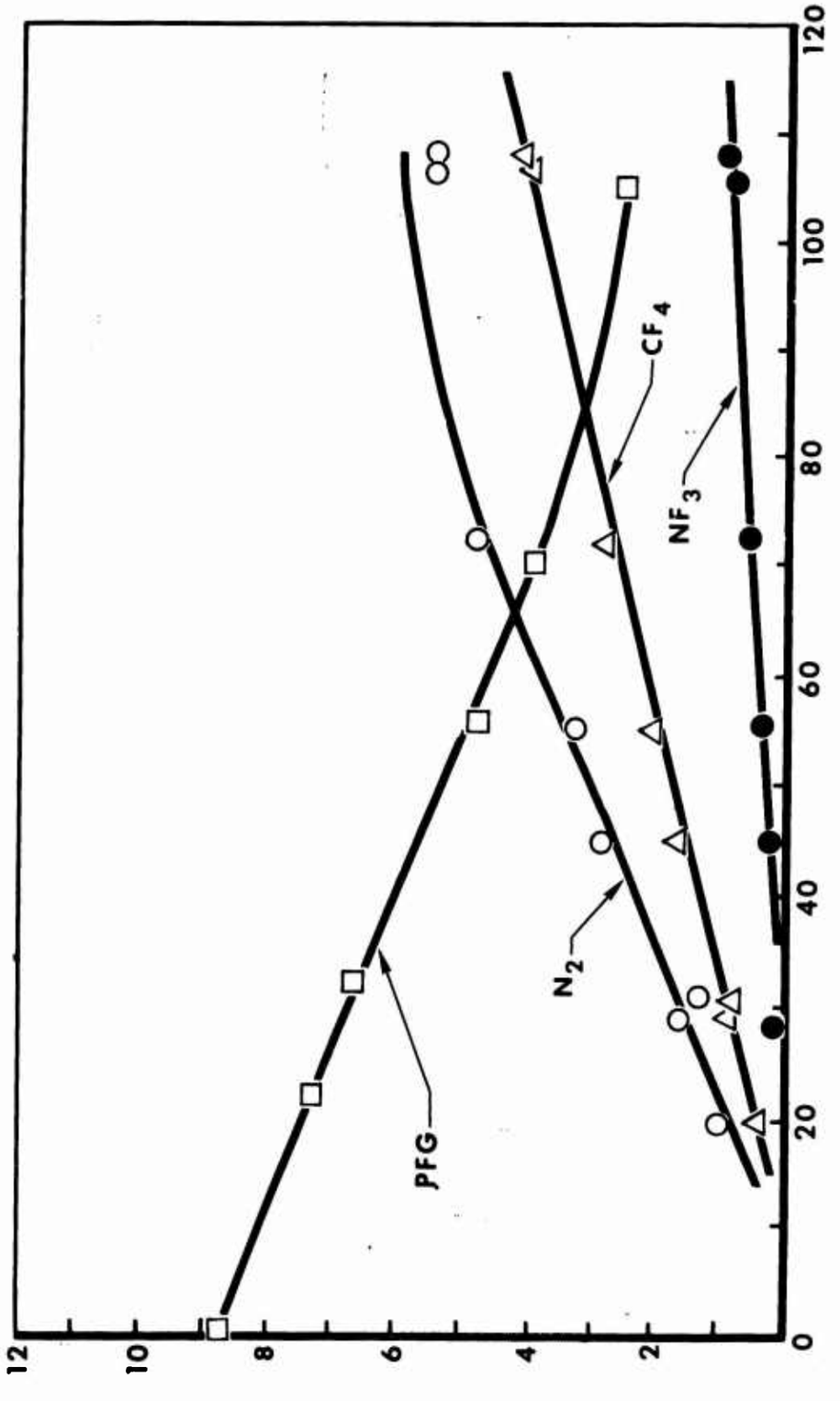


Figure 24. Products of PFG Pyrolysis at 252 C

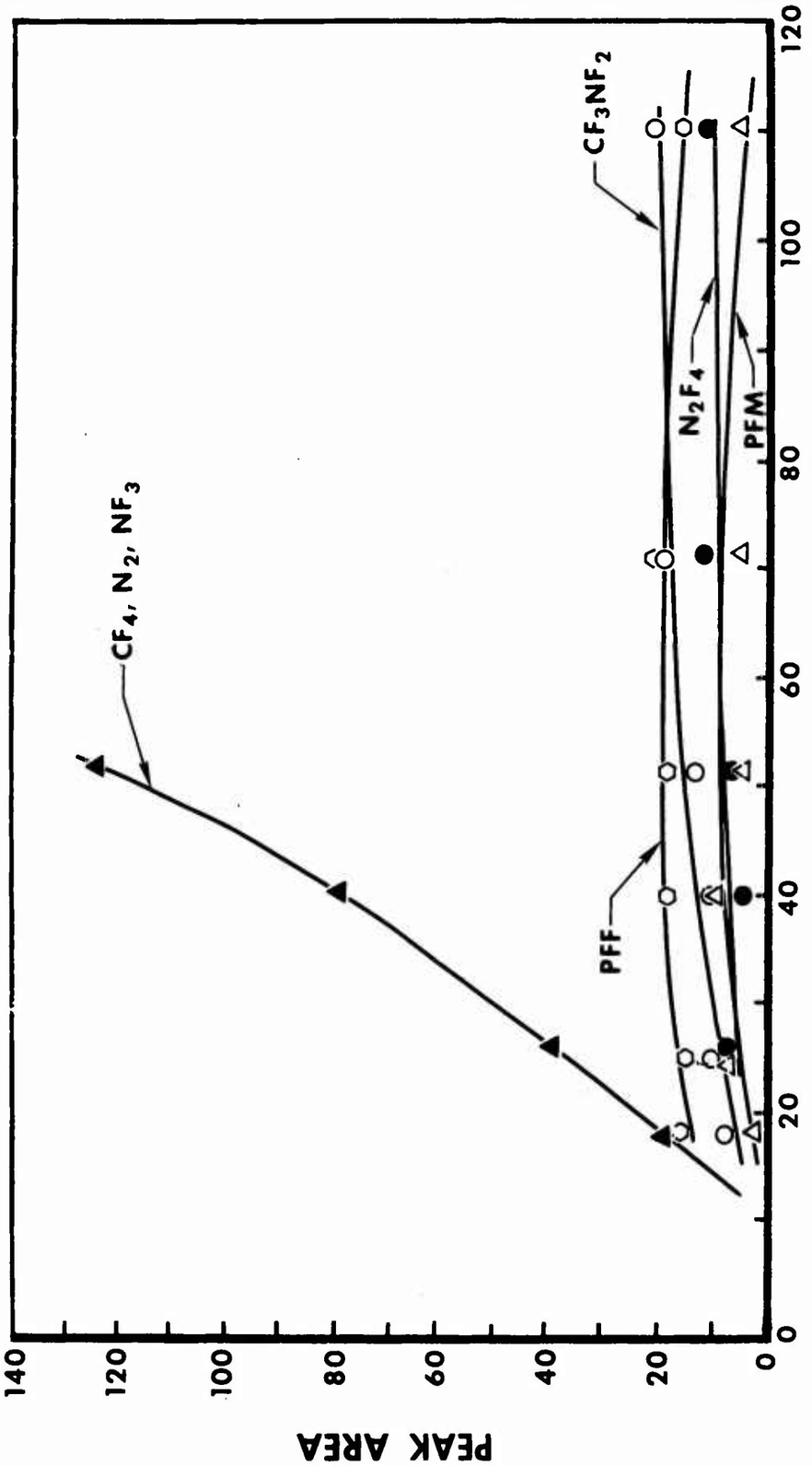


Figure 25. Products of PFG Pyrolysis at 252 C

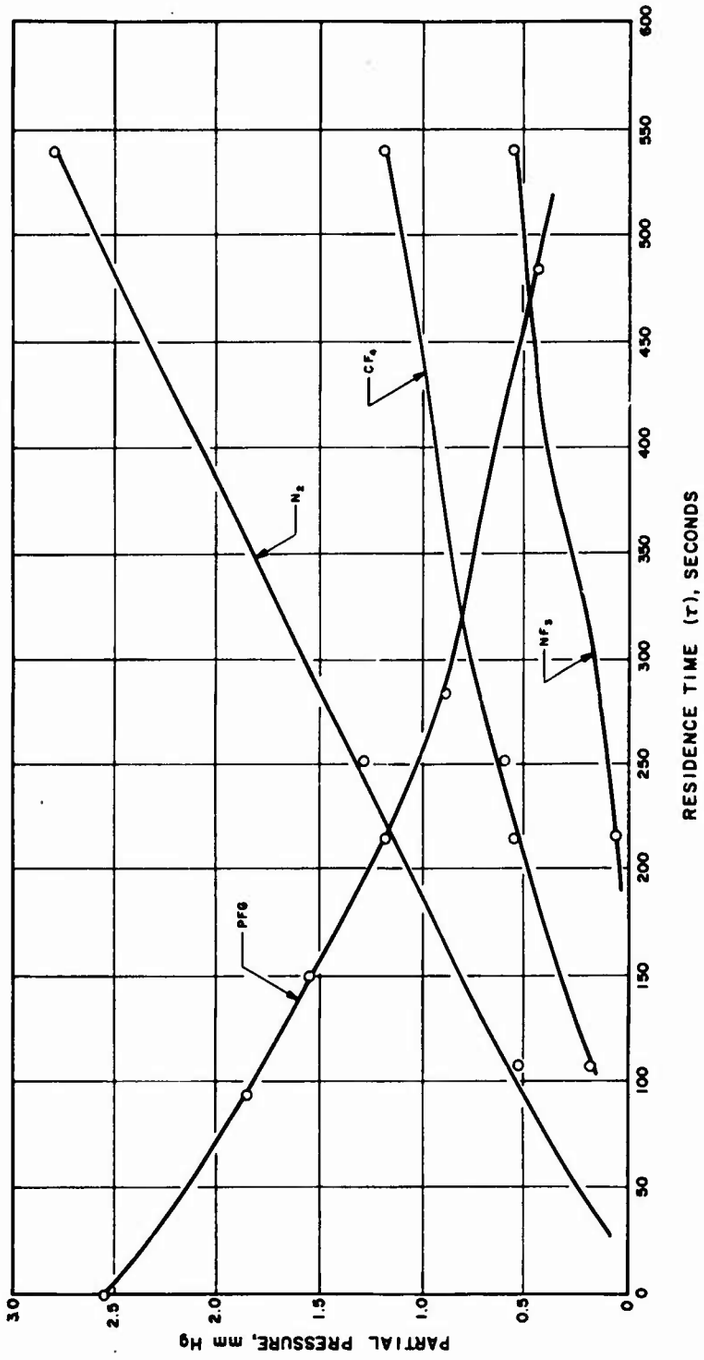


Figure 26. Products of Pyrolysis of 91-Percent Purity PFG at 272 C

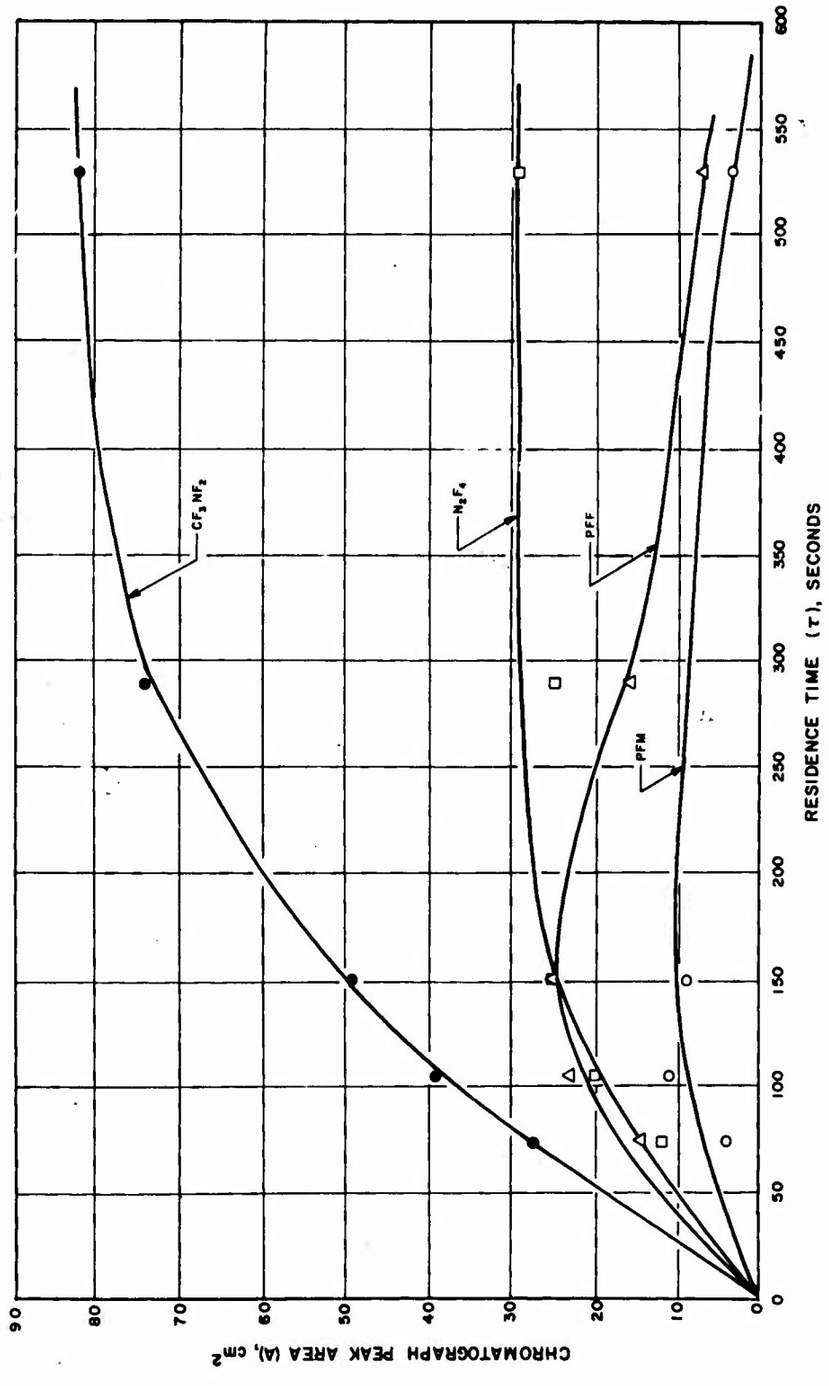


Figure 27. Products of Pyrolysis of 91-Percent Purity PFG at 272 C

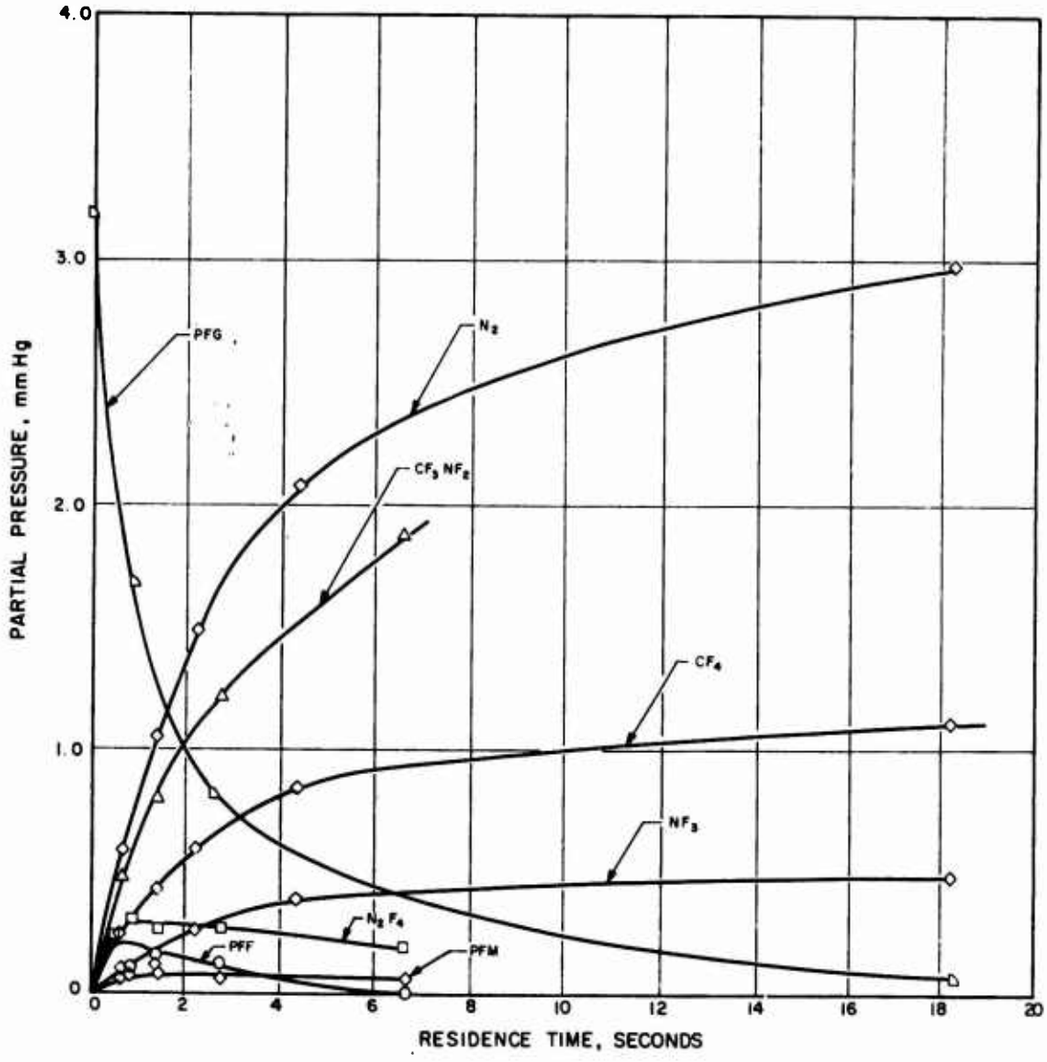


Figure 28. Product Distribution From PFG Homogeneous Pyrolysis at 416 C

The results presented thus far indicate that the decomposition of Compound T follows the steps:

$$T \longrightarrow PFG + xN_2F_4 + yNF_3 \longrightarrow \text{products} \qquad (15)$$

The reaction scheme shown in Eq. 15 requires that the products of the pyrolysis of Compound T and of the pyrolysis of PFG be the same under similar conditions, except that the Compound T should yield larger quantities of NF_3 and N_2F_4. To establish definitely that the reaction scheme in Eq. 15 is valid at higher temperatures, where the pyrolysis of PFG is homogeneous, both PFG and Compound T were decomposed under similar conditions at 528 C. The results are shown in Fig. 29 and 30. It may be seen that the products form in similar concentrations during each of these experiments, except that more NF_3 and N_2F_4 are formed from Compound T.

These experiments were conducted in a 2.4-milliliter, copper, tubular reactor which allowed the employment of much shorter residence times than the 95-milliliter, stirred-flow reactor. At this high temperature, the decomposition of Compound T was much too rapid to follow analytically. Thus, the Compound T decomposed rapidly to PFG which, in turn, decomposed to the remaining products. The much higher concentration of N_2F_4 and NF_3 obtained from Compound T are predicted from Eq. 15 (Fig. 20). The remaining species, N_2, CF_3NF_2, CF_4, PFM, and PFF, resulted from the decomposition of PFG, and were formed in similar amounts during each experiment.

Effect of Additives on PFG Pyrolysis

It was shown under the previous contract that additives did not affect the rate of pyrolysis of Compounds R and T but that they had a marked effect on the distribution of products (Ref. 1). Because PFG is apparently a true intermediate in the decomposition of Compound T, as represented by Eq. 15 (discussed in more detail in a subsequent section), the effect of additives on the rate and stoichiometry of PFG pyrolysis was studied.

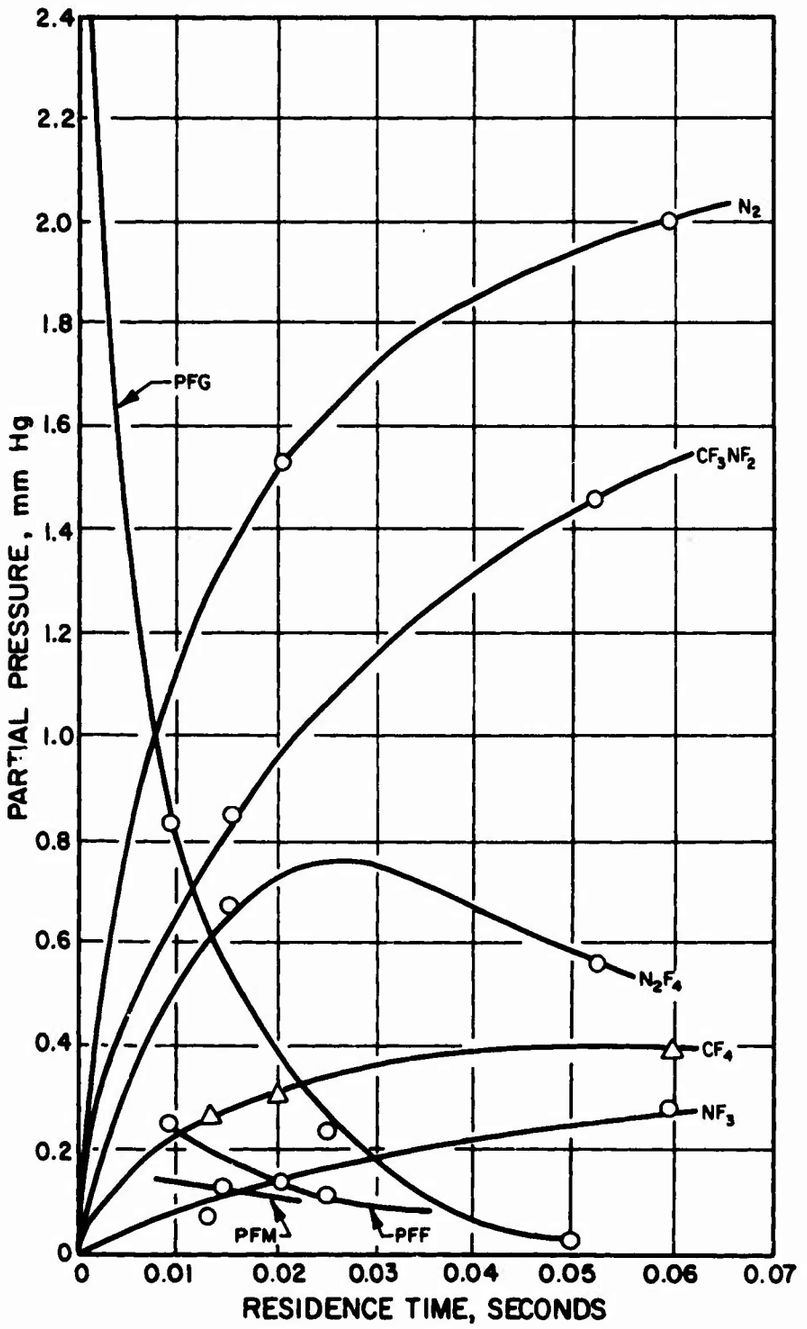


Figure 29. Pyrolysis of PFG at 528 C (initial pressure PFG = 3.08 millimeters)

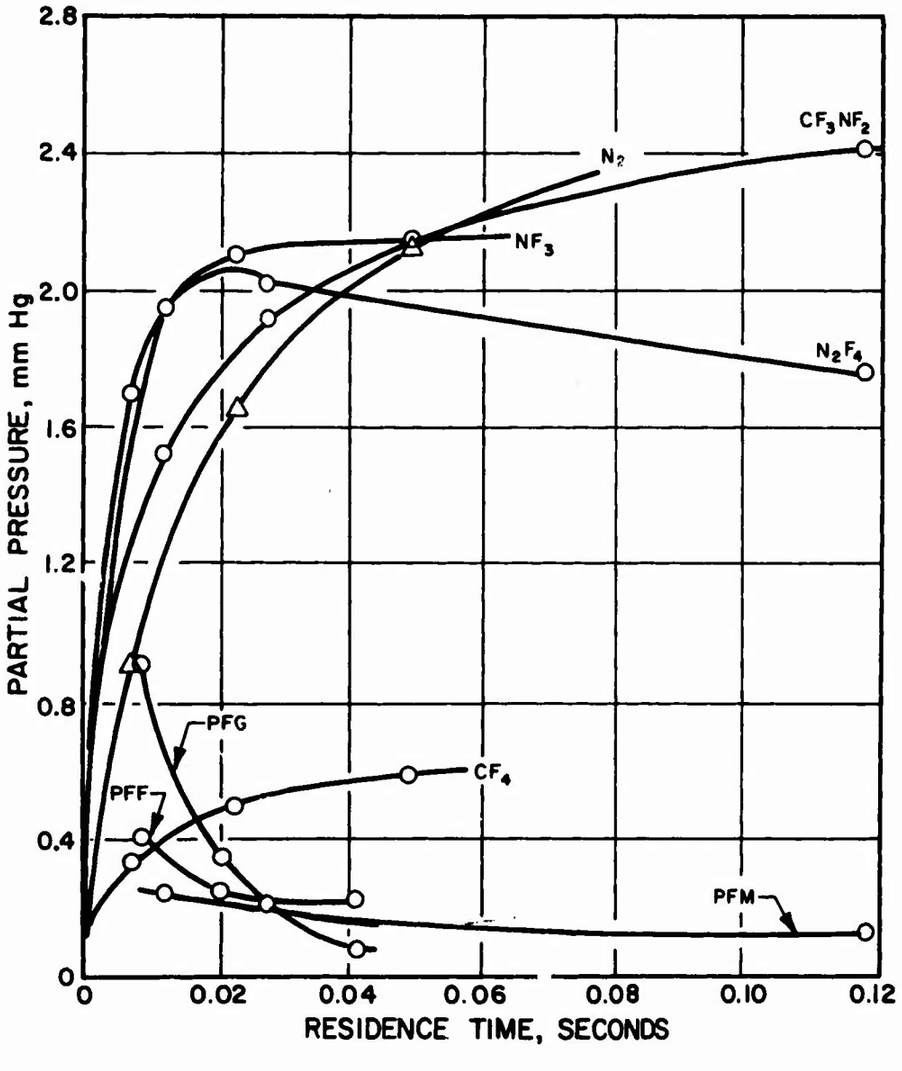


Figure 30. Pyrolysis of Compound T at 528 C (initial pressure Compound T = 3.77 millimeters)

Addition of a relatively high concentration of N_2F_4 was found to have little effect on the low-temperature (predominantly heterogeneous) rate of pyrolysis of PFG. These results are presented in Table 17. The addition of an excess of N_2F_4 (NF_2/PFG = 23.2/7.8) causes a negligible change in the first-order rate constants at 271 C. However, the addition of N_2F_4 was found to increase greatly the concentration of NF_3 formed at this temperature. For example, the addition of 26.2 mm Hg of N_2F_4 to 2.6 mm Hg of PFG, at 281 C and a residence time of 200 seconds, increased the concentration of NF_3 from 0.05 (Fig. 26) to 1.2 mm Hg. The concentration of nitrogen increased slightly, and the amount of CF_4 formed remained unchanged. During similar experiments, F_2 appeared to cause a slight increase in rate (Table 17). However, these rates may be within the range of reproducibility under these heterogeneous conditions.

In contrast to results obtained in the lower temperature region, N_2F_4 was found to reduce slightly the rate of PFG pyrolysis at 415 C (based on the result of a single experiment). This result is presented in Table 18. The addition of 9.3 mm Hg of N_2F_4 to 3.2 mm Hg PFG was found to lower the first-order rate constant by approximately 25 percent. Similar experiments indicate that the addition of smaller amounts of N_2O_4 increases the rate of PFG pyrolysis by approximately 40 percent (Table 18).

Because N_2F_4 appeared to reduce slightly the rate of PFG pyrolysis at 415 C, similar experiments were conducted at much higher concentrations of N_2F_4. Table 19 shows the results obtained on the addition of 165 mm Hg of N_2F_4 to 3.5 mm of PFG; the previously obtained effect of 9.3 mm Hg of N_2F_4 is included for comparison. Table 19 shows that the decrease in rate caused by the addition of 165 mm Hg of N_2F_4 is not appreciably different from that obtained with 9.3 mm Hg of N_2F_4. These results are not quantitative because the N_2F_4 dissociation reaction cooled the reactor and the exact temperature of the reacting gases is not known. It is apparent, however, that N_2F_4 does not appreciably inhibit the rate of PFG pyrolysis.

TABLE 17

EFFECT OF ADDITIVES UPON THE RATE OF THE LOW-TEMPERATURE PYROLYSIS OF PFG

Temperature, C	τ, seconds	Additive	Initial Partial Pressure PFG, mm Hg	Partial Pressure Additive, mm Hg	$k_1 sec^{-1}$
270.8	110.0	None	16.7	0	0.00436
270.8	112.0	None	16.7	0	0.00410
270.5	115.0	N_2F_4	7.8	11.6	0.00473
270.7	115.0	N_2F_4	7.8	11.6	0.00462
271.0	125.0	F_2	8.0	9.3	0.00536
271.0	127.0	F_2	8.0	9.3	0.00518

TABLE 18

EFFECT OF ADDITIVES UPON THE RATE OF THE HIGH-TEMPERATURE PYROLYSIS OF PFG

Temperature, C	τ, seconds	Additive	Partial Pressure of PFG, mm Hg	Partial Pressure Additive, mm Hg	k_1, sec^{-1}
415.2	1.45	None	4.6	0	0.896
415.2	0.957	None	4.6	0	0.925
415.3	0.900	N_2F_4	3.2	9.3	0.710
416.0	0.906	N_2O_4	3.2	3.6	1.30
415.5	0.923	N_2O_4	3.2	3.6	1.20

TABLE 19

EFFECT OF N_2F_4 ON THE RATE OF PYROLYSIS OF PFG

Temperature, C	Flow, $\frac{\text{milliliter}}{\text{seconds}}$	τ, seconds	Partial Pressure of PFG, mm Hg	Partial Pressure of N_2F_4, mm Hg	k_{exp}, sec^{-1}	$k_{1\,calc}$, sec^{-1}	$\frac{k_{exp}}{k_{calc}}$
415.3	104.9	0.90	3.2	9.3	0.710	1.02	0.696
404.0	83.7	1.12	3.5	160	0.382	0.538	0.710
400.8	79.4	1.19	3.5	166	0.350	0.446	0.784
398.8	75.4	1.25	3.5	166	0.288	0.389	0.740

The influence of N_2F_4 and N_2O_4 on the formation of the stable products N_2, CF_4, and NF_3 is presented in Table 20. It is shown that both N_2F_4 and N_2O_4 are effective in modifying the distribution of the stable products N_2, CF_4, and NF_3. In the case of N_2F_4, the percent reduction in CF_4 formation is approximately equal to the percent reduction in pyrolysis rate, while the N_2 appears to increase slightly even at the reduced extent of reaction. Similar to the low-temperature results, N_2F_4 was found to increase greatly the concentration of NF_3.

It is shown in Table 20 that N_2O_4 is more effective than N_2F_4 in eliminating the normal stable products (probably by reacting with radical intermediates). It was demonstrated that N_2F_4 and N_2O_4 react completely at room temperature to give FNO and FNO_2 as major products. This would account for the virtual elimination of NF_3 as a product in the presence of N_2O_4, because NF_2 radicals would react with NO_2 before they could react further to form NF_3.

RELATIONSHIP OF PFG PYROLYSIS RESULTS TO COMPOUND T DECOMPOSITION MECHANISM

The species PFG is always observed as an intermediate in the decomposition of Compound T, i.e., its concentration increases with time initially, reaches a maximum value, and then decreases. The maximum concentration of PFG varies from a few percent of the initial concentration of Compound T to more than 80 percent, depending on the temperature (Fig. 19 and 20). The question which was not resolved until the present study was undertaken was whether the PFG is a true reaction intermediate, as represented in Eq. 15, or merely an unstable side product formed by some reaction path other than that which produces the major reaction products.

The results of the present study establish rather conclusively that PFG is a true reaction intermediate and also permit the previous observations concerning the appearance of PFG in the decomposition of Compound T to be

TABLE 20

INFLUENCE OF ADDITIVES UPON THE STABLE PRODUCT FORMATION FROM PFG AT HIGH TEMPERATURE

Temperature, C	τ, seconds	Additive	Partial Pressure PFG, mm Hg	Partial Pressure Additive, mm Hg	Peak Area		
					N_2	CF_4	NF_3
413	2.35	None	3.3	0	63	33	10
	2.46	None	3.3	0	55	33	10
	2.52	N_2F_4	3.3	8.9	71	20	95
	2.56	N_2F_4	3.2	9.7	75	20	108
414	2.60	None	2.4	0	68	31	8
	2.67	None	2.4	0	59	31	9
	2.77	N_2O_4	2.4	5.9	32	1	0
	2.86	N_2O_4	2.3	6.0	29	1	0
414	2.61	None	3.6	0	67	36	10
	2.68	N_2O_4	3.6	2.6	49	16	2

explained. The results of the investigation of the products from PFG pyrolysis are certainly consistent with this conclusion because all of the products of Compound T decomposition are found in the PFG products. Moreover, the relative amounts of each product is as expected if PFG were a true intermediate. This is quite apparent from a comparison of Eq. 15 with the results shown in Fig. 29 and 30.

It must now be determined if the rate data obtained for PFG pyrolysis are consistent with the reaction scheme shown in Eq. 15. For comparison, Fig. 31 summarizes on one plot all the Arrhenius plots obtained during this study (including those from Ref. 1). The PFF results shown will be presented and discussed later in this report. It is apparent from Fig. 31 that PFG is much more stable than Compound T at elevated temperatures where the homogeneous decomposition mechanism prevails. However, at lower temperatures, the tendency for PFG to decompose heterogeneously at the reactor surface reduces its stability relative to Compound T, and at temperatures around 210 C, they have equal rate constants for decomposition (the exact temperature where this occurs will be influenced by the condition of the reactor surface).

These considerations readily explain, in qualitative terms, the PFG concentrations observed during the experiments shown in Fig. 19 and 20. At 198 C, the PFG formed as the Compound T decomposes homogeneously in the gas-phase diffuses to the reactor surface and decomposes at a rate which is rapid enough relative to its rate of formation that the PFG concentration remains small. This also explains the similarly low PFG concentrations in the Dow Chemical Company study of Compound T decomposition at 175 C (Ref. 8). At 250 C (compare Fig. 19 and 31), the PFG is sufficiently stable with respect to Compound T that it can build up to a moderate concentration. At 340 C (compare Fig. 20 and 31), the rate constant for the heterogeneous decomposition of PFG is several orders-of-magnitude smaller than that for the homogeneous decomposition of Compound T (because of the difference in activation energy). This accounts for the high yield of PFG shown in Fig. 20. Actually, these

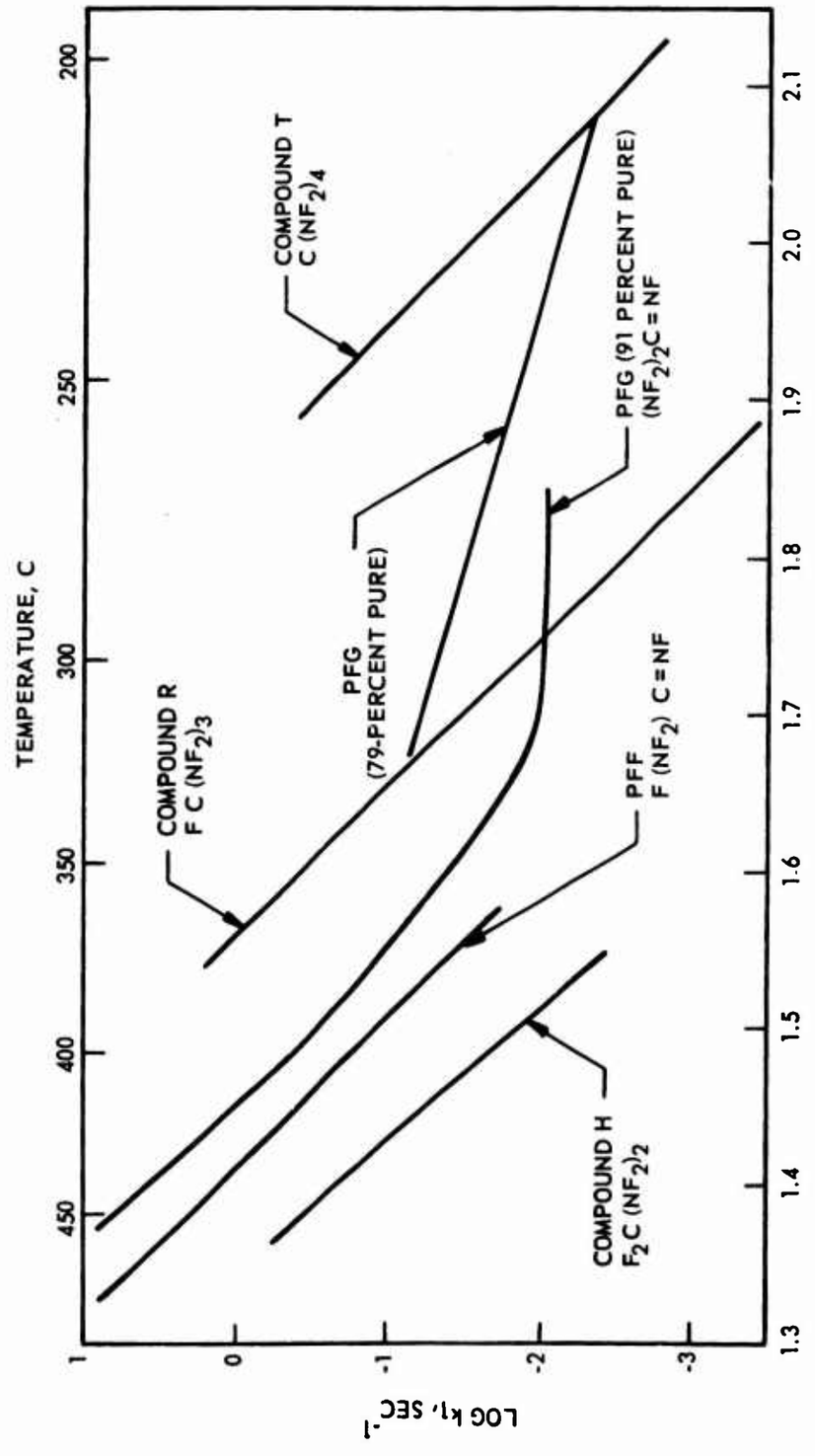


Figure 31. Comparison of Pyrolysis Rates

considerations would predict nearly a quantitative yield of PFG at 340 C rather than the 85 percent shown in Fig. 20 . This suggests that either calibration errors occurred or Compound T does not form PFG quantitatively. The latter is actually to be expected because other minor products must be formed to balance Eq. 15 , i.e., for each N_2F_4 formed, two F-atoms must react to form additional products.

The above considerations concerning the observed maximum concentration of the intermediate PFG in the decomposition of Compound T can be put on a more quantitative basis. According to Eq. 15 , the pyrolysis of Compound T is of the type:

$$A \xrightarrow{k_1} B \xrightarrow{k_2} \text{products} \qquad (16)$$

where

A = concentration of Compound T

B = concentration of PFG

If it is assumed that B decomposes by a first-order process, then for a stirred-flow reactor:

$$\frac{dB}{dt} = k_1A - k_2B - \frac{B}{\tau} = 0 \qquad (17)$$

where

τ = residence time = V/U

By differentiation of Eq. 17 , it can be shown that the residence time, τ_{max}, at which B reaches a maximum ($dB/d\tau = 0$) is given by:

$$\tau_{max} = \sqrt{\frac{1}{k_1k_2}} \qquad (18)$$

In a stirred-flow reactor, the percent reaction at a residence time τ for a first-order process is given by:

$$\text{percent reaction} = \frac{k_1 \tau}{k_1 \tau + 1} \times 100 \qquad (19)$$

It can be shown, therefore, that:

$$\text{percent reaction at maximum B} = \left(1 + \sqrt{k_2/k_1}\right)^{-1} \times 100 \qquad (20)$$

Equation 20 is in agreement with the experimentally observed shifting of the PFG maximum to higher percent reaction (Fig. 19 and 20) at higher temperature. The observed and calculated residence times and percent reactions at which the maximum PFG concentrations occur are presented in Table 21. The qualitative agreement is strong evidence for the proposed model, considering that the value of k_2 (PFG decomposition) is dependent on the reactor surface.

TABLE 21

FORMATION OF PFG FROM COMPOUND T AS A FUNCTION OF TEMPERATURE

Temperature, C	τ_{max} Observed, seconds	τ_{max} Calculated seconds	Percent Reaction at Maximum PFG	
			Observed	Calculated
198	180	260	19	39*
250	7	17	58	73*
340	0.03	0.09	99	99**

*The calculated percent reactions were obtained from Eq. 20 using the kinetic data for PFG from Eq. 20 and rate constant for Compound T (k_1) from Ref. 1.

**Calculated using tubular reactor equations

considerations would predict nearly a quantitative yield of PFG at 340 C rather than the 85 percent shown in Fig. 20. This suggests that either calibration errors occurred or Compound T does not form PFG quantitatively. The latter is actually to be expected because other minor products must be formed to balance Eq. 15, i.e., for each N_2F_4 formed, two F-atoms must react to form additional products.

The above considerations concerning the observed maximum concentration of the intermediate PFG in the decomposition of Compound T can be put on a more quantitative basis. According to Eq. 15, the pyrolysis of Compound T is of the type:

$$A \xrightarrow{k_1} B \xrightarrow{k_2} \text{products} \qquad (16)$$

where

A = concentration of Compound T

B = concentration of PFG

If it is assumed that B decomposes by a first-order process, then for a stirred-flow reactor:

$$\frac{dB}{dt} = k_1A - k_2B - \frac{B}{\tau} = 0 \qquad (17)$$

where

τ = residence time = V/U

By differentiation of Eq. 17, it can be shown that the residence time, τ_{max}, at which B reaches a maximum ($dB/d\tau = 0$) is given by:

$$\tau_{max} = \sqrt{\frac{1}{k_1k_2}} \qquad (18)$$

On the basis of Eq. 16, it is possible to predict a maximum concentration of PFG as a function of temperature. From Eq. 17, the ratio of PFG to Compound T is given by:

$$\frac{B}{A} = \frac{k_1}{k_2 + \frac{1}{\tau}} \tag{21}$$

Thus, the ratio of PFG concentration to initial Compound T concentration is given by:

$$\frac{B}{A^\circ} = \frac{k_1 A}{\left(k_2 + \frac{1}{\tau}\right) A^\circ} \tag{22}$$

The calculated and observed ratios of PFG/initial Compound T at τ_{max} for the three temperatures investigated (Fig. 19 and 20) are presented in Table 22. As shown, the ratios increase in the predicted order. Again the lower values of the observed ratios, as compared to the calculated values, must be considered because of the uncertainty in k_2. For example, if the surface of the reactor used during the experiment at 198 C were particularly active, the increased value of k_2 would greatly improve the agreement in Tables 21 and 22 between the calculated and observed values.

TABLE 22

MAXIMUM CONCENTRATION OF PFG FROM COMPOUND T
AS A FUNCTION OF TEMPERATURE

Temperature, C	Maximum PFG Concentration/Initial Compound T	
	Observed	Calculated
198	0.044	0.22*
250	0.26	0.54*
344	0.89	0.99**

*Using Eq. 19 and 22
**Calculated using tubular reactor equations

Because it has been established that Compound T forms PFG as a true reaction intermediate, the problem of determining the mechanism of decomposition of Compound T becomes one of determining the mechanism of PFG decomposition. It was shown in Ref. 1 that N_2 is the reaction product from Compound T that is the most difficult to account for mechanistically. The observation that nitrogen is a major product of the homogeneous (and heterogeneous) decomposition of PFG shifts the problem to one of determining the mode by which N_2 forms from PFG.

RELATIONSHIP OF PFG DECOMPOSITION MECHANISM TO THE DETONATION SENSITIVITY OF COMPOUND T

The results obtained during this mechanism study are encouraging because they suggest that Compound T decomposes through a series of processes which do not involve C-F bond rupture or N_2 formation until the later stages. It may be possible, therefore, to reduce the initial heat release from the decomposition of Compounds R and T markedly if an additive can be found which prevents the formation of compounds containing CF bonds or N_2, even through it is apparently not possible to reduce the rate of decomposition of Compounds R and T. For example, if the reaction of Compound R with N_2O_4 could be caused (by the addition of a suitable catalyst) to follow the stoichiometry:

$$3R + 5NO_2 \longrightarrow 7NF_3 + 3CO + 7NO \qquad (23)$$

only 4 percent of the heat of pyrolysis of Compound R would be generated. A partial shift toward this desired stoichiometry would be beneficial in increasing the critical temperature for explosion.

The first step in the pyrolysis of Compound T is a unimolecular bond rupture to form an NF_2 radical and a $C(NF_2)_3$ radical (Eq. 8); the latter radical then eliminates a fluorine atom to form PFG. The results reported here suggest that the PFG then decomposes either heterogeneously or

homogeneously, depending on the temperature, to still another species; this species is the precursor to the final stable products (N_2, NF_3, and CF_4). This last conclusion is based on the observations that both the low- and high-temperature pyrolyses of PFG give the same products, and the product distributions are affected to a similar extent by the addition of N_2F_4.

INHIBITION OF THE HETEROGENEOUS DECOMPOSITION OF PFG

Because the extreme detonation sensitivities of PFG and Compound T may result from the tendency of PFG to decompose heterogeneously at moderate temperatures, i.e.,

$$T \xrightarrow[\text{small } \Delta H]{\text{homogeneous}} PFG \xrightarrow[\text{large } \Delta H]{\text{heterogeneous}} \text{Products}$$

a small effort was devoted toward determining if coating the surface of a reactor with Teflon would markedly decrease the rate of the heterogeneous decomposition of PFG.

Pyrolysis experiments were conducted with PFG at 191 C, using both an untreated, static Monel reactor and a similar reactor coated with Teflon (DuPont 851-204). The initial pressure of PFG was approximately 100 mm Hg during all of the experiments. The results are presented on the following page.

Run No.	Surface	Percent Reaction After 2000 Seconds
1	Untreated	19
2	Untreated	35
3	Untreated	45
4	Coated	94
5	Coated	84
6	Coated	82
7	Coated	83

The untreated reactor gave rates that increased with consecutive runs. This suggests the Monel surface may be activated by contact with PFG or its decomposition products.

Disappointingly, the Teflon-coated reactor gave rates faster than those obtained in the uncoated reactor. These remained essentially constant after the initial run. The heterogeneous rate constants obtained in the untreated reactor were 10 to 100 times smaller than those obtained previously in the various flow reactors employed. However, those observed rates were still faster by a factor of more than 10^4 than those predicted for the homogeneous reaction at this temperature.

PYROLYSIS OF PFF

Because the major heat release (> 80 percent) in the reaction sequence represented by Eq. 15 occurs in the decomposition of PFG to stable products, the mechanism of PFG decomposition becomes an important consideration in examining routes to desensitive Compound T. The behavior of PFF as an intermediate in PFG pyrolysis (reaching a maximum, then decreasing with time), as shown in Fig. 28, suggested that PFF might be a precursor to the stable products N_2, CF_3NF_2, and CF_4, i.e., the reaction sequence might be of the type

$$T \longrightarrow PFG \longrightarrow PFF \longrightarrow \text{products} \qquad (24)$$

It should be noted, however, that if PFF is a direct intermediate in the pyrolysis of PFG, as indicated in Eq. 24, the thermal stability of PFF must be less than that of PFG. If this were not the case, the maximum concentration of PFF would be much greater than is observed. To determine the role of PFF in the pyrolysis of PFG, the pyrolysis of PFF was studied.

Kinetics of PFF Pyrolysis

The rate of the thermal decomposition of PFF was investigated over the temperature range 358 to 477 C using a Monel, stirred-flow reactor. In the higher temperature regime (> 410 C), the decomposition was first order and apparently homogeneous. Figure 32 is a plot of $(A^{\circ}-A)/A$ vs residence time at 428.5 C. A straight line through the origin is obtained as predicted for a first-order decomposition. All of the first-order rate constants are presented in Table 23. The Arrhenius plot of these data in Fig. 33 gives first-order rate constants for the higher temperature region which fit the equation:

$$k_1 = 10^{15.22} \exp(-49{,}279/RT) \text{ sec}^{-1} \qquad (25)$$

The rate constants at lower temperatures (< 400 C) tend to be above the line, suggesting that the decomposition becomes heterogeneous at lower temperature.

Comparing Fig. 33 with Fig. 31 , it may be seen that PFF is slightly more stable than PFG (by about a factor of three) and has nearly the same decomposition activation energy.

Products of PFF Pyrolysis

The products obtained from PFF at 426 C are shown in Fig. 34 . The product distribution from this species is very similar to that obtained from

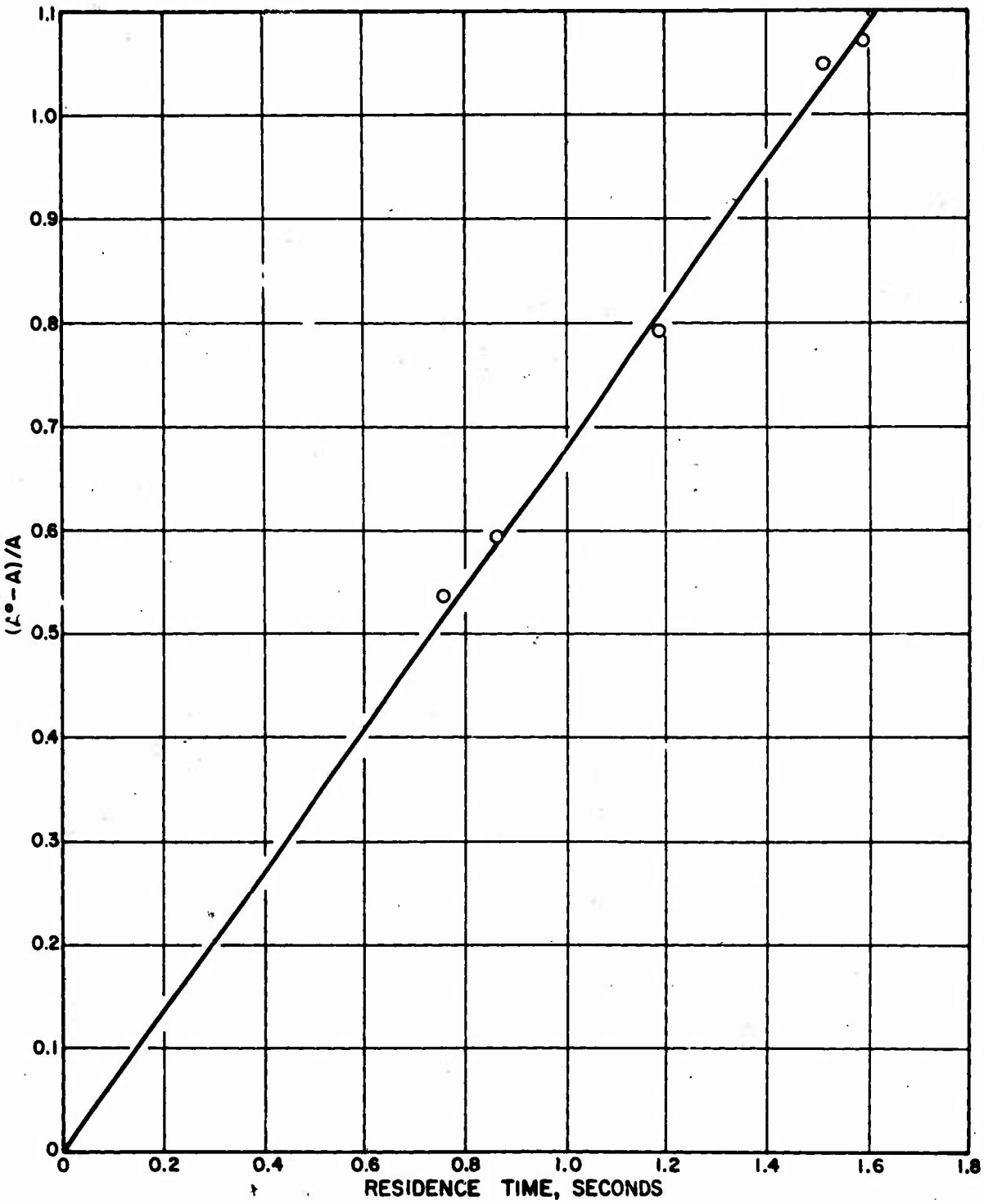


Figure 32. First-Order Plot for the Pyrolysis of FFF at 428 C

TABLE 23

FIRST-ORDER RATE CONSTANTS FOR THE PYROLYSIS OF PFF (AT 7.8 mm Hg OF PFF)

Temperature, C	τ*, seconds	Initial PFF, A° (chromatographic peak area, cm^2)	Final PFF, A (chromatographic peak area, cm^2)	k_1, sec^{-1}
357.8	25.5	176	113	0.0219
358.8	20.7	176	116	0.0250
361.2	14.4	176	122	0.0307
398.0	17.9	167	39	0.183
398.0	11.9	167	54	0.175
398.0	8.09	167	72	0.164
398.0	6.32	167	82	0.164
396.8	4.94	167	98	0.143
397.2	1.78	167	131	0.154
412.2	3.34	164	77	0.338
412.2	1.79	164	100	0.358
412.2	1.84	164	102	0.330
420.8	1.75	168	90	0.495
419.2	1.78	168	88	0.510
426.2	4.51	165	39	0.716
426.0	4.65	165	38	0.718
427.8	3.74	165	42	0.783
427.8	3.19	165	45	0.787
429.6	1.55	165	78	0.720
429.6	0.961	165	95	0.766
428.2	1.58	172	83	0.677
428.8	1.51	172	84	0.694
428.5	0.758	172	112	0.707
428.8	0.861	172	108	0.688
428.2	1.18	172	96	0.669
443.7	1.17	169	63	1.44
443.7	0.726	169	81	1.50
441.0	0.518	169	98	1.40
451.0	0.791	161	60	2.13
449.8	0.453	161	79	2.27
461.0	0.730	169	45	3.78
460.0	0.455	169	67	3.34
477.4	0.386	168	37	9.17
477.2	0.343	168	42	8.77

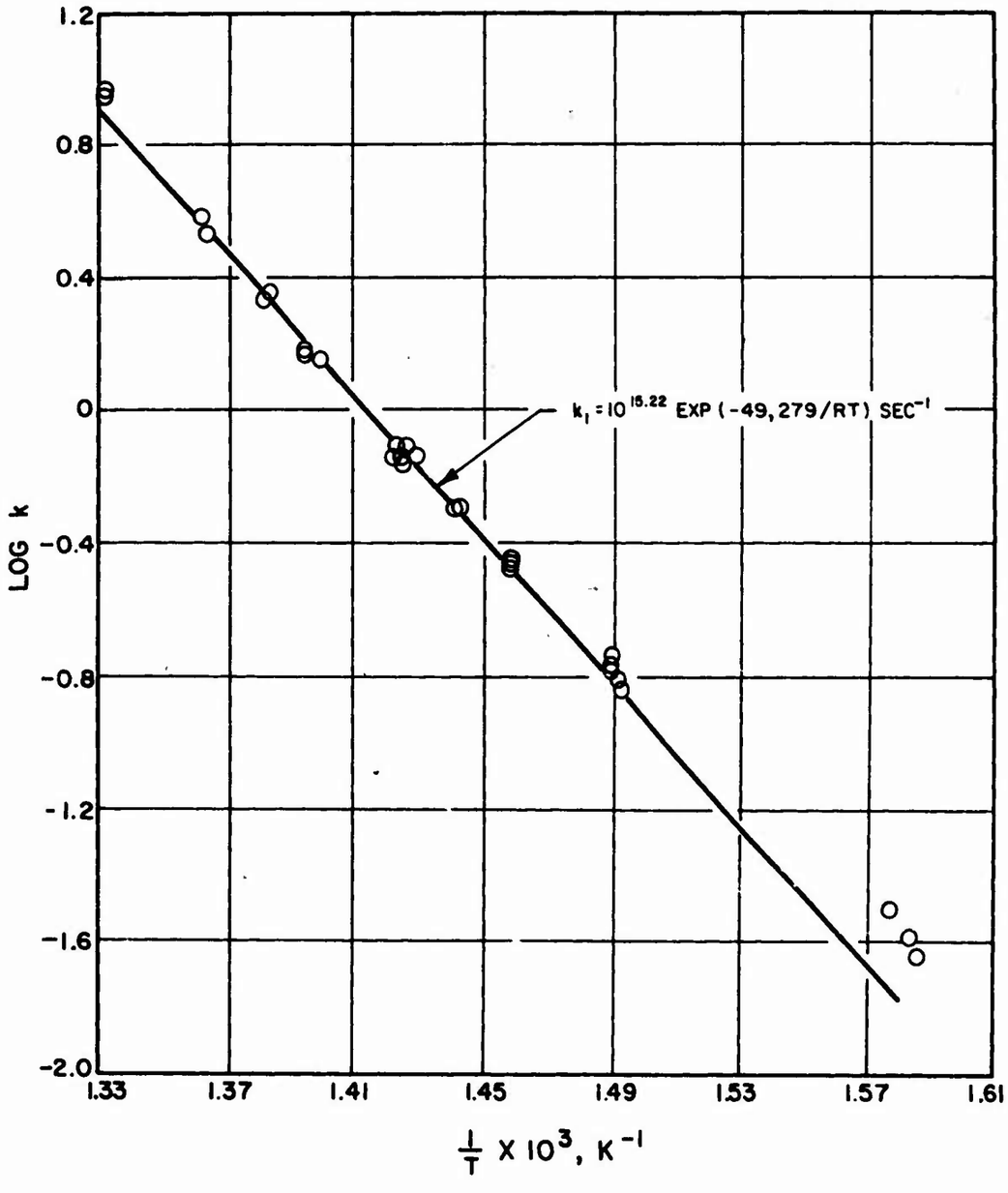


Figure 33. Arrhenius Plot for Thermal Decomposition of PFF

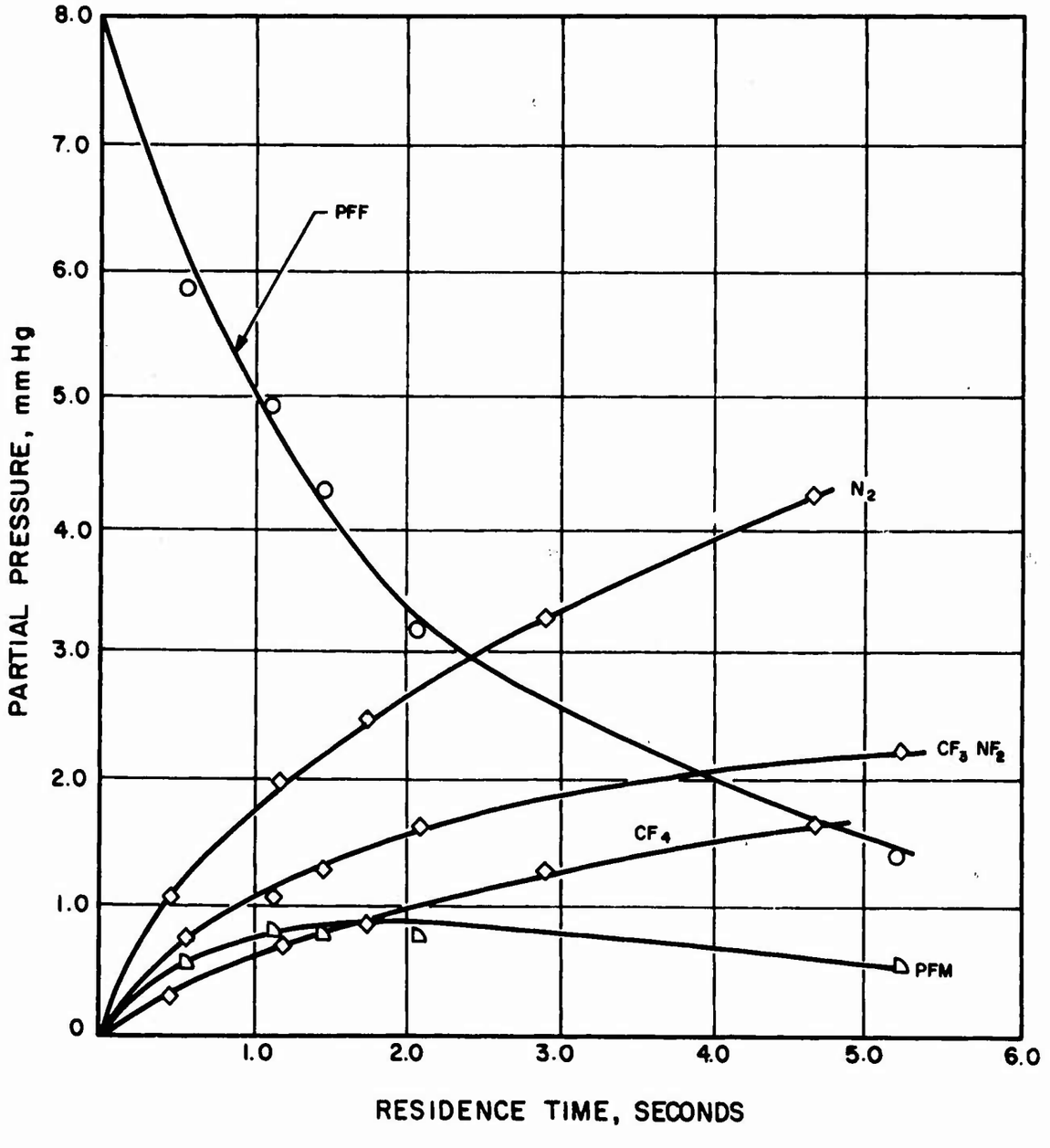


Figure 34. Product Distribution From PFF at 426 C

the homolog PFG (Fig. 28). The major products are N_2, CF_3NF_2, CF_4, and PFM. At high percent reaction, another product peak appeared on the gas chromatograms. This species was not identified.

Effect of Added N_2F_4 on PFF Pyrolysis

N_2F_4 and NF_3 were not found in the products from the pyrolysis of PFF. However, the addition of N_2F_4 to the initial PFF gas stream resulted in the formation of large amounts of NF_3. This result shows that no NF_2 radicals are formed in the pyrolysis of PFF, regardless of the exact mechanism of NF_3 formation in the absence of added N_2F_4. It is probable, however, that fluorine atoms form as intermediates in the pyrolysis of PFF and these react with the added NF_2 to form NF_3.

RELATIONSHIP OF PFF PYROLYSIS RESULTS TO MECHANISM

The mechanism by which PFG forms the observed products that include a large amount of N_2 has not been established. It can be shown that, if PFF were a direct intermediate in the pyrolysis of PFG, as depicted in Eq. 24, the ratio of PFF partial pressure to PFG partial pressure in the stirred-flow reactor would obey the relationship:

$$\frac{PFF}{PFG} = \frac{k_2}{k_3 + \frac{1}{\tau}} \qquad (26)$$

where

k_2 = first-order rate constant for the pyrolysis of PFG

k_3 = first-order rate constant for the pyrolysis of PFF

τ = residence time

At 416 C and a residence time of 1 second, the ratio of PFF PFG predicted by Eq. 26 would be 0.72. The experimentally observed ratio (Fig. 28) is 0.16. These results strongly indicate that PFF is not a direct intermediate in the pyrolysis of PFG if its only mode of reaction is that of pyrolysis.

This also can be seen qualitatively as follows. Because PFF is more stable than PFG by about a factor of three (Fig. 31), PFF should reach a rather high concentration. Instead, it appears only as a minor reaction intermediate.

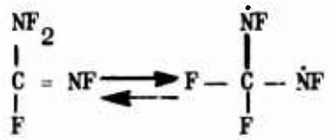
The next point to consider is the initial step in the pyrolysis of PFG and PFF. In the pyrolysis of Compounds T, R, and H, all experimental evidence suggests that the initial and rate-determining step is the rupture of a C-N bond (Eq. 8) to give $\cdot NF_2$ and the corresponding CNF radical. The replacement of successive ·F-atoms with $\cdot NF_2$ groups in the series H, R, and T was found to lower the C-N bond energy (activation energy) by approximately 6 kcal each (Ref. 1).

In the case of the double-bond-containing difluoramino compounds, the low concentration of N_2F_4 and NF_3 from PFG (Fig. 28) and the absence of N_2F_4 and NF_3 from PFF (Fig. 34) indicate that C-N bond rupture is not the initial step for these species. Also, the activation energies are in the reverse order to that expected from the previous results with the difluoramino methane series. Thus, the activation energy for PFG is approximately 4 kcal higher than that for PFF even though PFG contains one more NF_2 group. The slower rate of pyrolysis of PFF compared to PFG is caused by its lower pre-exponential factor.

It is possible in these compounds that the N-F bond on the imine nitrogen is the weakest bond in the molecule. The initial step in the pyrolysis of PFF might be, therefore:

$$F(NF_2)C = NF \longrightarrow F(NF_2)C = N\cdot + \cdot F \qquad (27)$$

Another possible initial step would be:



(28)

It has been shown during this study that (1) the formation of nitrogen is difficult to account for mechanistically, (2) nitrogen is formed from the double-bond-containing intermediates, and (3) there is no simultaneous formation of NF_2 radicals (at least for PFF). Following Eq. 27 or 28, the nitrogen could form by the following types of processes:

$$2 > C = N\cdot \longrightarrow C = N\text{-}N = C < \longrightarrow \dot{C}\ N = N\ \dot{C} < \qquad (29)$$

$$F_2C(\dot{N}F)_2 \longrightarrow PFM + :NF \qquad (30)$$

$$2\ :NF \longrightarrow N_2 + 2F\cdot \qquad (31)$$

Reactions of the types depicted in Eq. 29 through 31 are quite unusual; however, they must be considered in the absence of other possible mechanisms.

PYROLYSIS OF COMPOUND T IN STATIC REACTORS

Other investigators (Ref. 8 and 9) have reported rates for the low-temperature decomposition of Compound T which do not agree with those of this investigation (Ref. 1). Therefore, Compound T was studied in the static reactors used to study the pyrolysis of PFG.

The rate of Compound T decomposition at 190 C was found to be the same in the untreated and Teflon-coated reactors. These rates, obtained in static reactors, were in very good agreement with those predicted from previous stirred-flow experiments with Compound T (Ref. 1). These

results substantiate the previous conclusion that Compound T decomposes by a homogeneous, first-order reaction. During the present experiments, the Compound T pressure was higher by a factor of about three than the Compound T partial pressures employed during the flow reactor study, and no helium was present in the static reactors.

EXPERIMENTAL TECHNIQUE

The experimental data presented in this task were determined using stirred-flow reactors, tubular flow reactors, and static reactors.

FLOW REACTORS

The experimental procedure, description of apparatus, and method of data analysis are discussed in detail in Ref. 1 for the 90-milliliter, stirred-flow reactors and the 60-millilieter, tubular flow reactor.

The small tubular reactor used for the high-temperature pyrolysis was constructed from 1/8-inch copper tubing. The length of the heated tube is 112 centimeters and the wall diameter is 0.165 centimeter. Thus, the volume of the heated tube is 2.4 cm^3. The reactor is coiled and thermostated in an electric furnace. Even heating of the reactor is ensured by packing the furnace with aluminum foil. The temperature is determined from three thermocouples located at different positions along the reactor.

STATIC REACTORS

The static reactor consists of a 160-milliliter, Monel, static reactor connected directly to a Beckman gas chromatographic sampling valve. Samples are taken by evacuating the sample loop, expanding gases from the reactor into the loop, and rotating the loop into the carrier gas stream of the chromatograph. The chromatograph is the same as that used with the stirred-flow reactors. The stirred, constant-temperature bath consists of a large, dewar flask filled with Dow Corning 200 silicone fluid. The Teflon-coated reactor was similar except that it was coated with Teflon 851-204 (from aqueous solution) and baked at 250 C.

PRODUCT ANALYSIS

The rates of pyrolysis were followed gas chromatographically using a 7.5-foot, 1/4-inch column packed with 30 w/o Halocarbon oil on Chromosorb-W (acid washed). The column was at ambient temperature and the helium flowrate was 60 ml/min. Under these conditions, the products and intermediates gave composite peaks at 2-1/2 and 3 minutes, while PFG was eluted at 5-1/2 minutes.

N_2, NF_3, and CF_4 were measured using a 10-foot, 1/4-inch column packed with activated alumina. Again, the column was thermostated at -22 C and the helium flow was 60 ml/min. The following retention times were measured: N_2, 3.3 minutes; CF_4, 9.8 minutes; and NF_3, 11.2 minutes.

The chromatograph was calibrated for each species by introducing known pressures of the compound under conditions identical to those used for product analysis, and measuring the area of the evolved peak.

CONCLUSIONS

The results of this study establish with some certainty that Compound T decomposes via a C-N bond rupture and PFG is a direct intermediate (i.e., essentially all of the Compound T molecules decompose to PFG before forming the observed stable products). PFG is much more thermally stable than Compound T (when considering only homogeneous decomposition), but PFG is not found in high yields in the low-temperature pyrolysis of Compound T because of PFG's tendency to decompose heterogeneously on the reactor surface.

The similarity of products suggests that the homogeneous and heterogeneous decomposition mechanisms for PFG are the same except that the rate-determining step occurs on the reactor surface in the heterogeneous case. The initial process in the decomposition of PFG is apparently not a C-N bond rupture. The additives N_2O_4, N_2F_4, and F_2 had only minor effects on the rate of PFG pyrolysis but had a marked effect on the product distribution. PFG decomposes as readily on a Teflon-coated surface as on a Monel surface.

The large amount of nitrogen in the products of the pyrolysis of Compound T actually is formed from the pyrolysis of the intermediate PFG. Although this limits the problem somewhat, a satisfactory detailed mechanism for the formation of nitrogen is not apparent.

PFF is slightly more stable than PFG but is not a direct intermediate in the decomposition of PFG. The initial step in the pyrolysis of PFF cannot be the rupture of a C-N bond.

PFF is more thermally stable (toward homogeneous decomposition) than Compound R by approximately a factor of 100. PFF may be a direct intermediate in the decomposition of Compound R but is not found as a major product because it decomposes heterogeneously at the temperature where

Compound R has been decomposed. However, this point cannot be settled definitely because the PFF pyrolysis study was not extended to low enough temperatures.

The kinetic results indicate that the decomposition of CNF compounds may not be amenable to chemical inhibition. The initial step in the pyrolysis of Compound T is a unimolecular bond rupture which is not reversible. The initial step in the subsequent pyrolyses of the direct intermediate PFG is apparently not a C-N bond rupture but, again, does not appear to be reversible. Because neither of these reactions appears to involve chain reaction or autocatalysis, the additive approach to inhibition does not seem promising. No further studies of these decomposition mechanisms are planned.

TASK 3: HETEROGENEOUS PROPELLANTS

CONVENTIONAL GELLED PROPELLANTS

INTRODUCTION

The objectives of this task were:

1. To continue the development of high-energy, storable, heterogeneous propellants begun under an earlier contract, AF04(611)-9380
2. To prepare the promising propellants in quantities sufficient for engineering characterization tests
3. To develop new heterogeneous propellants

At the beginning of the current program, five heterogeneous propellants, listed in Table 24, were in the early stages of development. No further effort was accomplished on R-1 (LMH-1 in hydrazine) because the available solid aluminum hydride was too unstable to permit its incorporation into a storable propellant. During the course of the program, work on R-4 was suspended; studies on R-4 described herein are fragmentary.

A highly loaded R-2, designated R-2 HL was formulated, the composition of R-5 monopropellant was refined, and a new promising gelled heterogeneous fuel, R-6, was developed. The effort on R-6 is discussed in detail under Advanced Heterogeneous Propellant. Techniques for preparing the gels and for their characterization are detailed in the Experimental section.

TABLE 24

HETEROGENEOUS PROPELLANTS SELECTED FOR STUDY

Designation	Solid	Liquid	Oxidizer	Volume-Percent Solid	Specific Impulse (1000 psia → 14.7), seconds
R-1	AlH_3	N_2H_4	N_2O_4	40	318
R-2	Be	N_2H_4	H_2O_2	18	336
R-3	BeH_2-Be 2:1	MMH	H_2O_2	35	334
R-4	Be	H_2O-N_2H_4-HN 9·1:37·7:53·5	None	13	315
R-5	BeH_2-Be 8:3	H_2O-N_2H_4-HN 47:22:31	None	35	323

HN = Hydrazinium nitrate

Liquid compositions are given in weight percent

DISCUSSION AND RESULTS

R-2 Gel

At the end of the preceding program (Ref. 1), mechanically stable beryllium-in-hydrazine gels had been prepared (Ref. 1) using Kelzan-aluminum octanoate (AO) as the gelling agent. These gels contained Beryllium Corporation Lot No. R-2360 metal powder. (The vendor's analyses on various lots of beryllium powder are presented in Table 37, page 161). This lot was completely consumed, and initial attempts to prepare gels with the nominally similar lot R-3913 failed under apparently identical conditions. The difficulty was traced to deterioration of solutions of AO in hydrazine on storage. Cohesive, elastic gels were formed when solid AO was premixed with the metal powder and Kelzan, and subsequently added to the hydrazine, by mixing for a minute in a Waring Blendor and allowing the mixture to stand for 1/2 hour.

Unloaded Kelzan-N_2H_4 and Kelzan-H_2O Formulations. Unmetallized dispersions of Kelzan in hydrazine and in water were prepared in a Waring Blendor, centrifuged for 30 minutes at 500 g to remove air bubbles, and their rheological properties were determined with a Brookfield model HAF viscometer whenever possible. The mixtures prepared included the following:

1. 1- to 3-percent solutions of Kelzan with 0.2-percent AO in neat N_2H_4
2. 1- to 2-percent solutions of Kelzan with 0.2-percent AO in 95-percent N_2H_4 with 5-percent H_2O added
3. 1- to 3-percent solutions of Kelzan only in neat N_2H_4
4. 1- to 2-percent solutions of Kelzan only in distilled H_2O

Viscosity measurements were made using the Brookfield Helipath Stand with either disk-type or T-bar spindles. Typical results are listed in Table 25. The most significant results are as follows.

1. The apparent viscosity of Kelzan-N_2H_4 solutions (1 to 3 percent) varied from 400 to 5100 centipoises at 10 rpm with a size A, T-bar, and showed an exponential increase with concentration (Fig. 35). Kelzan concentrations greater than 3 percent produced gelled solutions. At less than 3 percent, the solutions possessed no yield strength.
2. Distilled H_2O solutions of 1- to 2-percent Kelzan displayed apparent viscosities of 2300 to 5200 centipoises with small yield stresses.

In addition to the tabulated results, the following observations were made:

1. Dispersions of 1- to 2-percent Kelzan-A0 in N_2H_4 formed gels with appreciable yield values and viscosities beyond the range of the Brookfield viscometer. Centrifuging the warm liquids caused some of the higher molecular weight portions of Kelzan to separate. Hence, the results for several solutions may be in error as far as consistency vs Kelzan concentration is concerned.
2. Kelzan-A0 dispersions in 95-percent N_2H_4-5-percent H_2O gelled more quickly than those without added H_2O, but the addition of 5-percent water apparently did not affect the ultimate rheological characteristics of the gel. Thus, Kelzan is a good gellant for propellants containing N_2H_4 and relatively small amounts of H_2O.

Information on the structure of water and hydrazine thickened with Kelzan was obtained by measuring the variation of light scattering intensity with scattering angle. The results are plotted in the form

TABLE 25

APPARENT VISCOSITY OF KELZAN SOLUTIONS
IN HYDRAZINE AND WATER

Liquid	Spindle Speed, rpm	Apparent Viscosity (cps) in Solutions of Kelzan (weight percent)				
		1	1.5	2	2.5	3
N_2H_4	10	400	800	1,500	3,300	5,100
	5	480	960	1,900	4,480	7,040
	2	800	1,200	2,400	6,400	10,400
H_2O	10	2,300		5,200		
	5	3,700		8,640		
	2	7,200		16,000		

NOTE: Measurements made with T-A spindle and Brookfield HAF viscometer

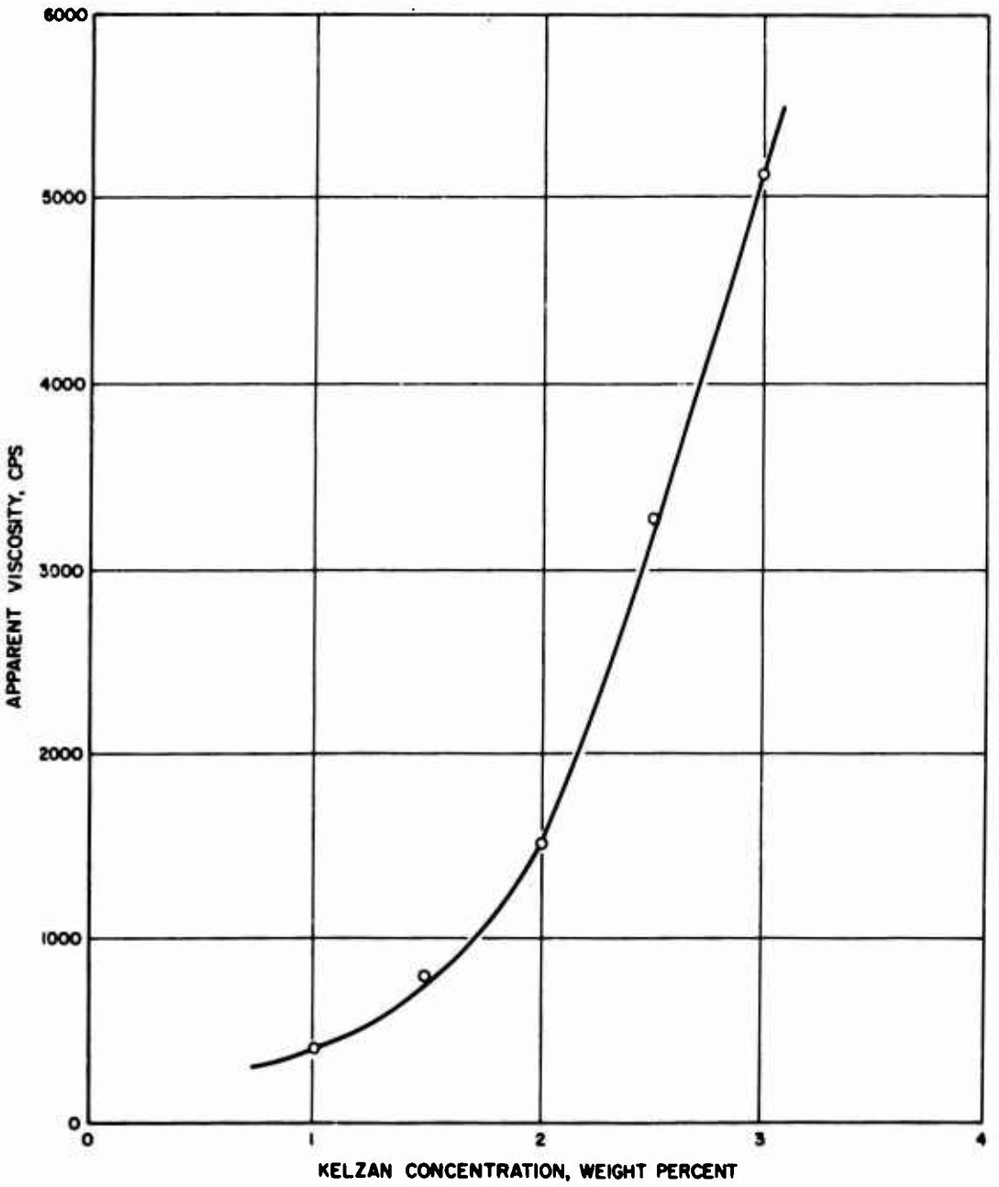


Figure 35. Dependence of Hydrazine Apparent Viscosity on Kelzan Concentration at 24 C Measured With Brookfield Spindle T-A at 10 rpm

of log $I\theta^2$ vs log θ, where I is the relative intensity of light scattered at an angle θ from the transmitted beam. The angular position of the maximum in the curve is related to the size of the predominant scattering center (Ref. 10). As shown in Fig. 36, the predominant size of the light scattering center decreases with increasing Kelzan concentration in each liquid. This observation implies that the major scattering unit, as determined in the 1- to 30-degree angular range, is a cell of liquid partially immobilized by the swollen Kelzan. The diameter of the cells in a 1-percent solution is approximately 1 micron in water and approximately 8 microns in hydrazine. Instrumental limitations precluded investigations at greater scattering angles. More effective cross-linkages exist in water solutions than in hydrazine solutions with the same Kelzan concentration, resulting in both higher viscosity and smaller scattering units in the aqueous solutions (Table 25).

Normal R-2 Gels (28.5 Weight Percent Be in N_2H_4). The particular beryllium powder incorporated into the thickened hydrazine solution has a profound effect on gelation. This has been confirmed by using Brush IV-195 and Berylco R-3913 in otherwise identical formulation procedures. The Brush sample gelled rapidly upon blending into Kelzan-hydrazine solutions containing 1.0 and 0.75 percent Kelzan without the use of AO. Under identical conditions, the Berylco sample did not gel immediately. However, after addition of AO or standing for 1 week, gelation began and eventually stiff gels formed.

On the basis of manufacturers' specifications, the Brush beryllium probably contains more oxide than the Berylco material, and this oxide on the surface may be responsible for cross-linking the Kelzan even in the absence of AO.

Mechanically stable, cohesive gels containing Beryllium Corporation Grade PS-98 beryllium powders of various average particle sizes from 8 to 24 microns were prepared with Kelzan and AO as gelling agents. Different orders of addition of the components included:

1. Adding the metal to Kelzan solution, then adding solid AO

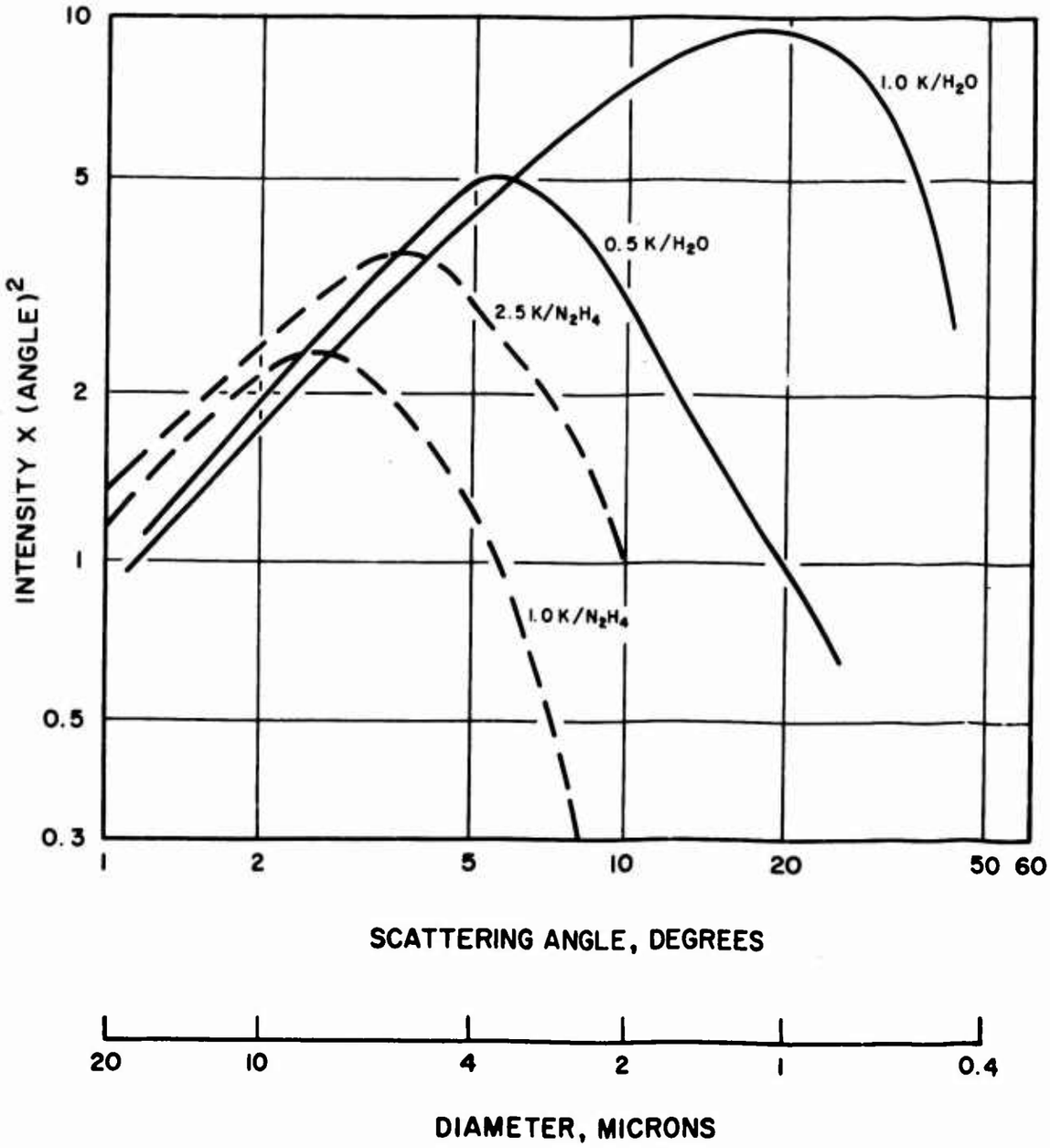


Figure 36. Light Scattered by Kelzan Solutions

2. Adding premixed solids to hydrazine

3. Adding metal to Kelzan solution, then adding fresh AO solution

No difference in behavior of the final mixture was ascribable to differences in the order of adding of the components. However, AO solutions in hydrazine deteriorate when stored and lose their ability to cross-link the Kelzan. This behavior contrasts with the stability of Kelzan-AO gels in hydrazine whether loaded with beryllium or not. Apparently the bond formed between Kelzan and AO in hydrazine gels is sufficiently strong to inhibit the deterioration of AO by hydrazine.

The concentration of gellant required to produce a particular rheological behavior depended on which lot of beryllium powder was used. Satisfactory gels were obtained with Kelzan and AO concentrations as low as 0.35 and 0.25 w/o, respectively, when 15-micron-diameter particles were used (lot R-4464). On the other hand, powder consisting of 7.7-micron-diameter particles (lot R-4391) required higher Kelzan concentrations (Fig. 37) to form gels with equal apparent viscosities. This behavior may result from a greater amount of Kelzan adsorbed by the smaller particle powder, thereby tying up sites that would otherwise be available for cross-linking by AO. However, it may also be caused by unidentified differences in the nature of the metal surface which are unrelated to differences in particle size. For example, an old lot (R-3913) of 24-micron powder required as much gellant as the 7.7 mic material to produce the same apparent viscosity.

Some properties of the prepared normal R-2 gels are summarized in Table 26. Gel stability was observed in screw cap jars. Low-temperature cycling involved freezing the gel in a Dry Ice bath and warming it to room temperature three times. No deterioration of the gel was observed.

In an effort to further improve gel stability and to decrease viscosity, several other gelling and cross-linking agents were tested. Although Kelzan and AO are still preferable, mixtures of Kelzan, SeaTex, and AO

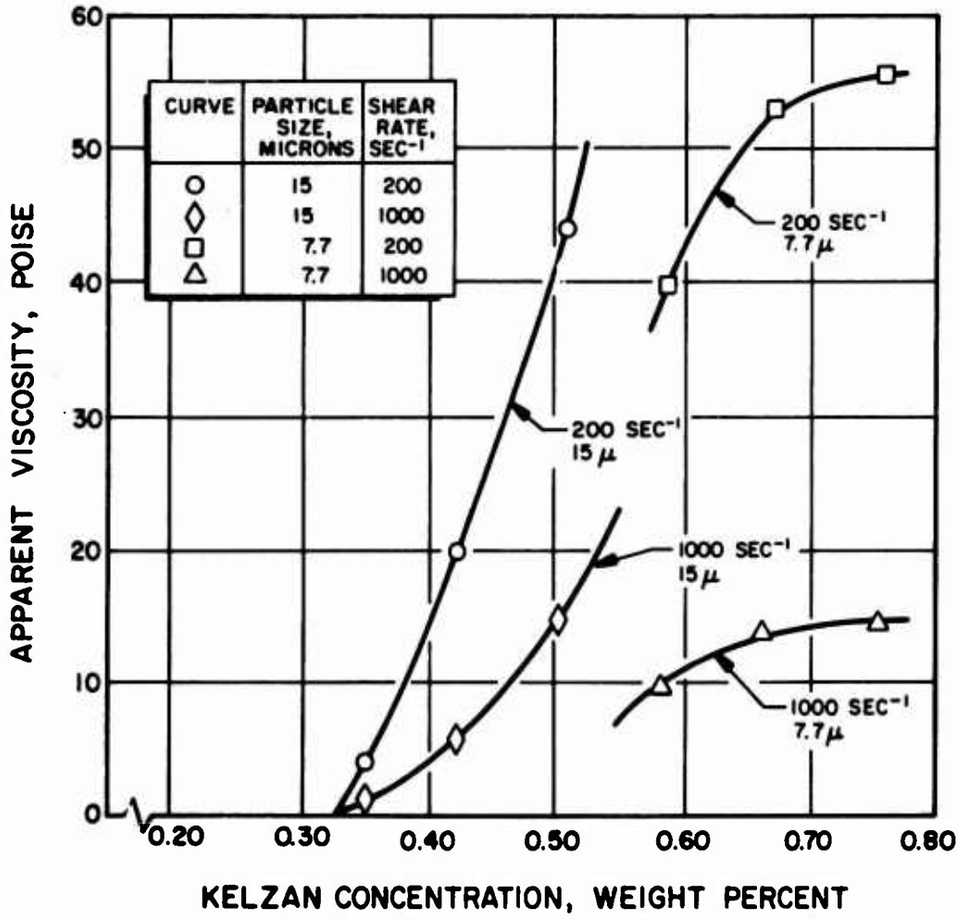


Figure 37. Effect of Particle Size of Beryllium Metal on Apparent Viscosity of Hydrazine Gels

TABLE 26

PREPARATION AND QUALITIES OF R-2 GELS

No.	Beryllium Lot	Particle Size, microns	Total Weight, gm	Kelsan Concentration, w/o	AO Concentration, w/o	Method	Stability, Ambient	Stability, 120 F	Low-Temperature Cycling	Stability on Centrifuging, g		Apparent Viscosity (Poise) at Shear Rate, sec^{-1}		
										50	200	10^2	10^3	10^4
1	3913	24	50	0.3	0.15	2	0	0						
2			50	0.5	0.15	2	3	1		2	1			
3			50	0.5	0.25	1	3			2				
4			50	0.5	0.25	2	3	3		2				
5			50	0.5	0.5	2	1							
6			50	0.75	0.25	2	2							
7			100	0.5	0.25	1	3	3	3			25	5	1
8			100	0.5	0.25	2	2	3	3			25	4	1
9			100	0.75	0.25	2	2	3	3		2	40	17	
10	3938	24	50	0.5	0.25	1	2	3						
11	2905	15.2	50	0.5	0.25	1	3	3		3				
12	2649	11.5	50	0.5	0.25	1	3							
13	2649	11.5	50	1.0	0.25	2	3	3						
14	4391	7.7	50	0.3	0.3	2	1							
15	4391	7.7	50	0.5	0.25	2	1							
16	4391	7.7	250	0.75	0.25	2	2+			3				
17	4391	7.7	50	0.75	0.25	2	2+			3		100	16	
18	2283	7.7	50	0.75	0.25	2	3		3	3	2			
19	2283	7.7	50	1.0	0.25	2	3	3						
20	3741	4.7		0.5	0.25	1	1							

NOTE: Method 1 Metal was added to Kelsan solution, then solid AO was added
Method 2 Premixed solids were added to hydrazine

Stability 0 = no gel
1 = 1 week
2 = 1 week to 1 month
3 = over 1 month

Stability on centrifuging for 40 minutes 1 = over 10-percent liquid separated
2 = 5- to 10-percent liquid separated
3 = 5-percent liquid separated

Most preparations were 50-gram batches, except No. 7, 8, 9 (100 grams) and No. 17 (250 grams)

TABLE 26
(Concluded)

No.	Beryllium Lot	Be Particle Size, microns	Total Weight, gms	Kelzan Concentration, weight percent	AO Concentration, weight percent	Method	Ambient Stability	Stability on Centrifuging, g		Apparent Viscosity (Poise) at Shear Rate, sec^{-1}		
								50	200	10^2	10^3	10^4
21	4391	7.7	50	0.30	0.3	2	1					
22		7.7	50	0.50	0.25	2	1	< 3	2			
23		7.7	50	0.50	0.25	3	2					
24		7.7	50	0.75	0.25	2	2+	3				
25		7.7	50	0.75	0	3	0					
26		7.7	250	0.58	0.25	2	2	< 3		[illegible]		2
27		7.7	250	0.66	0.25	2	3	< 3		[illegible]	14	
28		7.7	250	0.75	0.25	2	3	1		70	16	
29	4464	15	50	0.35	0.20	2	3					
30		15	50	0.35	0.25	2	2					
31		15	50	0.42	0.20	2	2					
32		15	50	0.42	0.25	2	1					
33		15	50	0.50	0.25	2	1					
34		15	50	0.50	0.25	1	1					
35		15	50	0.75	0	3	0					
36		15	50	0.75	0.25	2	1					
37		15	250	0.35	0.20	2	2					
38		15	250	0.35	0.25	2	3			5	1.5	0.4
39		15	250	0.42	0.25	2	2			30	7	1.3
40		15	250	0.50	0.25	2	2			70	15	
41	4391	7.7	50	0.25 Kelzan 0.75 SeaTex	0.20	3	2	1				
42		7.7	50	0.5 Kelzan 0.5 SeaTex	0.20	3	3	3				
43		7.7	50	0.75 Kelzan 0.25 SeaTex	0.20	3	3	3				
44		7.7	50	0.40 + 1% H_2O	0.20	2	3	2				
45		7.7	50	0.50 + 1% H_2O	0.25	2	3	2				

NOTE: Methods: 1 - metal was added to Kelzan solution then solid AO was added
2 - premixed solids were added to hydrazine
3 - metal was added to Kelzan solution, then AO solution was added

Stability: 0 - no gel
1 - 1 week or less
2 - 1 week to 1 month
3 - over 1 month

Stability on centrifuging for 40 minutes: 1 - over 10-percent liquid separated
2 - 5- to 10-percent liquid separated
3 - 5-percent liquid separated

did produce satisfactory gels. Addition of 1-percent H_2O seemed to improve the stability of Kelzan-A0 gels at ambient conditions. Other possible cross-linking materials tested for use in the R-2 formulation included Cab-O-Sil M-5, calcium citrate, and a fine particle alumina. None of these were effective.

On the basis of these results, the final formula selected for regular R-2 that was used in preparing gallon batches for firing tests is that listed in Table 27. All the beryllium powder in the large batches was nominally 7-micron material from manufacturer's lots R-4391, -4949 or -5075.

TABLE 27

COMPOSITION OF REGULAR R-2

Component	Concentration	
	Weight Percent	Volume Percent
Hydrazine	70.8	82
Beryllium	28.4	18
Kelzan	0.58	--
Aluminum Octanoate	0.24	--

Swelling. When stored, some of the small batches of R-2 gel described in Table 26 were observed to swell noticeably. In 3 weeks at room temperature, some gels containing lot R-4464 beryllium swelled approximately 40 percent. Accordingly, more quantitative measurements were made by placing loaded and unloaded hydrazine gels in passivated Babcock bottles. The gel was covered with a few drops of Nujol, and the advancing meniscus of the oil was observed as the gel expanded. The swelling rates at ambient temperature are presented in Table 28; the data represent average

TABLE 28

SWELLING RATE OF LOADED AND UNLOADED HYDRAZINE GELS

Test Number	Metal or Be Lot Number	Concentration		Average Swelling Rate, (volume percent/min) x 10^5
		Kelzan Weight Percent	Aluminum Octanoate Weight Percent	
I	None	0.83	0.35	6.3
II	None	0.58	0.25	3.6
III	None	0.83	0.35	8.2
IV 1	None	0.95	0.51	6.4
IV 2	None	0.47	0.25	6.1
D	Al	0.30	0.15	9.4
E	Al	0.30	0.15	9.3
F	Al	0.27	0.14	9.8
G	Al	0.30	0.15	8.5
K	Al	0.30	0.15	9.3
M	Al	0.30	0.15	6.5
B1	R 4391	0.58	0.25	21
B2	R 4391	0.58	0.25	17
B3	R 4464	0.47	0.25	47
B4	R 4464	0.47	0.25	42
B5*	R 4391	0.58	0.25	24
B6	R 4391	0.58	0.25	12
B6N*	R 4391	0.58	0.25	11
B7*	R 4464	0.47	0.25	27
B8*	R 4949	0.58	0.25	23
B9	R 4949	0.58	0.25	18
A14**	R 4949	0.60	0.075	70
A20**	R 4949	0.68	0.075	85
4	None	0.58	0.35	6.2
S IV	Type 321 Stainless Steel Strips	0.58	0.25	35

NOTES: Ambient temperature (75 F)
Metal loading = 19 volume percent except during tests A14 and A20
Test duration = 60 days except for A14 and A20 = 12 days
B6, B6N—Metal powder was washed with water and dried before preparation of gel
S IV—Strips were passivated by rinsing in hydrazine several times and immersing for several days in fresh hydrazine at 110 F before placing in gel.
M—Al was precoated with 0.07 percent of a perfluorinated silane.
*Prepared under nitrogen
**Metal loading = 38 volume percent

values for the entire period of up to 60 days. Sample B5 was an exception, as it was prepared in a nitrogen atmosphere and no swelling occurred for the first 25 days; the tabulated value is for the subsequent swelling rate. Attempts to duplicate a gel with this long induction period were not successful.

Unloaded hydrazine gels exhibited the lowest swelling rates. All the beryllium-containing gels swelled faster than those containing aluminum. Washing the lot R-4391 beryllium powder with water before its incorporation into a gel (Samples B6 and B6N) reduced the swelling rate 50 percent. Highly loaded R-2 gels swelled three to four times faster than normal R-2, presumably because a larger area of solid surface contacted the hydrazine. Lot R-4464 produced slower swelling when the gel was prepared in a nitrogen atmosphere than when it was prepared in air. However, the beneficial effect of excluding oxygen did not occur with lots R-4391 or R-4949 of beryllium powder. Passivated type 321 stainless steel having a total surface area of approximately 10 cm^2 increased the swelling rate of gelled hydrazine nearly as much as loading with 18 v/o beryllium powder which exposes about 1000 times more surface area. Precoating aluminum with a perfluorinated silane, which is strongly adsorbed, reduced the swelling rate nearly to that of unloaded gel. In unloaded gels, doubling the gellant agent concentration did not increase the swelling rate; the gelling agent itself apparently may not contribute to those processes that cause swelling. It is possible, however, that small amounts of gelling agents cause gassing, and that further addition does not have a proportional effect.

At 43 C, swelling rates were generally 10 times faster than at 25 C, corresponding to an activation energy of 24 kcal/mole. Although this activation energy may be that of the heterogeneous decomposition of liquid hydrazine there is as yet not sufficient evidence to ascribe swelling to any particular process.

Flow Properties. A rheogram of a typical normal R-2 gel used for engineering characterization is shown in Fig. 38. This gel exhibits the required shear-thinning characteristics; its apparent viscosity falls from a 2.8 poise at 1000 reciprocal seconds to a 1.0 poise at 6000 seconds.

Highly Loaded R-2 Gels (R-2HL)

The combustion efficiency of the Be-N_2H_4/H_2O_2 propellant system might be improved by the use of a tripropellant two-stage combustion concept. The concept involves the development of a highly loaded R-2 heterogeneous fuel which would be combusted with hydrogen peroxide in the first stage of the engine. Neat hydrazine would be introduced downstream in the thrust chamber as required to maintain the overall mixture ratio identical to that of the normal R-2/H_2O_2 propellant system having maximum specific impulse. The effect of solids loading on the theoretical chamber temperature and mixture ratio of the first stage are shown in Fig. 39. If the beryllium in a 35 v/o gel were efficiently combusted, the theoretical chamber temperature was predicted to be increased 500 K over that obtainable with a conventional formulation containing 18 v/o beryllium. It was hoped that the increased chamber temperature would yield greater combustion efficiency with respect to beryllium and thus higher delivered performance.

Gels containing 38 v/o beryllium were prepared in the laboratory, and were mechanically stable for more than 7 months. These gels were more thixotropic than normal R-2 preparations, probably because they were formulated with a lower ratio of the cross-linking agent to the gelling agent. A suitable composition is listed in Table 29.

The Kelzan concentration based on the hydrazine content was essentially the same in both the normal and the highly loaded gels, but the AO content of the highly loaded gels had to be kept low to prevent formation of highly elastic mixtures. Apparently in the highly loaded systems, the metal powder participates in cross-linking the Kelzan and thus allows a reduction in the quantity of AO.

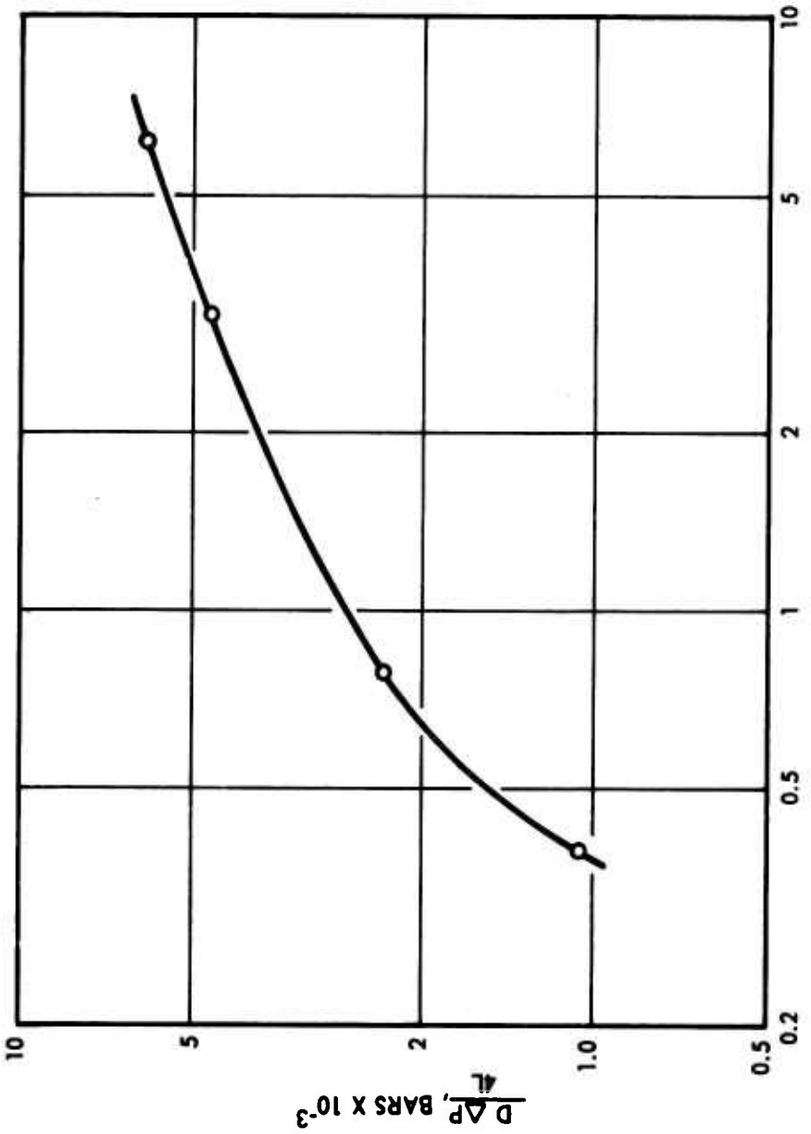


Figure 38. Rheogram of Typical Normal R-2 Gel

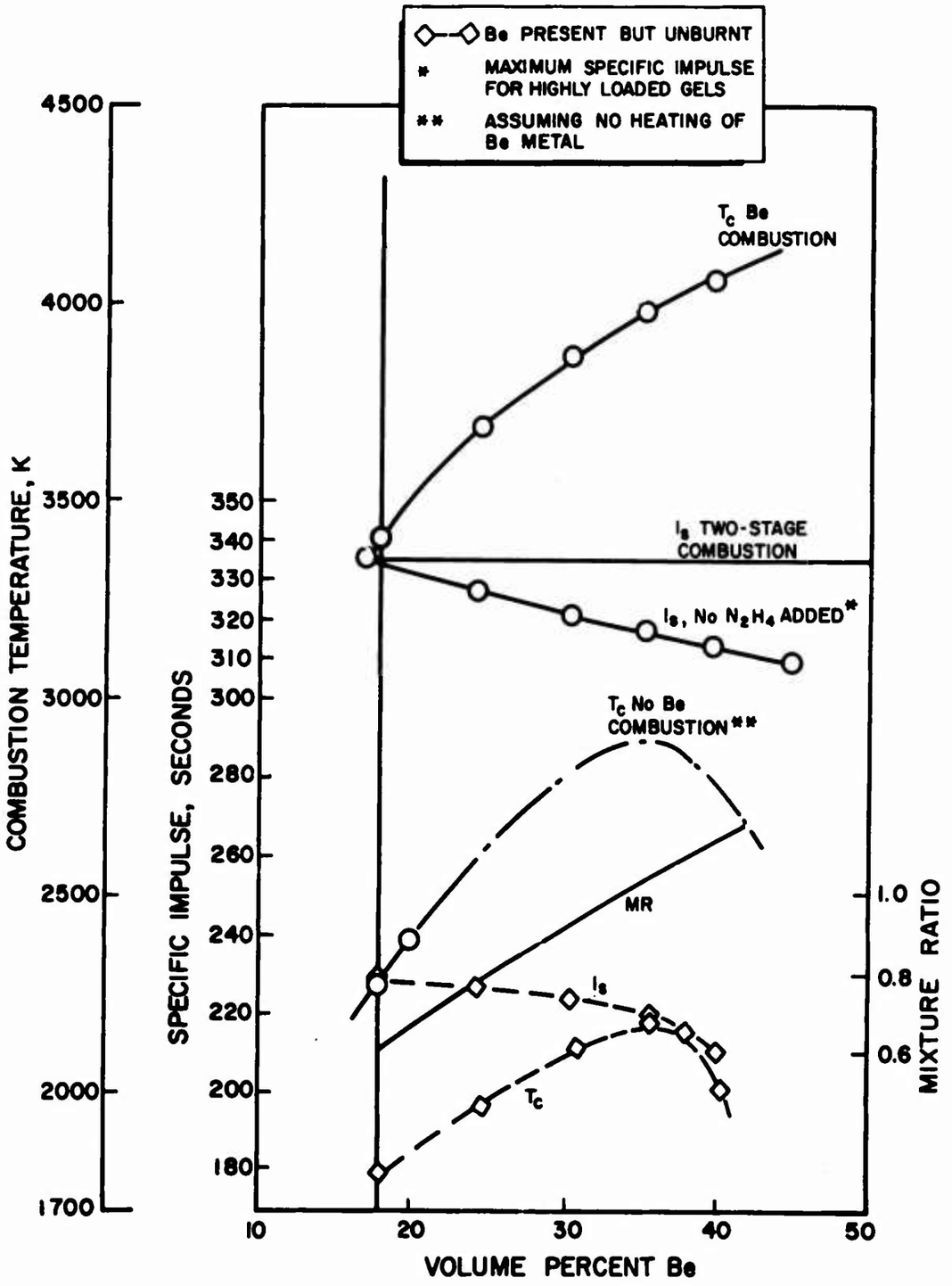


Figure 39. Performance of Be-N_2H_4/H_2O_2 System at Various Loadings

TABLE 29

COMPOSITION OF HIGHLY LOADED R-2HL

Component	Concentration	
	Weight Percent	Volume Percent
Hydrazine	47.0	62
Beryllium	52.6	38
Kelzan	0.40	--
Aluminum Octanoate	0.05	--

R-3 Gel

To formulate the composition R-3 (Table 24) into a useful gelled propellant, it was first necessary to find the most suitable gelling agents and preparative techniques. The search for the optimum conditions cannot be conducted by testing one factor independently of the other because the properties of the final gel depend on interacting variables involved in its preparation. Furthermore, the rheological properties of highly loaded gels are so dependent upon the degree of solids loading that the investigation of these variables must be carried out using loaded compositions. Hence, experiments were designed to optimize these mixing parameters, using at least 35 v/o of solids.

The first set of these experiments was conducted using Microthene instead of beryllium hydride in the formulation. Microthene is a polyethylene powder produced by the National Distillers Company and has been recommended as a simulant for beryllium hydride (Ref. 11). Its use during these tests permitted an appreciable saving in time and costs and the results were more significant than the use of unloaded MMH gels.

The experiment, which consisted of 44 tests, was intended to identify the effects of eight variables on the flow properties of gelled MMH. These variables were:

1. Purity of MMH
2. Concentration of gelling agent
3. Concentration of cross-linking agent
4. Addition of cellulose acetate
5. Order of addition of ingredients
6. Preheating of MMH
7. Duration and intensity of mixing
8. Intermittent vs continuous mixing

The identity of the gelling agent is really an additional variable.

It would have required many thousands of experiments to test all possible combinations of these variables at several levels. However, a statistically designed experiment, which is described in Appendix B, yielded the following results:

1. MMH which had been well exposed to the atmosphere and contaminated with 2-percent H_2O, produced gels which were slightly inferior only with respect to adhesion and shear thinning. Elaborate precautions for ensuring MMH purity appear unjustified.
2. Higher concentrations of gelling agents resulted in improved gelation as expected; higher concentrations of gelling agents did not contribute significantly to the plugging of viscometer capillaries (which was encountered occasionally). Therefore the higher concentrations were used for the next experiment.

3. Higher concentrations of cross-linking agent were found to give inferior gels; concentrations were lowered during subsequent tests.

4. The addition of cellulose acetate seemed to provide no advantage over using a higher concentration of gelling agents. Accordingly, the use of cellulose acetate was abandoned.

5. Premixing of all solids had a beneficial effect on some gel properties and a harmful effect on others. Because it was found to simplify the preparation of gels significantly, it was adopted on an interim basis. It will be seen that with the agent finally selected, this choice no longer existed.

6. Preheating of the MMH is of questionable advantage and was abandoned.

7. High shear mixing resulted in a firmer product which was lumpy and plugged the viscometer. Therefore, the technique adopted was to apply the same number of turns at a lower rate.

8. Interrupting the mixing process was found desirable.

9. Seven gelling agents were used but none were rejected on the basis of this series of experiments using simulants.

The same gelling agents were evaluated during the following experiment under the selected conditions in the presence of beryllium and beryllium hydride. A total of 20 runs were conducted; the results are presented in Table 30. It appears that any of the seven agents could be used at some concentration to obtain a gel with adequate rheological properties. Jaguar 315, Klucel HA, and Jaguar A20-B were eliminated from further consideration because of excessive gassing and swelling.

Larger batches (approximately 200 milliliters each) were then prepared with the remaining four candidates, using the best concentrations for each one. The gels were first evaluated at room temperature; then they were observed for 1 week at 120 F in closed test tubes. The formulations tested are shown in Table 31 together with the experimental results. In

TABLE 30

PROPERTIES OF R-3 MIXTURES

Gelling Agent	Concentration of Gelling Agent, percent	Type of Cross-Linking Agent	Concentration of Cross-Linking Agent	Pressure Buildup	Syneresis	Spontaneous Flow When Tilted	Appearance	η at 100 sec^{-1}, centipoise	$\frac{d(\log \tau)}{d(\log \dot{\gamma})}$	Strand Length, inches
Jaguar 415	1	—	—	Yes	Yes	Yes	Much too thin	—	—	—
Jaguar 415	2	— —	—	Yes	Yes	Yes	Much too thin	—	—	—
Jaguar 315	3	—	—	No	Yes	Slight	Somewhat thin	—	—	—
Jaguar 315	4	—	—	No	No	No	Much too thick	—	—	0.5 to 1
Natrosol 250 HHR	1	—	—	No	Slight	Yes	Too thin	3,700	0.156	—
Natrosol 250 HHR	1.5	—	—	No	No	No	Good	10,700	0.226	1.5
Natrosol 250 HHR	2	—	—	No	No	No	Good	8,000	0.218	>3.5
Cellosize QP100M	1	—	—	No	No	Slight	Fair	6,650	0.500	0.5
Cellosize QP100M	2	—	—	No	No	No	Good	3,250	0.0970	2.5
SeaTex	0.5	Boric acid	22.5 ppm	No	Slight	Slight	Somewhat thin	1,660	1.00	—
SeaTex	1	Boric acid	45 ppm	No	No	No	Thick	—	—	—
SeaTex	1.75	Boric acid	22.5 ppm	No	No	No	Good	11,600	0.126	>4
SeaTex	1.75	Boric acid	45 ppm	No	No	No	Much too thick	—	—	—
Klucel	1	Aluminum octetate	0.25 percent	Slight	Slight	—	Somewhat thin	2,850	0.671	1
Klucel	2	Aluminum octetate	0.25 percent	Yes	No	Very slight	Thick	—	—	>4
Klucel	2	Aluminum octetate	0.5 percent	Yes	No	Very slight	Good	5,440	0.359	2.5 to 3
Jaguar A20-B	1	Boric acid	20 ppm	No	Yes	Yes	Much too thin	—	—	—
Jaguar A20-B	2	Boric acid	20 ppm	Yes	No	No	Good	7,000	0.215	>4
Jaguar A20-B	2	Boric acid	40 ppm	Yes	No	No	Much too thick	11,400	0.553	~2.5
Gelcarin	3	—	—	No	No	No	Good	12,200	0.429	~2

TABLE 31

SUMMARY OF R-3 FORMULATIONS

Properties	Gelling Agent			
	SeaTex	Cellosize QP 100M	Natrosol 250 HHR	Gelcarin
Order of Preference	1	2	3	4
Concentration of Gelling Agent, percent	1	1.5	1.5	2.5
Cross-Linking Agent	Boric Acid	--	--	--
Concentration of Cross-Linking Agent, ppm	22.5	--	--	--
Pressure Buildup	No	No	Yes	Yes
Syneresis	No	No	No	Slight
Spontaneous Flow Upon Tilting	No	No	Slight	Slight
Appearance, Ambient Temperature	Good	Good	Good	Contained bubbles
η_2	6,400	11,100	18,700	8500
$\frac{d(\log \tau)}{d(\log \dot{\gamma})}$	0.21	0.36	0.15	0.28
K_s	16	38	21	24
Strand Length, inches	1.5 to 2	3	3	1.5 to 2
Appearance After 1 Week at 120 F	No change	Slight Thinning	Drier	Slight Syneresis

η_2 = Apparent Viscosity expressed in centipoises at $\dot{\gamma} = 10^{-2}$ sec^{-1}

τ = Stress, e.g., $dynes/cm^2$

$\dot{\gamma}$ = Shear rate, e.g., sec^{-1}

$N_t = \sqrt{\eta_2}\left(\frac{d \log \tau}{d \log \dot{\gamma}}\right)$

Table 31 N_t, the shear thinning index is defined as $N_t = \overline{\eta_2}\ (d \log \tau / d \log \dot{\gamma})$. Where τ = stress, e.g., dynes/cm^2; $\dot{\gamma}$ = shear rate, e.g., sec^{-1}, and η_2 = apparent viscosity expressed in centipoises at $\dot{\gamma} = 10^{-2}$ sec^{-1}.

This value should be as low as possible to obtain a gel which exhibits minimum pressure drop when flowing through hardware. The formulations are listed in order of preference based on the evaluation of these results. SeaTex is the most desirable gelling agent with Cellosize QP 100 being the next alternative.

Additional experiments were conducted on unloaded gels to learn more about the behavior of SeaTex and Cellosize in MMH. Since the compositions were not loaded with any solid, relatively higher concentrations of gelling agents were required.

A fresh gel containing 1 percent SeaTex and 45-ppm boric acid produced bubbles for the first several hours. The gel swelled more than 10 percent, but the gas escaped after 1 to 2 days, and the gel volume decreased and thereafter remained essentially constant. This gas evolution was not observed in the loaded SeaTex gel described in Table 31 for the following reasons:

1. The loaded gels were older and some of the gassing had already occurred when the gels were stored.
2. The ullage in the loaded R-3 storage jars was larger than in the vessels in which gassing of the unloaded gels was detected.
3. The loaded R-3 gels were blanketed with nitrogen.
4. Detection of pressure buildup in screw cap jars is a less sensitive method of detecting gassing than bubble formation in an unloaded gel.

It is believed that the gas evolution problem is associated with a reaction between MMH and the gellant or with air adsorbed on its surface, because the problem disappeared with aging. Preparation and storage of the gels in the absence of oxygen appeared to improve gel stability.

Centrifuging tests were conducted to learn whether gassing was caused by a reaction with air entrapped during the gel preparation. In each case, duplicate compositions were prepared and one of these was centrifuged within 1 hour after preparation. This treatment apparently had no effect since after 1 or 2 days there was no difference between the centrifuged samples and the corresponding controls.

A comparison of cross-linking efficiency was made between freshly-prepared boric acid solutions and those which were several months old. No noticeable difference was found. However, a solution of SeaTex in MMH generated gas as it aged and became more and more difficult to gel. After a few days, it requires a tenfold excess of boric acid to achieve gelation.

Even as much as 2.5 percent Cellosize did not gel MMH. No swelling could be observed because the gas was released from the viscous liquid.

The final composition of R-3 actually scaled up for engineering characterization is presented in Table 32.

TABLE 32

COMPOSITION OF R-3

Component	Concentration	
	Weight Percent	Volume Percent
MMH	66.3	65.2
Beryllium	11.2	5.2
Beryllium Hydride	22.3	29.7
SeaTex HCB	0.27	
Boric Acid	0.0003	

After SeaTex was selected as the preferred gelling agent, batches of R-3 were prepared and its physical properties were studied. The method of preparation used is described in the Experimental section of this Task.

The flow curves obtained by means of the capillary viscometer are shown in Fig. 40. At a shear rate of 100 sec^{-1}, the apparent viscosity measured was from 340 to 700 centipoises, depending on the length of the capillary used. This behavior is typical of thixotropic (time-dependent) materials; that is, once the gel had passed through the first 10 centimeters of capillary tubing, its resistance to flow decreased. Consequently, when gels were passed through a thinner needle of equal length they exhibited a lower apparent viscosity. Furthermore, the mere introduction of gel into the instrument caused some thinning. After storage in the instrument reservoir for 55 hours, the measured apparent viscosity was higher than when it was measured shortly after introduction of the gel. This thixotropy was not unexpected because SeaTex was chosen (among other reasons), for its outstandingly low shear thinning index, N_t.

Swelling and Gas Evolution

Gas evolution measurements on mixtures of BeH_2 and MMH had already been conducted under the preceding contract (Ref. 1 , page 284). A sample of a complete R-3 gel was tested for gas evolution. The gel was several weeks old and the Pyrex apparatus had been passivated with MMH. Nevertheless, when the gel was transferred, it gassed rapidly for approximately 4 hours and then the gas evolution rate dropped drastically, as shown in Fig. 41. It is suspected that sensitivity to air is responsible for this phenomenon.

Similar observations were made in the case of swelling measurements which were carried out in Babcock bottles extensively pretreated with MMH. The experiments showed that an aged gel swells rapidly when it is first transferred, but the reaction moderates after a few hours. After swelling for several hours, the rate fell in 1 month to 5×10^{-5} volume percent per minute.

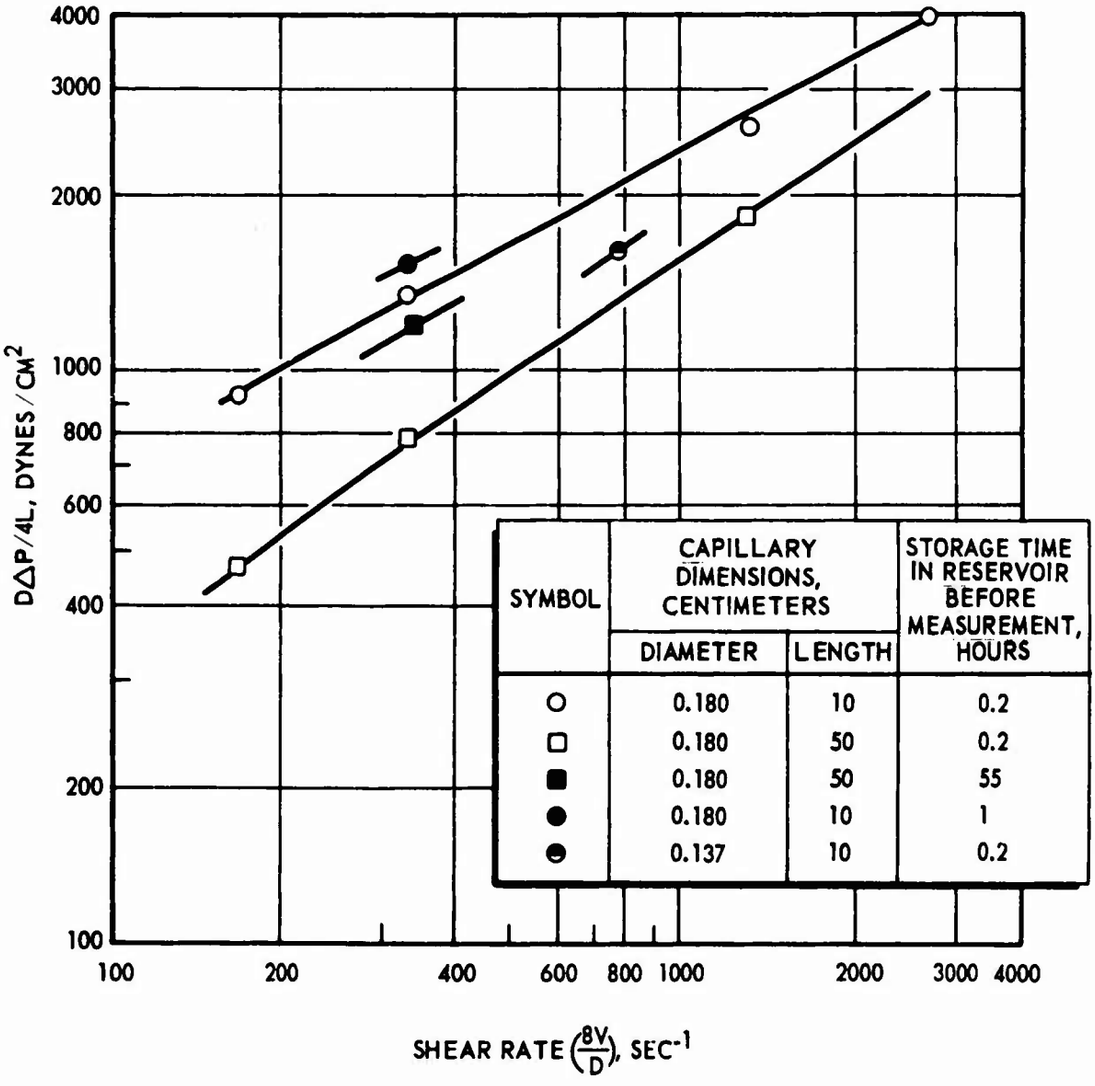


Figure 40 Rheogram of R-3 Gel

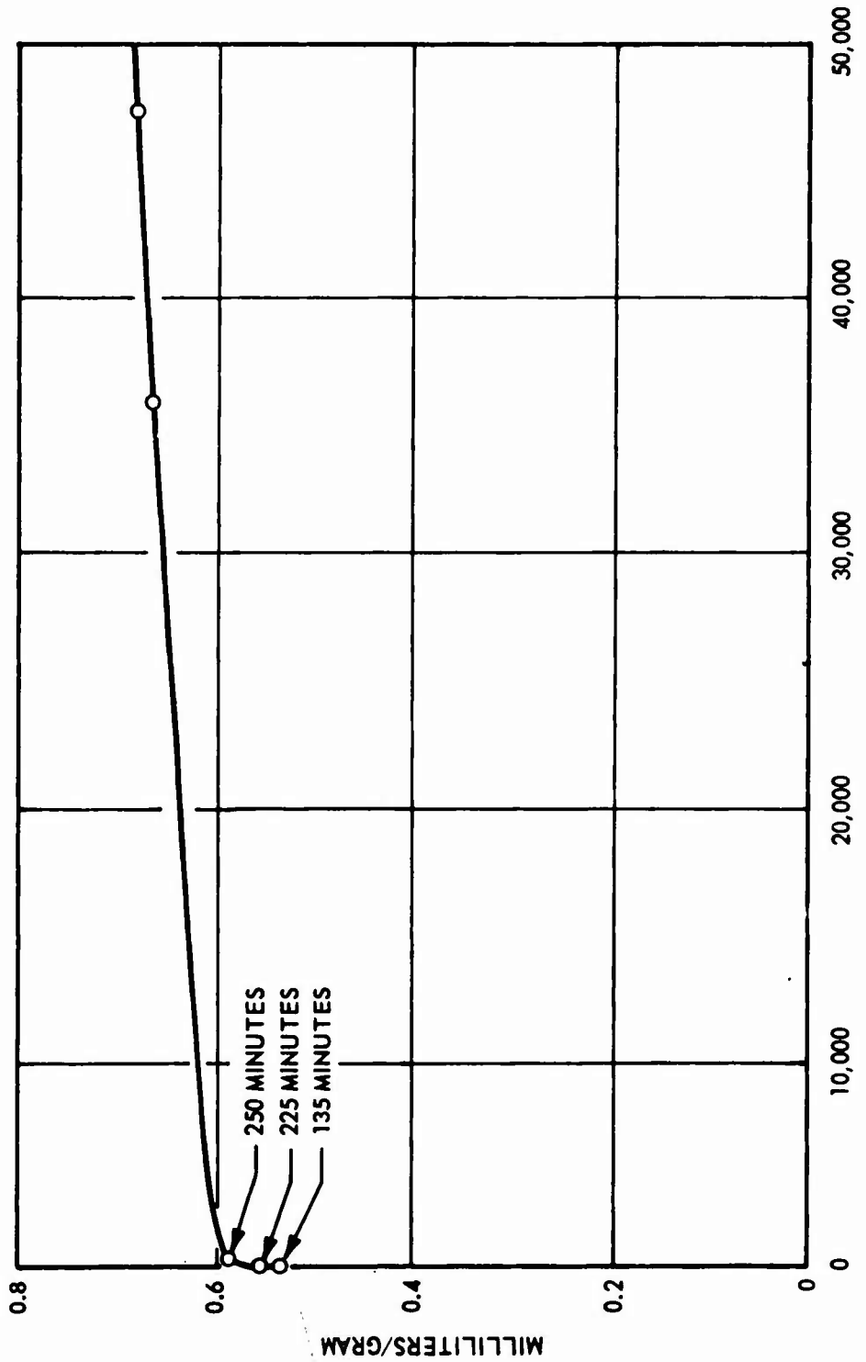


Figure 41. Gas Evolution From R-3 Gel

R-4 Gel

Before continuing development of R-4, begun under an earlier contract (Ref. 1), measurements were made of the compatibility of the major components at elevated temperatures. Gas evolution measurements from a mixture of Be, N_2H_4, $N_2H_5NO_3$, and H_2O at 160 F revealed that a sample containing 1 milliliter of liquid phase generated gas at the rate of 0.2 milliliter/day (converted to STP). In the absence of Be, gas evolution from the liquid phase was one-tenth as rapid, as shown in Table 33.

Analysis of the gases evolved from the metal-containing mixtures showed nitrogen and ammonia to be the major components, the balance being mostly hydrogen and a trace of methane.

TABLE 33

GAS EVOLUTION FROM N_2H_4-H_2O-$N_2H_5NO_3$ (38-24-38)

Time, Days	Cumulative Volume of Gas Evolved, cc STP	
	Neat Liquid	Liquid + 0.23 gram Be
1		0.15
2	0.01	0.32
3		0.44
6	0.12	0.90
7	0.15	1.05
8	0.16	1.46
9	0.19	1.58
12	0.22	2.3

NOTE: Volume of liquid, 1 milliliter
Temperature, 160 F

A search for suitable gelling agents for the liquid vehicle of R-4 included the following candidates:

1. Kelzan (Kelco Co.)
2. SeaTex HCB (Marine Colloids, Inc.)
3. Gelatin (E. H. Sargent and Co.)
4. Natrosol 250HHR (Hercules Powder Co.)
5. Cellosize QP100 (Union Carbide Corp.)
6. CMC 7HXP (Hercules Powder Co.)
7. Klucel HA (Hercules Powder Co.)
8. Jaguar 315 CM (Stein-Hall Co.)
9. Guartec XO-402 (General Mills, Inc.)

During initial tests, conducted with a liquid of composition 24 w/o H_2O-38 w/o N_2H_4-38 w/o $N_2H_5NO_3$, the best gelling agents were apparently Guartec XO-402 and SeaTex HCB cross-linked with boric acid. Gels were formed by the addition of 0.45-percent SeaTex, 0.04-percent boric acid, and 1.2 w/o KCl to the liquid. They were elastic and stable for more than 1 month. The other candidates exhibited one or more serious deficiencies. Kelzan plus AO formed good gels initially but after several hours, gas bubbles were produced and the gels exhibited syneresis. Klucel, Jaguar, and gelatin neither thickened nor gelled the liquid; Natrosol, Cellosize, and CMC merely thickened the liquid.

Reversible transformation of the SeaTex-boric acid gel to a sol occurred at moderate temperatures. Although this behavior limits the maximum temperature at which the gel may be stored, it may permit regenerative cooling if the detonation sensitivity is low. The behavior of various gels on heating and cooling is presented in Table 34. The gel-sol transformation temperature was raised at higher SeaTex concentrations.

TABLE 34

BEHAVIOR OF H_2O-N_2H_4-$N_2H_5NO_3$ GELS ON HEATING AND COOLING

Composition (Additives)	Transition Temperature, F			
	On Heating		On Cooling	
	Elastic Gel to Liquid With Structure	Liquid With Structure to Liquid Without Structure	Liquid Without Structure to Liquid With Structure	Liquid With Structure to Elastic Gel
0.45-Percent SeaTex 0.036-Percent H_3BO_3	98	112	108	94
0.6-Percent SeaTex 0.036-Percent H_3BO_3	107	128	127	107
0.75-Percent SeaTex 0.036-Percent H_3BO_3	118	150	146	122
0.45-Percent SeaTex 1.2-Percent KCl 0.030-Percent H_3BO_3	101	113	114	96

Small samples of R-4 containing 12.6 v/o beryllium in 24 w/o H_2O-38 w/o N_2H_4-38 w/o $N_2H_5NO_3$ (theoretical specific impulse of 311 seconds) were gelled with 0.6 w/o SeaTex and 0.04 w/o boric acid. These samples remained stable for more than 1 month at room temperature, and exhibited good stability on centrifuging at 50 g.

To attain a theoretical performance of 315 seconds with R-4, it is required that the liquid contain less than 9.1 w/o H_2O and more than 53 w/o $N_2H_5NO_3$. SeaTex gels prepared with this composition were observed to thin out in a few days at room temperature.

The loaded R-4 mixtures prepared are listed in Table 35. These gels were elastic, nonadherent, and several showed good storage stability at ambient temperature.

Several gelling agents were tested for the R-4 system, and Guartex XO-402 and SeaTex HCB cross-linked with boric acid were most promising. Several methods were used to prepare the mixtures, and satisfactory gels were produced by most procedures. However, it was not found satisfactory to hand stir the premixed solids (including hydrazine nitrate) into a solution of the gelling agent. This did not produce sufficiently uniform gels to prevent settling of the metal powder.

Most of the R-4 mixtures remained cohesive and elastic for more than 1 month and only a few mixtures (No. 7 and 9) increased in volume. Further work on R-4 was suspended at the request of the Air Force.

R-5 Gel

Theoretical Calculation. The R-5 monopropellant as first conceived, contained a mixture of beryllium and BeH_2 powders dispersed in a mixture of nitric acid, water, and more than sufficient hydrazine to neutralize all

TABLE 35

PREPARATION OF R-4 GELS

Number	Be Lot	Gelling and Cross-Linking Agent	Method	Gelling Agent Concentration, weight percent	Cross-Link Agent Concentration, weight percent	Composition, weight percent				Ambient Stability*
						Be	H_2O	$N_2H_5NO_3$	N_2H_4	
1	3913	SeaTex/Boric acid	1	0.45	0.02	18.7	19.5	30.9	30.9	0
2	3913	SeaTex/Boric acid	1	0.45	0.04	18.7	19.5	30.9	30.9	0
3	3913	SeaTex/Boric acid	1	0.60	0.04	18.7	19.5	30.9	30.9	3
4	3913	SeaTex/Boric acid	1	0.70	0.04	18.7	19.5	30.9	30.9	3
5	4464	SeaTex/Boric acid	3	0.70	0.016	16.5	20	30	33	3
6	4391	SeaTex/Boric acid	2	0.70	0.016	16.5	20	30	33	3
7	4391	Guartec X0-402	2	0.70	--	16.5	20	30	33	3
8	4464	Guartec X0-402	4	0.50	--	16.5	20	30	33	settling
9	4464	Guartec X0-402	3	0.70	--	16.5	20	30	33	3
10	4464	Guartec X0-402	4	0.75	--	16.5	20	30	33	settling

Method:
1. The SeaTex solution, R-4 liquid (H_2O, $N_2H_5NO_3$, and N_2H_4), and metal powder were mixed by hand; H_3BO_3 was then stirred in.
2. The solids were premixed, added to the liquid, and blended.
3. Solid gelling agent was mixed with the liquid in the blendor; the metal powder was then blended in
4. Solid $N_2H_5NO_3$ was stirred into a solution of gelling agent; metal powder was then stirred in by hand.

*Stability: 0 = few hours; 1 = 1 week; 2 = 1 week to 1 month; 3 = over 1 month

AFRPL-TR-66-294

of the nitric acid. This mixture had been optimized theoretically for maximum impulse at 35 v/o solid loading. It was hoped that the excess water would reduce the rate of reaction between BeH_2 and N_2H_4 to an acceptable level.

However, when these mixtures were prepared in small quantities, they were found to bubble at a rate which appeared somewhat excessive. Additional theoretical calculations were performed using vehicles which did not contain free hydrazine, because such liquids were believed to be less reactive with beryllium hydride. The theoretical specific impulse and chamber temperature for such a neutral R-5 are shown as functions of composition in Fig. 42. For a stoichiometric mixture of BeH_2 in 40 60 H_2O $N_2H_5NO_3$, the specific impulse is 336 seconds.

Except for mixtures near stoichiometric composition, the impulse is nearly independent of the concentration of hydrazine nitrate in the liquid phase, but decreases sharply with decreasing solids loading. The calculated chamber temperature decreases with increasing solids loading and with decreasing hydrazine nitrate content. Theoretical impulses of 315 to 336 seconds are attained at loadings from 36 to 49 v/o. These compositions exhibit flame temperatures from 3150 to 2890 K when using the 40/60 H_2O/ $N_2H_5NO_3$ liquid. Hydrazine nitrate concentration also influences detonation propagation characteristics and combustion properties. Furthermore, the maximum solids loading acceptable is a function of acceptable rheological properties. Therefore, the optimum composition must be a compromise reflecting impulse, safety, flow properties, flame temperature, and combustion.

The optimum ratio of Be to BeH_2 varies with solids loading. The concentrations of Be and BeH_2 (amorphous) R-5 which give the highest theoretical impulses at various loading levels are shown in Fig. 43. At the lowest loading (20 v/o), the solid is preferably entirely metal, and at 48 v/o solids loading (stoichiometric maximum specific impulse) the mixtures involve BeH_2 only.

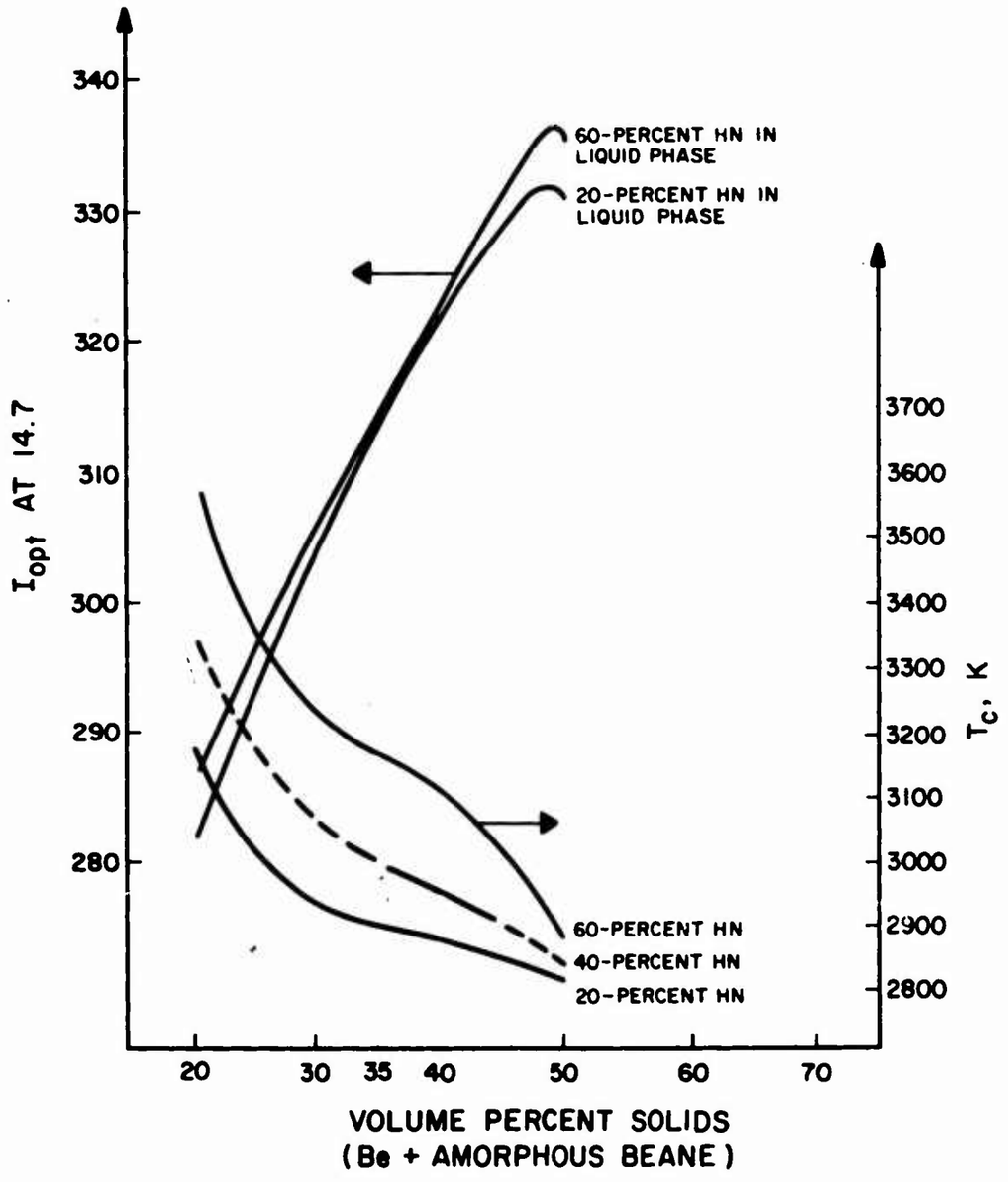


Figure 42. Be and BeH_2/Hydrazine Nitrate in H_2O, Specific Impulse and Temperature vs Volume Percent Solids

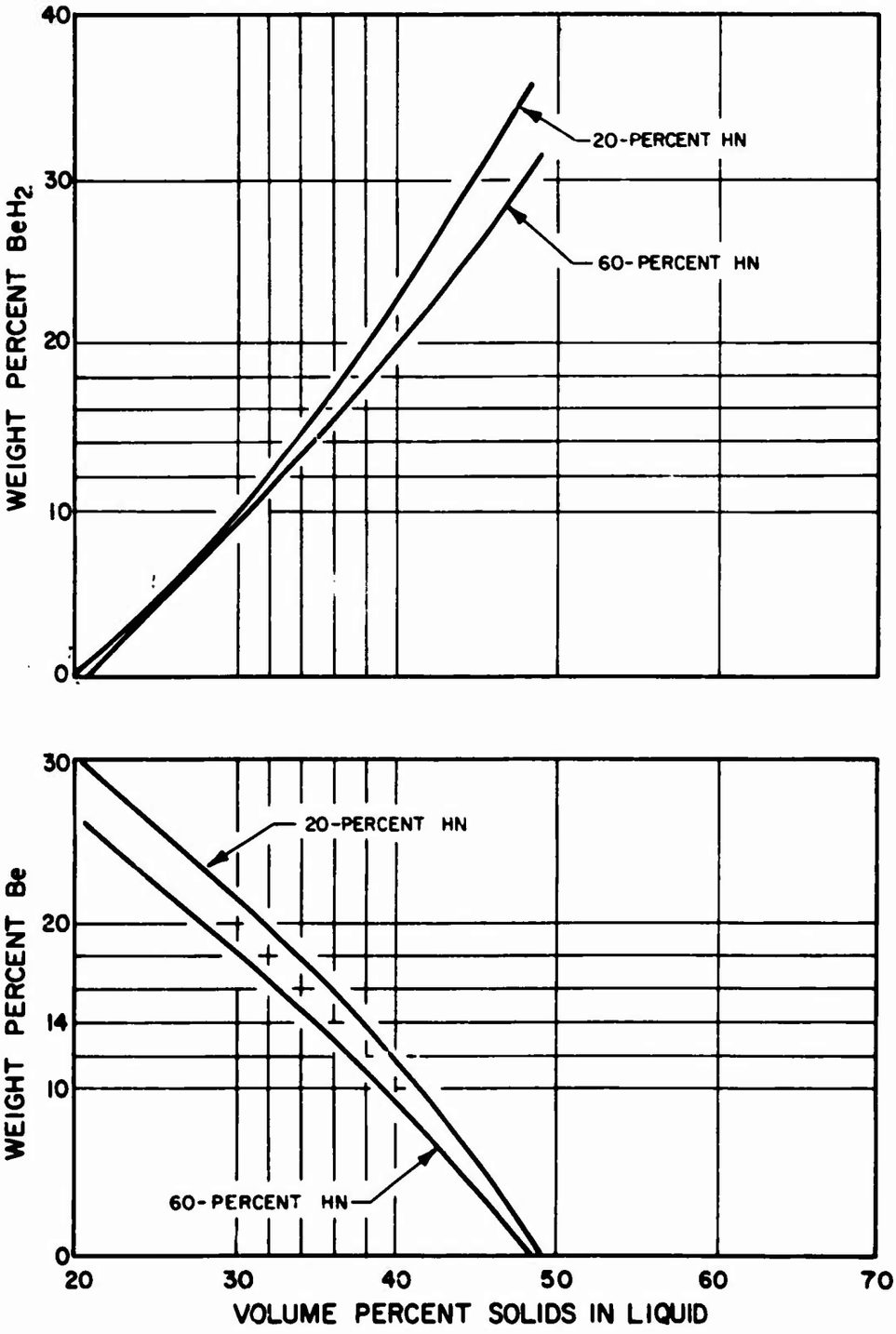


Figure 43. Be and BeH_2/Hydrazine Nitrate in H_2O, Weight Percent Be and BeH_2 vs Volume Percent Solids

Formulation. Preparation of R-5 mixtures at low hydrazine nitrate concentration was initiated before the detailed theoretical calculations described previously were completed. The work was first designed to select suitable gellants, and to determine the maximum loading that could be achieved while retaining fluid properties.

Before preparing loaded R-5 mixtures, unloaded gels were prepared with a liquid containing 31 w/o $N_2H_5NO_3$ and 69 w/o H_2O. The following gelling agents were tested:

1. Guartec XO-402 (General Mills)
2. Cab-O-Sil M-5 (Cabot Corp.)
3. Jaguar 315CM (Stein-Hall Co.)
4. SeaTex HCB (Marine Colloids, Inc.) and boric acid
5. Kelzan (Kelco Co.) and aluminum octanoate
6. Natrosol 250 HHR (Hercules Powder Co.)
7. Klucel HA (Hercules Powder Co.)
8. CMC 7HXP (Hercules Powder Co.)
9. Gelcarin SI (Marine Colloids, Inc.)
10. Gelatin (E. H. Sargent and Co.)
11. Thixcin R, GR, and E (Baker Castor Oil Co.)

Only the first five agents formed promising gels. They were subsequently tested on a loaded system.

It was found that relatively large quantities of Cab-O-Sil would be required, which is undesirable because silica compromises specific impulse. The R-5 gels prepared with Jaguar and SeaTex deteriorated with time, especially at high nitrate concentrations. Thus Guartec XO-402 and Kelzan are the preferred gelling agents. There was little difference between

these, except that the gelation speed for Guartec XO-402 is reported to be pH dependent. For example, complete gelation of 60-percent ammonium nitrate occurs in 30 minutes at a pH value of 3.5 but requires 16 hours at a pH value of 6.7. Kelzan does not exhibit this marked pH dependence and is superior to Guartec in this respect.

Loading of R-5 Gels. Loaded R-5 compositions were prepared both with amorphous Beane (Ethyl Corporation Lot No. 44) and with dense Beane (Lot No. E 121). The use of amorphous Beane resulted in a stiff paste at 40 v/o loading when an R-5 composition was prepared, using equal weights of beryllium and Beane in a liquid containing 40-percent hydrazine nitrate in water.

At 35 v/o loading, amorphous Beane formed satifactory gels. However, dense Beane formed fluid slurries at much higher loadings. A mixture was prepared corresponding to the stoichiometric composition, containing 45 v/o dense Beane in a 60/40 solution of $H_2O/N_2H_5NO_3$. It was found to be a free-flowing slurry. However, dense Beane was found to react faster with the liquid than did amorphous Beane. After ball-milling samples of each type and treating them with water for 1 week, the beryllium hydride assay of the amorphous material remained unchanged, whereas the assay of the dense Beane was reduced to less than one-third of its original value. This disqualified dense Beane as an ingredient in R-5. Ball-milling the amorphous Beane appeared to be a useful tool for permitting increased loading of amorphous Beane.

Sensitivity of R-5. The thermal stability of the R-5 monopropellant was investigated in the JANAF thermal stability apparatus. This test consists of heating a sample of the material in a closed bomb at a constant rate. The sample temperature and the temperature difference between the sample and the bath are measured as a function of time. Exothermic reactions in the sample are indicated when the rate of temperature increase of the sample exceeds that provided by the heating bath. Results are reported

as "self-heating rate" vs reciprocal absolute temperature. Data are evaluated using two criteria: (1) the temperatures at which some arbitrary rate of self heating occurs, usually the lowest practical rate observable, and (2) by the slope of the self-heating rate curve vs reciprocal temperature, which is related to the activation energy in the Arrhenius rate equation. A more detailed description of the test and its interpretation is presented in Ref. 36. The test was slightly modified in that a 30-cc Hoke cylinder was attached to the burst diaphragm in such a way that all reaction products would be contained. The entire apparatus was discarded after the test.

Two tests were conducted. During both tests an observable reaction first occurred at approximately 330 F which drove both the sample temperature and the temperature difference recorders off scale in less than 1 minute. Because the self-heating rate curve was very steep, data reduction proved difficult. The data for these tests are plotted in Fig. 44 , with reference curves for hydrazine and ethyl nitrate. The results indicate that R-5 is more temperature sensitive than hydrazine and ethyl nitrate. However, it is not so sensitive on the basis of this test as to preclude engine testing if suitable precautions are taken.

The drop weight sensitivity was also investigated. Six tests were conducted using the Olin Mathieson drop weight tester, three with freshly prepared gel and three with a gel prepared several weeks earlier. All of the tests were conducted at 10 ft-lb or more; none gave positive reactions. However, n-propyl nitrate showed a 50-percent probability level at less than 6 ft-lb while ethyl nitrate showed a 50-percent level at less than 1/3 ft-lb. (The values quoted for standard materials are higher than normal because the apparatus was modified by enclosing the sample holder in a plastic bag to contain the combustion products.)

The sensitivity of an R-5 composition with respect to electric discharges was also checked. The liquid phase of the mixture contained 40-percent hydrazine nitrate in water. The material was probed repeatedly with the arc from a Tesla coil, but no visible reaction took place.

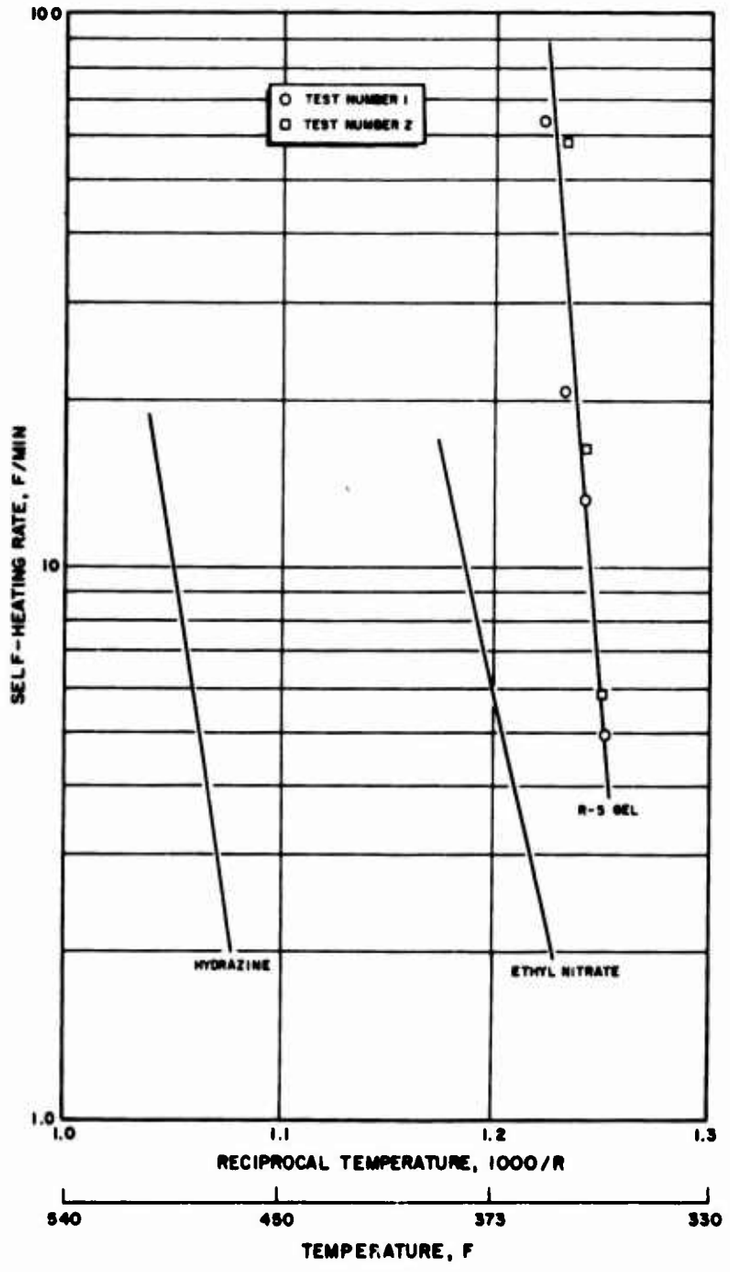


Figure 44. Thermal Stability of R-5 Gel

Detonation propagation tests with R-5 are described in the Engineering Characterization section of this report.

The composition of the R-5 gel prepared in sufficient quantity for engineering characterization is presented in Table 36.

TABLE 36

COMPOSITION OF R-5 GEL

Component	Concentration	
	Weight Percent	Volume Percent
Water	35.4	65.2
Hydrazinium Nitrate	35.4	
Beryllium	14.4	9.0
Beryllium Hydride	14.4	25.9
Kelzan	0.5	--

EXPERIMENTAL

Mixing Facility

To prepare batches of heterogeneous propellants in sufficient quantity for use in ignition and motor firing tests, a propellant formulation plant was constructed. To minimize toxic hazards, this was contained in an enclosed booth and most operations were conducted remotely. The plant had a 1-gallon capacity, and consisted basically of two cylinders made of 4-inch ID glass pipe, each with a capacity in excess of 1 gallon. Mixing was achieved by forcing the components of the propellant mixture back and forth between the cylinders and through the revolving blade of a Polytron mixer located in the bottom flange of one of the columns (Fig. 45).

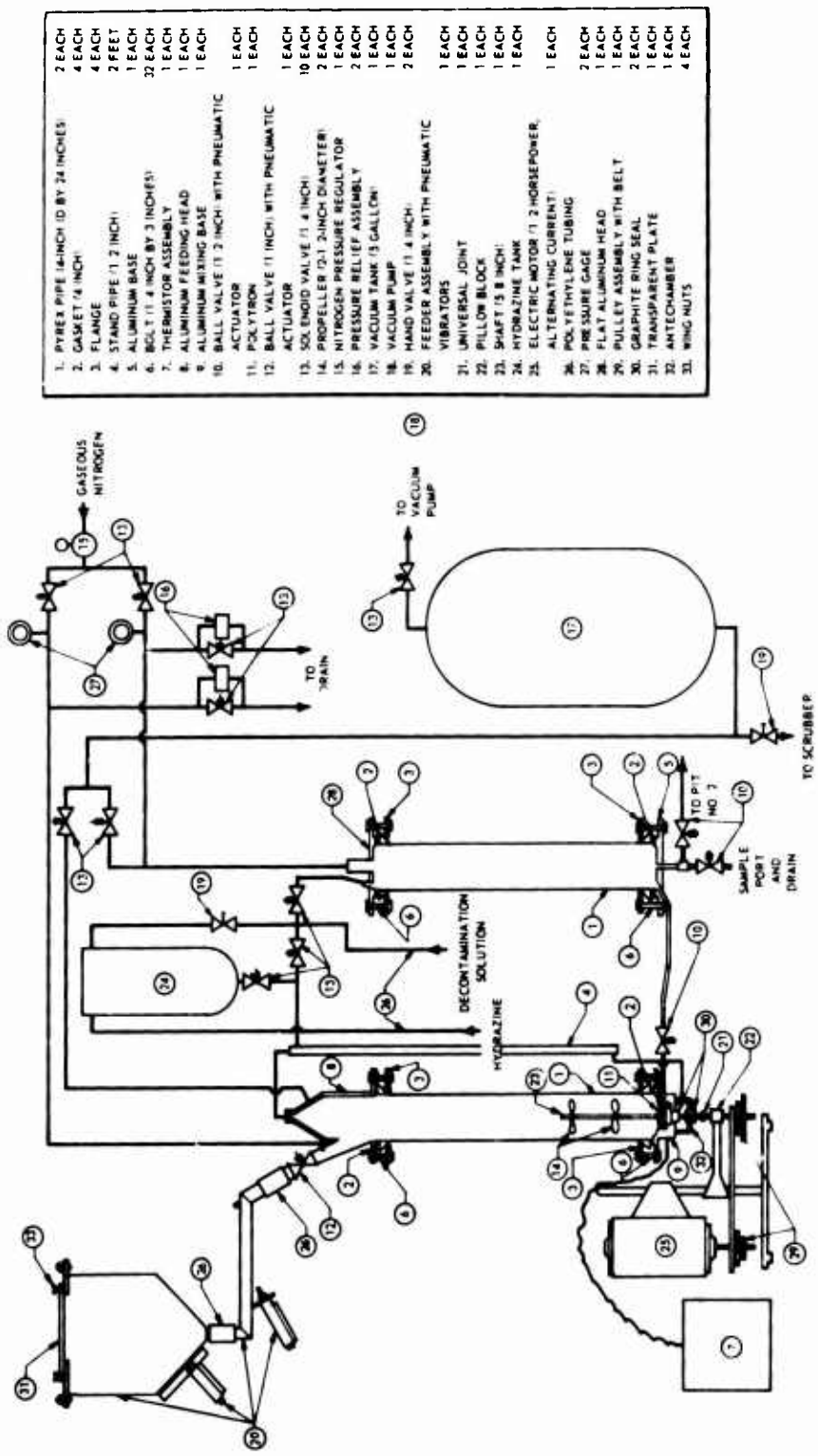


Figure 45. Gel Mixing Facility

The mixing equipment was operated as follows. The hydrazine storage tank was first charged by placing the required amount in a polyethylene jug and then transferring it in a flexible line under vacuum. The solid powders were premixed, weighed, and bagged in a glove box before bringing them to the equipment. The bag was placed inside another larger bag, the opening of which had been taped to a cardboard cylinder (a 1-gallon paper cup with the bottom removed). This receptacle fitted the opening on the feeder so that feeder, cup, and large bag formed an airtight envelope, i.e., the powder could be poured into the solid feeder without scattering toxic dust. From this time on, the mixing operation was carried on from a control panel outside the mixing booth.

Next, some hydrazine was gravity fed into the left column and incremental amounts of powder were added. This mixture was stirred by paddles attached to the electric motor. More hydrazine and solids were added and the process was repeated. When the left column was approximately one-third full, the contents were drawn by vacuum into the right column. Feeding of solids and liquids was continued. This was repeated until all the components had been introduced.

Mixing was continued by passing the gel back and forth from one column to the other with the mixing motor on.

Finally all of the gel was pushed into the right column under nitrogen pressure. Thereupon the line between the columns was closed and the line leading to the firing pit was opened so that the gel could be transferred under nitrogen pressure. Gel samples were taken at the time of the transfer and were used to determine the Be content and physical properties.

While the facility functioned smoothly during the original shakedown with inert ingredients, several mechanical problems slowed down the subsequent operation. The various components are discussed in the following paragraphs.

Feeder. The feeder used was a Cleveland Model FM-A-112-50 Special Air-Powered Vibrator Feeder Machine with 1/2 cu ft supply hopper, Drawing S-1234, feeding into a 1-inch horizontal tube also supplied with an air-powered vibrator. The contact surfaces were constructed of Type 304 stainless-steel. While this feeder was capable of feeding some powders with a 90-degree angle of repose at rates up to 25 lb/min, it was found that the exit would often bridge when feeding the fine beryllium powder, even though the hopper itself vibrated. It was clear that future installations should feed straight down, preferably through tubes somewhat larger than 1 inch. Because the transparent top plate became quite dusty, good lighting or a level indicator was also desirable.

Valve. The valve used in the powder chute was a Pacific 1-inch ball valve with a pneumatic operator. No problems were encountered. In future installations, it appears appropriate to place it into a vertical powder feed line connecting the hopper and mixer.

Glass Vessels. The cylindrical glass vessels, fabricated of 4-inch Pyrex pipe, were pressure tested in situ at 65 psi. No failures were encountered but two shortcomings were noted. First, the glass did not remain transparent once the loaded gels had contacted it. It therefore took an intense light source to find the liquid levels, especially in the case of the more adhesive, less cohesive compositions. The second shortcoming was the fact that the Pyrex pipe was not a true cylinder, rather it was manufactured from tubing and flanges, the axes of which were offset more than 1/8 inch. This prevented the smooth functioning of floating pistons intended to maintain the levels in the gel. These pistons were eventually removed.

Introduction of Liquids. The introduction of the liquids into the system was not a problem; small pneumatic pumps were used at first, but these were almost unnecessary because liquids, i.e. hydrazine or wash solution, could be drawn into the storage vessel under a slight vacuum.

Mixing Blades. The Polytron mixing blades performed satisfactorily shearing the gel, but some of the drier portions of the mixture did not feed readily into the blade. For this reason the drive shaft was extended and additional 2 1/2-inch propeller blades were added to force the mixture downwards.

Submerged Rotary Seal. The submerged rotary seal of the Polytron unit caused more problems than all other components combined. The seal wore out quickly and the gel leaked out. To prevent this, the seal was rebuilt using spring-loaded graphite rings. Even then, there was considerable wear and a second set of seals was added. The volume between the seals was filled with neat liquid at a pressure slightly higher than the mixing vessel, so that any leaking encountered would be that of pure hydrazine either to the outside or into the vessel. As a result of these difficulties, the rotary seal has been avoided in the more recent design of a large mixing facility.

Pipe Lines. The pipe lines, through which the gels passed, plugged occasionally. The lines were fabricated of 1/4-inch tubing; no further problems were encountered when 3/8-inch tubing was substituted.

Materials

Amine Fuels. The hydrazine used throughout was propellant grade. Its composition was determined periodically and was assayed from 98.5- to 98.9-percent N_2H_4, 0.3- to 0.7-percent NH_3, and 0.7- to 1.1-percent water.

The MMH used was propellant grade and was taken from a single 55-gallon drum. Periodic analysis showed that it contained 0.5-percent water, 0.2-percent ammonia, a trace of monomethylamine, 0.1-percent other soluble impurities and assayed 99.2-percent MMH. Its density was 0.872 gm/cc.

Beryllium. Except during a few experiments, the beryllium powder used in the preparation of R-2 mixtures was Beryllium Corporation's Grade PS-98. The manufacturer's specifications for this material and for their PS-97 grade include the following chemical compositions:

	Grades	
Component	PS-97, percent	PS-98, percent
Beryllium Oxide	< 0.5	< 0.5
Carbon	< 0.3	< 0.3
Magnesium	< 0.3	< 0.1
Chromium	< 0.4	< 0.3
Other Metallics (total)	< 0.8	< 0.3
Beryllium Assay (total)	>97.0	>98.0

The vendor's chemical analysis and size distribution of the particular lots of PS-98 beryllium powder are listed in Table 37.

During several experiments described earlier, beryllium powder was used as supplied by Brush Beryllium Company (designation FP-17). However, because greater gel stability of R-2 was observed generally with the Beryllium Corporation product, the latter was used exclusively in the later formulations.

Beane. The BeH_2 used was amorphous material (lots No. 44 and 49, Ethyl Corporation). Dense Beane, used in the preparation of R-5, was from the manufacturer's lot No. E 121. The manufacturer's analyses for these lots is reproduced in Table 38.

Although the particle size distribution for lots No. 44 and 49 suggest that particles larger than 100 microns in diameter were completely absent, a few hard clinkers up to several millimeters in size were found. If these large particles had not been broken up during preparation of heterogeneous propellants, they could have plugged the injector orifice (0.060-inch diameter). Accordingly, beryllium hydride was screened through a

TABLE 37

COMPOSITION AND SIZE DISTRIBUTION OF BERYLLIUM POWDERS

Component	Weight Percent in Lot Number						
	R-2360	R-3913	R-2283	R-4464	R-4391	R-4949	R-5075
BeO	< 0.5	< 0.5	< 0.5	< 0.5	< 0.5	< 0.5	< 0.5
C	0.100	0.09	0.44	0.23	0.43	0.45	0.41
Fe	0.170	0.095	0.132	0.067	0.068	0.092	0.100
Al	0.061	0.088	0.210	0.174	0.091	0.083	0.069
Ni	0.017	0.008	0.019	0.008	0.013	0.018	0.015
Si	0.050	0.035	0.049	0.062	0.060	0.083	0.082
Mg	0.065	0.109	0.063	0.050	0.095	0.050	0.038
Mn	0.010	0.011	0.011	0.012	0.014	0.009	0.013
Cr	0.075	0.080	0.470	0.200	0.340	0.420	0.355
Average Particle Size, microns	24	23*	7.7	15.5**	7.7**	7.3**	6.8**
Particle Size, microns	Cumulative Weight Percent Smaller Than Specified Size						
44	99.7						
37	98.0	96.5					
35			98	92	99	99	99
30	68.9	71					
20	36.1	40	93	66	90	92	93
15			82	48	83	85	84
10			63	33	64	68	70
5			25	10	24	28	28

*Determined by microsieve
**Determined by Coulter Counter

TABLE 38

COMPOSITION AND CHARACTERISTICS OF BEANE

Component	Weight Percent in Lot Number		
	44	49	E 121
Total Carbon	1.78	1.76	
Total Hydrogen	17.39	17.36	
Total Chloride	0.11	0.61	0.8
Beryllium Hydride	93.5	92.9	88.4
Beryllium Metal	2.2	2.3	2.5
Beryllium Alkyls			3.0
$(t\text{-}Bu)_2$ Be	1.4	2.7	
$(C_3H_7)_2$ Be	0	0.1	
(C_2H_5) Be	0.6	1.5	
Beryllium Alkoxides	0.67	1.15	0.3
Volatiles	0.25	0.22	Nil
Lithium			1.6
True Density, gm/cc	0.64	0.65	0.77 to 0.79
Bulk Density, gm/cc	0.27	0.28	
Particle Size, microns	Cumulative Weight Percent Greater Than Specified Size		
30	100	100	
40	96	99	
50	74	86	
60	42	54	
70	14	27	
80	18	7	
90	1	2	
100	0	0	

U.S. Standard sieve number 80 (177-micron opening) in the dry box before incorporating it into the propellants used for motor firing tests.

Gelling Agents. Kelzan was the preferred gellant for R-2 and R-5 propellants. It is a high molecular weight biosynthetic polysaccharide supplied by Kelco Company. Kelzan solutions have several useful properties including the following:

1. Viscosity shows practically no change with temperature variation
2. Excellent stability in alkaline solutions
3. Good freeze-thaw stability
4. High viscosity at low concentrations
5. Extreme pseudoplasticity

The aluminum octanoate used to cross-link the Kelzan-hydrazine solution was supplied by Leffingwell Chemical Company (designation Aluminum Okto-8). A similar product of Witco Chemical Company behaved identically.

Preparation of R-2

Batches of R-2 for laboratory characterization were mixed in a Waring Blendor. Large batches for engine testing were prepared either in the mixing facility described above, or in Waring Blendors. The following procedure was used to minimize escape of toxic dust. Preweighed quantities of Kelzan and aluminum octanoate were added to the weighed metal powder in screw cap polyethylene bottles in a dry box and shaken to blend the dry ingredients. The required quantity of hydrazine was poured into a Waring Blendor jar. The blendor jar and polyethylene bottle were placed in a polyethylene bag so that it could be flushed with nitrogen in a fume hood. Next, the bag was sealed with tape and placed on the blendor base in such a way as to cut a clean hole in the bag where the stud of the drive motor engaged the socket head drive shaft of the blending assembly. The motor speed was controlled with a variable transformer. With the motor running at low speed, the mixed solid was gradually added to the hydrazine.

Then, the motor speed was increased as addition of solids proceeded. After addition of all the solid, the blendor was run at high speed for a minute. The polyethylene bag was opened, and the gelled mixture was poured into a passivated polyethylene bottle for storage. The bag and its contents were taped up and discarded in the toxic waste container. A clean bag was used for preparing each batch of gel.

Small batches (150 grams or less) of gel were generally prepared with a Monel semi-micro Waring Blendor or by stiring manually. Larger batches were prepared using Pyrex blendor jars.

Preparation of R-3

Based largely on the statistical test program (Appendix B), the following formula was arrived at for preparing laboratory-size batches of gelled R-3 propellant.

Beryllium powder (57.3 grams) was mixed with 114.6 grams of beryllium hydride and 1.37 grams of the SeaTex gelling agent. A Waring Blendor was then loaded with 390 milliliters (340 grams) of MMH. The powder was then added in five or six portions while the mixer was turning slowly, always waiting more than 10 seconds to permit dispersion of the powder. When all of the powder was well dispersed, the mixer was speeded up and 1.5 milliliters of an MMH solution containing 1.0 mg/ml of boric acid was added quickly into the vortex of the dispersion by means of a hypodermic syringe. The batch stiffened within seconds.

Preparation of R-5 gel

To prepare a batch of R-5 gel in the laboratory, the following procedure was developed.

The liquid phase was first prepared by placing 68.2 grams of hydrazine and 100 grams of water into a beaker cooled with ice water or a colder

mixture. Dry Ice presents problems because of CO_2 dissolving in the product. The beaker was provided with a magnetic stirrer. A mixture of 189 grams of 70-percent HNO_3 and 43 grams of water, no warmer than ambient temperature, was then placed into a dropping funnel. The acid was added dropwise to the hydrazine as it was being stirred. The acid flow was stopped temporarily whenever the hydrazine reached room temperature. This procedure produced 400 grams of 50-percent hydrazine nitrate solution.

When all the acid had been added, the pH values of the mixture was adjusted by the addition of a few drops of either hydrazine or nitric acid solution. Most of the hydrazine nitrate solutions prepared in this manner were made just slightly acid to methyl red.

The gel itself was made by mixing the powdered beryllium with sieved Beane and Kelzan, the gelling agent. The hydrazine nitrate solution was then measured into a Waring Blendor and the powder mixture was added in four or five increments, mixing each one of them into the propellant before adding more. Mixing was then continued intermittently for several minutes at low speed to avoid overheating.

The quantities used were changed from time to time. In the case of the 50/50 hydrazine nitrate/water solution, 91.5 grams of powdered beryllium, 91.5 grams of the amorphous Beane, and at least 3.0 grams of Kelzan were blended into 357 milliliters of the liquid. This concentration of gelling agent represents the one that was used, but slightly higher values may be desirable.

The entire procedure must be considered potentially hazardous, despite the fact that one test was conducted with a 60/40 HN/water R-5 gel which was allowed to churn at top speed in a Waring Blendor, at a remote location and at a safe distance for 10 minutes without incident. Any droplets or residue on hardware, stirring rods, or disposal bags must not be permitted to dry, because the residue contains crystaline hydrazine nitrate.

Another necessary precaution is to avoid direct sunlight. Being quite black, the material will heat rather rapidly.

Swelling Measurements

Swelling measurements were made in Babcock bottles previously passivated by the following procedure:

1. Washing with Alconox and water
2. Rinsing three times with distilled water
3. Heating with 50-percent hydrazine at 120 F for 24 hours
4. Rinsing with fresh 50-percent hydrazine

The bottles were filled with gel to the lowest mark on the neck by expelling the gel from a large syringe or by suction. Passivation with MMH was used prior to making similar measurements on R-3.

Adhesion

A simple test device was used to measure the amount of a gel which adhered to the inside of an aluminum tube after the gel had been expelled by the sudden application of gas pressure. The device consisted of a 200-milliliter metal chamber and a 5-milliliter glass syringe, which were attached through quick-opening valves to a metal tee at the ends of a 0.25-inch steel tube.

The chamber was first pressurized with nitrogen at 30 psi and closed off. Then the open end of the steel tube was dipped into the gel so it could be withdrawn by means of the syringe. After 2-milliliters of gel had been introduced, the valve leading to the syringe was closed carefully, the outside of the tube was wiped and the gel was expelled by opening the valve to the pressure chamber.

The gel retention was calculated from weights of the tube before and after extrusion. Some dramatic differences were observed; for instance, 2-gram samples of hydrazine-Kelzan gel left only a 0.005-gram residue, while a water-Carbopol gel left 0.234 gram. This technique was used in evaluating the various R-3 formulations prepared in the statistical experiment described previously.

Flow Properties

Rheograms of R-2 (Fig. 39) and R-3 (Fig. 40) were measured with the capillary viscometer. Because it has been described in an earlier report (Ref. 1 , p. 338), the details will not be repeated. The equipment consisted of a syncronous motor which expelled oil from a cylinder at a known rate by means of a gear-driven piston. The oil was transmitted by flexible tubing into the top of a vertical cylinder filled with the gel. The gel was expelled downwards through capillary tubing. The latter can be changed readily. A free-floating Teflon piston prevented mixing of oil and gel. The pressure in the oil was measured by gages which operated over high (0 to 150 psi) or low (0 to 50 psi) pressure ranges. The rate of flow was known from the gear ratio of the syncronous motor.

Industrial Hygiene

Because of the toxicity of beryllium and its compounds, precautions were taken to protect personnel working on this program and to prevent the spread of toxic dust within and outside the laboratory areas. These precautions are described in Appendix C, Safety Standard Operating Procedure, Toxic Chemicals Laboratories.

CONCLUSIONS

Four high-energy storable propellant compositions were formulated. These gels had excellent physical characteristics because they were cohesive and did not adhere to container surfaces; they exhibited shear-thinning

and were mechanically stable. Three of these were prepared in quantities sufficient for engineering characterization.

The preferred gellant for R-2 (Be-N_2H_4) formulations was a mixture of Kelzan and aluminum octanoate (AO). The concentration of gellant required to produce a mixture with a given apparent viscosity was dependent on the characteristics of the beryllium powder and on its loading. Finer powders (Beryllium Corporation lots No. R-2283 and R-3913) required a higher concentration of Kelzan than a coarser one (lot No. R-4464). Highly loaded (52 w/o Be) gels were formulated with lower concentrations of AO than normally loaded ones (28.5 w/o Be). The highly loaded gels were noticeably thixotropic, whereas the normally loaded gels were not.

Addition of either aluminum or beryllium increased the swelling rate of Kelzan-AO hydrazine gels. The swelling rate of R-2 gels depended on both the particular lot of beryllium powder and on the solids loading. Lot No. R-4464 beryllium powder produced gels that swelled faster than lots No. R-4391 or R-4949 which consisted of smaller particles and had a higher chromium content. Because excessive swelling renders the gel nonstorable, the behavior of normal R-2 gels containing lot No. R-4391 beryllium was investigated. The swelling rate was reduced to one-half by washing the metal powder with water before incorporating it into a gel. Highly loaded gels swelled three to four times faster than normally loaded ones, presumably because the surface area of metal in contact with a given quantity of hydrazine was higher in the highly loaded than in normal R-2 gels.

A statistical design was used to optimize mixing conditions for the preparation of R-3 (Be + BeH_2 in MMH), and to select the most suitable gelling agent. The preferred gellant was SeaTex HCB which was cross-linked with boric acid. It exhibited the greatest amount of shear-thinning of the four candidates that survived extensive testing. The final R-3 gel was distinctly thixotropic.

A monopropellant (R-5) was produced with 35 v/o solids loading (1:1 mixture by weight Be and B_2H_2) in gelled 50/50 water/hydrazine nitrate; it had a theoretical specific impulse of 315 seconds. Sensitivity was determined by drop weight and JANAF thermal stability tests. Detonation propagation tests were accomplished and are reported elsewhere in this Document.

MECHANISM OF HETEROGENEOUS PROPELLANT INCOMPATIBILITY

INTRODUCTION

The goal of this task was to elucidate the mechanisms of the gas-forming reactions which occur during the storage of heterogeneous propellants. The specific points which appeared particularly important to resolve were (1) the site and products of the gas-forming reaction in the Be/N_2H_4 system, (2) the effect of oxygen on the rate of gas formation, (3) the role of impurities present in the hydrazine, and (4) nature of the gaseous decomposition products from the interaction of BeH_2 and MMH. The study was concerned with both the gas-phase and the liquid-phase decompositions.

DISCUSSION AND RESULTS

Vapor Decomposition Study

The kinetics of decomposition or hydrazine vapor was investigated to determine the extent of vapor reaction which might occur in the ullage of propellant tanks and laboratory reactors. Decomposition of hydrazine vapor in the tank ullage will not cause swelling of a gelled propellant. Therefore, in laboratory studies of liquid or gelled hydrazine, gas formed in the reactor ullage is not relevant and should be corrected for or minimized. It is nevertheless possible, that vapor-phase reaction may be the cause of swelling of heterogeneous propellants since rapid reaction may occur in bubbles trapped during mixing or formed at the surface of the metal powder.

Previous investigations of the gas-phase decomposition of hydrazine in flow reactors and shock tubes, generally involved very high temperatures. A lower temperature range, more relevant to the present problem was employed. In a study by Hanratty (Ref. 12) Henratty investigated the pyrolysis of hydrazine over the temperature range of 301 to 637 C using a silica glass reactor, and found the data to be best represented by first-order kinetics. He showed the reaction to be heterogeneous and obtained an activation energy of approximately 16 kcal/mole.

The objectives of the present vapor-phase study were (1) to obtain data at a low enough temperature that a meaningful extrapolation to storage temperatures could be made, and (2) compare the catalytic activities of various metal surfaces.

The decomposition of hydrazine was investigated over the temperature range 199 to 340 C in a Pyrex stirred-flow reactor. Because of the experimental difficulties discussed later in this section, it was not possible to determine the exact order of the reaction under these conditions. The average values of the apparent first-order rate constants are presented in Table 39. An Arrhenius plot of these results is presented in Fig. 46, along with the data of Hanratty for comparison.

The Arrhenius plot in Fig. 46 gives a good straight line over the entire temperature range from 199 to 637 C for both the current Rocketdyne data and Hanratty's results. The rate expression for this best line is given by the equation:

$$k = 10^{5.94} \exp(-19{,}064/RT) \text{ sec}^{-1}$$

The above equation yields a somewhat higher activation energy, 19 kcal/mole, than the value of 16 kcal/mole obtained by Hanratty (principally because Hanratty ignored his point at 301 C, apparently feeling it was an anomaly).

Because the Arrhenius plot in Fig. 46 is linear over a range of more than 400 C, it should be possible to extrapolate these heterogeneous rate constants with some confidence in the significance of the results. Extrapolation gives a time for 1-percent decomposition of hydrazine vapor in glass of 4.6 hours* at 70 C and 12.6 days at 25 C. These extrapolated results can be used to predict the amount of reaction which will occur in the ullage of a glass reactor. For example, if liquid hydrazine is present with an ullage of 50 percent and only vapor reaction is assumed, a gas

*This value was incorrectly listed as minutes in AFRPL-TR-66-167, page 18, line 23.

TABLE 39

PYROLYSIS OF HYDRAZINE VAPOR

Temperature, C	Number of Tests	k_{1}', sec^{-1}	Average Deviation
Pyrex Flow Reactor			
199	4	0.00134	0.0005
229.0*	2	0.00357	0.0002
235.6	8	0.00784	0.0017
274.1	8	0.0494	0.013
299.2	4	0.0308	0.007
329.6	2	0.105	0.014
339.6	2	0.100	0.008
Static Aluminum Reactor			
202	1	0.0000761	
195	1	0.0000714	
245	1	0.00108	
241	1	0.00112	

*0.456-gram aluminum powder added

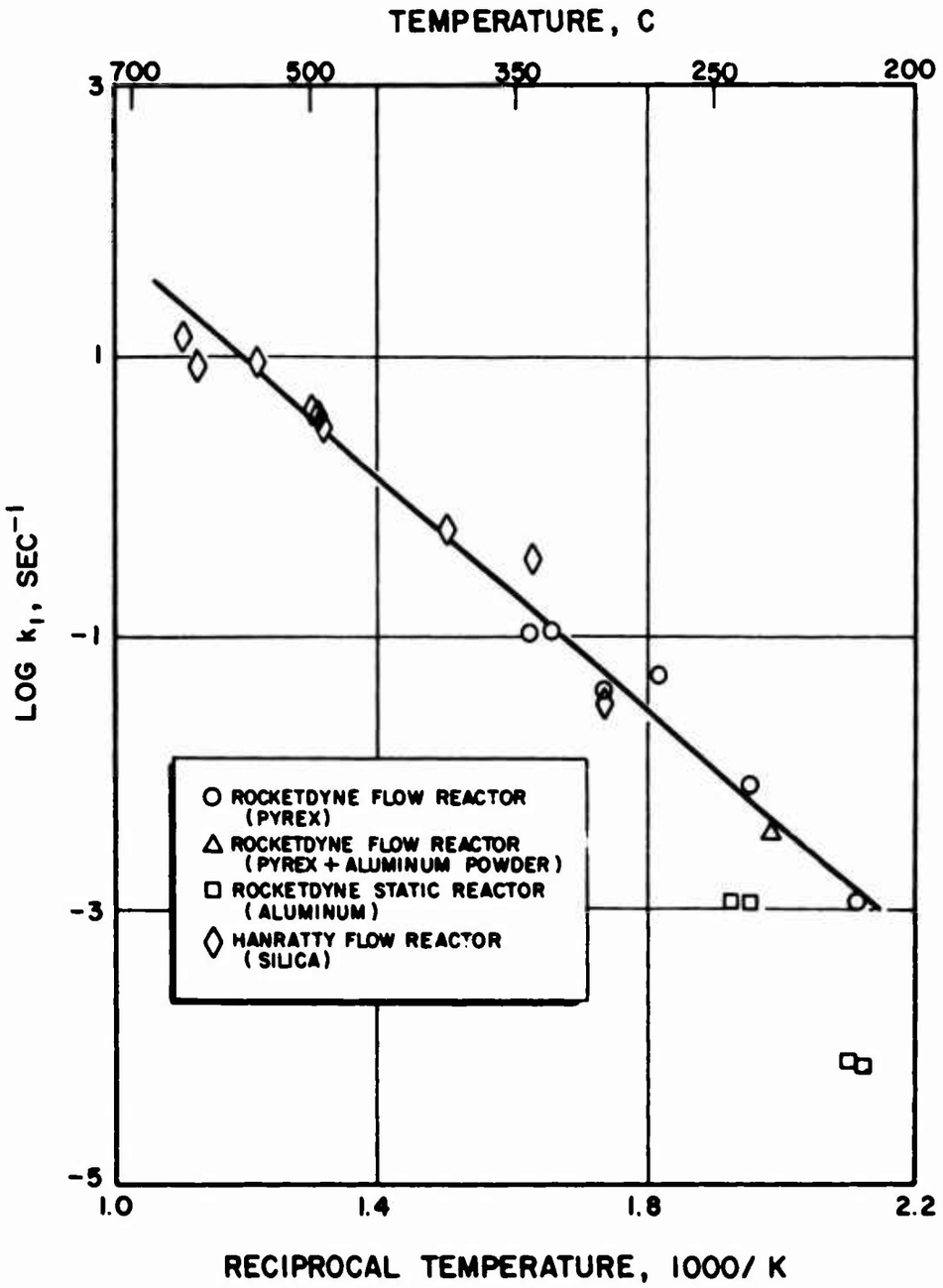


Figure 46. Arrhenius Plot of Hydrazine Vapor Decomposition in Flow Reactors

evolution rate of approximately 2 x 10^{-6} cc/lb-min is predicted at 25 C in Pyrex. This assumes that the glass surface has the same activity toward the heterogeneous decomposition as the reactors employed at the higher temperatures and that the surface-to-volume ratio is approximately the same.

Extrapolation of Fig. 46 to higher temperatures is of interest though not of direct consequence to the present study. In Fig. 47 the Arrhenius plot obtained in this study is extrapolated upward and compared with the Arrhenius plots obtained at higher temperatures by other investigators (Ref. 13 to 17).

The shock tube results represent the homogeneous rate of decomposition. It appears that the mode of decomposition of hydrazine vapor changes from a surface reaction to a homogeneous reaction in the temperature region of 600 to 700 C. It is apparent also that Eberstein and and Glassman may have had some heterogeneous reaction occurring in their flow reactor.

Attempts were made to measure the relative effect of various metals in promoting heterogeneous decomposition of hydrazine at elevated temperatures. Experiments were conducted at 229 C with 0.456 gram of Reynolds 1-511 "Atomized" aluminum powder at the bottom of the flow reactor. No influence upon the rate of hydrazine pyrolysis was noted (Fig. 46). However, the rates obtained using the 400-milliliter static aluminum (6060 T-6) reactor were lower by factors of 18 and 8 at 200 and 245 C, respectively (Fig. 46 and Table 39). These results indicate that aluminum surfaces are less active in promoting heterogeneous decomposition of hydrazine at elevated temperatures than is the Pyrex surface (the exposed surface was still mainly Pyrex when the metal powder was placed in the flow reactor). Therefore, relative activities of metal surfaces cannot be compared in the glass flow reactor.

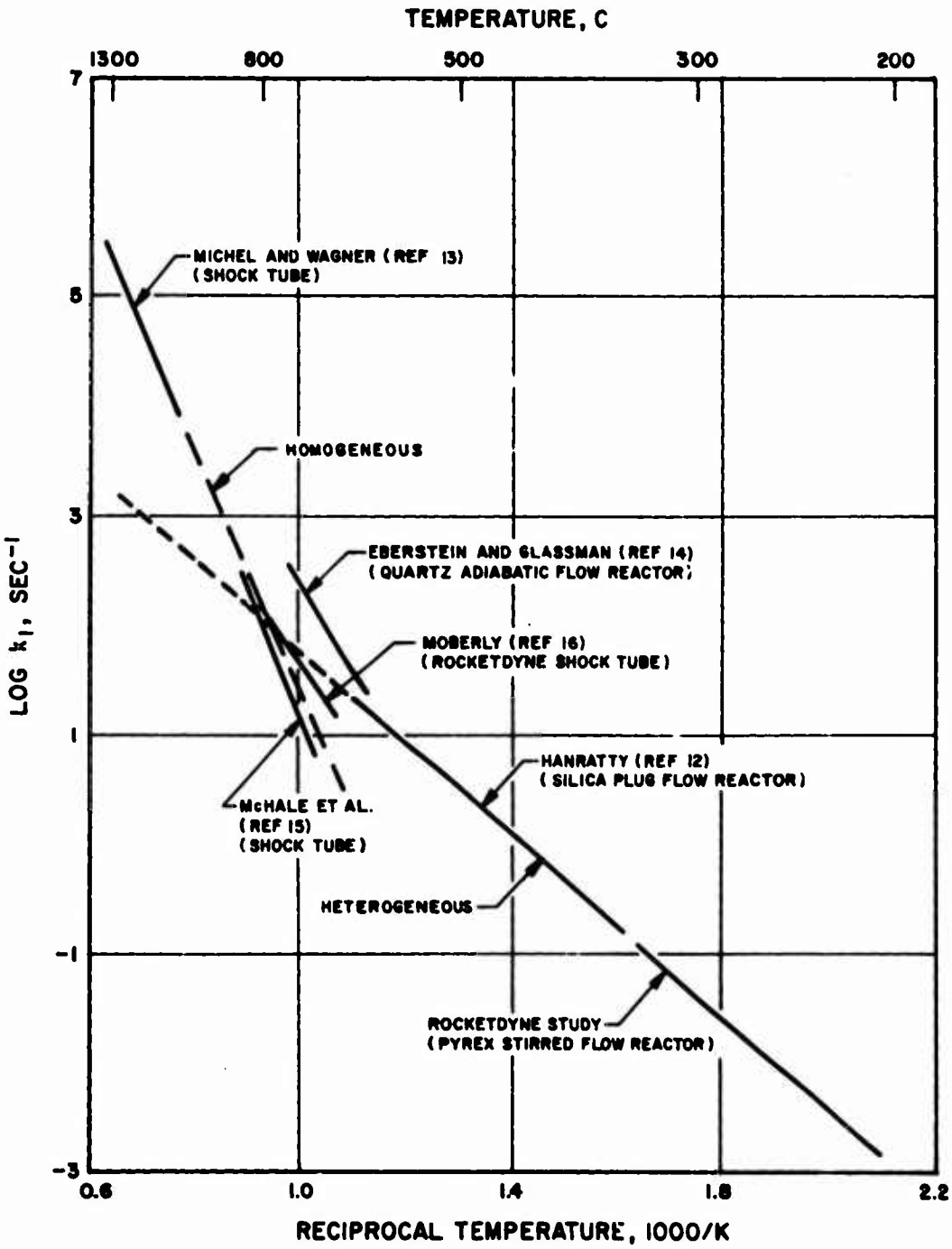


Figure 47. Comparison of Arrhenius Plots for Decomposition of Hydrazine Vapor

Liquid Decomposition Study

The liquid decomposition experiments involved both the neat vehicles and solid/vehicle systems. They were performed mostly at 71 C, a temperature at which the rate of gas evolution was rapid enough for measurement in a practical time period. Some long-term experiments at ambient temperature were also carried out, but proved to be less informative. Answers were sought to the four specific points listed before, i.e., the site of reaction, the effect of oxygen, the role of impurities, and the BeH_2-MMH interaction. The results would be important in elucidating the reaction mechanism, and thereby in the development of methods of eliminating gas formation.

Reaction Site and Reaction Products. In 1953, Mason at the Jet Propulsion Laboratory (Ref. 18) and Troyan of the Mathieson Chemical Company (Ref. 19) presented evidence that hydrazine vapor decomposes (heterogeneously) considerably more rapidly in stainless steel than does liquid hydrazine. The conclusion was reached by comparing the rates at different ratios of ullage to liquid volume, e.g., Troyan reported that decreasing the ullage from 87 to 26 percent at 50 C decreased the rate of decomposition (percent per day) by a factor of 16. These early studies had some weak points (stainless-steel reactor, large ullage, probable presence of air, inordinately high gas evolution rates, particularly in Mason's work). If, however, the conclusions are valid, solid/vapor interactions (e.g., bubbles at the surface of the metal) might control the rate of gas evolution in gelled propellants.

The first attempt to investigate the reaction site in the Be/N_2H_4 system was made during experiments at room temperature. Three glass containers connected to mercury manometers were filled, degassed, and sealed off under vacuum. The samples were: (1) hydrazine, (2) hydrazine with Be powder (0.5 gram) in the liquid, and (3) hydrazine with Be powder in a side tube in contact with the vapor. Equal amounts of hydrazine (4 grams) were used during each experiment and the ullage was approximately the same (31 cc) so that direct manometric comperisons could be made.

When stored at room temperature, the pressure increase over the vapor pressure was very slow (e.g., 8 torr after 50 days). The sample containing Be powder in contact with the vapor showed a slightly higher rate of gas evolution than did the other two. Unfortunately, the experiment with neat hydrazine was inconclusive (up to 30-day storage, the pressure buildup was lower than in the other samples, but later an anomalous behavior was observed and eventually the glass cracked). The average rates of gas evolution during room temperature storage are shown in Table 40.

TABLE 40

GAS EVOLUTION DURING ROOM-TEMPERATURE STORAGE

Sample	Average Rate After Days of Storage x 10^4, cc/lb-min					
	14	29	41	58	89	130
Neat N_2H_4	4.1	3.3	---	---	---	---
N_2H_4 + Be (liquid)	5.4	4.3	4.0	3.3	2.9	2.5
N_2H_4 + Be (vapor)	7.1	6.5	5.5	5.1	3.9	3.1

There were some unsatisfactory features of this experiment (large ullage, possible inadequate passivation of the apparatus, and possible condensation of a liquid film on the walls and on the powder in contact with the vapor) preventing definite conclusions.

The study of the site of the interaction was accelerated by increasing the temperature to 71 C. Specially designed glass ampoules equipped with break seals were employed. Three pairs of experiments were conducted in which the ampoules contained: (1) neat hydrazine to serve as a control, (2) hydrazine with Be powder in the liquid phase, and (3) hydrazine with the Be powder in a glass side arm, i.e., in the vapor phase.

Each sample was carefully degassed, evacuated, sealed, and placed in a constant temperature bath at 71 C for 110 hours. The ampoules were then removed, the hydrazine was frozen with liquid nitrogen, and the pressure was measured using a glass manometer in a special vacuum apparatus. The noncondensable reaction products, nitrogen and hydrogen, were collected by means of a Toepler pump and analyzed in the mass spectrometer.

The results of these experiments are presented in Table 41.

TABLE 41

THERMAL DECOMPOSITION OF LIQUID HYDRAZINE AT 71 C

Hydrazine, milliliters	Be Powder, grams	Noncondensable Gases Partial Pressure*, mm Hg	Mole Percent Nitrogen	Mole Percent Hydrogen
2	0	19	98	2
2	0	9	97	3
2	0.410 (liquid phase)	76	49	50
2	0.352 (liquid phase)	57	63	36
2	0.445 (vapor phase)	38	43	46
2	0.530 (vapor phase)	38	36	64

*Measured at room temperature

These results show that Be powder markedly increases the rate of hydrazine decomposition when contacting the liquid and is less effective when in contact with the vapor, but still results in an increased rate over neat hydrazine. The higher percentage of hydrogen in the products from samples containing Be, indicates that this lot of beryllium catalyzed the formation of hydrogen. Aerojet-General (Ref. 20) obtained similar nitrogen/hydrogen ratios with some Be samples.

A third series of experiments was performed to clarify the issue. This time, special precautions were taken to ensure the absence of condensation of hydrazine vapor on the Be powder in the side arm. A thermostatic

bath at 65 to 68 C was placed inside another bath at 71 C and the ampoules with liquid hydrazine were maintained at the lower temperature, while their limbs, with Be exposed to hydrazine vapor in two cases, were at 71 C. The results obtained during these four experiments, after 510 hours heating, are presented in Table 42.

TABLE 42

GAS EVOLUTION FROM Be/N_2H_4 SYSTEM

Sample	Average Rate x 10^{-3}, cc/lb-min	Volume Percent Nitrogen	Volume Percent Hydrogen
Neat N_2H_4	5.9	97	2
N_2H_4 + Be (in liquid)	13.0	46	53
N_2H_4 + Be (in vapor)	6.5	90	9
N_2H_4 + Be (in vapor)	8.0	85	14

These results confirm a higher rate of decomposition when Be is in contact with liquid hydrazine, and again reveal a high proportion of hydrogen in the volatile products. Under these conditions, Be powder in contact with vapor has little or no effect on the rate or stoichiometry.

The higher rate of decomposition of hydrazine at 71 C observed when Be is in contact with the liquid rather than with the vapor suggests several possibilities. One is that impurities in hydrazine (present in the liquid and presumably absent in the vapor) play a considerable role in the decomposition, and may be more significant than impurities on beryllium (accessible to hydrazine in both cases). Another is that impurities on beryllium are leached by liquid hydrazine and only then become effective. Still another possibility is that the decomposition of liquid hydrazine at the metal surface involves an ionic reaction (no ionic reactions occur in the vapor phase). Clarification of these points requires a methodical basic study.

The results of this investigation of the reaction site indicate that the role of the vapor-phase reaction may not be as pronounced as the data of Troyan would suggest. However, further study of the reaction site would appear warranted because the addition of metal powder to the liquid only increased the decomposition rate by a factor of two in some experiments.

Because the ampoule method yields only one data point per experiment, selected experiments with neat hydrazine at various heating times are compared in Table 43 to determine if any trends appear as a function of time, e.g., an induction period. No such trend can be drawn from these data although there does appear to be considerable difference in rates among the experiments (perhaps because of differences in surface conditions).

TABLE 43

GAS EVOLUTION FROM NEAT HYDRAZINE AT 71 C

Hydrazine, milliliters	Time of Heating, hours	Pressure, torr	Average Rate x 10^{-3}, cc/lb-min
2	110	9	3.1
2	142	9	2.4
2	310	13	1.7
2	510	74	5.9

Effect of Oxygen. A series of experiments was conducted in which neat hydrazine was placed in four ampoules; oxygen was bubbled through one pair, and helium through the other pair for approximately 30 minutes. The hydrazine was frozen with liquid nitrogen, the ampoules evacuated, sealed, and placed in the constant temperature bath at 71 C. The results of these experiments are presented in Table 44.

TABLE 44

INFLUENCE OF OXYGEN UPON THE RATE OF HYDRAZINE DECOMPOSITION AT 71 C

Hydrazine, milliliters	Gas Added	Hours in Bath	Noncondensable Gases Partial Pressure*, mm Hg	Mole Percent Nitrogen	Mole Percent Hydrogen
2	Helium	142	9	98	2
2	Helium	310	13		
2	Oxygen	142	27	99	1
2	Oxygen	310	45		

*Measured at room temperature

These results show that oxygen pretreatment increases the rate of hydrazine decomposition.

Role of Impurities in Hydrazine. In all cases of prolonged heating of hydrazine at 71 C, the liquid acquired a degree of yellowish coloration. The liquid phase from several series of experiments was examined to determine the nature of the color-producing products. Neither infrared nor gas chromatographic techniques revealed any significant difference between the heated liquids (these had been heated in sealed ampoules) and the initial propellant-grade hydrazine. However, ultraviolet spectrophotometry (using a Cary double-beam instrument) revealed pronounced absorption in the 300- to 350-millimicron range with heating time (curves D and E in Fig. 48). These spectra were obtained with untreated hydrazine present in the reference beam. This indicates that one or more species (probably more than one from the shape of curve D) which can be easily followed by their strong ultraviolet absorption are being formed during heating. They may be products or even catalysts for the decomposition reaction (because decomposition occurred during the heating period). However, the relationship of the species to decomposition must yet be established.

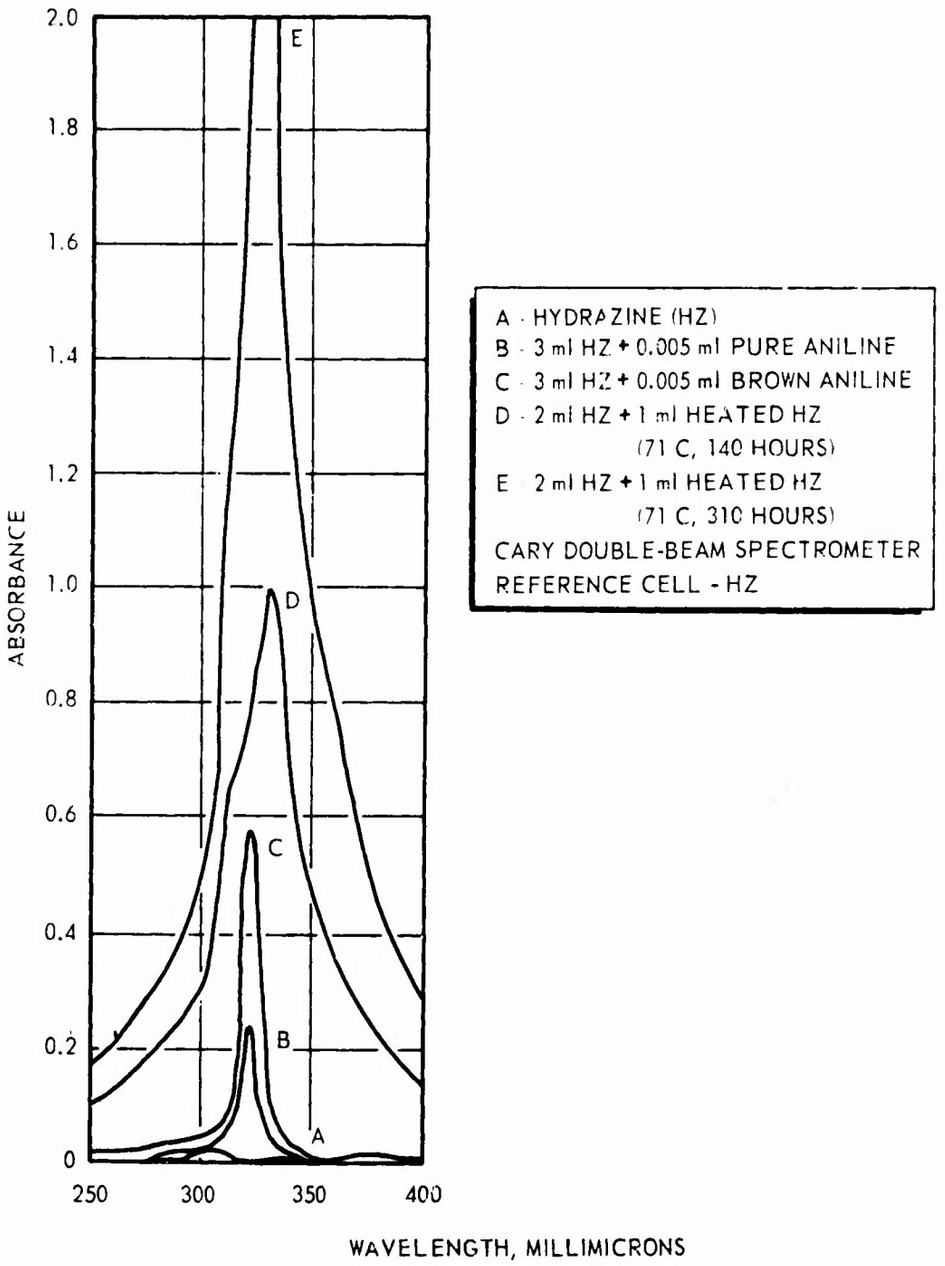


Figure 48 Ultraviolet Spectra in Hydrazine

Several agents were added to propellant-grade hydrazine in the sample cell and the ultraviolet spectra from 250 to 400 millimicrons were determined (again propellant-grade hydrazine was present in the reference cell). Ammonium hydroxide had no effect on the ultraviolet spectrum, and water caused a slight depression in the baseline over this spectral range. The addition of 0.16 v o freshly distilled aniline, however, produced a sharp peak at 325 millimicrons. An older sample of aniline which had turned brown gave a higher peak at this wavelength than the colorless distilled aniline (curves B and C in Fig. 48). The difference in maximum absorbance between curves B and C indicates that either (1) the absorption is not by aniline itself but rather a species which is at a high concentration in the brown aniline or (2) a concentration error occurred. It is apparent from Fig. 48 that the species present in heated hydrogen which absorbs the most strongly is not aniline (or the species present in aniline) because the wavelength at maximum absorption is shifted slightly. The shoulder on curve D indicates that, as expected, aniline is also present.

A series of ultraviolet spectra was taken using cyclohexane as the solvent (Fig. 49). Propellant-grade hydrazine showed the presence of species absorbing at 288 and 245 to 248 millimicrons. An older sample of hydrazine, brownish in color, showed the same two peaks but of much higher intensity; the increase in the 288-millimicron peak was much greater than that of the 248-millimicron peak. Absorption spectra for aniline in cyclohexane, available in the literature (Ref. 22), show major ultraviolet peaks at 287 and 234 millimicrons, the extinction coefficient for the shorter wavelength band being approximately four times greater than that for the 287-millimicron band. It thus appears that the species responsible for the spectra in Fig. 49 is not aniline but is similar in that it absorbs strongly at 287 millimicrons (but not at 234 millimicrons).

Propellant-grade hydrazine contains aniline as a residue from the azeotropic distillation process. Although the aniline content of hydrazine cannot increase during aging, the species which do form could arise

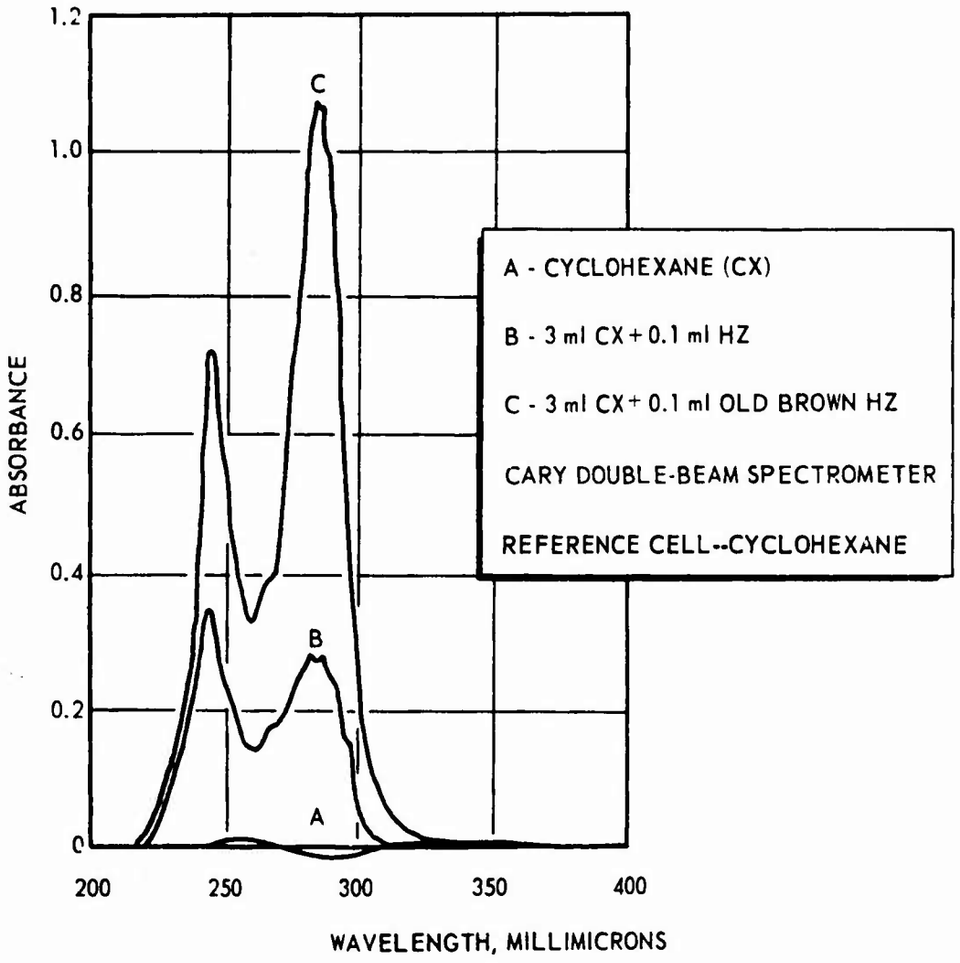


Figure 49. Ultraviolet Spectra in Cyclohexane

from aniline as a precursor. The results in Fig. 48 strongly suggest this possibility. Whether alone or in the presence of hydrazine, aniline can produce a number of species of the imino, nitroso, etc., type. Some of these species resemble intermediates in the decomposition of hydrazine and would be expected to participate in the overall degradation. A further systematic study is needed to utilize the leads provided.

Interaction of BeH_2 With MMH. The products from the decomposition of liquid MMH at 71 C, which are noncondensable in liquid nitrogen, were analyzed in the mass spectrometer. These were consistently nitrogen and methane (in approximately equal amounts) along with small amounts of hydrogen. However, the nitrogen/methane ratio was not constant. It was suspected that, with the small amount of reaction involved, some of the observed nitrogen may have resulted from traces of residual air. When a small amount of air was introduced initially, most of the oxygen did react and the nitrogen/methane ratio increased markedly. This again emphasizes the possible role of oxygen in the degradation of heterogeneous propellants.

These MMH results are of considerable interest because no product analyses have been reported previously for MMH at low temperatures. The noncondensable products, nitrogen and methane with practically no hydrogen, are the same as those reported by Cordes (Ref. 23) from the decomposition of UDMH at 400 C. Cordes found, however, that these gaseous reaction products only represented a very minor fraction of the total reaction products for UDMH. If this should also be the case for MMH at storage temperatures, MMH might be an inherently better vehicle than hydrazine, i.e., hydrazine always forms a gaseous product, nitrogen, whereas MMH might only form liquid products. It is also possible, however, that a product is formed which is volatile at room temperature but condensable in liquid nitrogen. This would result in swelling at room temperatures even if the MMH only formed small amounts of nitrogen and methane.

Because there is a possibility that MMH may react directly with BeH_2 to form hydrogen, a series of experiments was conducted to determine the nature of the noncondensable reaction products from MMH in the presence of BeH_2. The MMH/BeH_2 mixture was outgassed and heated at 71 C for several hours (usually 4 hours). This gave again nitrogen and methane (the ratio being approximately 1), and practically no hydrogen. This indicates that BeH_2 does not interact with MMH to form hydrogen (at least during the initial stages of the propellant degradation).

Because Be powder was observed to change the mechanism of hydrazine decomposition from one in which virtually no hydrogen forms to one in which equal amounts of hydrogen and nitrogen form, MMH was heated in the presence of beryllium and aluminum powders. Under these conditions, the noncondensable products still consisted of only nitrogen and methane.

EXPERIMENTAL

Vapor Decomposition

The stirred-flow reactor system was similar in design to that used to investigate the pyrolysis of Compounds T and R (Ref. 1). Helium carrier gas was passed through two bubblers in series containing liquid hydrazine (thermostated below room temperature), and then through the stirred-flow reactor. The gases leaving the reactor were analyzed for hydrazine using a Beckman gas sampling valve coupled to a 20-foot gas chromatographic column consisting of 10-percent Quadrol on Kel-F-6 at 110 C. The system was equipped with a bypass to allow analysis of hydrazine entering the reactor.

Difficulties were involved in obtaining reproducible peaks for equal concentration samples of hydrazine vapor introduced into the gas chromatograph. It was believed that these difficulties resulted from an interaction of hydrazine with the grease used to lubricate the Beckman gas

sampling valve. However, the use of a variety of greases (Kel-F, Halocarbon, Silicone, etc.) failed to alleviate the problem. Although these experimental difficulties led to a rather large average deviation in the results, it is believed that the conclusions drawn from the data obtained are valid.

Liquid Decomposition

Experiments on the liquid-phase decomposition of hydrazine (in the absence or presence of Be powder) were conducted in glass ampoules, shown in Fig. 50. Some ampoules also had glass side arms (not shown) so that Be powder could be kept out of contact with the liquid. After filling the ampoule with reactant(s), it was sealed off under vacuum (normally after degassing of contents) and placed in a thermostatic bath for a desired period of time. It was then attached to the vacuum apparatus, as shown in Fig. 51. The tip was cooled to freeze the hydrazine, the break seal was broken, and the pressure was measured. The noncondensable gases were then transferred by means of a Toepler pump into a detachable sampling bulb for subsequent mass-spectrometer analysis. The ampoules were passivated before filling by the following procedure: (1) rinse with distilled water, (2) fill with distilled water and place in a water bath at 91 to 98 C for 2 hours, (3) replace the water with a 50/50 v/o mixture of water and hydrazine, and place in a water bath at 91 to 98 C for 2 hours, and (4) rinse with distilled water and dry at 100 C overnight.

The investigation of the decomposition of MMH was conducted in a 150-cc flask which contained 10 to 15 milliliters of liquid and approximately 0.5 gram of solid (during some experiments). After loading the flask, the side arm was sealed shut and the flask was thoroughly outgassed by alternately freezing in liquid nitrogen and pumping through a Teflon needle valve. At the end of the reaction period (at 71 C) the flask was frozen in liquid nitrogen and the noncondensable products were analyzed in the mass spectrometer.

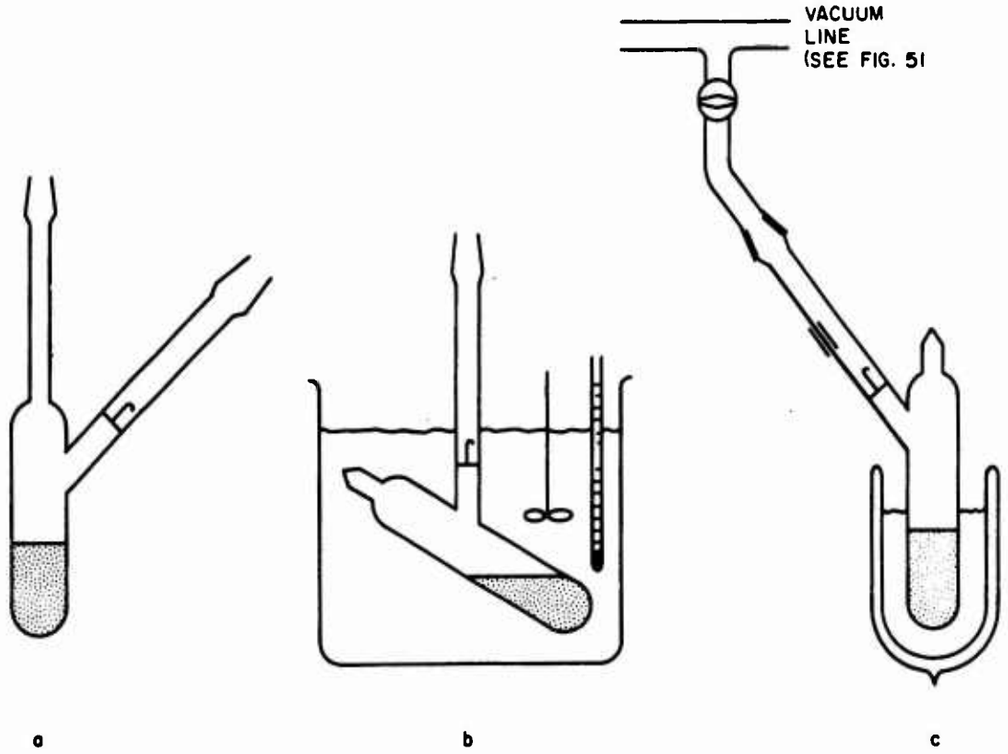


Figure 50. Sample Holders

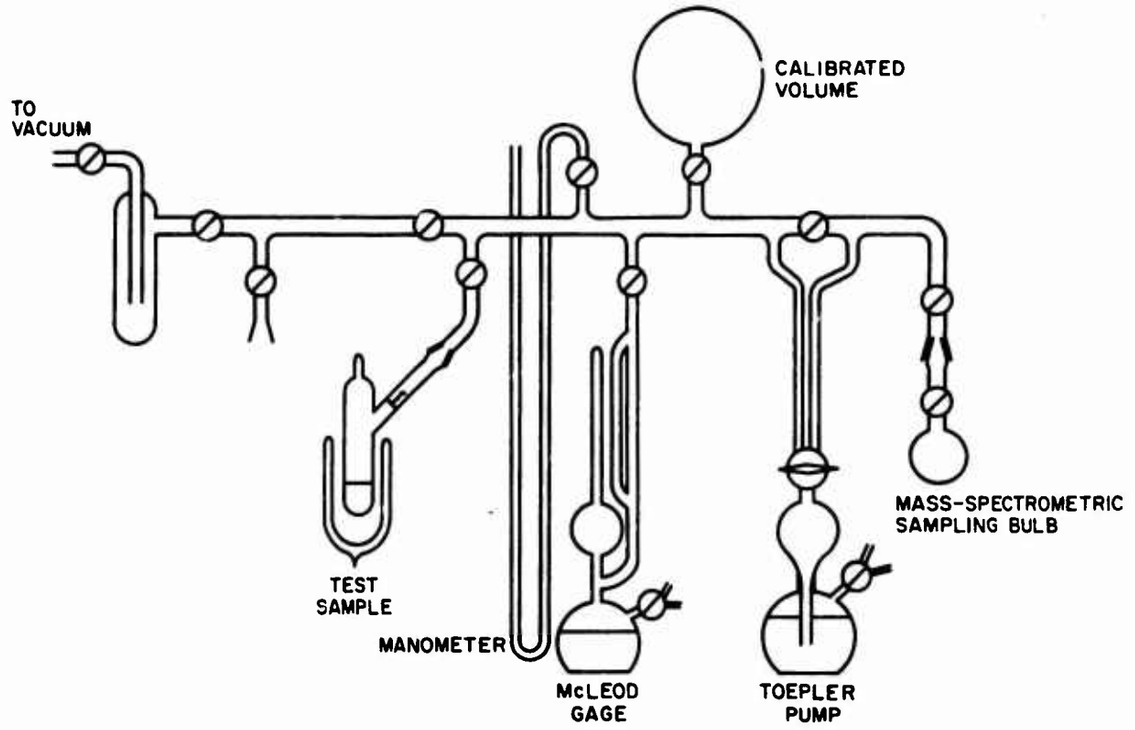


Figure 51. Vacuum Apparatus

CONCLUSIONS

Hydrazine vapor decomposition in the ullage could lead to an apparent gas evolution rate of approximately 2×10^{-6} cc/lb-min at 25 C in glass reactor with 50-percent ullage. The presence of beryllium powder accelerates the decomposition rate of hydrazine; this enhancement is greater when Be powder is in contact with hydrazine liquid than with hydrazine vapor at 71 C. Oxygen treatment accelerates the decomposition of neat hydrazine in glass at 71 C. Residual aniline or its decomposition products seem to play a role in the degradation of hydrazine (although its effect on the reaction rate was not investigated during this study). The noncondensable products from MMH decomposition at 71 C are nitrogen and methane along with a smaller amount of hydrogen. Decomposition of BeH_2 does not occur during the initial stages of degradation in the BeH_2/MMH system.

INTRODUCTION

The objective of this phase of the program was to investigate the feasibility of formulating high-performance heterogeneous systems based on beryllium hydride in various borane- and alane-terminated beryllium hydride liquids. Liquid beryllium hydride compounds are attractive storable vehicles for heterogeneous fuels containing solid beryllium hydride. They possess several distinct advantages over other vehicles:

1. These liquids themselves are more energetic than any of the other liquids which have been suggested as storable vehicles for solid beryllium hydride; therefore, the propellants formulated with liquid beryllium hydride compounds are also more energetic. For example, a fuel containing 35 volume percent solid beryllium hydride in various presently available liquid beryllium hydrides exhibits a specific impulse of 335 to 343 seconds with 98-percent H_2O_2 (Fig. 52).
2. They are chemically similar to beryllium hydride; therefore, heterogeneous fuels should be more stable chemically than those containing some other vehicles, e.g., MMH.
3. The liquids are readily oxidized; combustion efficiency of corresponding heterogeneous fuels is expected to be higher.
4. The density of these liquids (d = 0.72 gm/cc) matches the density of both amorphous Beane (d = 0.65 gm/cc) and crystalline Beane (d = 0.78 gm/cc) more closely than other liquids. Thus, mechanical stability of heterogeneous fuels with these components is facilitated.
5. The chemical similarity of BeH_2 and the liquid beryllium hydrides results in only slight changes of mixture ratio as the impulse varies along any of the curves in Fig. 52. Because the density of BeH_2 and the liquid media are also very similar, hardware

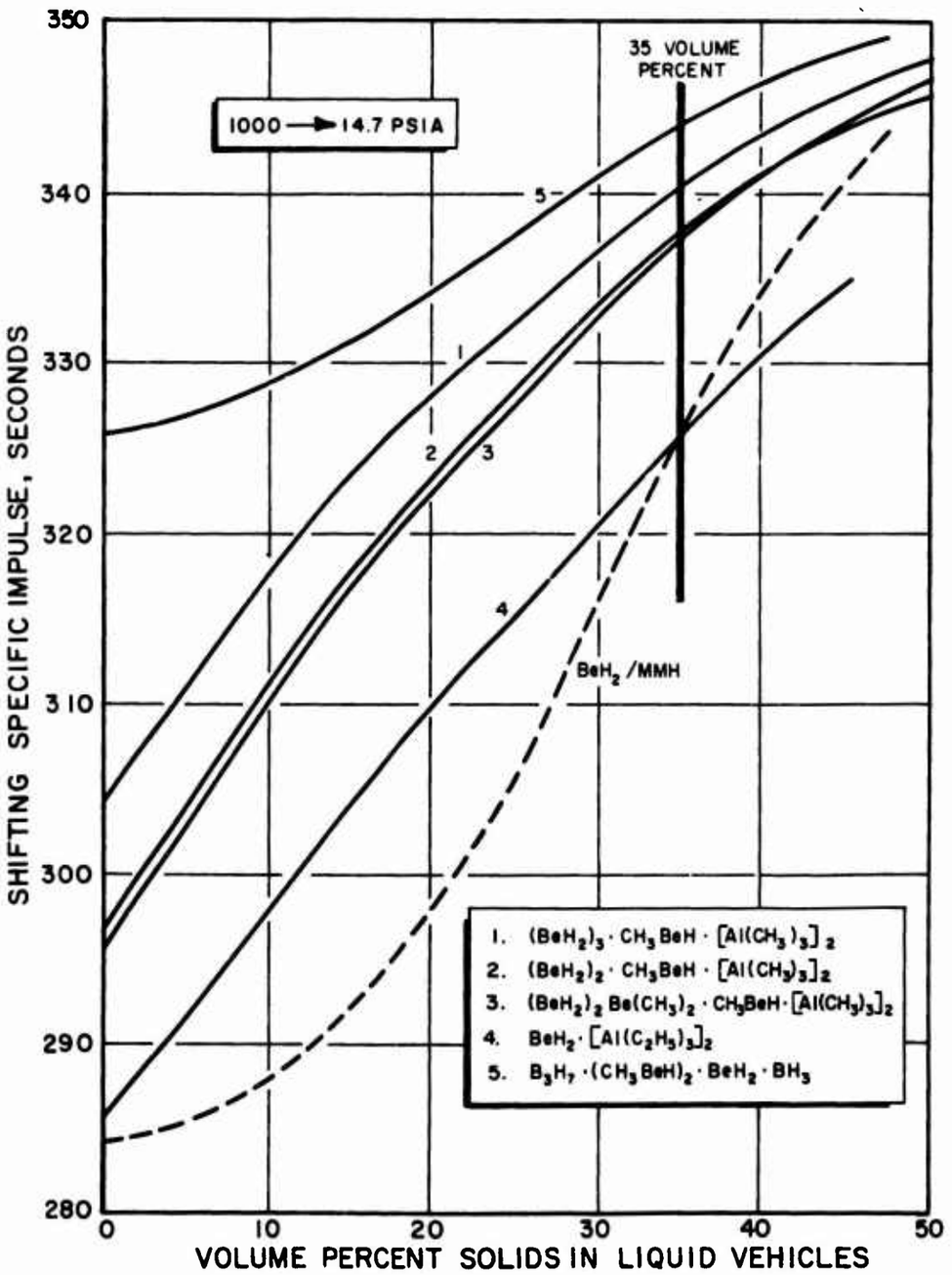


Figure 52. Theoretical Performance Comparison of BeH_2-Beryllium Hydride Liquid Gelled Fuels and BeH_2-MMH Gelled Fuels With 98-Percent H_2O_2

designed to fire a 330-second specific impulse formulations would still be close to optimum when firing a 340- or a 350-second specific impulse formulation. Accordingly, a single engine might be adjusted to meet many different mission requirements merely by varying the fuel composition.

It has been demonstrated at Rocketdyne that the alane-terminated beryllim hydride (ATBH) possessed excellent potential as the vehicle in high-performance BeH_2-containing heterogeneous propellants. From the standpoints of stability, compatibility with beryllium hydride, and actual demonstrable formation of stable gels, the ATBH liquid appears to be one of the better candidates for future investigations in the field of heterogeneous propellants.

It has also been demonstrated that the preparation of the ATBH liquids is amenable to scale-up, and batches up to the 100-gram level have been prepared.

DISCUSSION AND RESULTS

Preparation of Beryllium Liquids

The synthesis efforts under this task consisted of preparing beryllium-containing liquids which had previously been prepared at Rocketdyne.

The reaction between dimethyl beryllium and diborane proceeded smoothly, as reported previously (Ref. 24), producing a clear, mobile liquid. The liquid had an average empirical formula of $H_3B(CH_3BeH)_7BH_3$.

The reaction in a solvent medium between dimethyl beryllium and tetraborane was found to proceed in a different fashion than reported (Ref. 24). In a solvent system, no isolable liquid was produced. In the absence of a solvent, and utilizing an excess of B_4H_{10} (molar ratio: $B_4H_{10}/Be(CH_3)_2 = 3.2:1$), the reaction was observed to proceed smoothly

overnight. However, some difficulty was encountered in the isolation of the liquid. The liquid was lost when attempts were being made to separate a small amount of unreacted solid from the liquid.

The preparation of the ATBH liquid was carred out essentially as it was done originally (Ref. 25) by dissolving Beane (pyrolytic BeH_2-Ethyl Corp.) in trimethyl aluminum at elevated temperatures. At the refluxing temperature of $Al(CH_3)_3$, the reaction was complete in 15 to 16 hours. The viscosity of the final liquid was found to be dependent on the length of evacuation on the high vacuum system. $Al(CH_3)_3$ could be removed with prolonged pumping and the liquid became more viscous correspondingly. The desired viscosity could thus be easily attained by the addition or removal of a small amount of $Al(CH_3)_3$. Only a small amount of $Al(CH_3)_3$ was necessary to change the viscosity substantially.

The average empirical formula of the liquid prepared can be written in the following manner (based on 97-percent analytical mass balance): $2BeH_2 \cdot CH_3BeH \cdot 2Al(CH_3)_3$.

The scale-up preparations of the ATBH liquids were carried out essentially as outlined previously. The first scale-up reaction produced 14 grams of a clear, mobile liquid with an empirical formula of $2BeH_2 \cdot CH_3BeH \cdot 2Al(CH_3)_3$. The second reaction was of a larger scale and was carried out at a slightly lower temperature, for a longer time, and at a lower molar ratio of $Al(CH_3)_3$ to BeH_2. This reaction yielded 25 grams of a liquid of similar properties as the first liquid. Its empirical formula of $2BeH_2 \cdot 0.5CH_3BeH \cdot 2Al(CH_3)_3$ may indicate a possible mixture of $2BeH_2 \cdot 2Al(CH_3)_3$ and $2BeH_2 \cdot CH_3BeH \cdot 2Al(CH_3)_3$. The third reaction of a still larger scale, was carried out at a slightly higher temperature than either of the first two reactions. At higher temperatures, the heating period required was found to be less. This reaction produced 68 grams of a liquid with the empirical formula $2BeH_2 \cdot CH_3BeH \cdot 2Al(CH_3)_3$. An initial reaction designed to produce at least 100 grams of the liquid was lost because of a malfunction in the heating system. However, this reaction was repeated and successfully completed.

Thermal Stability Studies

The thermal stability of four liquids was investigated in the glass thermal stability apparatus (Fig. 53). The rate of gas evolution was measured. The evolved gases were identified by infrared spectroscopy and mass spectrometry. Other observations were made such as change of viscosity and clarity of the liquid. The compatibility of Beane (BeH_2) with the aluminum-terminated liquid was also investigated in the thermal stability apparatus. The experimental data are summarized in Table 45. As can be observed in Table 45, the liquids can be arranged in the following order of decreasing stability: $(CH_3BeH)(BeH_2)_2[Al(CH_3)_3]_2 >> (CH_3BeH)_3BeH_2(CH_3B_3H_6)_2 > (CH_3BeH)_7(BH_3)_2 >> 1.8(CH_3)_2Be/Be(BH_4)_2$.

Beane was found to be compatible with $(CH_3BeH)(BeH_2)_2[Al(CH_3)_3]_2$. The rate of gas evolution (Table 45) was similar to that of the neat liquid and no dissolution of the solid was observed.

Long-Term Storage Stability Study

An ATBH liquid with an average empirical formula of $2BeH_2 \cdot CH_3BeH \cdot 2Al(CH_3)_3$ was used in a low ullage, long-term storage stability determination at ambient temperatures. The apparatus utilized was similar to, but smaller than, the one used during the thermal stability studies. The ullage was approximately 15 percent. Over a period of 5-1/2 months, the average rate of gas evolution was found to be 1.1×10^{-4} cc/min/lb of liquid (Table). The rate appears to decrease slowly with time. The rate during the last 12 weeks was 0.9×10^{-4} cc/min/lb as compared to 1.2×10^{-4} cc/min/lb during the first 10 weeks (or 1.0×10^{-4} cc/min/lb during the second 5 weeks as compared to 1.5 cc/min/lb over the first 5 weeks). Little change was noted in the appearance of the liquid over the entire period; the liquid was still clear and quite mobile.

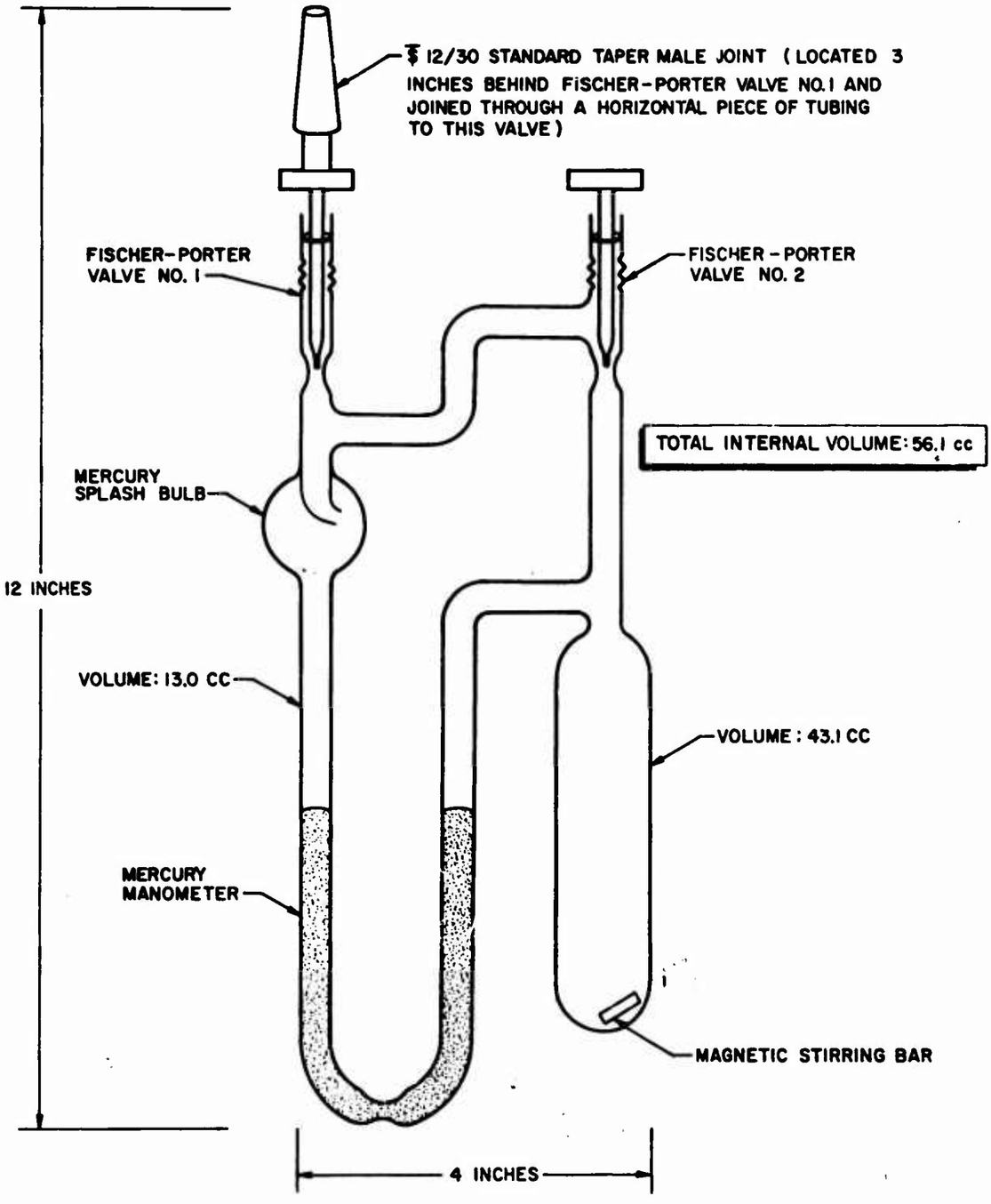


Figure 53. Glass Thermal Stability Apparatus

TABLE 45

THERMAL STABILITY OF BORON- AND ALUMINUM-TERMINATED BERYLLIUM HYDRIDE LIQUIDS

Empirical Formula of Liquid	Reactants for Preparation	Gas Evolution Studies				Gases Evolved*	Other Observations
		Liquid Weight milligrams,	Temperature, C	Period of Study, hours	Average Gas Evolution Rate, cc/min/lb		
$1.8(CH_3)_2Be/Be(BH_4)_2$	$Be(CH_3)_2$, $Be(BH_4)_2$	443	71.0	4.38	125 (rate decreasing slowly)	$B(CH_3)_3$	Viscosity remained constant; white insoluble solid precipitated during test
$(CH_2BeH)_3BeH_2(CH_3B_3H_6)_2$	$Be(CH_3)_2$, B_4H_{10}	263	71.0	18.2	13.4 (rate decreasing slowly)	$B(CH_3)_3$	Viscosity remained constant; no precipitate
		263	20.2	120	1.1×10^{-2} (constant rate)		
$(CH_3BeH)_7(BH_3)_2$	$Be(CH_3)_2$, B_2H_6	285	71.0	14.0	14.3 (rate increasing rapidly)	$B(CH_3)_3$	Large viscosity increase; no precipitate
$(CH_3BeH)(BeH_2)_2[Al(CH_3)_3]_2$	BeH_2(Beane), $Al(CH_3)_3$	310	71.0	70.3	5.9×10^{-2} (constant rate)	Not determined	Small viscosity decrease, no precipitate
$(CH_3BeH)(BeH_2)_2[Al(CH_3)_3]_2$ compatibility with Beane	Beane, $Al(CH_3)_3$	310 (liquid) 90 (Beane)	71.0	100	2.1×10^{-2} (constant rate)	Not determined	No viscosity change; solid Beane disperses easily in liquid; no solid dissolution observed
$(CH_3BeH)(BeH_2)_2[Al(CH_3)_3]_2$	Beane, $Al(CH_3)_3$	8420	Ambient	3696	1.1×10^{-4} (rate decreasing slowly)	Not determined	No viscosity change, no change in appearance

*H_2 may have been evolved in these studies.

Density Determination

The density of an ATBH liquid, empirical formula: $2BeH_2 \cdot CH_3BeH \cdot 2Al(CH_3)_3$, has been determined to be 0.72 gm/cc at 29 C.

Gel Formation

Gels containing solid BeH_2 dispersed in these liquid vehicles were designated R-6. ATBH liquids are expected to behave as nonpolar substances and accordingly materials suitable for gelling hydrocarbons (e.g., soaps and fine-particle gellants) were expected to gel ATBH if they did not react chemically. Gelling agent candidates selected for preliminary testing on ATBH included Alumagel, aluminum octanoate, and Cab-O-Sil M-5.

Alumagel (Witco Chemical Company) is a proprietary aluminum soap that gels nonpolar solvents including kerosene at room temperature. However, on addition of triethyl aluminum (TEA) or ATBH to the solid, visible gassing occurred and no gel was formed at the 2-percent concentration level. Heating and stirring at approximately 150 F did not induce gelation.

Aluminum octanoate A (Witco) appeared to dissolve in TEA and did not gel it even on warming. Addition of ATBH to this soap resulted in a vigorous, immediate reaction with the formation of some black material (possibly metallic aluminum, beryllium, or both); no gel was produced.

The addition of 4 weight percent Cab-O-Sil M-5 to either TEA or ATBH resulted in immediate gelation at room temperature with no visible reaction. Complete R-6 formulations consisting of 35 volume percent Beane (Ethyl Corporation Lot No. 44) have also been gelled with 1- to 2-percent Cab-O-Sil. These formulations have been stable for more than 3 months and have a theoretical specific impulse of approximately 335 seconds (1000 → 14.7 psia) with 98-percent H_2O_2 as oxidizer. The results of these experiments are presented in Table 46.

TABLE 46

EFFECT OF GELLANT CANDIDATES ON PYROPHORIC LIQUIDS

Gellant	TEA	ATBH IV	R-6 Formulation
Alumagel	No gel	No gel	---
Aluminum octanoate	No gel	Vigorous reaction	---
Cab-O-Sil M-5	Stable gel	Stable gel	Stable gel

NOTE: TEA = triethyl aluminum

ATBH = alane-terminated beryllium hydride, $(BeH_2)_2 \cdot CH_3BeH \cdot 2Al(CH_3)_3$

R-6 = 35 volume percent Beane in ATBH

EXPERIMENTAL

$(CH_3BeH)_7(BH_3)_2$ System

Dimethyl beryllium (40 mmoles) was placed in a 500-cc bulb reactor equipped with a Fischer-Porter needle valve. The reactor was evacuated on the vacuum system and B_2H_6 (15 mmoles) was condensed in. The reactor was allowed to warm up to room temperature and then was immersed in a preheated oil bath (90 C). The first appearance of a liquid occurred within 5 minutes of heating. In 15 to 20 minutes, a large amount of liquid had been formed. At the end of the heating period (1 hour) a small amount of unreacted solid remained suspended in the liquid. When the reaction mixture had attained room temperature, all volatiles were removed. The volatiles consisted of: a small amount of noncondensables (not measured), $(CH_3BeBH_4)_2$ (1.0 mmole), and $B(CH_3)_3$ (14 mmoles). The liquid product was removed from the reactor as a hexane solution. The solid was filtered off and the solvent was stripped off of the filtrate. A clear syrupy liquid remained as the final product. Analysis of the liquid revealed the following: gas evolved upon hydrolysis, 86.5 mmoles/gm sample which included 65.2 w/o H_2 and 34.4 w o CH_4; Be, 25.4 w/o, and B, 8.7 w/o.

Attempts to Prepare Other B_3H_7 Terminated Liquids

Dimethyl beryllium (25.6 mmoles) was placed in a 200-cc bulb reaction and n-hexane (15 milliliters) was added as a solvent. Tetraborane (10.8 mmoles) was then condensed into the reactor using the usual high vacuum techniques. The mixture was allowed to warm to room temperature and stirred at ambient condition by means of a magnetic stirrer. After 6 days, a -80 C bath was placed around the reactor and all volatiles were removed. The volatiles consisted of: noncondensables (not measured), and $B(CH_3)_3$ (1 mmole). Because a large amount of solid remained unreacted, an additional amount of B_4H_{10} (7.25 mmoles) was added to the reaction mixture. After 3 additional days of stirring at room temperature, the volatiles were again removed. Noncondensables, $(CH_3BeBH_4)_2$ (trace), and $B(CH_3)_3$ (0.9 mmole) were produced. The reactor was broken open and the reaction mixture was filtered. Upon stripping off the solvent, no liquid was isolated.

A second reaction was carried out similar to the preceding, without, however, the use of a solvent. B_4H_{10} (8 mmoles) was condensed over $Be(CH_3)_2$ (7.5 mmoles) in a bulb reactor and allowed to stand at room temperature. After 18 hours, all the solid had been converted into a liquid. All the volatiles were removed and an attempt was made to remove the liquid from the reactor as a solution in benzene. When the benzene was added, a large amount of solid precipitated out, and the liquid could not be recovered by stripping off the benzene. The condensables removed from the reaction were recondensed over the solid and allowed to stand overnight. Removal of the volatiles and extraction of the solid with benzene produced no liquid. The volatiles consisted of: noncondensables; $B(CH_3)_3$ (4.0 mmoles); some $(CH_3)_3B_2H_4$; and unreacted B_4H_{10} (16.3 mmoles).

$BeH_2/Al(CH_3)_3$ System

Beryllium hydride (Ethyl Corp. Lots No. 47 and 48) (92.3 mmoles) was placed in a thick-walled glass reactor equipped with a Fischer-Porter needle valve. $Al(CH_3)_3$ (156 mmoles) was added and the mixture was heated in an

oil bath (85 to 120 C) over a period of 4 days. The solid was then filtered, washed with benzene, and dried on the vacuum system. Approximately 30 w/o of the original solid was recovered. Upon removal of the benzene and excess $Al(CH_3)_3$, a clear viscous syrup (2.9 grams) was obtained. Fresh $Al(CH_3)_3$ (0.45 gram) was added to the thick syrup to thin it out to give a reasonably mobile liquid. A sample of this liquid was analyzed and revealed the following: gas evolved on hydrolysis, a 61.7 mmoles/gm sample of which included 59.0 w/o CH_4, and 38.7 w/o H_2; Be, 13.95 w/o; and Al, 27.6 w/o.

In a second reaction, BeH_2 (45.4 mmoles) was placed in a round-bottomed flask equipped with a water condenser. $Al(CH_3)_3$ (156 mmoles) was added to the BeH_2 and refluxed under a blanket of dry nitrogen. During overnight refluxing most of the solid had gone into solution and a small amount of gray material was deposited on the wall. The reaction mixture was filtered and the solid was washed with $Al(CH_3)_3$ and dried under evacuation. Approximately 12 w/o of the original solid was recovered. Excess $Al(CH_3)_3$ was stripped off the filtrate on the vacuum system. A clear, mobile liquid (2.19 grams) was obtained as the final product. Analysis of this liquid revealed the following: gas evolved on hydrolysis, a 60.1 mmoles/gm sample of which included 62.6 w/o CH_4 and 35.4 w/o H_2; Be, 12.35 w/o; and Al 22.5 w/o.

The scale-up reaction procedures were essentially the same as in the second reaction. The results of these scale-up reactions are summarized in Table 47.

Thermal Stability Studies

The two volumes of the thermal stability apparatus (Fig. 53) and the manometer correction were determined. The liquids were introduced into the apparatus with a syringe through Fischer-Porter valve No. 2. Hexane was used as a solvent to make a quantitative transfer of $(CH_3BeH)_3BeH_2$-$(CH_3B_3H_6)_2$ liquid and of $(CH_3BeH)_7(BH_3)_2$ liquid. In both cases, hexane

TABLE 47

RESULTS OF SCALE-UP PREPARATION OF ATBH LIQUIDS

No.	BeH_2, moles	$Al(CH_3)_3$, moles	Temperature, C	Period of Heating	Weight Percent Recovery of Solid	Analyses			
						H_2, moles/gm	CH_4 moles/gm	Be, weight percent	Al, weight percent
1	0.27	0.42	125	24 hours	19	24.5	36.9	13	30.2
2	0.55	0.71	115 to 120	3 days	20	22.3	31.5	10.9	26.3
3	1.09	1.35	130 to 145	2 days	8.1	26.7	36.5	15.3	30.9
4	2.18	2.71	125	5 days	9.4	--	--	--	--

CONFIDENTIAL

CONFIDENTIAL

caused precipitation of a finely divided insoluble solid which was transferred to the apparatus so as not to change the composition of the liquid. The solids redissolved in the liquids when the hexane was evaporated on the vacuum line. In the case of $(CH_3BeH)_3BeH_2(CH_3B_3H_6)_2$ liquid, the solid dissolved after overnight storage at room temperature, whereas, in the case of $(CH_3BeH)_7(BH_3)_2$ liquid, dissolution occurred as soon as the hexane was removed. The dry-box atmosphere (nitrogen) was admitted to the apparatus at atmospheric pressure (745 mm Hg) and both Fischer-Porter valves were closed. The loaded apparatus was removed from the dry box and the viscosity of the fluid was observed by moving the magnetic stirring bar around with a magnet. The apparatus was next immersed to the depth of the Fischer-Porter valves in a glass thermoregulated oil bath at 71.0 ±0.3 C.

Pressure readings were taken at intervals with a cathetometer to ±0.2 millimeter. The quantities of evolved gases were calculated utilizing the ideal gas law for each time interval and the known calibrated volumes of the apparatus. A vapor pressure of approximately 25 ±5 millimeters was observed when the 1.8 $Be(CH_3)_2/Be(BH_4)_2$ liquid was initially heated to 71 C. There was a large error in this measurement because the liquid decomposed rapidly at this temperature.

A vapor pressure of 51.0 millimeters was observed when the $(CH_3BeH)(BeH_2)_2$-$[Al(CH_3)_3]_2$ liquid was initially heated to 71 C. Vapor-phase analyses, as subsequently described, indicated that this observed vapor pressure was that of a complex mixture. The condensable vapor contained 60.2 m/o ethane, 10.3 m/o propane, 9.5 m/o acetylene, 9.3 m/o $B(CH_3)_3$, 6.0 m/o alkoxy compounds, 2.8 m/o other hydrocarbons, and 1.9 m/o $Al(CH_3)_3$.

Methane was found in the total gas sample. These gases, except $Al(CH_3)_3$, were probably generated from the reaction of impurities that were present in either the Beane or the $Al(CH_3)_3$ that were used for the synthesis of this liquid.

CONFIDENTIAL

After the stability studies were completed, gas samples were expanded into a vacuum line. A portion of these total gas samples were analyzed on the mass spectrometer. The remainder was passed through a trap cooled to -196 C with liquid nitrogen to collect the condensable gases. These condensable fractions were analyzed on an infrared spectrometer and on the mass spectrometer. Mass spectometric analysis of the dry-box atmosphere indicated the presence of hydrogen after overnight regeneration. Therefore, it was impossible to determine whether hydrogen was evolved during these studies. The viscosity of the liquids was re-examined with a magnet as previously described to observe viscosity changes. The experimental results of these studies are summarized in Table 45. It was impossible to determine the nature of the evolved gas during either the thermal stability study of $(CH_3BeH)(BeH_2)_2[Al(CH_3)_3]_2$ liquid or during the compatibility study. Only small quantities of gas were evolved which could not be distinguished in the complex mixture of gases present in the vapor phase.

Compatibility With Beane

The Beane (Ethyl Corporation Lot No. 44), 1 gram, which was used in a compatibility study with $(CH_3BeH)(BeH_2)_2[Al(CH_3)_3]_2$ liquid was pretreated with 5 milliliters of $Al(CH_3)_3$ in 15 milliliters of benzene overnight at room temperature to remove any reactive groups such as hydroxyl. The resulting solid was filtered, washed with benzene, and dried in vacuo. Some of this pretreated Beane (90 milligrams) was added with a funnel to the $(CH_3BeH)(BeH_2)_2[Al(CH_3)_3]_2$ liquid (310 milligrams) after the thermal stability study of this liquid was completed. The resulting mixture was investigated for thermal stability using the same techniques as were used for the neat liquids.

Long-Term Storage Stability Study

The liquid was introduced into the stability apparatus using a syringe and a long needle through the Teflon needle valve. With the dry-box atmosphere (nitrogen) in the free spaces, both needle valves were closed.

The apparatus was then immersed to the depth of the needle valves in a glass thermoregulated water bath at 25 C. Pressure readings were taken at intervals with a cathetometer. The quantities of evolved gases were calculated as above.

Density Determination

The density of the liquid was determined in a small ampoule equipped with a Teflon needle valve. The liquid was placed in the ampoule by using a needle and syringe. From the weight of the liquid and the calibrated volume of the ampoule, the density was obtained.

Gel Formulation

To test gelling agents for the ATBH liquid, a weighed quantity of the candidate gellant was placed in the dry box, and added to the liquid (1 milliliter) in a 4-milliliter vial while stirring magnetically. This procedure had been tested previously by using it to gel RP-1 outside the dry box. To prepare loaded gels, a weighed quantity of gellant was added in the dry box to a weighed amount of solid BeH_2. The mixed solids were added to a measured volume of the liquid and stirred manually, because magnetic stirring was completely ineffective in the loaded system.

CONCLUSIONS

It has been shown that an ATBH, $(BeH_2)_3 \cdot (CH_3BeH) \cdot [Al(CH_3)_3]$, is sufficiently stable at elevated storage temperatures, 165 F, to be used as the liquid vehicle for a heterogeneous fuel. It has also been demonstrated that Beane is completely stable in this vehicle at 165 F.

Approximately 300 grams of ATBH liquid have been prepared. Satisfactory storability has been demonstrated and the density of the liquid has been determined. A stable heterogeneous fuel consisting of BeH_2 suspended in the ATBH liquid has been prepared in the laboratory with Cab-O-sil as the gelling agent. These gels have been mechanically stable for more than 3 months. This approach shows promise for the preparation of storable heterogeneous fuels of 335 to 350 seconds specific impulse using H_2O_2 as the oxidizer.

TASK 4: ENGINEERING CHARACTERIZATION OF PROPELLANTS

INTRODUCTION

The objectives of this task were to determine the engineering characteristics of homogeneous oxidizer and heterogeneous fuel mixtures. The most promising mixtures were evaluated as to detonation sensitivity, thermal stability, and handling hazards. Performance evaluation tests were carried out in a small rocket engine system.

PROPELLANT SENSITIVITY MEASUREMENTS

U-Tube Adiabatic Compression Sensitivity

Principle of U-Tube Tester. The U-tube adiabatic compression tester consists of a U-shaped tube closed at one end and containing a slug of test liquid in the curvature of the tube. The test is conducted by suddenly pressurizing the open end of the tube, which forces the liquid slug violently into the closed end. Peak pressures many times greater than the driving pressure are attained in the closed end of the tube. The rate of pressurization is fast enough to provide adiabatic compression. A simplified schematic of the apparatus is presented in Fig. 54.

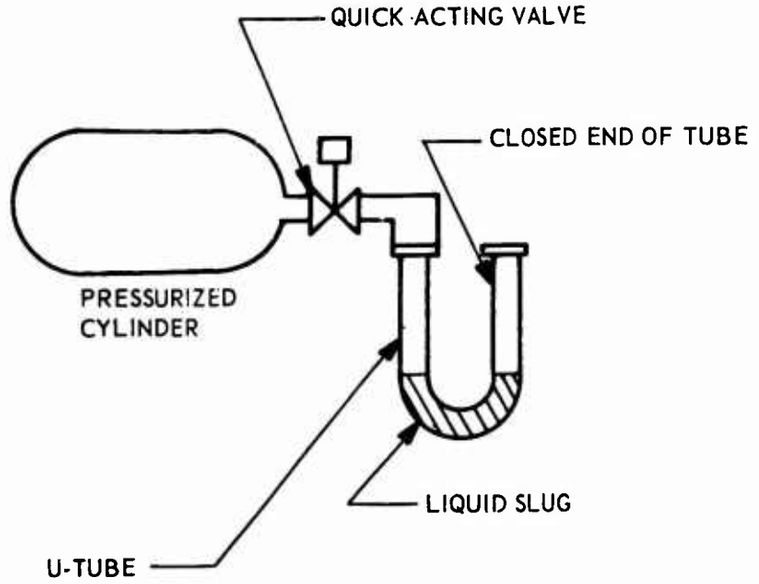


Figure 54. Simplified U-Tube Schematic

The U-tube test has several advantages over the drop weight test. The major advantage is that elastomeric seals were not required because the liquid slug acts as the piston. The only solid material in contact with the test fluid is the metal tube itself. Other advantages are that the composition and initial pressure in the gas phase are easily varied and volatile materials can be easily handled. Furthermore, temperature conditioning is greatly simplified. The major disadvantage of the apparatus

is the large sample size involved (2 milliliters) and the higher cost per test.

Theory. Verschoyle (Ref. 27) studied the dynamics of the U-tube apparatus and derived the following relationship of applied pressure, P_a, initial pressure, P_o, and velocity, v (Fig. 55):

$$P_a (X_o - X) - P_o X_o^{\gamma} (X^{1-\gamma} - X_o^{1-\gamma})/(\gamma-1) = 1/2\ l\rho v^2$$

where

l = length of liquid slug

γ = specific heat ratio

X = distance between liquid and end of tube

M = mass of liquid piston

ρ = liquid density

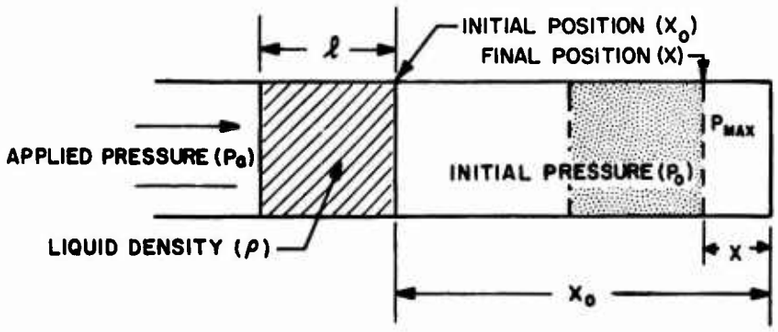


Figure 55. Schematic of U-Tube Section

The assumptions made in the derivation were:

1. Adiabatic, reversible compression of the gas bubble was achieved, i.e., $P_o X_o^{\gamma} = PX^{\gamma}$
2. The liquid moves as a slug (plug flow)

3. Frictional heating of the slug is negligible

The peak pressure (P_{max}) of the gas bubble is realized when the slug velocity is zero ($v = 0$ at $X = X_{min}$). At this point, X_{min}/X_o is negligible compared to 1. Furthermore, $X_o/X_{min} = (P_{max}/P_o)^{1/\gamma}$. With these relations, Eq. 25 can be rearranged to give:

$$P_{max}/P_o = \left[(\gamma - 1)\ P_a/P_o + 1 \right]^{\gamma/\gamma-1} \tag{26}$$

In terms of maximum temperatures, Eq. 26 becomes:

$$\frac{T_{max}}{T_o} = \left[(\gamma - 1)\ P_a/P_o + 1 \right] \tag{27}$$

Thus, the peak pressure, P_{max}, and peak temperature, T_{max}, depend only on the pressure ratio (P_a/P_o), and the specific heat ratio of the gas bubble. Based on this analysis, the criterion for sensitivity in the U-tube compression apparatus is reported as a 50 percent test rupture point vs pressure ratio, P_a/P_o. It should be noted that Eq. 26 is an ergery balance on the system. With the assumptions listed, the total energy was considered to be transferred to the initial gas bubble and the energy available for initiation of an explosion in the gas bubble is proportional to P_a/P_o.

Apparatus and Experimental Technique. The apparatus developed by Air Reduction Company (Ref. 26) was installed with minor modifications to simplify introduction of the oxidizer mixtures into the U-tube. The entire test apparatus was assembled in subdivided enclosures to minimize blast and shrapnel damage. Pressure transducers were installed to measure the pretest vapor pressure exerted by the confined liquid slug. As discussed in the foregoing Theory section, accurate measurement of the initial pressure is essential in the sensitivity test. Because of difficulties in condensing Compounds R and T, the apparatus was modified to accomplish a flow-through condensation technique, in which the U-tube was used as a cold trap. Additional modifications included an air-operated vibrator

attached to one leg of the U-tube to accomplish mixing of multicomponent oxidizers and a temperature-conditioning bath to control the test temperature. Early tests were made at ambient temperatures. Lower temperatures were, however, desirable with many mixtures to reduce the vapor pressure and hence increase the range of driving pressure ratios since the maximum driving pressure available was fixed at about 1800 psig. A test temperature of 32 F was selected for this purpose. A complete schematic diagram of the apparatus is presented in Fig. 56.

When loading mixtures, the volatile components were metered individually by pressure in the calibrated volume loading system and then were condensed sequentially into the U-tube at liquid nitrogen temperature. At the pressures used (less than atmospheric), all materials except N_2O_4 were assumed to be perfect gases. The Compounds R and T used for these tests contained significant amounts of contaminants which were noncondensable in liquid nitrogen. Correction factors were determined by condensing metered samples in the U-tube by the same techniques used in actual loading and revaporizing the samples into the loading system. Noncondensables comprised about 5 mole percent in all cases with these materials. Equilibrium data for the reaction $N_2O_4 \rightleftharpoons 2NO_2$ as a function of temperature and pressure (Ref. 30) were used in determining the amount of N_2O_4 loaded into the U-tube. Tetranitromethane was loaded by adding the desired amount into the U-tube with a calibrated syringe and freezing the sample as a film on the walls in ice water before the U-tube was installed in the apparatus.

All liquid compositions were corrected for losses to the vapor space in the apparatus. Because of the necessity for pressure transducers and connecting lines, this volume amounted to 88 to 101 milliliters, depending on the pressure transducers installed. Since the solutions were not ideal, an attempt was made to determine vapor-liquid equilibrium data for the R-N_2F_4-TNM system to determine accurately the composition of the vapor phase and the liquid composition.

An empirical correction factor (C, where PV = CnRT) for the nonideal behavior of N_2F_4 at 0 C was first determined to obtain more accurate

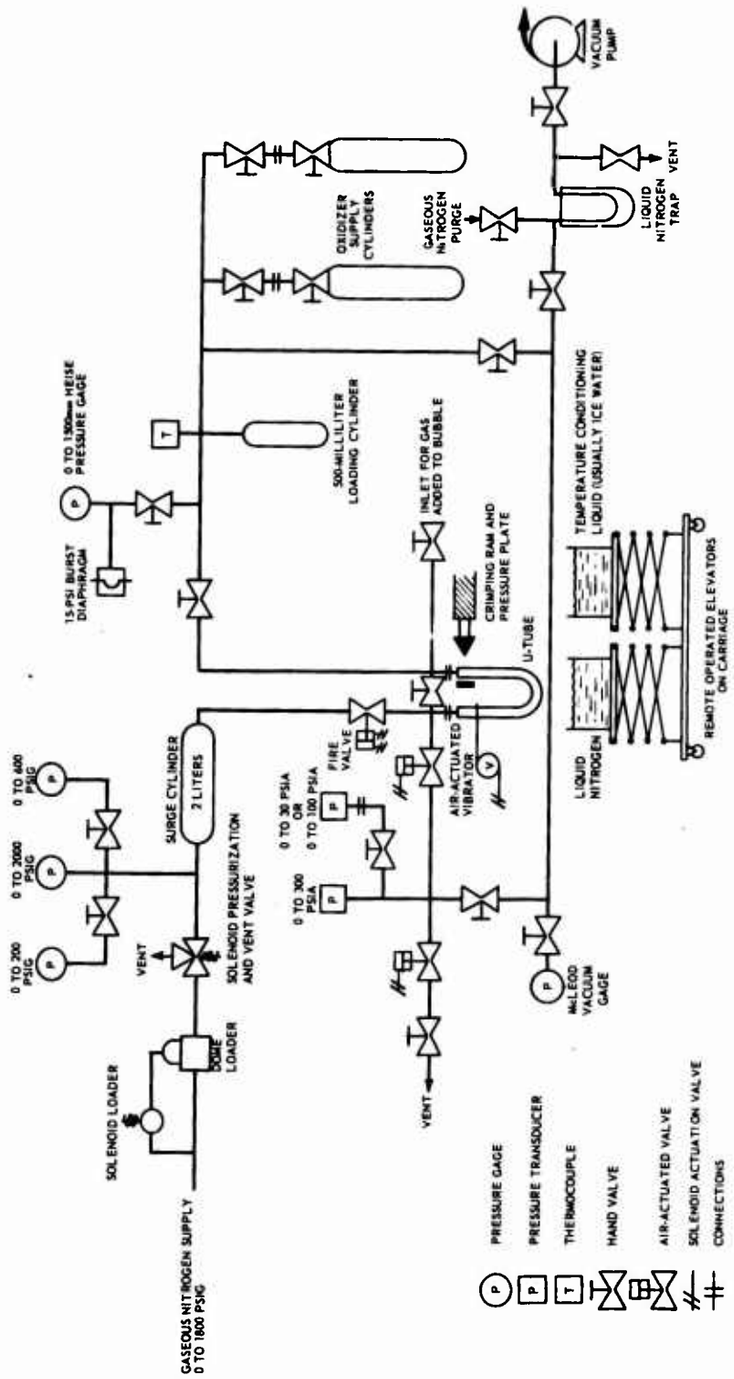


Figure 56. Schematic Diagram of U-Tube Adiabatic Compression Sensitivity Tester

calculations of the liquid compositions. The variation of C with increasing pressure is shown in Fig. 57 . The low-volume, vapor-pressure apparatus (Ref. 1) was modified to allow vapor sampling. Vapor analysis was accomplished by gas chromatography using the gel-column (50-percent halocarbon oil 13-21 on Kel-F) developed at Rocketdyne (Ref. 1). Results of the study are presented in Table 48 . The observed vapor pressures correspond with those observed previously on the N_2F_4-$FC(NF_2)_3$-$C(NO_2)_4$ system (Ref. 31). Mixtures rich in $C(NO_2)_4$ have a positive deviation from the vapor pressure expected for an ideal solution, and mixtures rich in $FC(NF_2)_3$ have a negative deviation. The liquid compositions calculated from vapor analysis, total composition, the correction for nonideal behavior of N_2F_4, and the known ullage of the vapor pressure apparatus are in agreement with the liquid compositions calculated by the previously reported computer program, which does not involve vapor analysis. However, in the absence of necessary equipment refinements, the accuracy of the data is not sufficient for the determination of activity coefficients of the constituents.

Consequently, all compositions were computed by assuming that TNM in the vapor phase was negligible, and the activity coefficients of all other components were equal, i.e., all nonidealities were shared equally by all components in the mixture except TNM. In addition, it was assumed that all components in the vapor except N_2O_4 behaved as perfect gases. Again, the dissociation of N_2O_4 was taken into account by using the data reported in Ref. 30.

Another possible source of error in the compositions reported was incomplete mixing of the components in the U-tube. This would be especially true in the case of the R-N_2F_4-TNM system where the melting points and vapor pressures of the individual components are so widely disparate. This was investigated by loading a typical ternary composition in a glass U-tube. The mixture was observed visually and photographically during all steps of the procedure leading up to the actual test. The standard test procedure was followed in all respects. First, the bottom of the U-tube was immersed in ice water, and the TNM was added using a 1-milliliter syringe. The TNM was frozen as a film on the walls of the tube

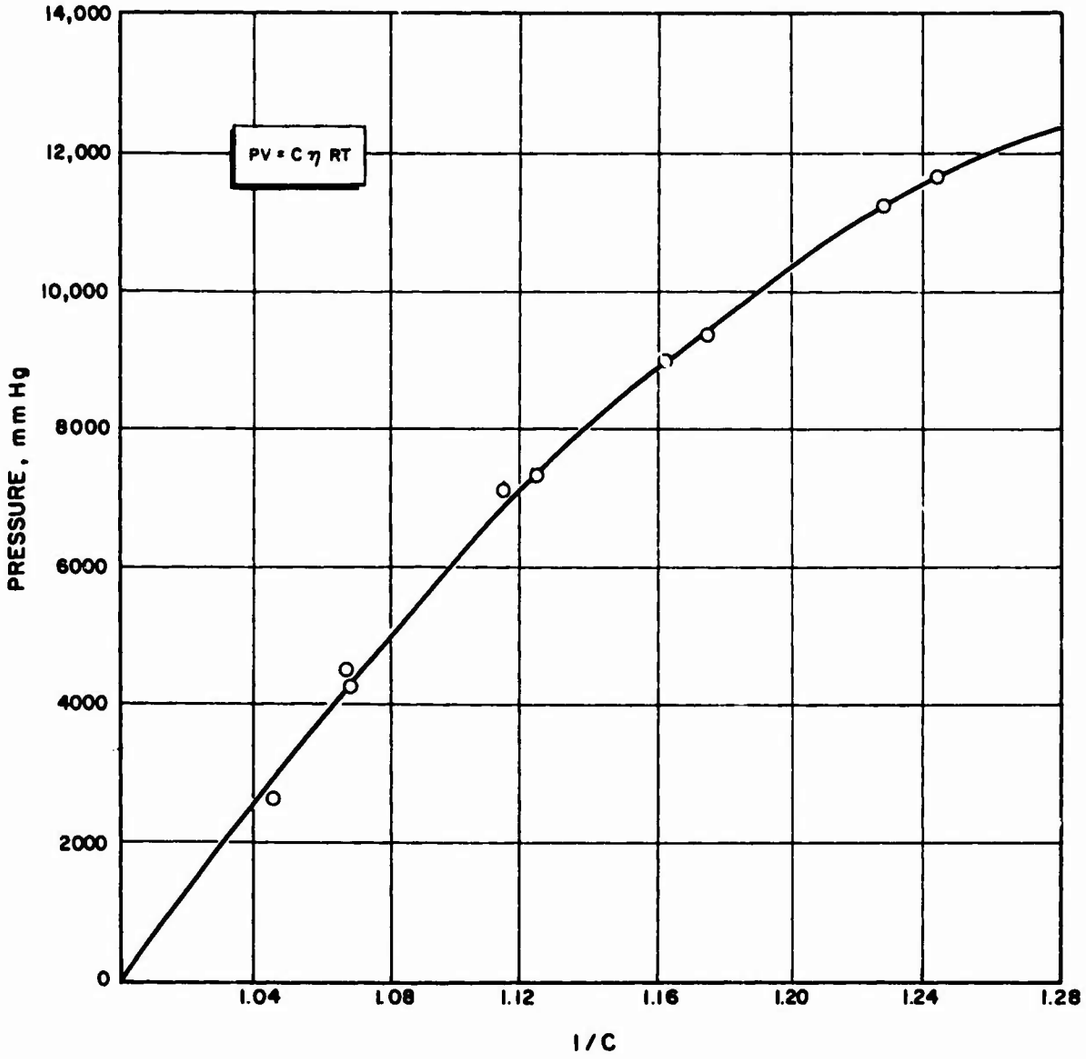


Figure 57. Empirical Correction Factor for Nonideal Behavior of N_2F_4 at 0 C

TABLE 48

VAPOR-LIQUID EQUILIBRIUM CONCENTRATION DETERMINATIONS AT 0 C FOR THE TERNARY SYSTEM (TNM-N_2F_4-R)

Mixture No.	Total Composition, m/o	Liquid[1] Composition, m/o	Analytical Vapor Composition, m/o	Pressure Observed, psia	Calculated Pressure[2] (ideal), psia	Calculated Liquid Composition[3], m/o
1	34.7	40.6				40.6
	27.1	15.9	93.1	58.8	43.8	16.7
	38.2	43.5	6.9			42.3
2	37.0	44.4				44.4
	33.8	20.7	98.6	70.8	54.4	21.9
	29.2	34.9	1.4			33.7
3	16.8	21.8				21.6
	46.9	31.3	99.2	88.4	81.6	33.6
	36.3	46.9	.8			44.8
4	10.2	13.7				13.5
	54.1	38.6	99.3	96.7	99.4	40.8
	35.7	47.7	.7			45.7
5	26.5	30.6				30.6
	36.7	27.4	97.0	73.4	71.5	28.0
	36.8	42.0	3.0			41.4
6	4.5	5.8				5.7
	53.9	41.5	96.2	93.9	107	42.5
	41.6	52.7	3.8			51.8
7	13.6	16.8				16.8
	40.1	27.6	94.6	68.1	73.6	28.0
	46.3	55.6	5.4			55.2
8	8.3	10.8				10.7
	53.2	40.9	92.1	94.4	105	40.7
	38.5	48.3	7.9			48.7
9	3.5	7.4				7.7
	62.1	17.9	88.0	52.4	52.3	19.5
	34.4	74.7	12.0			72.8

[1]Liquid composition calculated from total composition and analytical vapor composition.
[2]Ideal vapor pressure calculated from 1 above.
[3]Liquid composition calculated from total composition; ullage and vapor pressure by machine program.

by this means. The tube was then attached to the apparatus, the ice-water bath replaced with a liquid nitrogen bath, and the tube evacuated. The desired pressure of Compound R vapor was admitted to the evacuated metering volume and frozen out by drawing the mixture through the U-tube with a vacuum. The N_2F_4 was loaded using the same procedure. The vibrator was then turned on and the liquid nitrogen bath replaced with the ice water bath.

The mixing test was made with a feed calculated to provide a liquid composition of approximately 54 w/o R, 18 w/o N_2F_4, and 28 w/o TNM at 32 F in the test system.

The major agitation during warming was caused by boiling of the volatile components from the mixture. Melting and some boiling of the N_2F_4 began while the conditioning baths were being changed. Violent boiling began as soon as the ice bath reached the U-tube. This boiling occurred throughout the liquid, even at the bottom of the U-tube. In less than 2 minutes, all the solid TNM had disappeared. At this point, boiling had subsided although some bubbling was still observed. Some agitation from the vibrator was evident after the bubbling had subsided.

The liquid phase appears to be entirely homogeneous less than 5 minutes after immersion in the ice bath. On this basis, all mixtures were allowed at least 5 minutes to come to equilibrium. During tests, system pressures became constant well before this time.

Calibration Tests. A series of calibration tests was conducted with ethyl nitrate and n-propyl nitrate to check the operation of the tester, to confirm the theoretical conclusions stated previously, and to provide a basis for comparison of mixed oxidizers. These results are summarized in Table 49.

TABLE 49

U-TUBE SENSITIVITY CALIBRATION DATA

Calibrating Material	Gas Bubble Pressurant	Initial Pressure, atmospheres	50-Percent Positive Driving Pressure Ratio
Ethyl Nitrate	Air	1	7.3
Ethyl Nitrate	Air	2	7.9
Ethyl Nitrate	Air	3	8.6
Ethyl Nitrate	Air	5	8.0
Ethyl Nitrate	Nitrogen	3	24
n-Propyl Nitrate	Air	1	21
Nitroethane	Air	1	>120

All tests were conducted at ambient temperature ($\sim$ 70 F). The ambient pressure calibrations with ethyl nitrate were comparable with the results of both Minnesota Mining and Manufacturing Co. (Ref. 28) and Air Co. (Ref. 26). The n-propyl nitrate calibrations agreed with Air Co. but were in wide disagreement with the data of Minnesota Mining and Manufacturing Co. This was attributed to the anomalous behavior of n-propyl nitrate during this test. Frequently, at high driving pressure ratios, the tube was not ruptured, but obvious decomposition of the n-propyl nitrate had occurred. When rupture of the tubing occurred, it was in the upstream portion of the U-tube and inflicted considerable damage to the pressurization fittings and adapter. For this reason, the testing with n-propyl nitrate was limited and calibrations were conducted primarily with ethyl nitrate.

Individual data from the ethyl nitrate calibration tests at all initial pressures were analyzed as a group. The results of this analysis showed a driving pressure ratio to produce 50 percent positive results of 7.81 with a standard deviation of 0.71. Most important, however, this analysis showed there was no significant difference between sets, i.e., between the driving pressure required to obtain 50 percent positive results for the various initial pressures.

Test Results. The results of tests on individual components and various mixtures are presented in the ensuing paragraphs.

Tetranitromethane (TNM). Five tests were conducted to evaluate the sensitivity of TNM at ambient temperature. In all cases, dry air in the gas bubble and the maximum driving pressure of 1800 psi were used. The gas bubble was partially evacuated during some tests to obtain higher driving pressure ratios. No positive reactions were obtained up to the maximum driving pressure ratio of 256.

Compound R. Sensitivity test results of Compound R under its own vapor in the gas bubble are presented in Table 50. The driving pressure ratio for 50 percent positive results was 4.3. Additional tests were conducted on a later shipment of Compound R in conjunction with the tests on the R-N_2F_4-TNM system and are reported with that data.

Under company sponsorship, high-speed photographic coverage was made of special tests on Compound R, ethyl nitrate, and n-propyl nitrate in which glass U-tubes were used. The film showed both the liquid and vapor phase of Compound R participating in the explosion. This contrasts with the ethyl nitrate and n-propyl nitrate photographs where it can be seen that the explosion occurred only in the vapor phase. These observations were supported by the damage sustained by the stainless-steel U-tubes during the standard tests. During tests with Compound R, T, and mixtures containing these materials, 2 to 3 inches of tubing were completely fragmented in positive tests. During positive tests with ethyl nitrate only a small portion of the tubing next to the crimp was ruptured.

TABLE 50

U-TUBE SENSITIVITY DATA FOR COMPOUND R
WITH 1.0 ADDITIONAL GAS SPACE PRESS RATIO

Test Number	Pressure Ratio, P_d/P_i	Sensitivity
1	6.42	Positive
2	3.94	Negative
3	5.01	Negative
4	5.14	Negative
5	6.6	Positive
6	5.98	Positive
7	5.56	Positive
8	5.29	Positive
9	5.02	Positive
10	4.92	Positive
11	4.48	Positive
12	3.97	Positive
13	3.01	Negative
14	2.97	Negative
15	3.14	Negative
16	18.5	Positive
17	9.65	Positive
18	5.5	Positive
19	3.73	Negative
20	8.6	Positive
21	6.3	Positive
22	3.72	Positive
23	3.72	Negative
$\hat{\mu} = 4.32$	$\hat{\sigma} = 0.95$	
$\hat{\sigma}_{\hat{\mu}} = 0.34$	$\hat{\sigma}_{\hat{\sigma}} = 0.36$	

NOTE: $\hat{\mu}$ = 50-percent point

$\hat{\sigma}$ = estimate of standard deviation

$\hat{\sigma}_{\hat{\mu}}$ = estimate of standard deviation of sample mean

$\hat{\sigma}_{\hat{\sigma}}$ = estimate of standard deviation of sample standard deviation

A series of tests was conducted wherein air was introduced into the vapor space above Compound R liquid. The results of these tests are presented in Table 51 and Fig. 58. The straight line drawn through the data in Fig. 58 represents estimates of the 50-percent positive level boundary of the sensitive region. This line fits the equation:

$$P_d/P_i = 18.9 - 14.5\ Y_R$$

where

P_d/P_i = critical driving pressure ratio

Y_R = mole percent R in vapor

This equation should not be extrapolated to compositions lower than 60 m/o Compound R in the vapor.

Compound T. Six tests were conducted on Compound T under its own vapor in the gas bubble. These tests are presented in Table 52. The driving pressure ratio to cause 50-percent positive results was 4.4. These results contradicted earlier reports that Compound T was more sensitive than Compound R.

Compound R-N_2O_4. The results of sensitivity tests on liquid mixtures of Compound R and N_2O_4 are presented in Table 53 and Fig. 59. The sensitivity curve as a function of liquid composition compares favorably with the results of MMM "Schlagen Test" (Ref. 29). The decrease in sensitivity, however, is more gradual with decreasing Compound R concentrates than in Ref. 29. It was noted that positive tests were more exposively violent with R-N_2O_4 mixtures than for R by itself.

TABLE 51

U-TUBE SENSITIVITY DATA FOR PURE COMPOUND R
WITH DRY AIR AS A GAS SPACE PRESSURANT

Test Number	Mole Percent R in Vapor	Driving Pressure Ratio, (P_d/P_i)	Sensitivity
1	6.9	4.12	Negative
2	37.2	3.78	Negative
3	38.7	3.05	Negative
4	46	4.45	Negative
5	90.1	5.78	Positive
6	78.0	10.3	Positive
7	38	4.3	Negative
8	26	4.2	Negative
9	42.5	6.7	Negative
10	58	5.9	Negative
11*	33.3	6.15	Negative
16	81	10.3	Positive
17	84	6.16	Negative
18	62	7.96	Negative
19	70	8.66	Negative
20	87	8.94	Positive
21	48	8.99	Negative
22	93	8.89	Positive
23	92	9.04	Positive

*Tests 12 through 15 are deleted because of recorder malfunction.

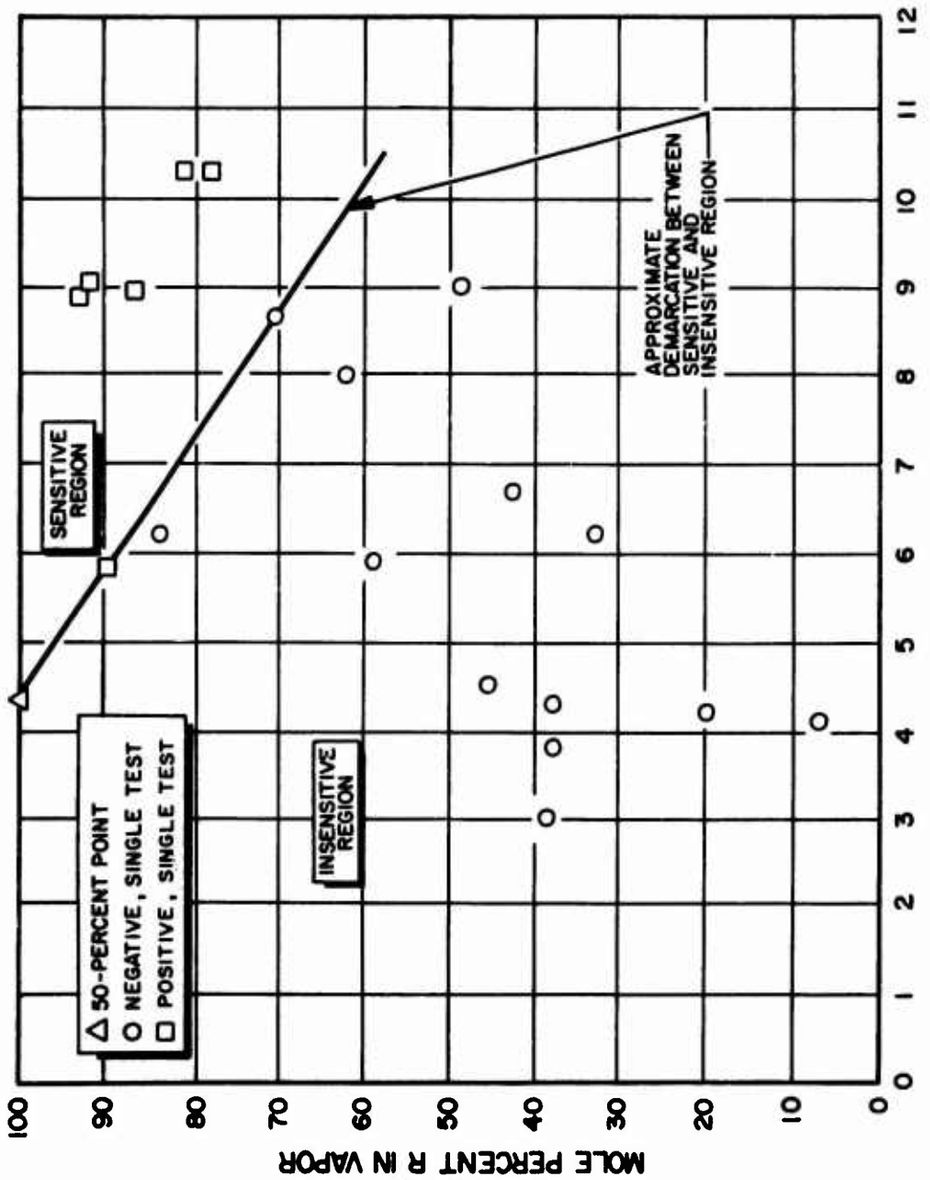


Figure 58. U-Tube Sensitivity of Compound R With Pure, Dry Air

TABLE 52

COMPOUND T TEST DATA

Test Number	Test Temperature	Driving Pressure Ratio	Result
1	83	2.2	Negative
2	67	3.5	Negative
3	68	5.2	Positive
4	48	4.4	Negative
5	51	4.8	Positive
6	50	4.4	Positive

Compound T-N_2O_4. Test results for mixtures of Compound T and N_2O_4 are given in Table 54 and Fig. 60. An unanticipated result was the apparent sensitization resulting from the addition of small amounts of N_2O_4 to Compound T. Except in this region, the sensitivities of Compound T-N_2O_4 mixtures were equal to those of Compound R-N_2O_4 mixtures.

Compound R-N_2F_4-TNM. The data from sensitivity tests on R-N_2F_4-TNM ternary systems are presented in Table 55 and Fig. 61. All tests were conducted at 32 F. The original test plan called for the determination of isosensitivity contours on the ternary composition diagram. This was to be accomplished by first determining 50-percent positive levels for the apexes and the center of the region of interest as shown by the numbered points in Fig.61 . These were to be supplemented by additional test as required.

Positive results could not be obtained with compositions 1 and 2 in this original test plan at the maximum driving pressure available. This was the result of the high vapor pressures and relatively low sensitivities of these compositions. For this reason, both compositions were shifted toward the Compound R apex of the ternary composition diagram until positive results

TABLE 53

U-TUBE SENSITIVITY FOR COMPOUND R

$-N_2O_4$ MIXTURES

Test Number	Liquid Composition		Liquid Composition Temperature, F	Pressure Ratio (P_d/P_i)	Sensitivity
	Mole Percent R	Weight Percent R			
1	85	92	25	6.4	Positive
2	85	92	71	5.0	Positive
3	69	82	64	6.0	Positive
4	43	60	59	6.9	Negative
5	75	86	60	4.8	Negative
6	43	60	68	9.0	Positive
7	24	39	67	14.4	Negative
8	24	39	67	21.4	Negative
9	24	39	67	31.3	Positive

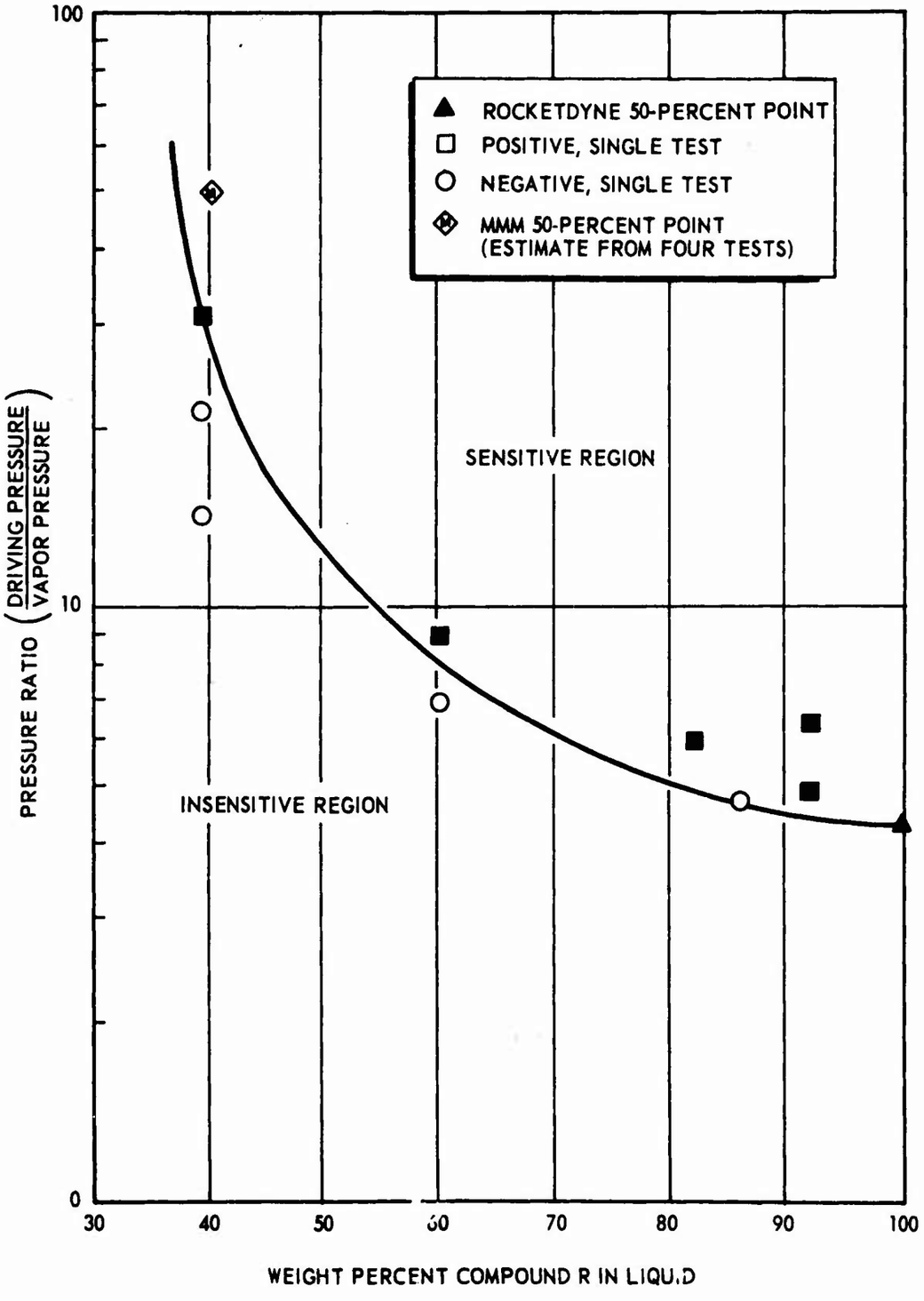


Figure 59. U-Tube Sensitivity of Compound R-N_2O_4

TABLE 54

RESULTS OF U-TUBE SENSITIVITY TESTS
ON MIXTURES OF COMPOUND T-N_2O_4

Test No.	Mole Fraction Compound T	Weight Fraction Compound T	Vapor Pressure, psia	Driving Pressure, psia	Pressure Ratio	Result	Comments
1	0.47	0.68	7.3	120	16.4	Positive	
2	0.49	0.70	7.0	75	10.7	Positive	
3	0.24	0.43	7.2	109	15.1	Negative	
4	0.25	0.44	6.5	195	30.0	Negative	U-tube bulged
5	0.25	0.44	6.3	424	65.7	Positive	
6	0.26	0.45	6.5	276	42.5	Negative	U-tube bulged
7	0.24	0.43	9.1	384	42.2	Positive	
8	0.24	0.43	7.8	324	41.6	Negative	
9	0.25	0.44	7.7	373	48.5	Negative	
10	0.23	0.42	6.3	393	62.4	Positive	
11	0.25	0.44	7.4	368	49.6	Positive	
12	0.25	0.44	7.4	338	45.7	Positive	
13	0.24	0.43	7.0	293	41.9	Negative	
14	0.47	0.68	8.1	47	5.8	Positive	
15	0.13	0.26	6.7	1674	250	Negative	
16	0.13	0.26	7.5	1740	232	Negative	
17	0.47	0.68	7.2	31	4.3	Positive	
18	0.33	0.54	7.0	74	10.6	Positive	
19	0.34	0.55	7.7	50	6.5	Negative	
20	0.36	0.57	7.3	63	8.6	Positive	
21	0.49	0.70	11.0	36	3.3	Negative	
22	0.46	0.67	8.5	32.5	3.8	Positive	
23	0.50	0.70	7.7	26	3.4	Negative	
24	0.37	0.58	8.5	65	7.6	Negative	
25	0.34	0.55	7.2	60	8.3	Positive	
26	0.37	0.58	7.8	58	7.4	Positive	
27	0.56	0.75	8.3	32	3.9	Positive	
28	0.57	0.75	7.6	23	3.0	Negative	

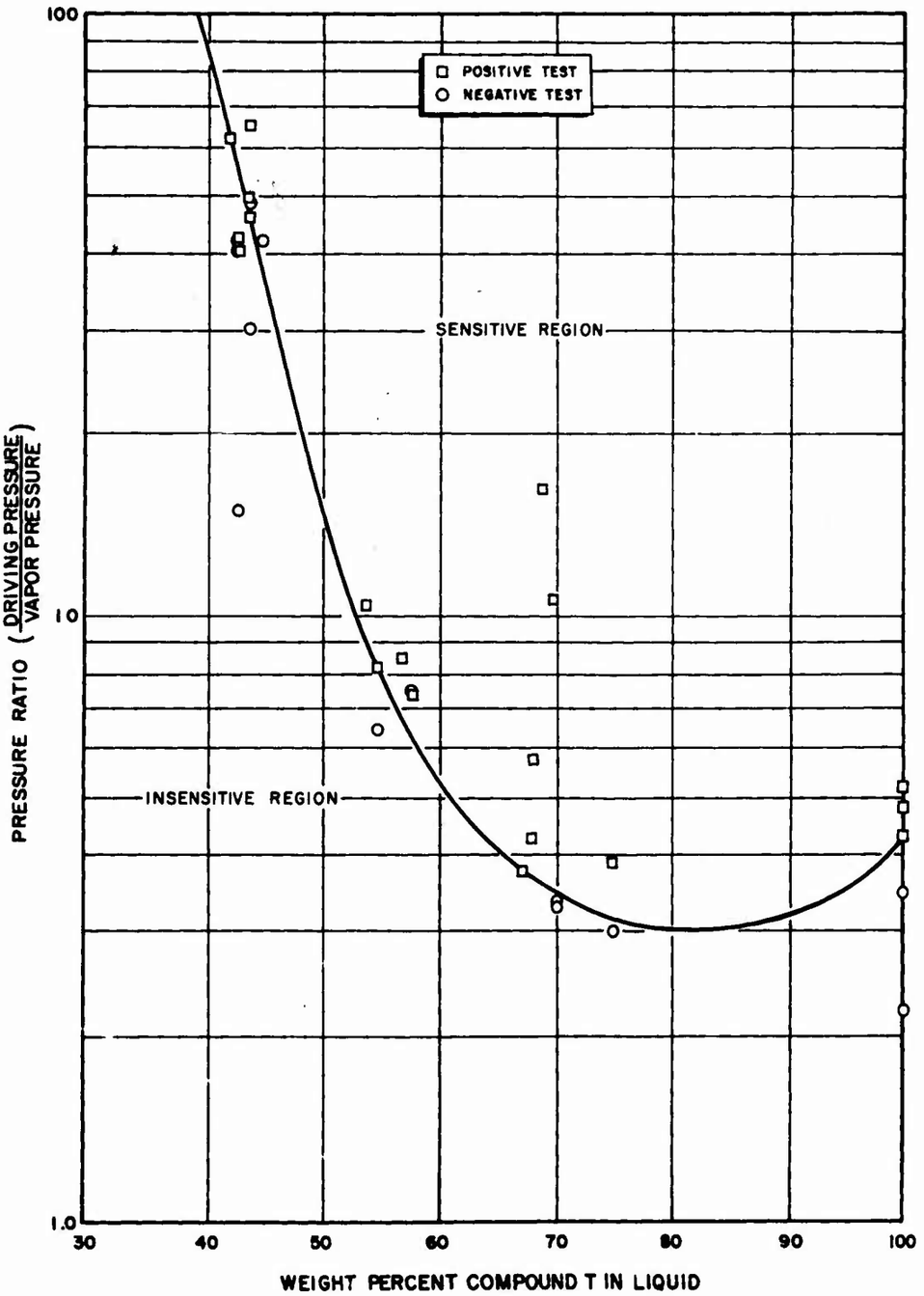


Figure 60. Sensitivity of Compound T-N_2O_4 Mixtures

TABLE 55

SUMMARY OF U-TUBE SENSITIVITY TEST RESULTS WITH R-N_2F_4-TNM MIXTURES

Test Number	Mixture Number	Initial Quantity millimoles			Liquid Composition Weight Fraction			Vapor Composition Mole Fraction		Initial Pressure, psia	Driving Pressure, psia	Driving Pressure Ratio	Results
		R	N_2F_4	TNM	R	N_2F_4	TNM	R	N_2F_4				
1	5	9.4	21.0	4.3	0.54	0.14	0.32	0.09	0.91	80	815	10.2	Negative
2	5	8.9	21.1	4.3	0.53	0.13	0.34	0.10	0.90	83	1245	15.0	Positive
3	1	8.3	39.3	--	0.58	0.42	--	0.04	0.96	130	1715	13.1	Negative
4	1A	11.1	29.0	--	0.70	0.30	--	0.06	0.94	93	1735	18.5	Negative
5	1B	13.5	20.2	--	0.81	0.19	--	0.10	0.90	64.7	1755	26.9	Positive
6	2A	4.5	31.1	7.4	0.25	0.25	0.51	0.03	0.97	105	1740	16.6	Negative
7	2B	6.5	25.1	6.3	0.37	0.17	0.46	0.06	0.94	90	1730	19.2	Positive
8	1B	12.7	20.0	--	0.82	0.18	--	0.11	0.89	68.2	1228	18.0	Negative
9	1B	13.8	20.2	--	0.82	0.18	--	0.11	0.89	66.8	1470	22.0	Positive
10	3	10.9	--	7.0	0.54	--	0.46	1.00	--	9.1	181	19.9	Positive
11	4	19.7	--	--	1.00	--	--	1.00	--	11.8	60	5.1	Positive
12	5	11.5	22.6	5.3	0.55	0.14	0.31	0.09	0.91	75.0	909	12.1	Positive
13	1B	15.4	21.7	--	0.81	0.19	--	0.12	0.88	67.1	1340	20.0	Positive
14	2B	7.6	26.5	3.7	0.49	0.21	0.30	0.06	0.94	92.5	1387	15.0	Positive
15	3	11.0	--	7.0	--	--	--	--	--	--	--	--	Exploded during warming
16	3	11.0	--	7.0	0.53	--	0.47	1.00	--	9.8	--	--	Exploded 6 minutes after warming
17	--	--	--	16.3	--	--	1.00	Ambient Air		13.8	1715	124	Negative
18	3	10.9	--	7.0	1.00	--	--	1.00	--	10.3	103	10.0	Positive
19	3	11.0	--	7.0	0.53	--	0.47	1.00	--	9.6	49	5.1	Positive
20	3	10.6	--	7.0	0.52	--	0.48	1.00	--	9.2	27	2.9	Positive
21	4	19.7	--	--	--	--	--	--	--	--	--	--	Exploded during warming
22	4	17.2	--	--	1.00	--	--	1.00	--	11.8	46	3.9	Positive
23	4	18.8	--	--	1.00	--	--	1.00	--	13.0	31	2.4	Negative
24	3	10.9	--	7.0	0.54	--	0.46	1.00	--	9.1	21	2.3	Negative U-tube exploded after removal
25	3	10.9	--	7.0	0.53	--	0.47	1.00	--	9.5	24	2.5	Negative
26	4	18.0	--	--	1.00	--	--	1.00	--	12.0	42	3.5	Positive
27	5	11.4	22.3	5.3	0.54	0.09	0.36	0.13	0.87	87.5	875	10.0	Negative
28	1B	15.6	21.2	--	0.83	0.17	--	0.12	0.88	70.6	1274	18.0	Negative
29	2B	7.4	26.0	3.7	0.47	0.20	0.31	0.06	0.94	87.3	1048	12.0	Negative
30	3	10.9	--	7.0	0.53	--	0.47	1.00	--	9.8	--	--	Exploded 5 minutes after warming
31	4	17.9	--	--	1.00	--	--	1.00	--	13.2	39.5		Negative

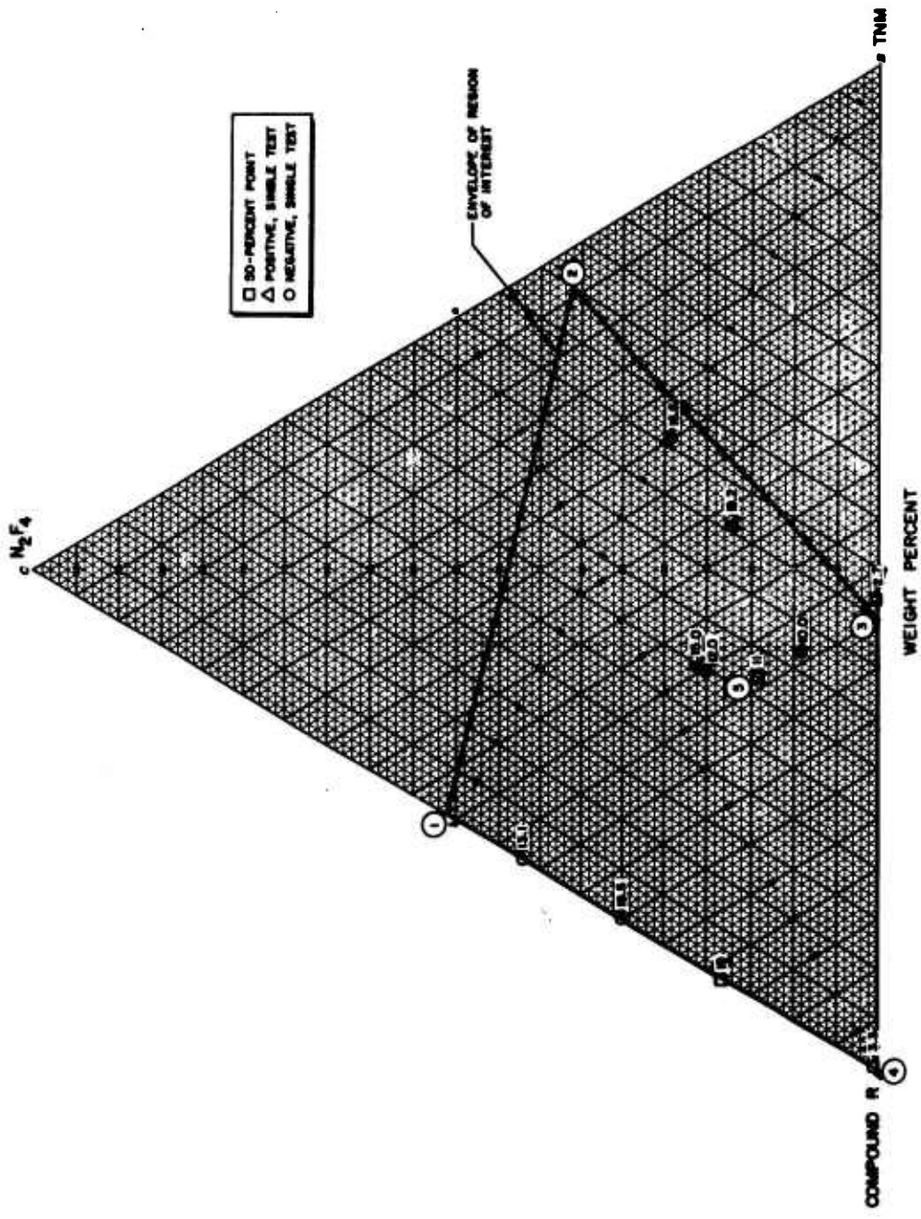


Figure 61. Results of U-Tube Sensitivity Test on Compound R-N_2F_4- TNM System

could be obtained. Tests No. 14 and 29 were intended to be conducted at composition 2B; however, an error in loading these compositions in the U-tube caused them to be shifted away from the TNM apex. Four premature explosions resulted. During tests No. 15 and 21, these occurred just as the ice water came in contact with the U-tube. Many instances of explosions occurring during melting of difluoramino compounds have been reported and these have also been attributed to that cause. The explosions during tests No. 16 and 30 are more baffling. In both cases, the explosions occurred with no apparent cause after equilibrium had been achieved. During test No. 16, the U-tube had been crimped for approximately 1 minute; however, no operations were taking place and the surge tank had not been pressurized at the time of the explosion. The tube had not been crimped during test No. 30. These explosions, indicative of a high order of sensitivity for the R-TNM mixture, have not been included in the analysis of the data subsequently presented. Previous experience had shown that a U-tube removed after a negative test with R-TNM mixtures would explode if dropped. Safety procedures call for evacuation of the tube after a negative test to eliminate propellants prior to removal of the tube from the system. Normally, this evacuation continued for several minutes. During test No. 24, the tube was evacuated for only approximately 20 seconds. This tube exploded when dropped after removal.

Although these results are not sufficient to show isosensitivity contours, certain conclusions can be drawn. The Compound R from the cylinder used during these tests is more sensitive to adiabatic compression than from the cylinder used for earlier tests. The addition of N_2F_4 markedly desensitizes Compound R. However, the addition of TNM not only does not desensitize Compound R but the mixtures actually appear to be more sensitive than pure R. This same sensitization by TNM seems to occur in mixtures containing R and N_2F_4 also.

Compound T-N_2F_4. The sensitivity of one Compound T-N_2F_4 mixture was determined at 32 F. The results of these tests are presented in Table 56. The 50-percent positive driving pressure level of 19 is equivalent to that of Compound R-N_2F_4 mixtures at the same composition.

Explosion of Compound T. Prior to initiating U-tube sensitivity tests on Compound T, the contents of four shipping cylinders, each containing approximately 75 grams of material at approximately 100 mm Hg absolute pressure, were consolidated into a single cylinder to provide a higher feed pressure for the U-tube apparatus. A constant temperature box maintained at approximately 90 F was installed around this cylinder to ensure that no Compound T would condense and form an explosion hazard. A remote handling system including part of the U-tube system was temporarily installed to condense the contents of the shipping cylinder into a 500-cc Hoke cylinder. The Compound T was then vaporized into the supply cylinder by a heating tape around the Hoke cylinder. Subsequent to the transfer of the final shipping cylinder, an explosion occurred which ruptured the Hoke cylinder and damaged the associated valves and tubing. The evidence indicated that some liquid Compound T remained in the Hoke cylinder and tha small amounts had condensed in at least two places in the transfer tubing. The cause of initiation is unknown because no operations were taking place at the time of the explosion and the heating tape had been turned off. Fortunately, the cylinder valves had been closed and the Compound T in the supply cylinder was not lost.

TABLE 56

RESULTS OF U-TUBE SENSITIVITY TESTS ON COMPOUND T-N_2F_4

Test Number	Mole Fraction N_2F_4	Weight Fraction N_2F_4	Initial Pressure	Driving Pressure	Driving Pressure Ratio	Result
1	0.27	0.15	73.4	1645	22.4	Positive
2	0.28	0.16	73.8	1175	15.9	Negative
3	0.27	0.15	73.3	1375	18.8	Negative
4	0.25	0.14	76.0	1555	20.5	Positive
5	0.25	0.14	75.9	1475	19.4	Positive
6	0.24	0.13	76.2	1435	18.8	Positive
7	0.24	0.13	74.8	1365	18.2	Negative

Wenograd Thermal-Sensitivity Tests

Apparatus and Procedure. The sensitivity of materials to high temperatures was evaluated in the Wenograd apparatus. This test was selected as an additional measure of sensitivity to supplement the U-tube adiabatic compression-sensitivity studies. The Wenograd apparatus uses electrical resistance heating to suddenly subject a sample to a high-temperature environment. This sample heating is accomplished by isolating a small sample in a length of capillary tubing and discharging a large capacitor at high initial voltage through the capillary tubing. The time delay to explosion is recorded. The temperature at explosion is dictated by the capacitor charge. The results, as in the U-tube tester, are empirical in nature. The sensitivity of the samples is rated in comparison to previously tested calibrating fluids. By comparing the sensitivity data produced by both the U-tube and Wenograd tests, a more complete sensitivity characterization is accomplished. These combined data provided additional insight into mechanisms controlling the initiation of an explosion.

The apparatus and procedure used was developed by Wenograd (Ref. 32 through 35). Explosion temperatures are determined by monitoring the resistance of the capillary tubing. Time to explosion is found either by observing with an oscilloscope the sudden change of electrical resistance when the capillary tubing ruptures, or recording the sound of the explosion by means of an electronic counter and a microphone. A Tektronix type 555 oscilloscope and a Beckman-Berkeley Model 7370 electronic counter were used. Figure 62 is a simplified circuit diagram of the apparatus. Details of the experimental procedure may be obtained from Ref. 32.

Data from the Wenograd apparatus are plotted as the logarithm of time delay to explosion vs reciprocal temperature. A linear correlation is usually obtained. A complete theoretical analysis is presented in Appendix D.

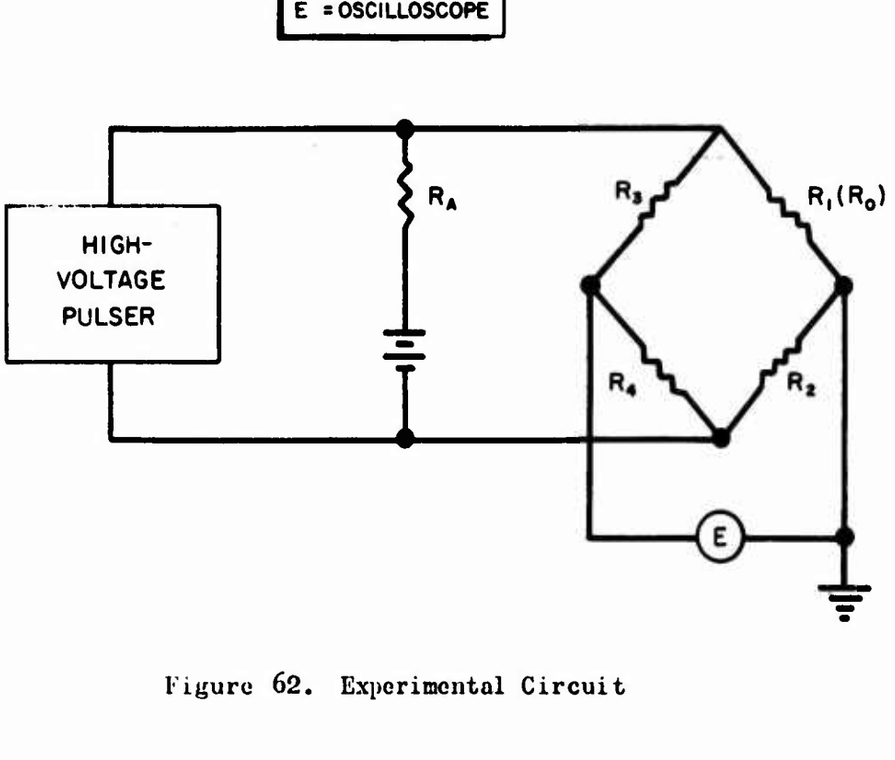


Figure 62. Experimental Circuit

Calibration Data. To establish a basis for comparison of the relative sensitivities of various propellants and propellant mixtures, data were obtained for several standard reference materials: Nitroethane, n-propyl nitrate, ethyl nitrate, and nitroglycerine. The data points for nitroethane, n-propyl nitrate and nitroglycerine are shown in Fig. 63. Considerable scatter is exhibited by all the data obtained with this apparatus. A least-squares calculation is used to determine a straight line through the points. Increasing sensitivity is manifested by either a shorter time delay to explosion or a lower explosion temperature. Therefore, a sensitive substance will exhibit either a shallower slope than a less sensitive material or be displace to the right in Fig. 63.

Test Results With Oxidizers. The results of tests on various oxidizer components are shown in Fig. 64. The curves for nitroethane, ethyl nitrate, and nitroglycerin are included for reference. Tetrafluorohydrazine and tetranitromethane show the same relative correspondence between slope and sensitivity as the standard calibration materials. Nitroglycerin and Compounds A, T, and R yield very steep slopes. For this reason, a relative comparison based on the temperature required to produce a standard time delay such as 0.25 millisecond could be confusing. In general, it is best to compare the curves over a fairly large range of time delays, particularly with compounds of different types. Compounds T and R exhibited a high degree of sensitivity during this test. Compound T gave the highest sensitivity of any material subjected to the Wenograd test. Both Compounds T and R were more sensitive than nitroglycerin. The apparent sensitivity of Compound A probably represents a reaction between the tube and the propellant at the indicated temperature rather than an explosion of the propellant itself.

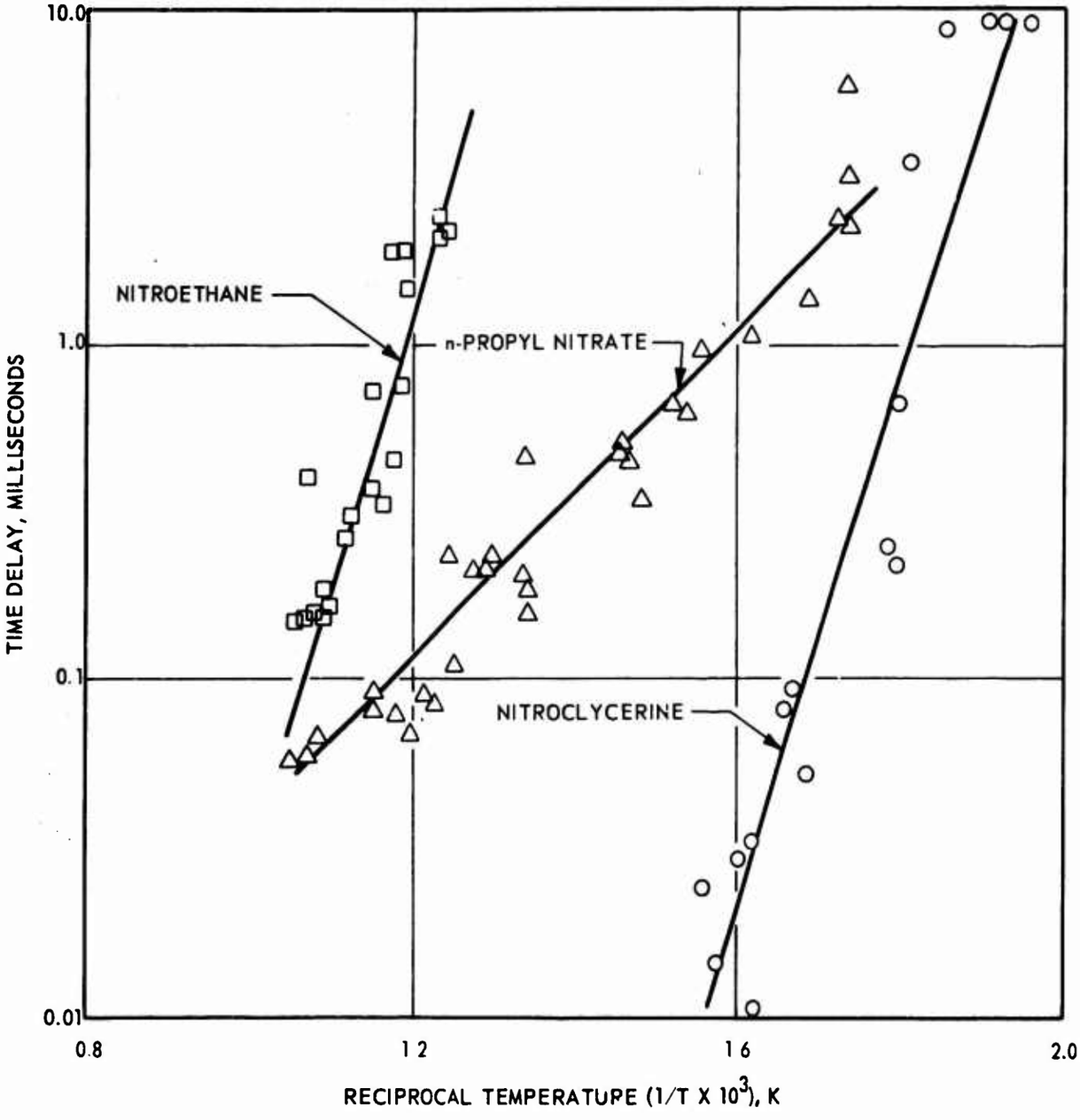


Figure 63. Time Delay as a Function of Temperature at Detonation

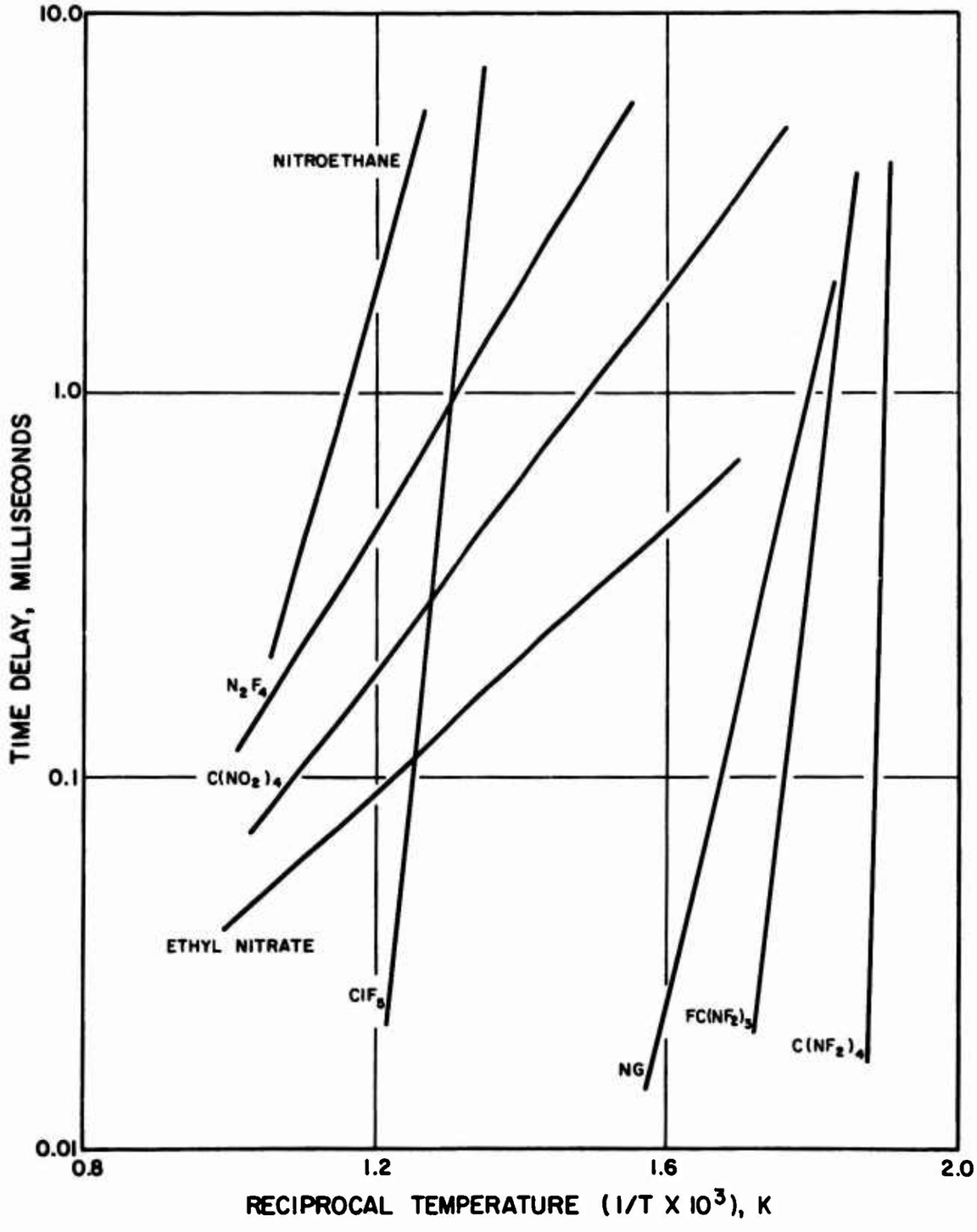


Figure 64. Wenograd Test Results for Various Oxidizers

The sensitivity of one oxidizer mixture, the Compound T-TNM system, was studied in the Wenograd apparatus. The results of these tests are presented in Fig. 65. To illustrate more clearly the effect of composition on sensitivity, the temperature which results in a 0.25-millisecond time delay to explosion was plotted as a function of composition in Fig. 66. This curve shows that the addition of a small amount of Compound T to TNM sharply increases the sensitivity while the addition of a small amount of TNM to Compound T has relatively little effect. This relationship is opposite to that desired. It had been hoped that the addition of small amounts of TNM would strongly desensitize Compound T.

Explosions in Compound T. In preparing the Compound T-TNM samples, accidental explosions which propagated through the hypodermic sample tubing were observed on two occasions. These explosions occurred during the process of sealing off the individual samples by crimping the hypodermic tubing at 2.5-inch intervals. An explosion which initiated at the point being crimped shredded the entire length of tubing (approximately 3 feet). In an effort to better analyze this phenomenon, a number of lengths of tubing were loaded with Compound T and deliberately exploded. It was found that an explosion which progagated through the entire length of tubing could always be initiated by either a thermal or impact stimulus.

Figure 67 shows the results of one of these tests. A 3-foot length of stainless-steel hypodermic tubing (0.007-inch ID and 0.014-inch OD) was loaded with liquid Compound T and the ends were sealed with clamps made from a 1/4-inch bolt and two tubing sleeves. The length of tubing was placed inside a polyethylene bag and then struck lightly near one end with a small hammer. The entire length of tubing was fragmented (Fig. 67). Figure 68 is a closeup of one of the fragments, showing that the tubing had split lengthwise and flattened into a ribbon.

To check the possibility of a surface reaction being responsible for the highly sensitive behavior, a length of tubing was passivated with liquid chlorine trifluoride for approximately 45 minutes, then flushed out and

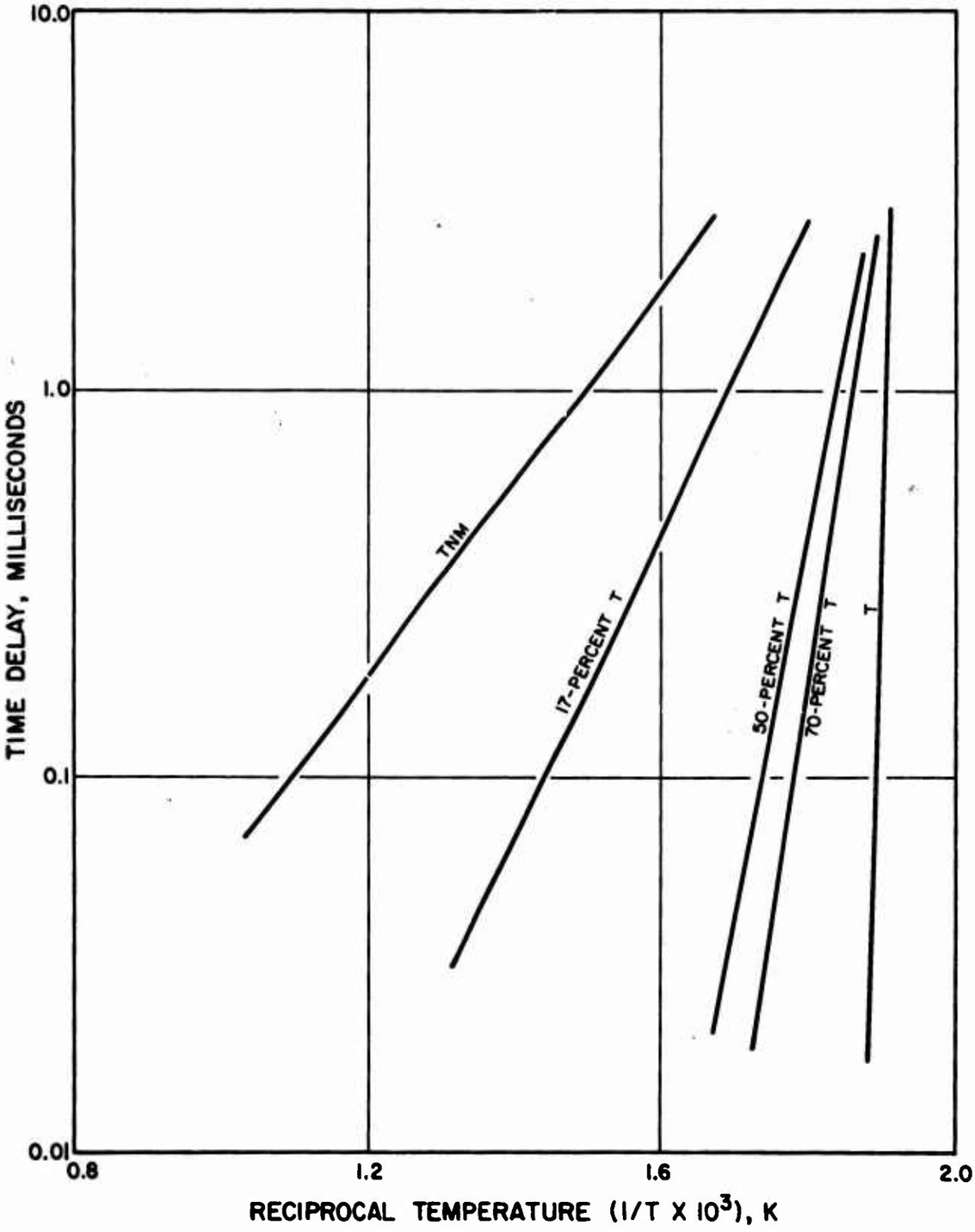


Figure 65. Wenograd Test Results for Mixtures of TNM and Compound T

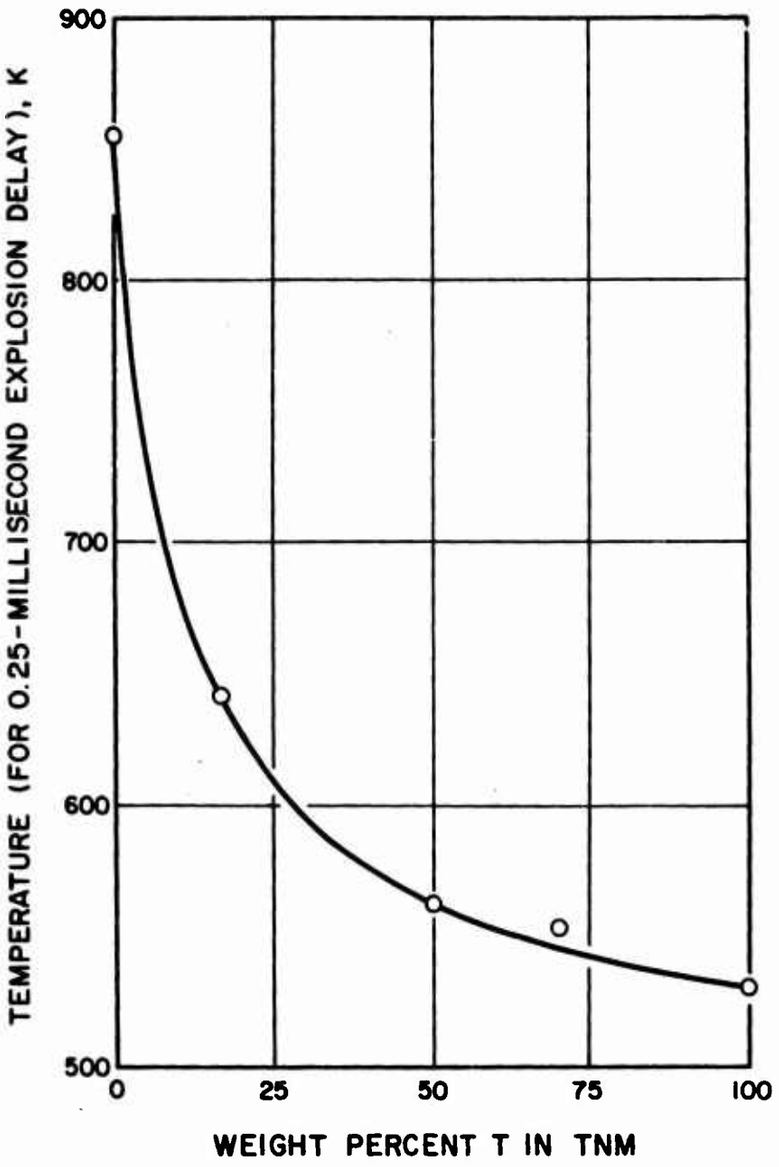
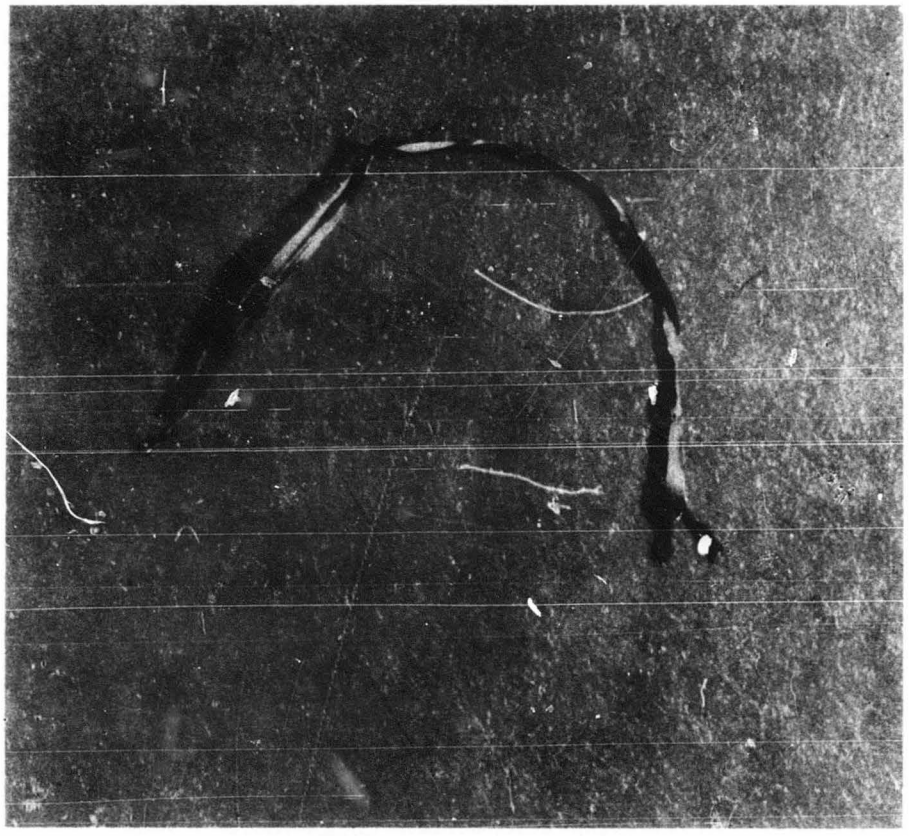


Figure 66. Sensitivity of Mixtures of T and TNM



5AC26-11/22/65-S1D

Figure 67. Explosion of Compound T in Hypodermic Tubing



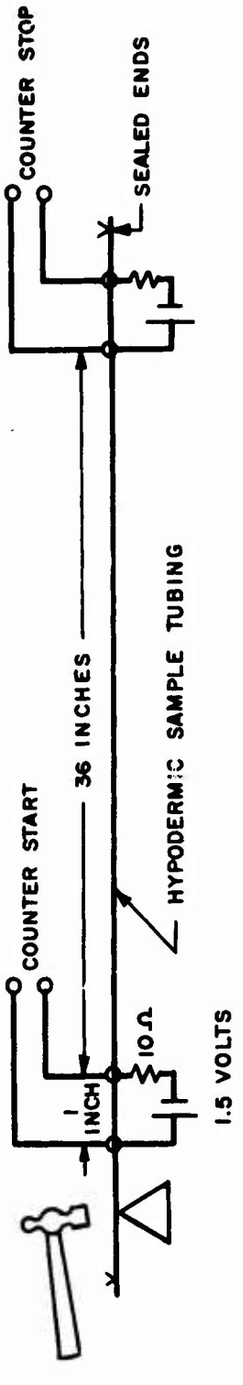
5AC26-11/22/65-S1C

Figure 68. Tubing Fragment

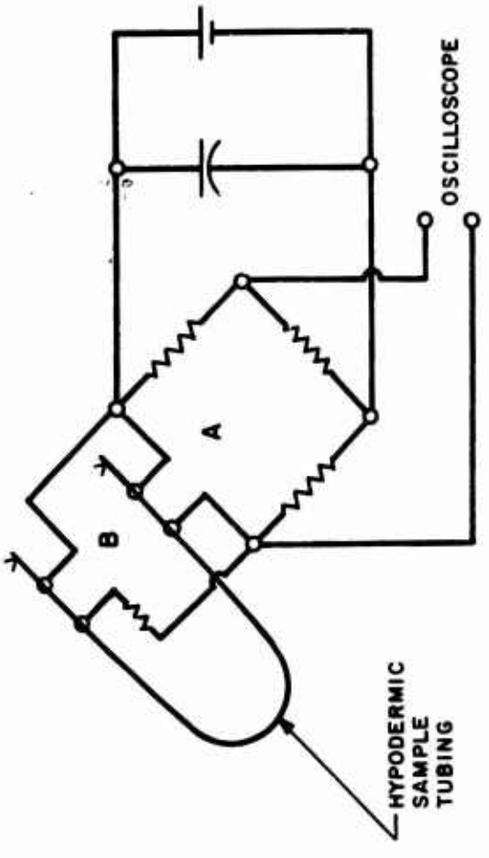
filled with Compound T. The supply of Compound T used during this and all other tests discussed had a stated purity of 99.5 percent. This sample exploded as easily and completely as the others.

A knowledge of the velocity of propagation of the explosion through the tubing would be of value in any detailed analysis. Two methods of measurement were devised (Fig. 69). System I utilizes an electronic counter and two simple triggering circuits which cause a voltage to be applied to the counter input when contact with the sample tubing is broken by the explosion. Explosion is initiated by impact. To provide a more reproducible initiation stimulus, System II was devised. This system makes use of the electronic circuitry of the Wenograd test apparatus. The high-voltage capacitor (Fig. 69) is discharged, causing a large current to flow through the low-resistance arm of the Wheatstone bridge arrangement and subsequent heating and explosion of sample section A. An abrupt change is then registered in the bridge voltage observed by the oscilloscope. The explosion progresses along the sample tubing, finally rupturing section B and producing another sharp change in the oscilloscope trace. Several runs were made with these two systems, and consistently comparable results (Table 57) were obtained for the propagation velocity.

The average of all the data in Table 57 is 187 meters/sec. This value indicates that propagation by means of a shock wave is not involved in these explosions. A much higher velocity would be expected for a detonation and self-supporting shock wave. A possible explanation is a chain reaction of initiations at local "hot spots" caused by adiabatic compression of small gas bubbles in the liquid. To check this hypothesis, a sample was loaded with liquid Compound T under a pressure of 10 atmospheres. Because the other samples had been loaded at a pressure of only slightly more than 1 atmosphere, this initial pressure substantially changed the compression ratio attainable in a gas bubble. This was expected to have a significant effect on the apparent propagation velocity. However, the observed value of 175 meters/sec for the one sample loaded under these



SYSTEM 1. IMPACT INITIATION



SYSTEM 2. THERMAL INITIATION

Figure 69. Propagation Velocity Measurements

conditions indicates that the gas bubble mechanism is probably not operative here. Further study is necessary to define the mechanism.

TABLE 57

VELOCITY OF PROPAGATION

System	Run No.	Sample Length, centimeters	Time, milliseconds	Velocity, meters/sec
I	1	104	5.1	204
I	2	95	6.0	158
I	3	101	5.7	177
II	4	80	3.5	228
II	5	81	4.4	184
II	6	68	4.0	170

In the process of loading more sample tubes for additional tests, an explosion destroyed the sample loading manifold. This explosion occurred when a valve was opened to evacuate the liquid Compound T remaining in the system after loading a sample tube. It is possible that "bumping" of the liquid when the vacuum valve was opened may have been responsible for initiating the explosion.

Test Results With Fuels and Monpropellants. The major objective in this area was to determine the sensitivity of the monopropellant gels. It was found, however, that even though the individual solid particles were considerably smaller than the ID of the capillary tube used for the Wenograd test, it was impossible to load the gel formulations into the tube. The use of larger-diameter tubes for the gel was considered, but the necessary

modifications to the apparatus and additional calibrations were considered unwarranted. Consequently, the only tests performed were on hydrazine, methyl hydrazine, and hydrazine-hydrazine nitrate mixtures. The results of these tests are presented in Fig. 70. The hydrazine-hydrazine nitrate solutions were prepared in a dry box by dissolving crystalline hydrazine nitrate in hydrazine. No significant difference could be detected in the test results with hydrazine and methyl hydrazine. The addition of hydrazine nitrate to hydrazine, however, did increase the the sensitivity significantly. To more clearly show this effect, the temperature required to cause an explosion at various time delays is plotted as a function of composition in Fig. 71. If 0.25 millisecond is chosen as the representative time delay, the critical temperature is reduced from 925 K for pure hydrazine to 650 K for 80 w/o hydrazine nitrate.

Detonation Propagation Tests

Theory and Procedure. For every explosive, there is a diameter below which a column of the explosion will not propagate a detonation. This "critical diameter" ranges from several inches for ammonium nitrate to several thousandths of an inch for nitroglycerin, and is not predictable from other sensitivity measurements. The critical diameter for a particular material varies with the confinement of the charge and with temperature; however, this variation is negligible over the normal range of feed system tubing wall thickness and ambient temperatures. The critical diameter has also been found to be a function of the tube material for many liquid propellants. Tests made in aluminum tubes are not necessarily applicable to stainless-steel tubes and vice versa.

A rocket engine test firing provides many potential sources of initiation of a detonation. Consequently, it is advisable to use feed lines smaller than the critical diameter of the propellant to eliminate the possibility of an explosion propagating back to the feed tank and creating a major disaster. Because the R-5 monopropellant is potentially capable of propagating a detonation, the critical diameter was found for several compositions to ensure that the test stand feed system would not permit a propagating detonation during test firings with this material.

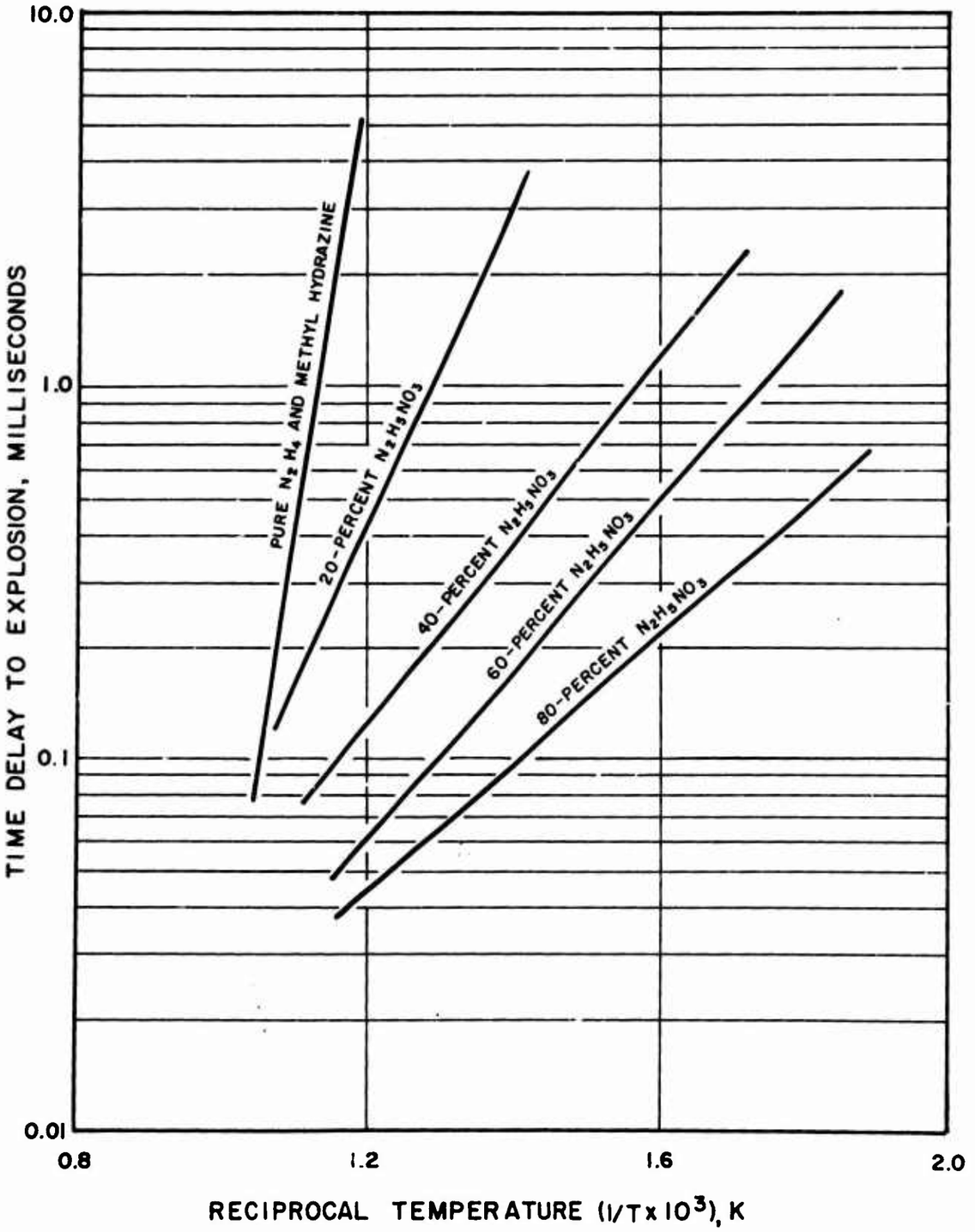


Figure 70. Wenograd Test Results for Mixtures of Hydrazine Nitrate in Hydrazine

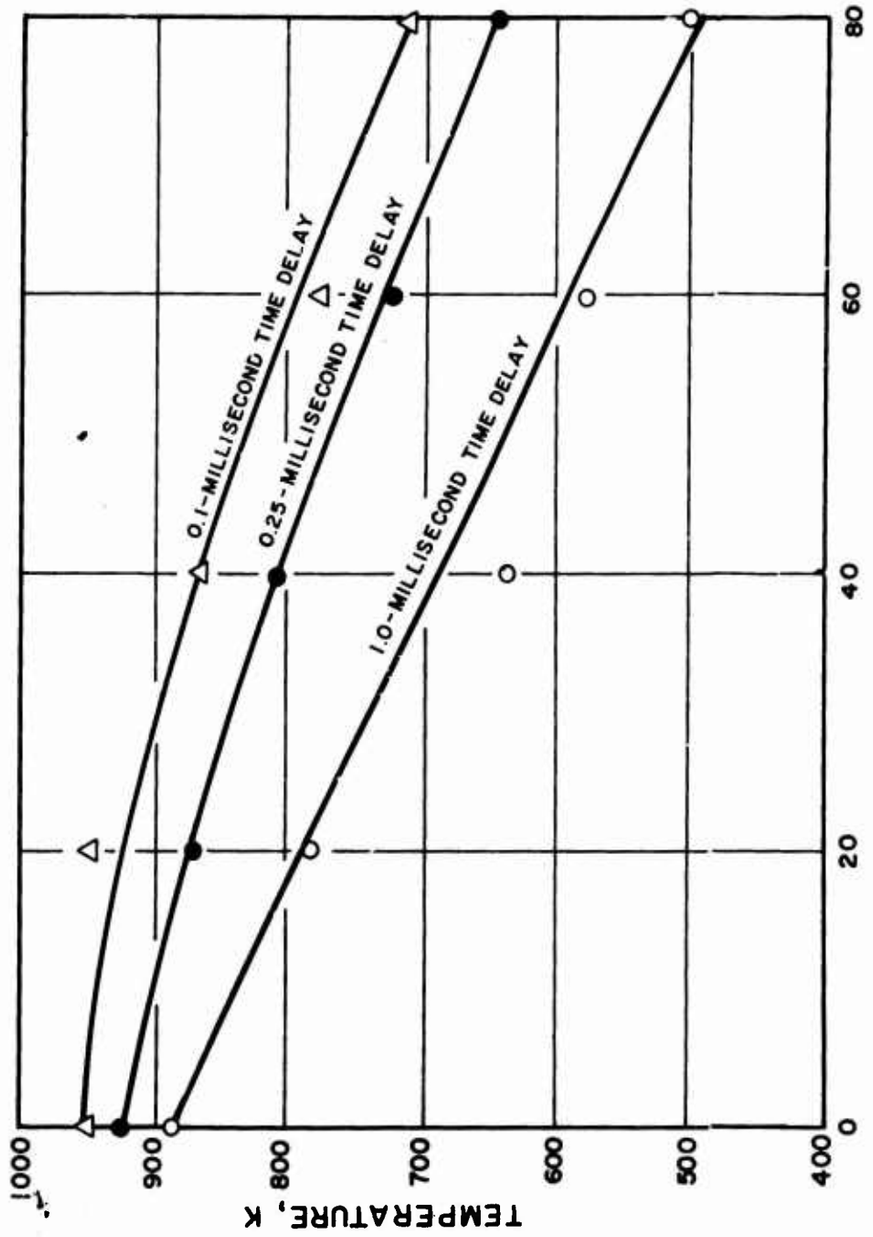


Figure 71. Wenograd Test Results for Mixtures of Hydrazine Nitrate in Hydrazine

Tests were conducted by filling 12-inch-long tubes of various diameters with the propellant formulation, sealing both ends of the tube with thin (0.002 inch) polyethylene sheets, and initiating one end of the propellant column with an explosive charge. To provide the maximum initiation potential, all initiators were at least as large in diameter as the test charge, and had a length-to-diameter ratio of at least 3 to provide a relatively flat shock wave at the interface with the propellant column. The surface of the explosion initiator was also covered only with a 0,002-inch polyethylene sheet and was attached directly to the propellant charge so that attenuation of the shock wave from the initiator was minimized. Two initiators were used for these tests. Both consisted of Composition C-4 explosive, which is a waxed RDX formulation, and were detonated with duPont E-83 commercial electric blasting caps. Initiator No. 1 consisted of 50 grams of Composition C-4 in a 1-inch OD by 0.049-inch wall aluminum tube, and initiator No. 2 consisted of 25 grams of explosive in a 3/4-inch OD by 0.049-inch wall aluminum tube. Both explosive charges were approximately 3 inches long.

Many liquid monopropellants exhibit two modes of propagation. A true high-order detonation propagates at a velocity between 4000 and 8000 meters/sec. The so called "low-order detonation" usually propagates at or slightly above the sonic velocity of the liquid. Although both can be equally damaging to a test facility, the low-order detonation usually requires less energy for initiation but has a larger critical diameter for propagation. The two modes of propagation can be differentiated by placing a "witness plate" of carbon steel sheet at the opposite end of the charge from the initiator. A high-order detonation will punch a hole in the witness plate. Complete fragmentation of the tube but no hole in the witness plate indicates a low-order detonation. Carbon steel witness plates 4 by 4 by 3/16 inches were used during all tests.

Results. Tests were made on four gel formulations in which the ratio of hydrazine nitrate to water in the liquid phase was varied. The compositions of these formulations are presented in Table 58 and the test results are presented in Table 59 All tests were conducted in stainless-steel

tubes 12 inches long. Tests 9 through 13 were conducted on one batch of gel on a very hot, dry afternoon. Although precautions were taken to minimize evaporation of water from the gel, it is certain that some evaporation did take place during mixing and loading of the tubes. Tests 14 through 17 were conducted on a new batch of gel the following morning, and more stringent precautions were taken against evaporation. It is believed that this evaporation of water is the explanation for the inconsistent results obtained with the R5-D formulation, and that the true critical diameter for this formulation is approximately 3/4-inch.

In addition to the detonation propagation tests, impact tests were conducted on the R5-A formulation. Tests were made in the standard JANAF drop-weight tester. The sample holder assembly was enclosed in a polyethylene bag to confine toxic products from a positive test. Negative results were obtained during all tests where a 2 pound weight was dropped 5-1/2 feet. Under identical conditions, n-propyl nitrate invariably gave positive results when the weight was dropped 3-1/2 feet.

A sample of R5-A gel was placed in a shallow plastic pan approximately 4 inches in diameter and 1/2-inch deep and ignited with a pyrotechnic igniter. The sample continued to burn in air after the igniter had burned out and until all the gel was consumed. The residue consisted of white solids.

TABLE 58

COMPOSITIONS OF R-5 MONOPROPELLANT GEL FORMULATIONS

Gel Designation	Concentrated HN In Liquid, weight percent	Gel Composition, weight percent				
		Be	BeH_2	HN	H_2O	Kelzan
R5-A	40	15.2	15.2	27.6	41.5	0.50
R5-C	50	14.9	14.9	34.9	34.8	0.48
R5-D	55	14.4	14.4	39.0	31.8	0.47
R5-B	60	13.8	13.8	43.1	28.8	0.46

TABLE 59

RESULTS OF DETONATION PROPAGATION TESTS ON R-5 GELS

Test No.	Gel Designation	Initiator	Tube Size, inches	Results
1	R5-A	1	1 OD x 0.065 wall	Negative-7-inch undamaged tube recovered
2	R5-A	1	1 OD x 0.065 wall	Negative-6-inch undamaged tube recovered
3	R5-B	1	1 OD x 0.065 wall	High-order detonation
4	R5-B	1	3/4 OD x 0.049 wall	High-order detonation
5	R5-B	2	1/2 OD x 0.035 wall	High-order detonation
6	R5-B	2	3/8 OD x 0.028 wall	High-order dotonation
7	R5-C	1	1 OD x 0.065 wall	Negative-6-inch undamaged tube recovered
8	R5-C	1	1 OD x 0.065 wall	Negative-6-inch undamaged tube recovered
9	R5-D	1	3/4 OD x 0.049 wall	Negative-5-inch undamaged tube recovered
10	R5-D	1	1 OD x 0.065 Wall	High-order detonation
11	R5-D	2	3/4 OD x 0.049 wall	High-order detonation
12	R5-D	2	5/8 OD x 0.065 wall	High-order detonation
13	R5-D	2	5/8 OD x 0.065 wall	High-order detonation
14	R5-D	1	1/2 OD x 0.035 wall	Negative-8-inch undamaged tube recovered
15	R5-D	1	5/8 OD x 0.065 wall	Negative-6-inch undamaged tube recovered
16	R5-D	1	5/8 OD x 0.065 wall	Negative-6-inch undamaged tube recovered
17	R5-D	1	3/4 OD x 0.049 wall	Negative-3-inch undamaged tube recovered

HETEROGENEOUS PROPELLANT FLOW AND
PERFORMANCE EVALUATION

Experimental System

An experimental flow system was designed and constructed to study the flow characteristics of heterogeneous fuels on an engineering scale. This flow system served as the fuel feed system for thrust chamber performance evaluation test firings. Figure 72 is a simplified flow diagram of the system. The gelled fuels are expelled by a positive displacement piston. Two identical expulsion tanks were used to permit recycling of the fuel from one tank to the other in a completely closed system. The piston in tank A is driven by liquid hydrazine forced from tank C under gaseous nitrogen pressure. Flowrates were determined by means of a turbine flowmeter in the hydrazine line. Tank levels were obtained by monitoring the position of the follower rod attached to the expulsion piston. Figure 73 is a cross-sectional view of the expulsion tank.

The basic thrust chamber assembly used consisted of a 2.4-inch ID, uncooled, solid-wall chamber with a characteristic length of approximately 150 inches, depending upon the particular injector and nozzle assembly used. A nominal thrust of 500 pounds at a 1000-psia chamber pressure was chosen. To contain the toxic exhaust products, the nozzle exhausts into a water-scrubbing and filtration system, shown schematically in Fig. 74 and photographically in Fig. 75. The method of connecting the nozzle to the scrubber by means of a rubber boot is shown in Fig. 76.

The chamber exhaust flows first through a cylindrical scrubbing section approximately 3 feet in diameter and containing a series of 30 large-capacity, water-spray nozzles along its length. A dense spray (approximately 400-gpm total flow) cools and removes most of the solid particles from the exhaust. Saturated vapors then pass through a demister and finally out through a bank of 22 ultrafilters (the approximately square

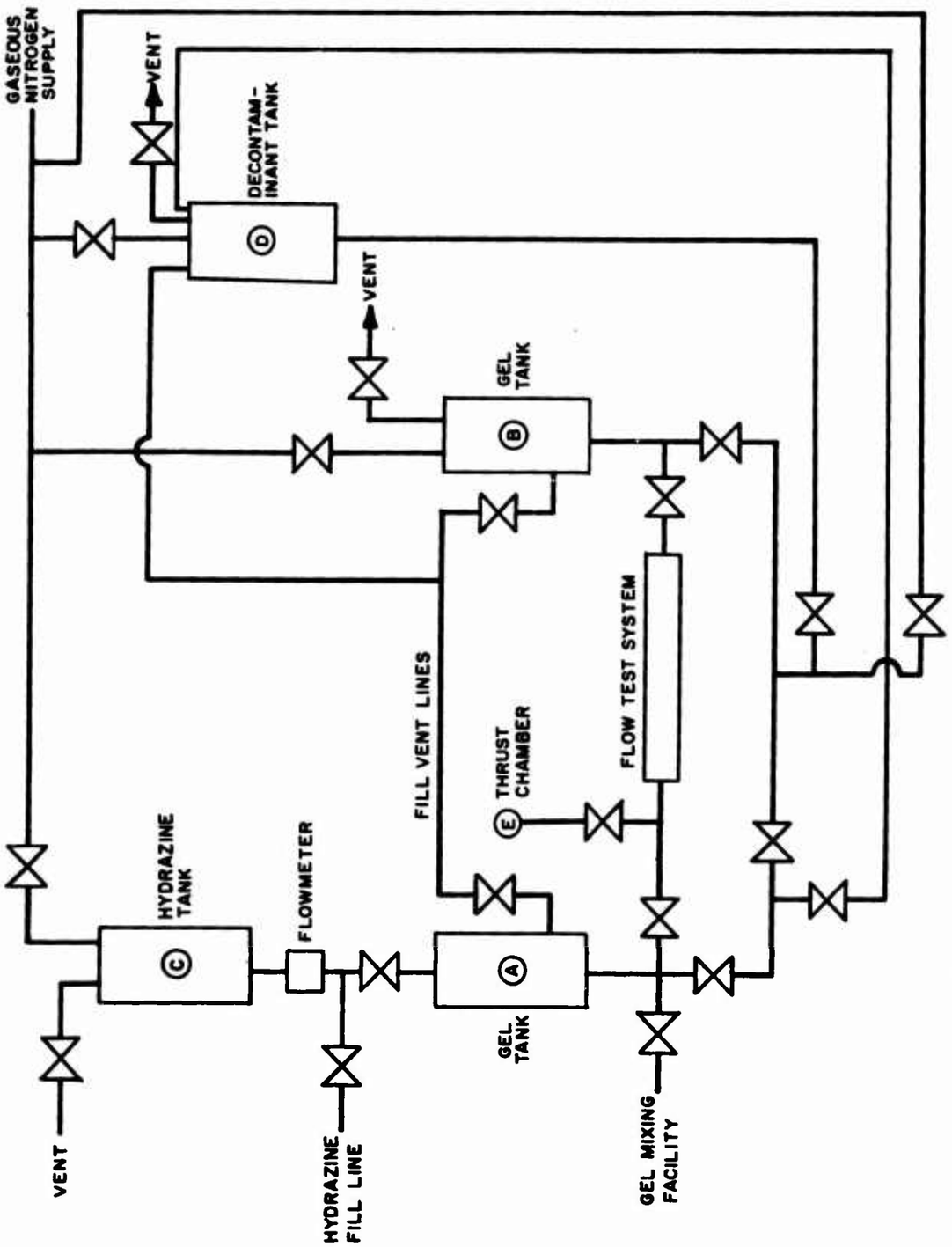


Figure 72. Heterogeneous Fuel Flow Characterization System

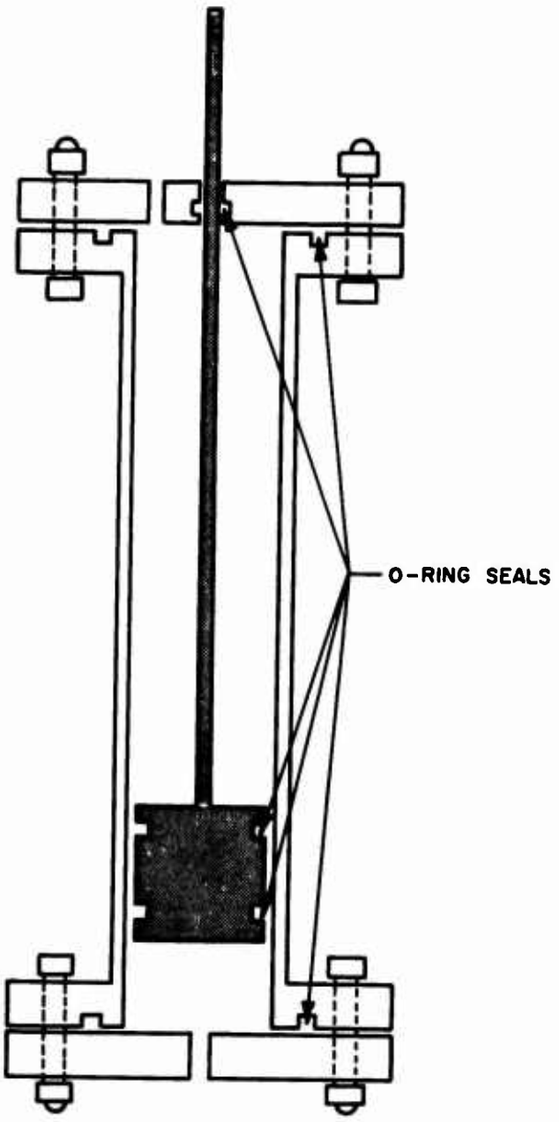


Figure 73. Gel Expulsion Tank

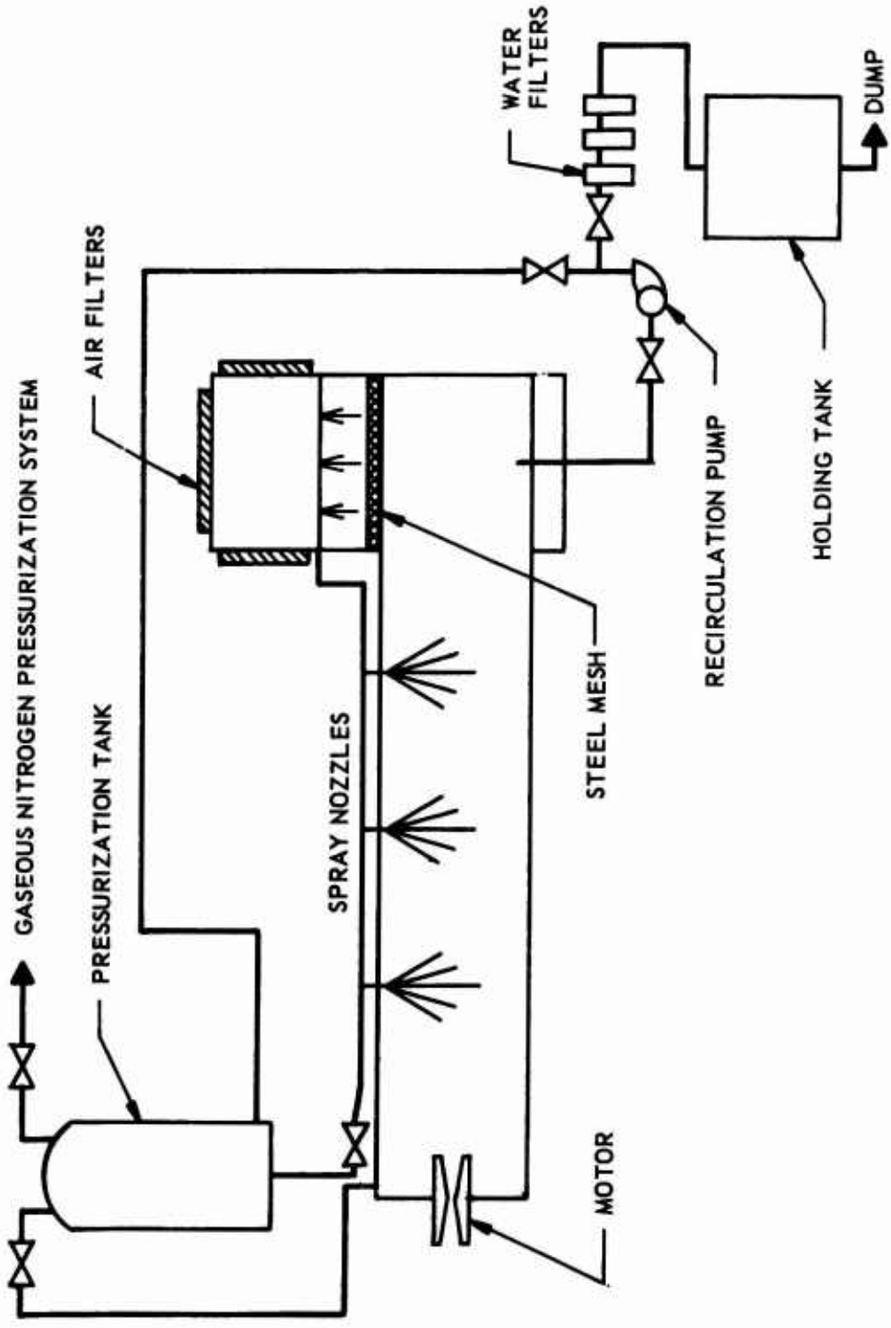
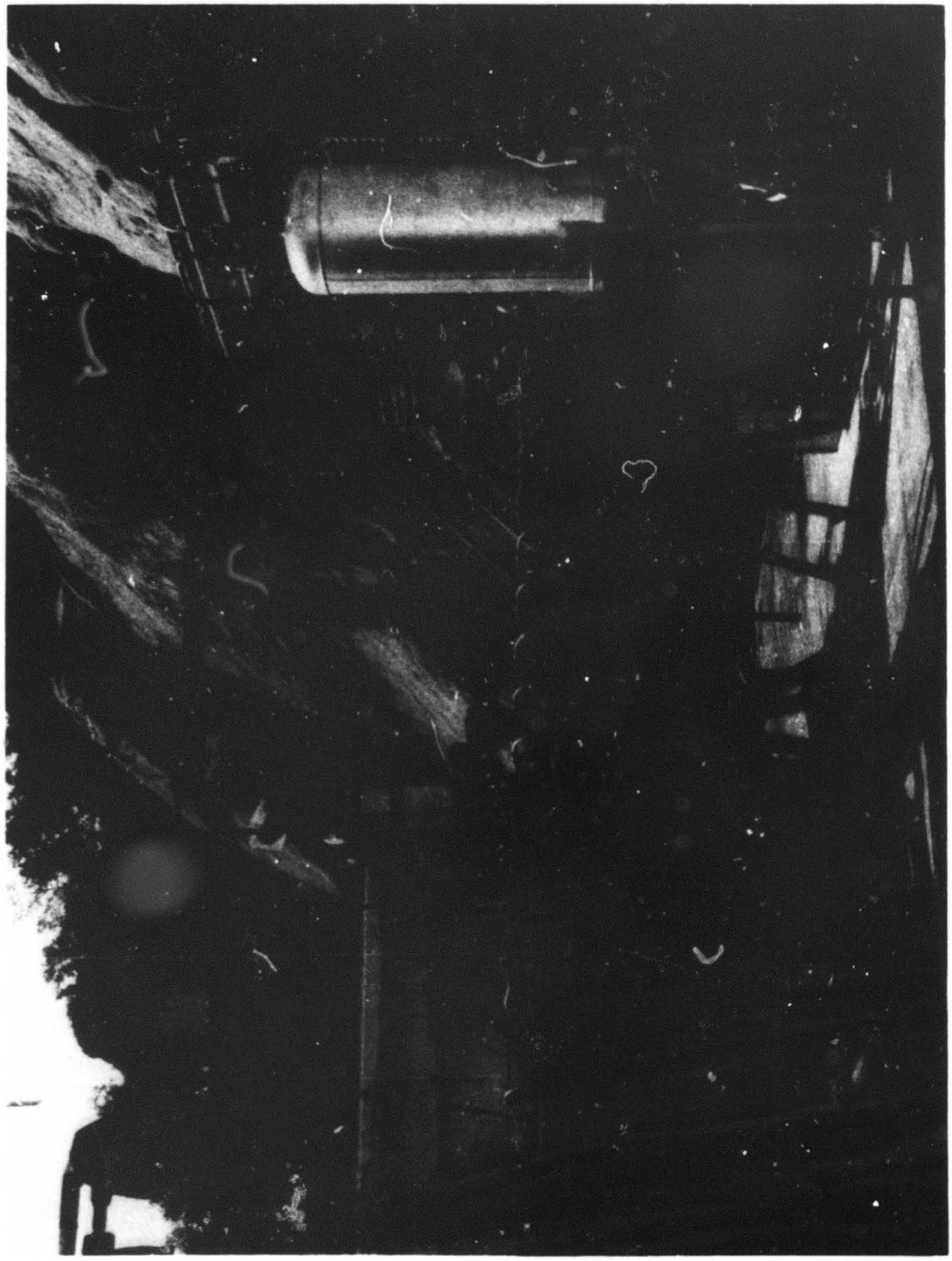
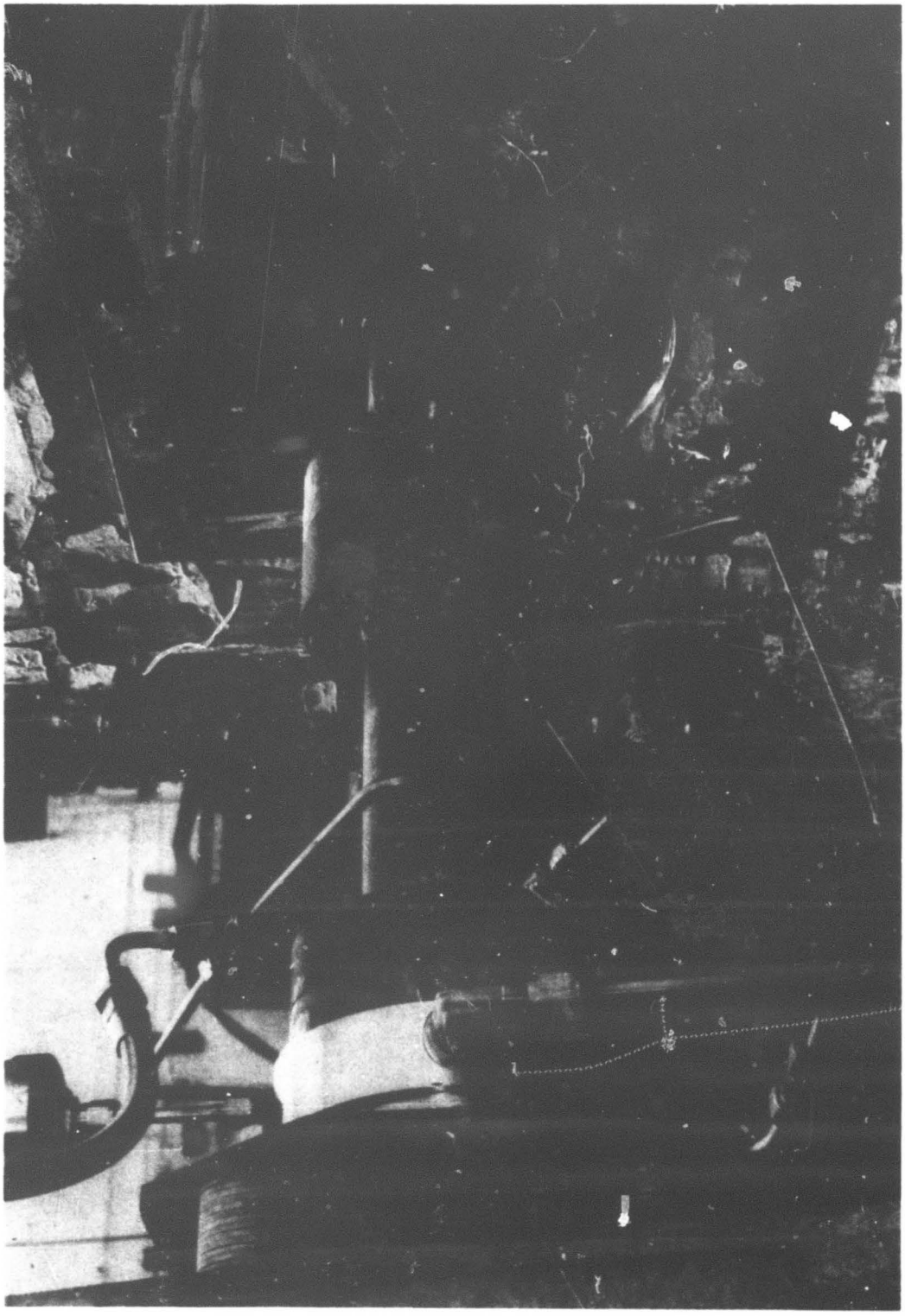


Figure 74. Scrubber System



5AA86-3/11/66-S1B

Figure 75. Exhaust Scrubber System



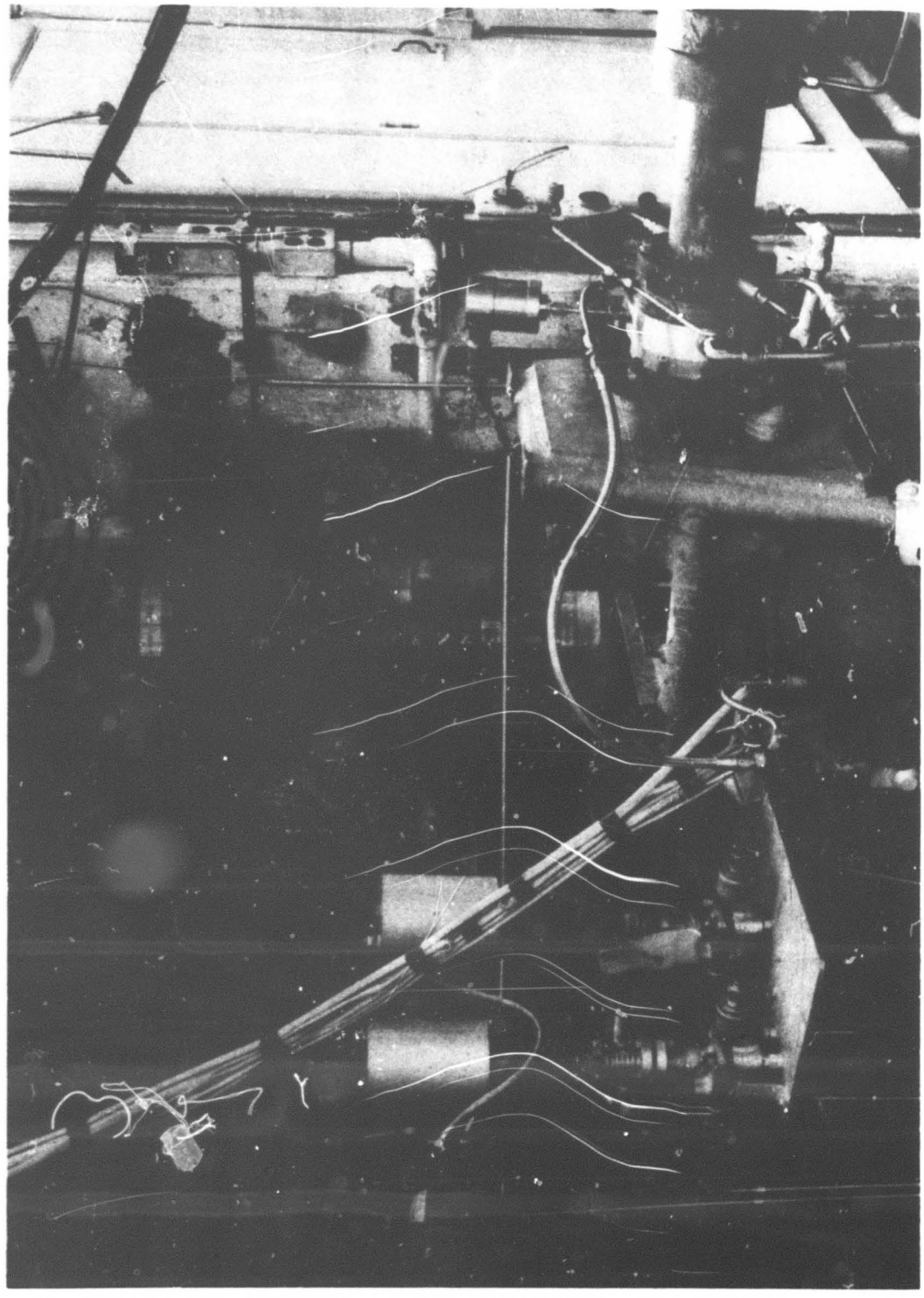
5AA86-3/11/66-S1C

Figure 76. Motor Connection to Scrubber

filters in the rectangular section of the scrubber, shown to the right in Fig. 75). These air filters have an efficiency of 99.97 percent in removing particles of 0.3-micron diameter or larger. Wash water from the nozzles is contained, and then it is recirculated for another test or filtered and pumped to a holding tank where it is analyzed for traces of beryllium. Noncontaminated filtrates are simply dumped. A complete discussion of air and water pollution control measures is given in Appendixes E through G .

The thrust stand and propellant tanks are shown in Fig. 77. Thrust was sensed by a dual-bridge, bonded strain-gage, Baldwin load cell. Propellant flowrates were measured with Fisher-Porter and Potter turbine flowmeters. Gel flowrate was derived indirectly by measuring the flow of hydrazine used to drive the piston displacing the gel. Preliminary printout of propellant flowrate was obtained using a-c to d-c converters and strip chart recorders. Taber pressure transducers and iron-constantan thermocouples were used for steady-state pressure and temperature measurements with cell and electromotive-force-type Foxboro Dynalog recorders. Chamber pressure, thrust, flowrates, injection pressure, and valve openings were recorded on a CEC galvanometer oscillograph.

For runs in which hydrogen peroxide was the only oxidizer, a small amount of N_2O_4 was used as an igniter fluid to ensure smooth hypergolic ignition. Typical operating procedures were as follows. With high-pressure injection purges on, the N_2O_4 flow was initiated, followed by the hydrazine flow and then the peroxide flow. Entry of the hydrazine gel into the chamber establishes mainstage operation. Chamber pressure buildup checks off the N_2O_4 flow and the main propellant purges; shortly afterward, the N_2O_4 valve is closed by the sequence timer. The shutdown sequence begins by opening the peroxide water purge, which remains checked off by the chamber pressure. An almost simultaneous cutoff of propellants was used. As the main valve closes and line pressures decay, the peroxide water purge begins and continues until it is shut off approximately 500 milliseconds after being turned on. As the gel line pressure drops below the purge pressure setting, purge gas flow begins,



5AA86-3/11/66-S1D

Figure 77. Thrust Stand and Propellant Tanks

emptying the line. The peroxide water purge valve then closes, allowing the peroxide purge gas flow to begin. A typical timer sequencing chart is shown in Table 60.

TABLE 60

TIMER SEQUENCE CHART

Time, seconds	Event
0	Scrubber water flow on
2.00	Igniter valve opens
2.20	Fuel valve opens
2.26	Peroxide valve opens
2.50	Igniter valve closes
3.50	Water purge valve opens
3.70	Fuel valve closes
3.70	Peroxide valve closes
4.00	Water purge valve closes
5.00	Scrubber water flow off

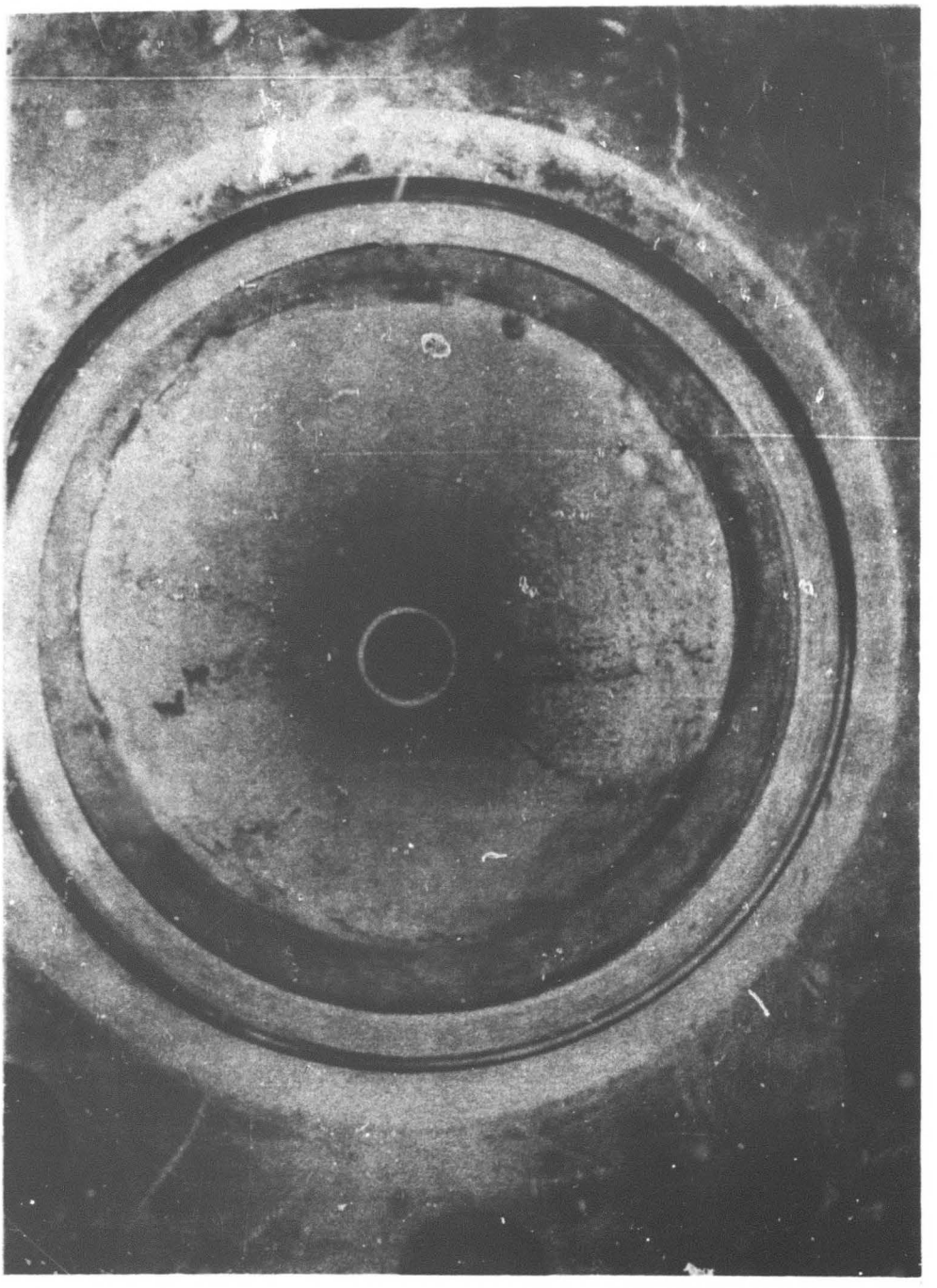
A lead of 2 seconds on the scrubber water flow was necessary to allow the Flex-Flow valve to open completely and ensure that no hot gases would be passing through the scrubber before start of water flow. An average run duration of 1.5 seconds was chosen to provide sufficient time for steady-state instrumentation response (approximately 1.0 second minimum time required) and yet conserve the amount of fuel used as much as possible. After the shutdown sequence has been completed, the gel line and injector are flushed with a high-pressure water purge. The transmission lines for the gel injection pressure and chamber pressure transducers, which are filled with water prior to the run, are then purged with nitrogen gas.

Test History

Al-N_2H_4-H_2O_2 System (Runs No. 1 Through 4). To establish system operation with nontoxic propellants, checkout firings were made with an aluminum-hydrazine gel (40-percent Al, 60-percent N_2H_4) and 98-percent hydrogen peroxide. An uncooled copper nozzle and a conventional impinging stream injector were used during the first series of test firings. The copper injector contained three quintuplet elements, consisting of four fuel streams impinging on one oxidizer stream. During the initial run, an explosion occurred in the peroxide line between the main valve and the injector during injector priming. It was postulated that the explosion resulted from concealed contamination in the bellows portion of the flexible metal hose comprising that part of the oxidizer line. The damage was minor and, on succeeding runs, Teflon-lined bellows were used to provide a smooth internal surface and avoid dead spots which could conceal contaminants.

Runs No. 2 and 3 were programmed for durations of 1.5 and 3 seconds, respectively. Smooth ignition and combustion resulted. Examination of the injector and chamber after run No. 2 revealed no damage; however, heavy deposits of unburned aluminum were found on the chamber walls and nozzle (Fig. 78). The light-colored ring visible at the center of the throat in Fig. 78 is a steel tube positioned at the throat to provide a known reference and allow the throat area to be determined from the photograph. Inspection after run No. 3 revealed lighter deposits but extensive erosion of the injector retaining ring and the chamber walls near the injector. Replacement of both items was necessary. This is attributed to a visible partial plugging of the fuel orifices, which caused distortion of the spray pattern and direct impingement of oxidizer on the chamber walls.

To eliminate the problem of injector plugging and attempt to provide better breakup of the fuel gel, a new injector was designed and built. This injector was also fabricated from copper and consisted of three



5AA36-1/27/66-S1

Figure 78. Throat Deposits

fuel, solid-cone spray nozzles and four oxidizer streams impinging on each fuel spray. Test No. 4 was run with this injector without incident. No chamber erosion was evident after testing.

A brief summary of test data obtained with the Al-N_2H_4-H_2O_2 system is presented in Table 61. A complete listing of all data is presented in Table

TABLE 61

THRUST CHAMBER TESTS, Al-N_2H_4-H_2O_2 SYSTEM

Run No.	Chamber Pressure, psia	Mixture Ratio, o/f	Specific Impulse, seconds	Specific Impulse Efficiency, percent
1	---	---	---	---
2	895	0.61	245	82
3	855	0.78	257	86
4	860	0.68	240	80

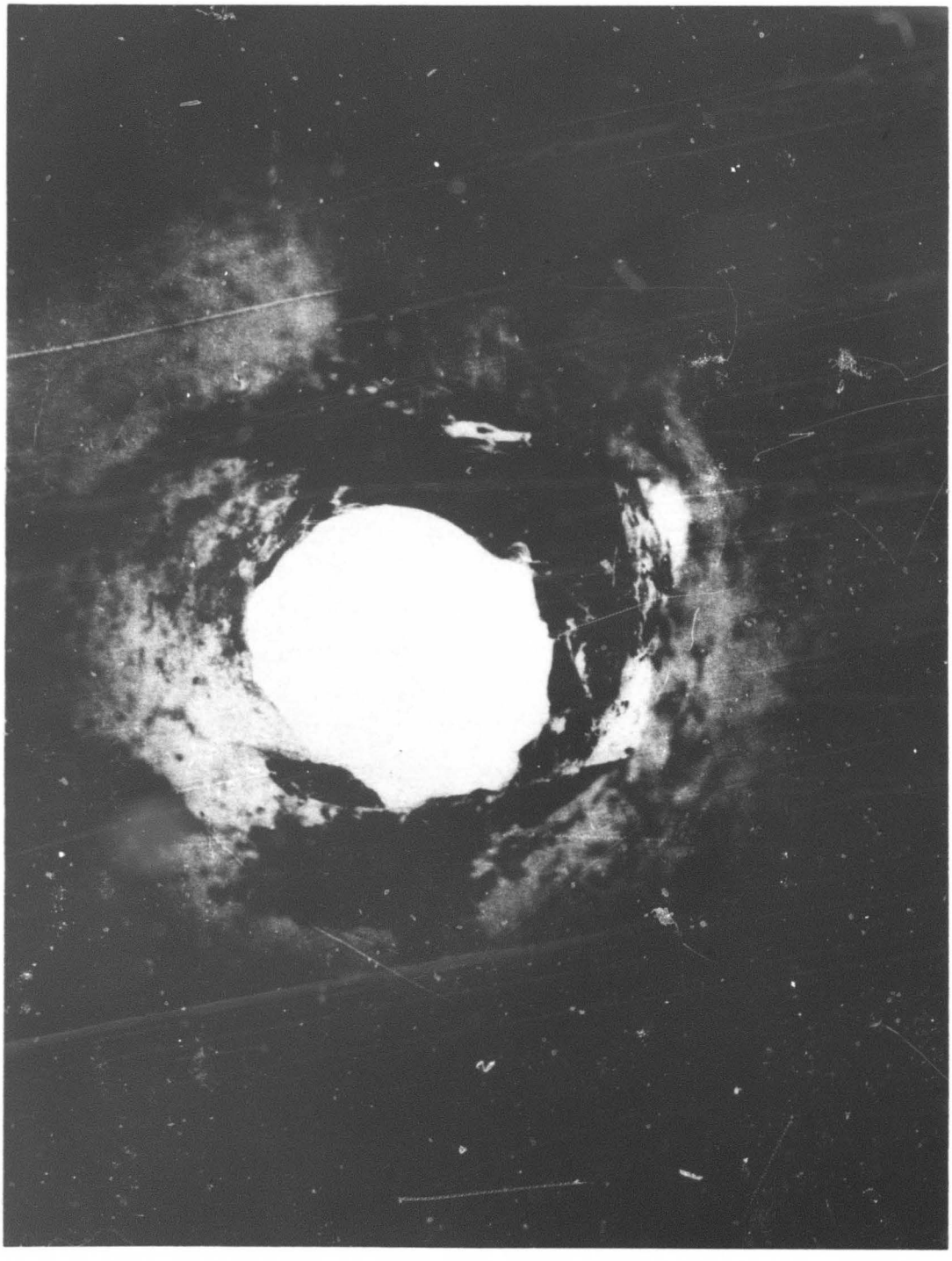
The results in Table 61 indicate low combustion efficiencies. This was to be expected from the evidence of unburned metal deposited on the chamber walls. The only purpose in making these tests was to check out the operation of the propellant feed system and no further evaluation of observed performance levels was made.

Be-N_2H_4-H_2O_2 System (Runs No. 5 Through 10). The first beryllium-containing fuel tested was that designated as R-2 (29 w/o Be, 71 w/o N_2H_4) using 98 percent hydrogen peroxide. Testing was conducted with the same hardware as that used for the aluminum system. Two operational problems appeared during this test series. During the first run (run No. 5), an explosion occurred in the peroxide injection manifold approximately 250 milliseconds after closing the main propellant valves in the shutdown

sequence. The explosion was audible inside the control center, but there was no external rupture of lines or hardware and there was no release of propellants to the atmosphere. Posttest inspection revealed that both peroxide injection pressure transducers suffered heavy internal damage. The explosion was attributed to inadequate purging of the peroxide line and heat soakback through the injector. The gaseous nitrogen purge pressures were increased for the next test and operation appeared to be satisfactory. During the third test (run No. 7), however, a similar explosion occurred. Two more transducers were destroyed and, in addition, the injector manifold was sufficiently deformed to require replacement. It was after this test that the high-pressure water purge of the peroxide line was added to the shutdown sequence. Subsequent tests proceeded without difficulty.

The second operational problem involved burning and erosion of the nozzle throat. Run No. 5 was completed without incident. During run No. 6, evidence of throat enlargement first appeared after 1.1 seconds of mainstage operation. The total run duration was 1.5 seconds and resulted in a badly eroded throat. The test duration was then reduced to 1.0 second in an attempt to avoid the problem.

Run No. 7 was satisfactory, but during run No. 8 throat enlargement began at 0.6 second, with the results shown in Fig. 79. This view is taken from the nozzle exit, looking upstream toward the throat. During run No. 9 evidence of throat enlargement began after 0.3 second. The variation of performance data with time is presented in Fig. 80. It became obvious that very oxidizer-rich mixtures could not be tested with the uncooled copper nozzle, even for short runs. A run duration of at least 1 second is desired to achieve satisfactory response of the steady-state instrumentation. Run No. 10 was completed at a lower mixture ratio without significant erosion. Because testing at relatively high mixture ratios for this propellant system was required, it was decided to build a water-cooled nozzle for use in subsequent tests.



5AA86-3/11/66-S1A

Figure 79. Eroded Throat

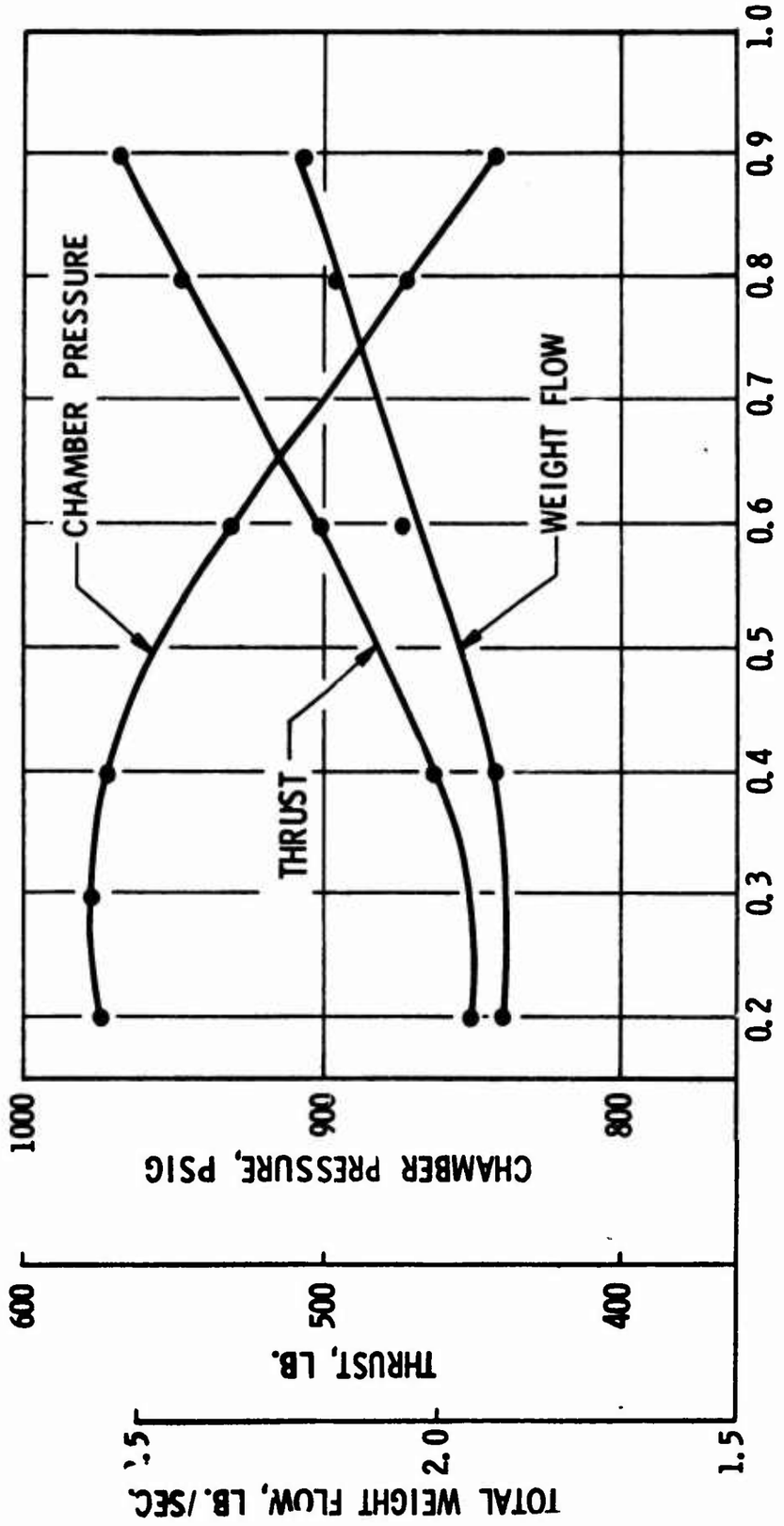


Figure 80. Test Data Showing Nozzle Throat Erosion

Table 62 contains a capsule summary of tests with the Be-N_2H_4-H_2O_2 system using the bipropellant copper injector and uncooled copper nozzle. Complete data are presented in Table 70.

TABLE 62

THRUST CHAMBER TESTS, Be-N_2H_4-H_2O_2 SYSTEM

Run No.	Chamber Pressure, psia	Mixture Ratio, o/f	Specific Impulse, seconds	Specific Impulse Efficiency, percent
5	1034	0.92	248	77.2
6	956	1.30	241	76.7
7	856	0.46	226	68.6
8	971	0.93	239	74.2
9	980	1.21	243	76.9
10	952	0.81	236	72.5

Runs No. 5, 6, and 10 were performed with the spray nozzle injector (injector No. 2) while runs No. 7 through 9 utilized the impinging stream injector (injector No. 1). Performance data are presented graphically in Fig. 81. The scope of this investigation did not include any injector optimization effort. The only objective of testing with two injectors was to decide on a basic design which would give acceptable performance without operating problems. All propellant evaluations were to be based on relative comparisons between different propellant systems tested in the same hardware. There appeared to be no significant difference in performance between the two injector types and both operated at a sufficiently high performance level for the purpose of the test program. Therefore, the fuel spray nozzle configuration (injector No. 2) was chosen for all future work to avoid the injector plugging problem experienced with the small orifices in the impinging stream injector.

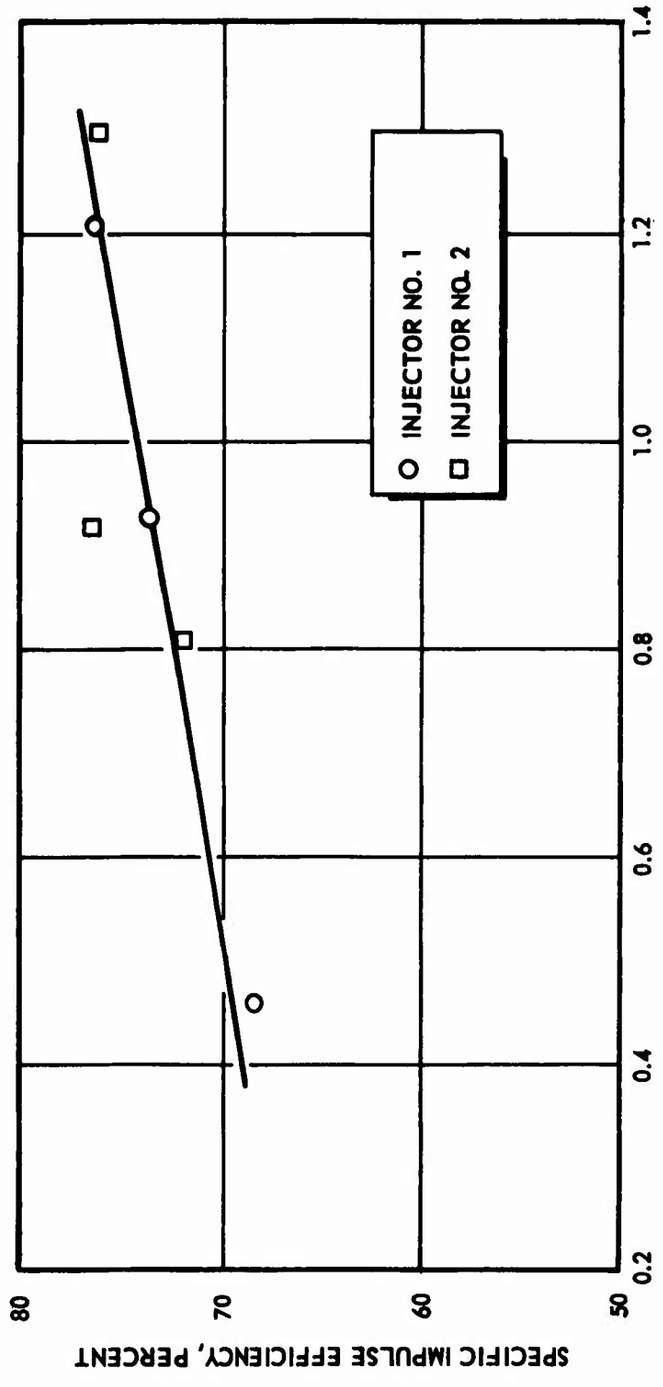


Figure 81. Injector Performance Data

Be-N_2H_4-H_2O_2-ClF_5 System (Runs No. 11 Through 20 and 27). This test series was designed to test the hypothesis that addition of fluorine to a Be-containing system would improve combustion efficiency. For this purpose, a homogeneous tripropellant injector was built. This injector (Fig. 82) was manufactured from nickel and consists of three fuel-spray nozzles, each surrounded by three oxidizer fans generated by H_2O_2-ClF_3 doublets. This injector design was chosen to obtain uniform distribution of the fluorine-containing oxidizer throughout the combustion chamber. Technical factors favoring the choice of a tripropellant test system were:

1. Allows use of incompatible oxidizers to give higher performance than otherwise possible
2. Eliminates problems of unknown mixture sensitivities and compatibilities
3. Eliminates necessity of building oxidizer mixing facility
4. Ensures exact knowledge of oxidizer composition (eliminates incomplete mixing, fractionation, etc.)
5. Gives more flexibility in varying oxidizer composition from run to run

The water-cooled nozzle assembly was first used during this test series. The four-piece nozzle assembly is seen in Fig. 83. It consists of a copper liner, a two-piece aluminum filler block, and a stainless-steel casing. The water flowrate at design conditions results in a velocity of approximately 100 ft/sec at the nozzle throat. Figure 84 is a view of the copper liner with one-half the aluminum filler block in place and showing the coolant passage between these two pieces. More than 20 tests were completed on the original assembly without visible or measurable erosion of the throat. However, in analyzing the oscillograph traces, it was observed that the throat diameter often appeared to decrease during the course of a test, probably because of the formation of deposits in the nozzle, similar to those in Fig. 78. In

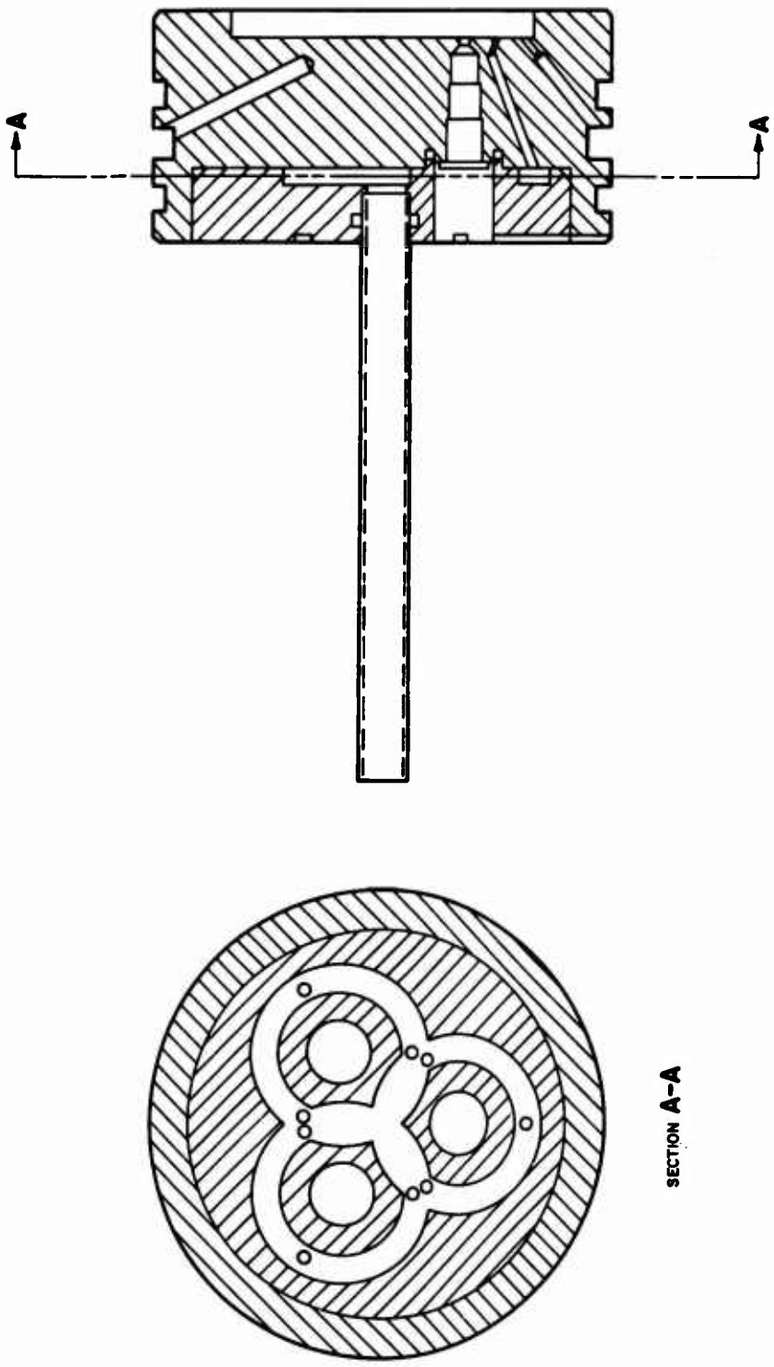
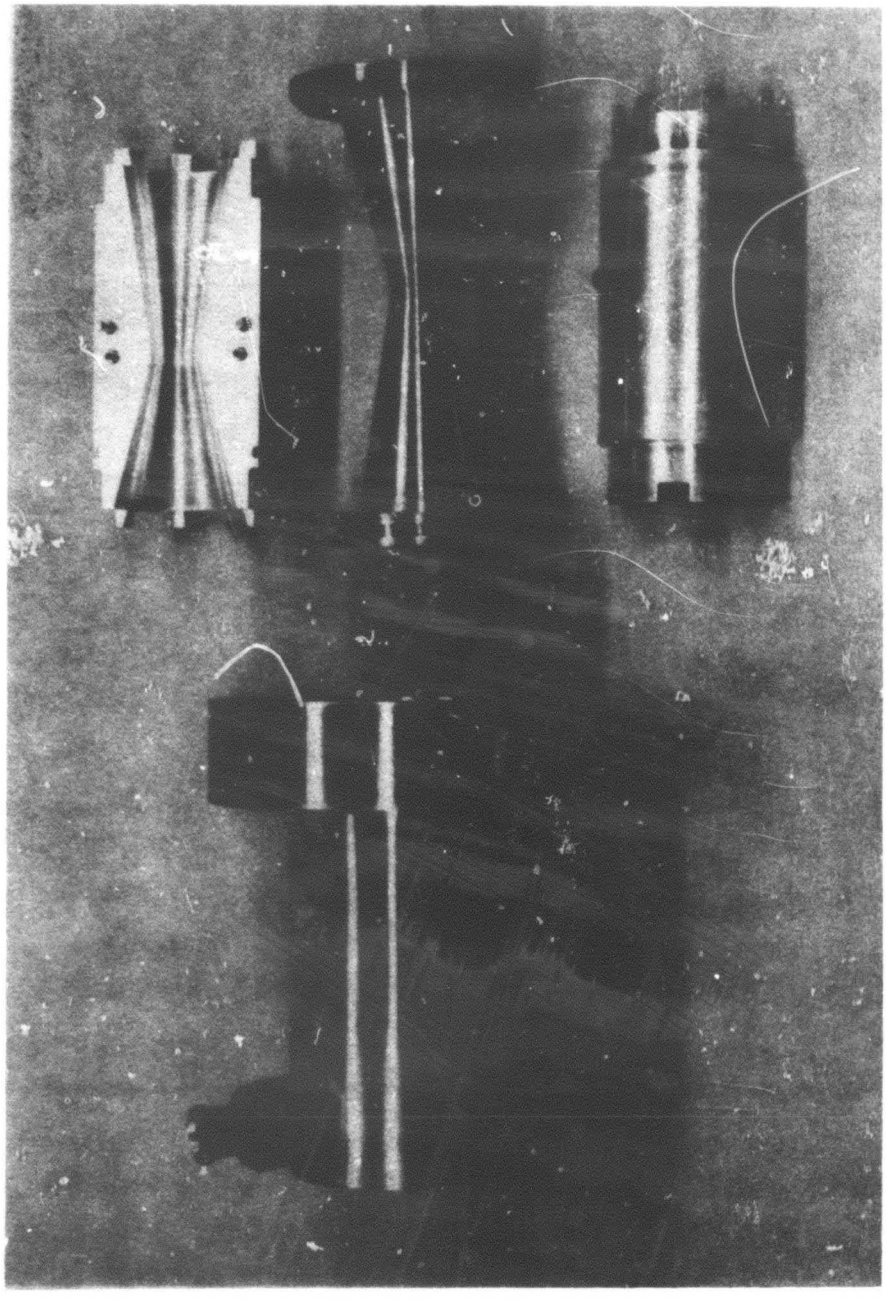
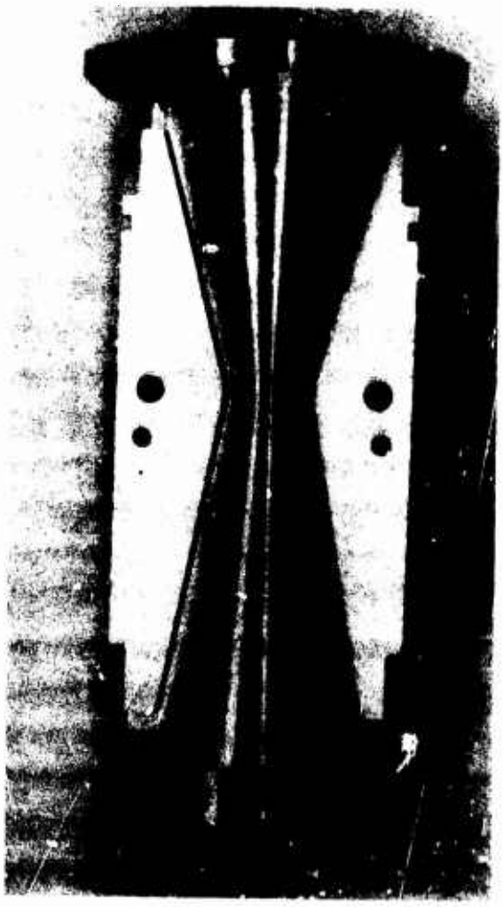


Figure 82. Tripropellant Injector



5AA31-8/1/66-S1D

Figure 83. Water-Cooled Nozzle Assembly



5AA31-8/1/66-S1E

Figure 84. Water-Cooled Nozzle Assembly

Fig. 85 , the variation of test parameters with time during a typical test is shown. The same data have been converted to characteristic velocity and specific impulse efficiencies in Fig. 86 . Specific impulse reaches a steady-state value approximately at the midpoint of the run, but the apparent characteristic velocity continues to rise during the entire test. No posttest evidence of a buildup of deposits in the throat was usually observed, but it is postulated that these deposits are removed by the high-pressure water purge during the shutdown sequence. Posttest measurements of the throat diameter of the water-cooled nozzle were made and found to be identical to pretest values.

During the first test of the series (No. 11), a valve failure resulted in no fuel flow to the chamber. The second test resulted in a normal run, but an instrumentation malfunction caused the loss of the oxidizer flowrate and no performance could be computed. Nine valid performance tests were obtained on following runs. The oxidizer flow in each case consisted of approximately 30 percent ClF_5. Runs No. 13 through 20 were programmed for 1.5 seconds duration. One run (No. 27) of 3 seconds duration was conducted to check the possibility of increasing performance with a longer run time. No thrust chamber hardware problems appeared during any of these tests. The results are presented briefly in Table 63 and completely in Table 70.

Be-N_2H_4-H_2O_2 System (Runs 22 Through 26 [illegible] and 29). To provide an exact estimate of the effect produced by ClF_5 during the tripropellant tests, a series of tests was conducted with the same tripropellant injector (injector No. 3) and other hardware, but with H_2O_2 in both oxidizer manifolds. Five tests (No. 22 through 26) were conducted, with the results shown in Tables 64 and 70.

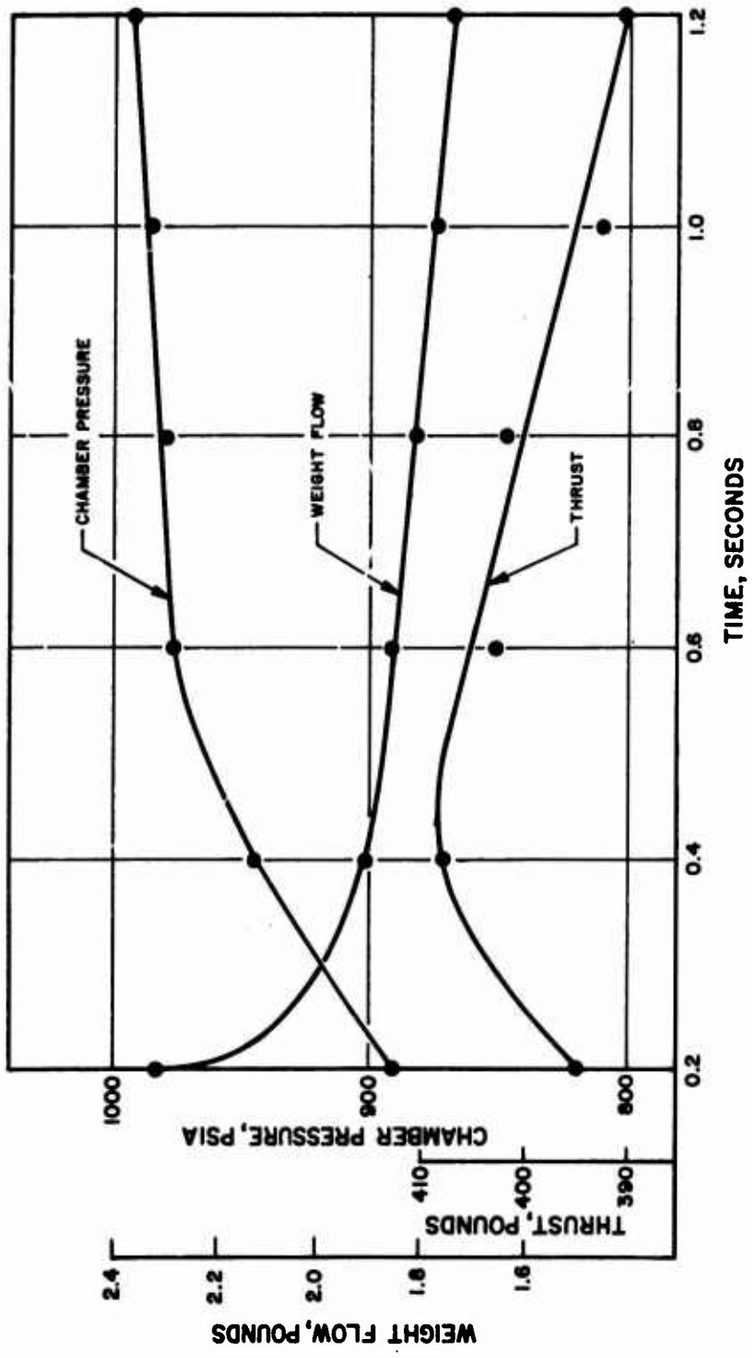


Figure 85. Thrust Chamber Trace Showing Throat Plugging

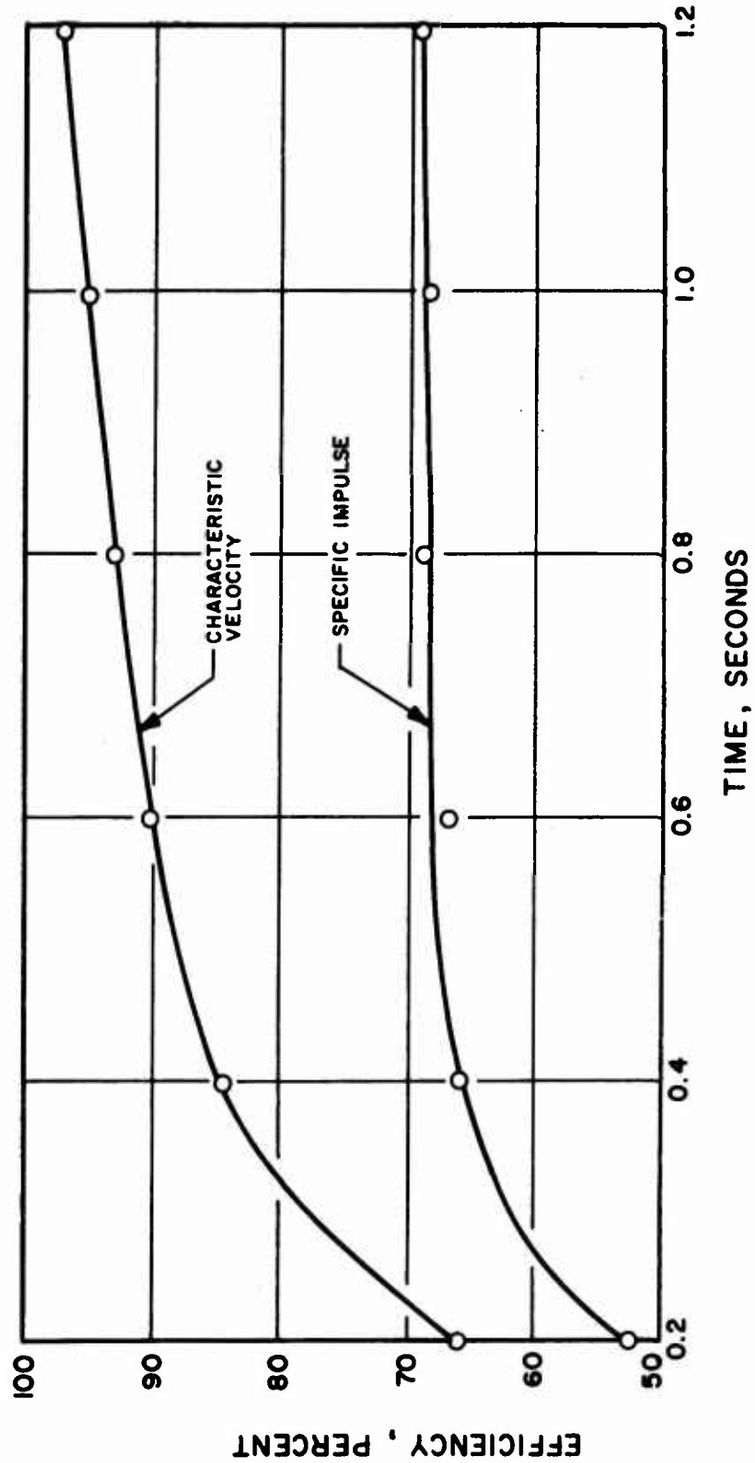


Figure 86. Thrust Chamber Trace Showing Throat Plugging

TABLE 63

THRUST CHAMBER TESTS, Be-N_2H_4-H_2O_2-ClF_5 SYSTEM

Run No.	Chamber Pressure, psia	Mixture Ratio, o/f	Specific Impulse, seconds	Specific Impulse Efficiency, percent
13	976	1.04	230	70.4
14	944	1.14	251	77.5
15	1007	0.64	227	69.0
16	1022	0.73	234	71.0
17	1054	1.47	241	75.6
18	995	1.21	236	72.9
19	1022	1.06	236	73.2
20	1050	0.60	229	68.9
27	1042	0.70	231	70.0

The above data are presented graphically in Fig. 87.

TABLE 64

THRUST CHAMBER TESTS, Be-N_2H_4-H_2O_2 SYSTEM
(TRIPROPELLANT INJECTOR)

Run No.	Chamber Pressure, psia	Mixture Ratio, o/f	Specific Impulse, seconds	Specific Impulse Efficiency, percent
22	963	0.85	239	73.9
23	1019	0.59	241	71.8
24	949	0.99	228	70.0
25	949	1.25	236	74.0
26	999	0.85	239	72.3

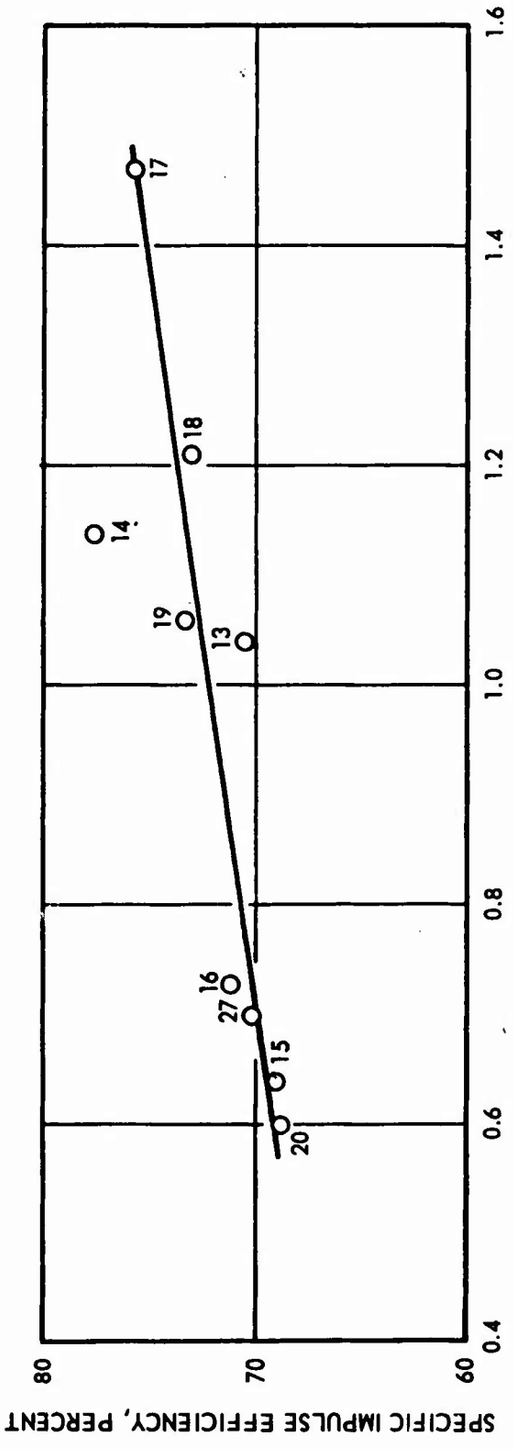


Figure 87. Tripropellant Test Data

The possible effect of increased chamber residence time on combustion efficiency was investigated during two tests (No. 28 and 29) made with a double-length chamber. Two standard chamber sections were bolted together, increasing the chamber characteristic length to 308 inches. Because this combination extended too far into the exhaust scrubber to make connections to the water-cooled nozzle, an uncooled nozzle was used. The bipropellant fuel spray injector (injector No. 2) was used. Data from these two tests are presented in Tables 65 and 70.

TABLE 65

THRUST CHAMBER PERFORMANCE, Be-N_2H_4-H_2O_2 SYSTEM
(308-INCH L*)

Run No.	Chamber Pressure, psia	Mixture Ratio, o/f	Specific Impulse, seconds	Specific Impulse Efficiency, percent
28	975	0.75	249	75.0
29	994	0.80	249	75.1

The data from Tables 64 and 65 are presented graphically in Fig. 88.

Be-N_2H_4-N_2O_4 System (Runs 30 Through 33). A series of four test firings was conducted under a company-sponsored program with the tripropellant injector (injector No. 3) and using N_2O_4 as the oxidizer with R-2 fuel gel. These tests were undertaken with the objective of determining whether a basic difference exists between the attainable combustion efficiencies with hydrogen peroxide and nitrogen tetroxide. During the last test of this series, the water-cooled nozzle assembly was destroyed. An explosion was audible at approximately the scheduled shutdown time. Posttest inspection revealed that the copper liner had burned through or parted at the throat. The expansion nozzle portion of the copper liner and the entire aluminum filler block were missing from the assembly, and a hole approximately 1 inch in diameter had burned through the outer stainless-steel case. Because no evidence of throat erosion was

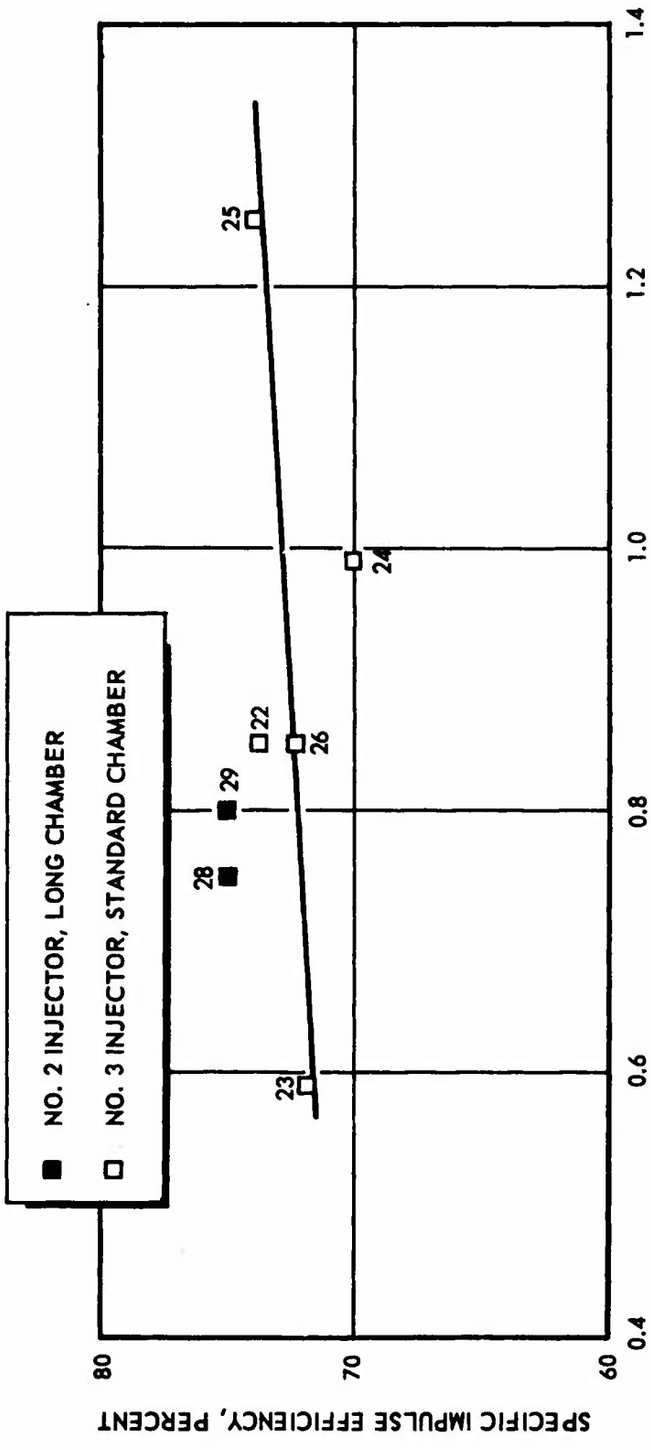


Figure 88. Be-N_2H_4-H_2O_2 System Test Data

seen during the main portion of the run, it is surmised that nozzle burning took place entirely at the end of the run, perhaps because of a coolant blockage and creation of a hot spot. The extremely oxidizer-rich mixture ratio achieved during this test also may have been a contributing factor. Data for this series are given in Tables 66 and 70, and Fig. 89.

TABLE 66

THRUST CHAMBER PERFORMANCE, Be-N_2H_4-N_2O_4 SYSTEM

Run No.	Chamber Pressure, psia	Mixture Ratio, o/f	Specific Impulse, seconds	Specific Impulse Efficiency, percent
30	986	1.03	253	80.4
31	1070	0.65	260	80.7
32	1026	1.22	253	81.5
33	1026	1.49	249	81.6

Be-BeH_2-MMH-H_2O_2 System (Runs 34 and 37 Through 42). This test series with the R-3 formula fuel gel was conducted with the spray nozzle injector (injector No. 2) and a new water-cooled nozzle. During the first run (No. 34), an explosion occurred in the peroxide manifold shortly after run start. No explanation for this explosion was found. Posttest inspection revealed that the copper liner and aluminum filler block in the water-cooled nozzle were both destroyed. The nozzle case was slightly eroded but repairable. Because no evidence of nozzle erosion could be discerned in the data before the peroxide explosion, it is thought that loss of the nozzle occurred on shutdown. The emergency shutdown switch closed all propellant valves and simultaneously shut off power to the nozzle water valve. There may have been enough propellant left in the chamber to cause a nozzle burnthrough after the water flow ceased. This is difficult to reconcile with the fact that

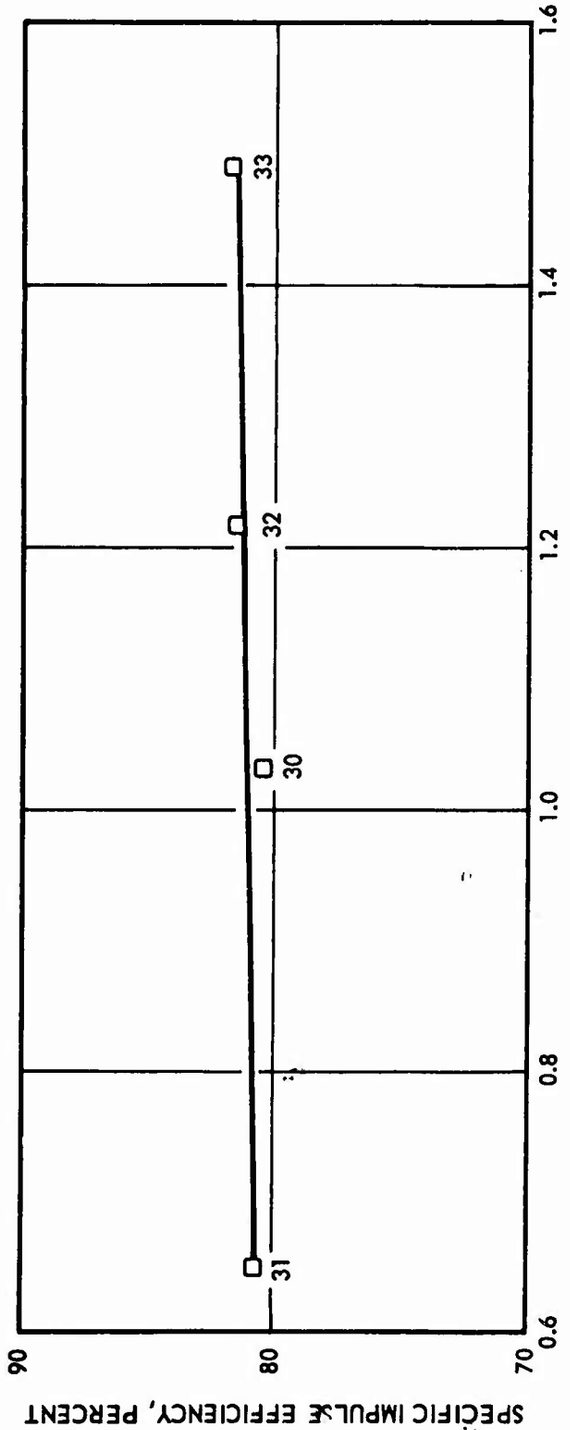


Figure 89. Be-N_2H_4-N_2O_4 System Test Data

the peroxide explosion destroyed the peroxide line and injector manifold and, therefore, there should have been no oxidizer left in the chamber by the time the emergency shutoff switch was observer-actuated. However, no other satisfactory explanation could be found. In succeeding runs, the emergency shutdown procedure was modified to leave nozzle coolant flowing during a shutdown.

A new water-cooled nozzle assembly was placed in operation during run No. 37 and the test series was completed without further incident. The data are presented in Tables 67 and 70, and Fig. 90.

TABLE 67

THRUST CHAMBER PERFORMANCE, Be-BeH_2-MMH-H_2O_2 SYSTEM

Run No.	Chamber Pressure, psia	Mixture Ratio, o/f	Specific Impulse, seconds	Specific Impulse Efficiency, percent
34	1003	1.46	265	81.6
37	1034	0.95	251	74.8
38	974	0.78	242	72.2
39	964	0.77	239	71.2
40	1014	1.33	254	77.6
41	1014	1.29	265	80.7
42	1024	0.93	248	74.1

Be-N_2H_4-H_2O_2-ClF_5 System, Hot-Core Injector (Runs 46 Through 53). These runs were conducted to test the hot-core injector concept. The hot core is produced by a central injector element which uses ClF_5 as the oxidizer. Three outer elements utilize H_2O_2. Each injector fuel-oxidizer element is identical to the injector elements of the bipropellant fuel spray injector (injector No. 2) and consists of a central fuel spray

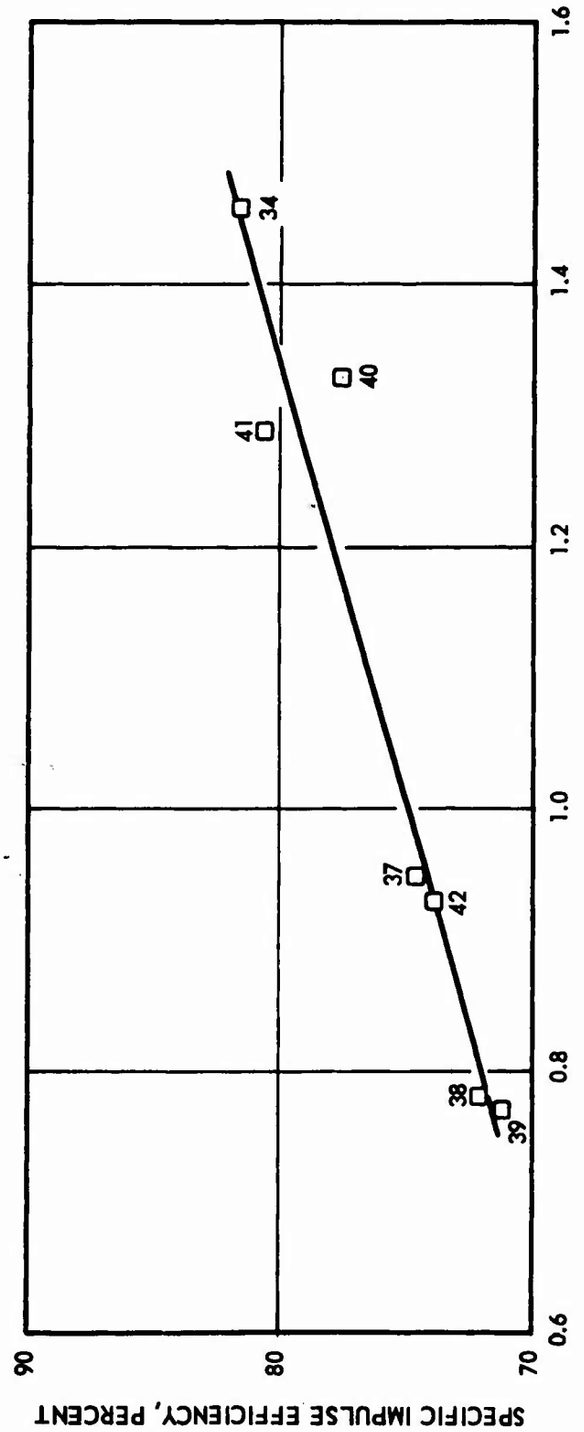


Figure 90. Be-BeH_2-MMH-H_2O_2 System Test Data

nozzle surrounded by four impinging oxidizer streams. This injector (injector No. 4) was fabricated from nickel and brazed to a one-piece, stainless-steel oxidizer manifold ring (Fig. 91).

During the first run of this series (No. 46), an instrumentation malfunction resulted in the loss of flowmeter data for the ClF_5 flowrate. All remaining runs were completed without difficulty. The results are presented in Tables 68 and 70, and in Fig. 92. Posttest inspection of the injector after run No. 53 revealed some erosion of the injector face around the hot-core (ClF_5) element. The injector was refinished by machining a 1-inch-diameter spot-face at the center of the injector to a depth approximately 0.03 inch below the original injector face.

TABLE 68

THRUST CHAMBER PERFORMANCE, Be-N_2H_4-H_2O_2-ClF_5 SYSTEM
(HOT-CORE INJECTOR)

Run No.	Chamber Pressure, psia	Mixture Ratio, o/f	Specific Impulse, seconds	Specific Impulse Efficiency, percent
46	983	---	---	---
47	971	0.67	230	69.8
48	964	1.07	248	77.6
49	943	1.04	244	76.4
50	999	0.84	246	75.4
51	979	1.28	237	75.1
52	1011	1.01	252	78.2
53	991	1.42	250	79.9

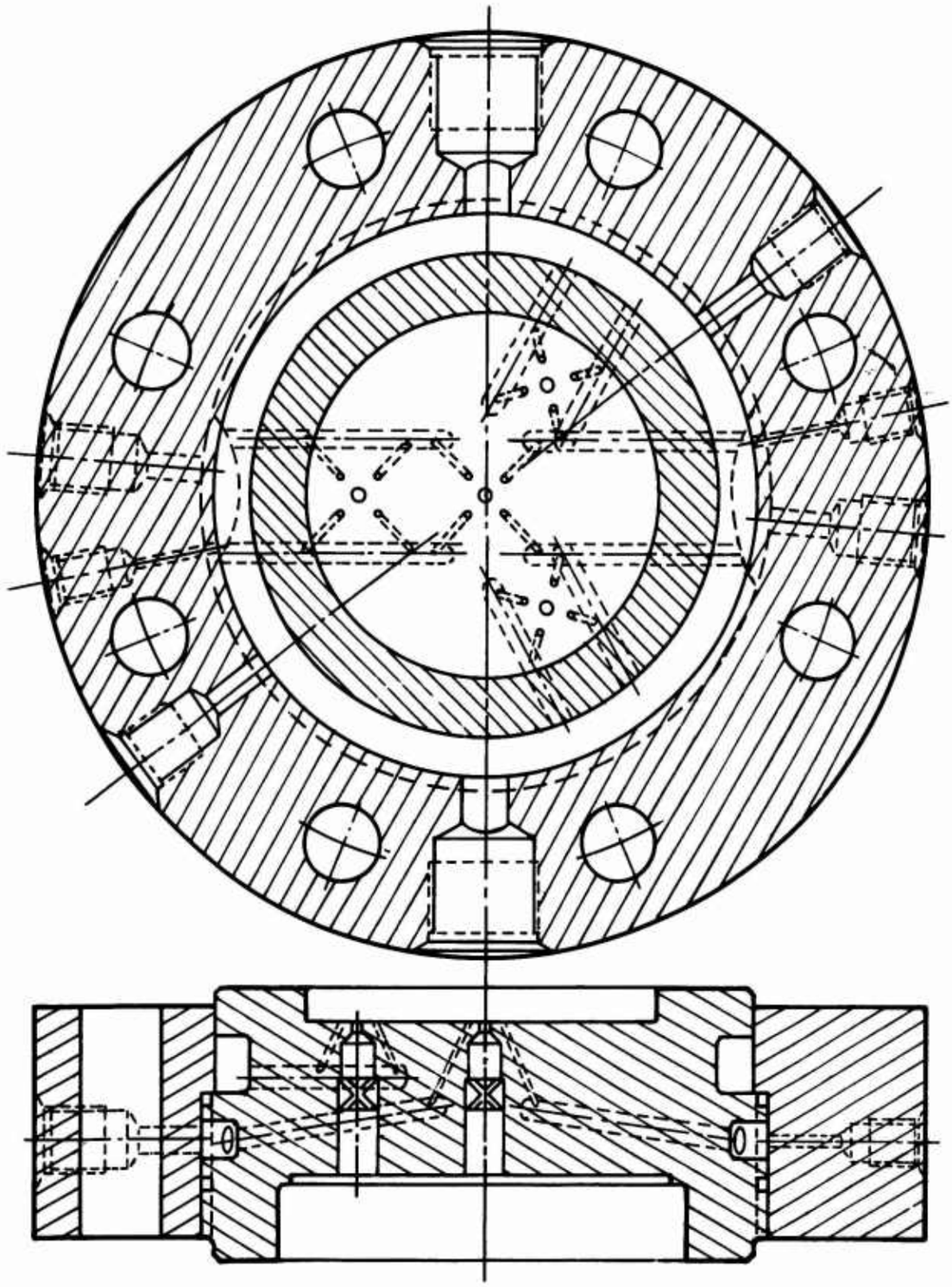


Figure 91. Hot-Core Tripropellant Injector

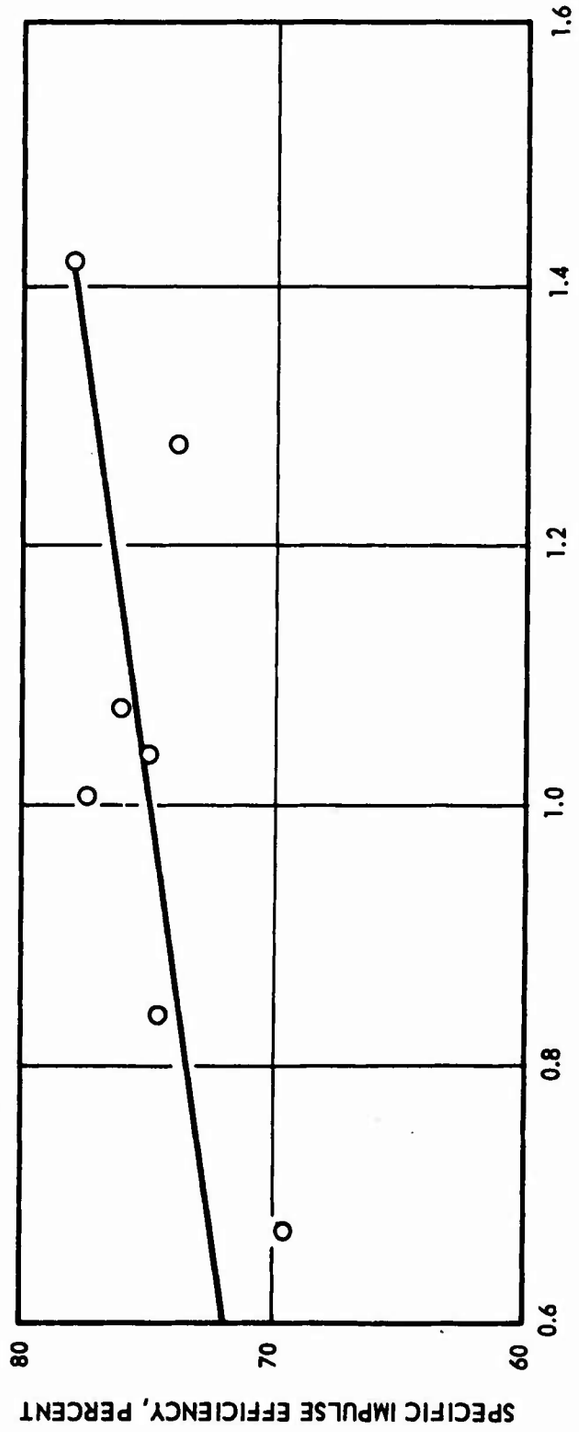


Figure 92. Hot-Core Injector Test Data

N_2H_4-H_2O_2 System (Runs No. 43 Through 45 and 54 Through 59). A series of tests with nonmetallized fuel in the same experimental hardware was desirable to establish baseline performance efficiencies. Three runs (No. 43 through 45) were conducted with 98-percent hydrogen peroxide and neat propellant-grade hydrazine using the No. 2, fuel spray injector and water-cooled nozzle. During the first run (No. 43), an explosion occurred in the peroxide injector manifold at the end of the run. The manifold ring was badly warped, necessitating replacement. Cause of this explosion is unknown. It appeared to be similar to those which occurred before the high-pressure water purge of the peroxide line was added to the shutdown sequence. Run No. 44 was completed without problem. It was followed immediately by run No. 45, which resulted in an explosion in the fuel injector dome. The explosion destroyed the injector, injector flow distributor, injector manifold, injector retaining ring, fuel injection pressure transducer, and thrust stand load cell. Based on observations of later tests, this explosion was attributed to insufficient cooling of the injector after run No. 44.

The second set of baseline firings (runs No. 54 through 59) was conducted with the hot-core (No. 4) injector configuration using hydrogen peroxide in both oxidizer manifolds. Gelled hydrazine was the fuel for this series. No malfunction occurred during the tests. The copper liner of the water-cooled nozzle became elongated gradually until it became unusable after run No. 59 because the O-ring seal at the exit was no longer contacting the sealing surface. The throat diameter did not appear to change significantly during this time. Compared to a design dimension of 0.650 inch, measurements between 0.638 and 0.663 inch were obtained after run No. 59. Test data are presented in Tables 69 and 70, and Fig. 93.

TABLE 69

THRUST CHAMBER PERFORMANCE, H_2O_2-N_2H_4 SYSTEM

Run No.	Chamber Pressure, psia	Mixture Ratio, o/f	Specific Impulse, seconds	Specific Impulse, Efficiency, percent
43	1014	1.16	240	86.9
44	1004	1.69	243	85.7
45	1014	1.74	241	84.9
54	896	1.34	235	85.1
55	944	1.92	236	83.1
56	954	2.26	233	82.5
57	954	2.03	236	82.9
58	944	2.15	235	82.4
59	921	1.58	237	84.5

Be-BeH_2-$N_2H_5NO_3$ System (Runs No. 35, 36, 60, and 61). Four attempts were made to test fire the R-5 monopropellant formulation consisting of a gelled mixture of beryllium, beryllium hydride, water, and hydrazine nitrate. The first tests were conducted with a small, expendable motor and tank system. A single, solid-cone spray nozzle injected the fuel into an uncooled, stainless-steel chamber and nozzle assembly. The design level was approximately 100 pounds of thrust. A 1-inch stainless-steel tube approximately 2 feet long served as the propellant tank. This allowed for a total run time of approximately 1 second. The fuel gel was forced out of the tank by nitrogen pressure above a close-fitting Teflon piston. A piston bypass at the bottom of the tank allowed the pressurizing gas to purge the propellant line after the piston had reached the bottom of the tube. Figure 94 shows the motor and tank assembly in place, with the motor exhausting into the scrubber. In operation, the tube-tank was filled with fuel at a separate location, the hand valve on the tank outlet being closed. After installation, as shown in Fig.94 , the hand valve was opened. The remainder of the operation was conducted remotely. Chamber pressure was the only test parameter recorded.

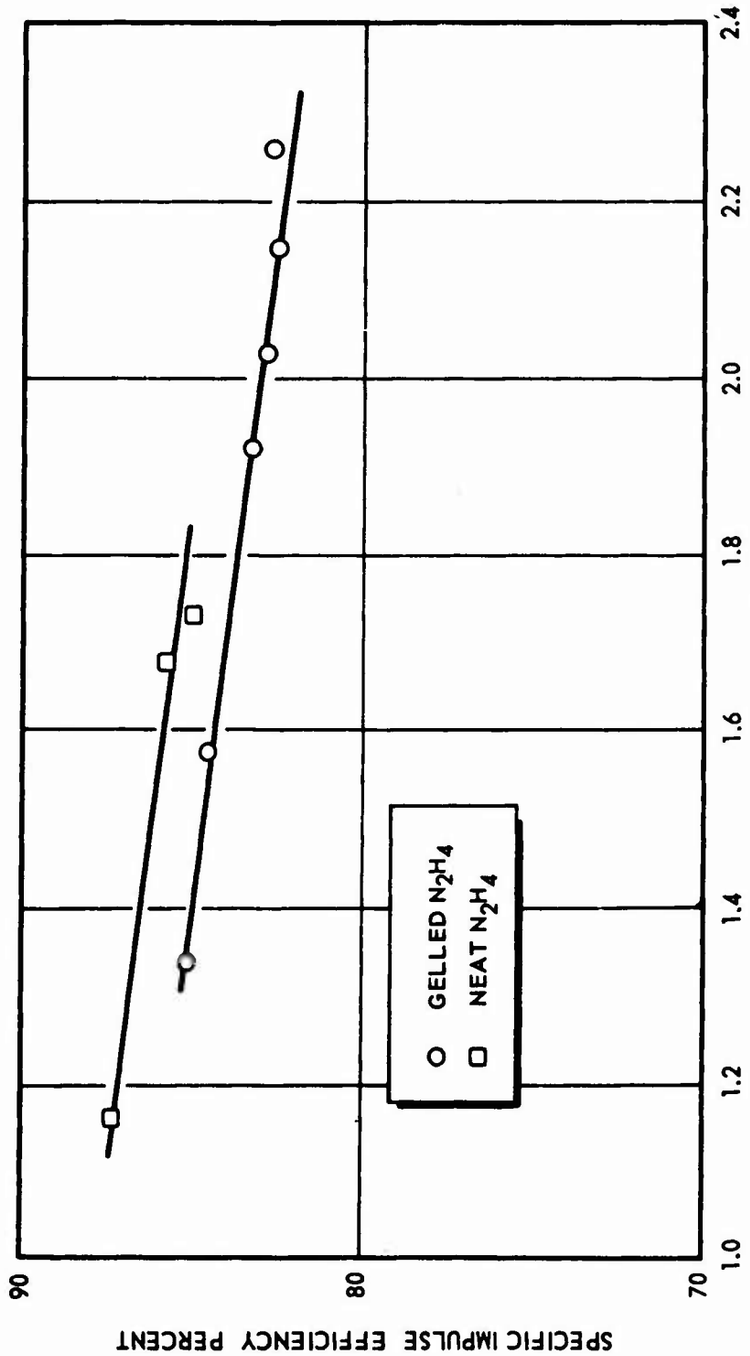
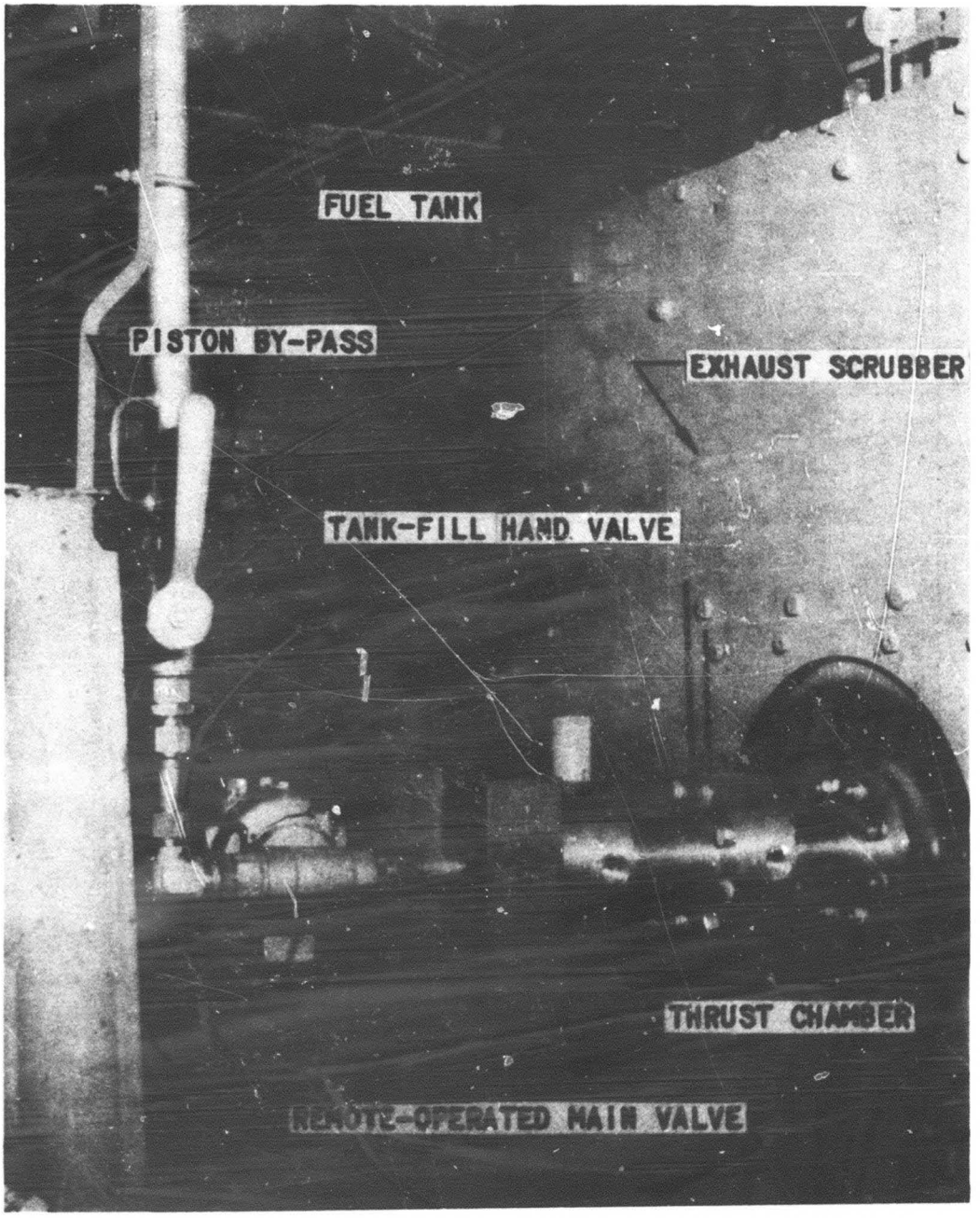


Figure 93. Performance of Gelled and Ungelled N_2H_4 With H_2O_2



5AA31-8/1/66-S1B

Figure 94. Expendable Monopropellant Test Stand

To provide ignition, ClF_5 was injected directly into the chamber, just in front of the injector face. The ClF_5 valve was sequenced to close shortly after the estimated time of ignition. A liquid base of 60-percent water and 40-percent hydrazine nitrate was used in formulating the first batch of fuel. For the initial test (No. 35), a ClF_5 flowrate equal to 10 percent of the fuel flowrate was selected. No detectable rise in chamber pressure was observed during the test.

For the second test, the igniter flowrate was increased to approximately 75 percent of the estimated fuel flowrate. The chamber pressure-time trace (Fig. 95) showed that ignition was achieved during this test, but chamber pressure decayed steadily after the igniter flow was shut off.

After conducting additional sensitivity tests, the liquid composition was changed to 50-percent water, 50-percent hydrazine nitrate with the objective of obtaining a mixture which would sustain combustion. The beryllium-beryllium hydride ratio remained as before. Test No. 60 on the small, expendable, 100-pound-thrust stand was somewhat inconclusive (Fig. 96). The final test (No. 61) was conducted at the 500-pound level using the hot-core injector and other hardware from previous tests. An uncooled copper nozzle was used. Fuel was injected through the injector spray nozzles as during the bipropellant and tripropellant tests. ClF_5 was injected through all oxidizer injector orifices to provide a strong ignition and an initial period of bipropellant operation. ClF_5 flow was then shut off. Chamber pressure dropped immediately, but then leveled off and maintained a new constant value, indicating sustained monopropellant operation (Fig. 97). The delivered specific impulse was 172 seconds, for an efficiency of 58-percent.

Flow Properties of Heterogeneous Propellants

As part of the thrust chamber performance testing effort, it was planned to obtain flow data concurrently with the performance tests. The dual-tank flow system (Fig. 54) was designed to allow cycling of the propellant between tanks prior to use in the thrust chamber. After loading the first batch of beryllium-containing fuel gel, the piston in the run

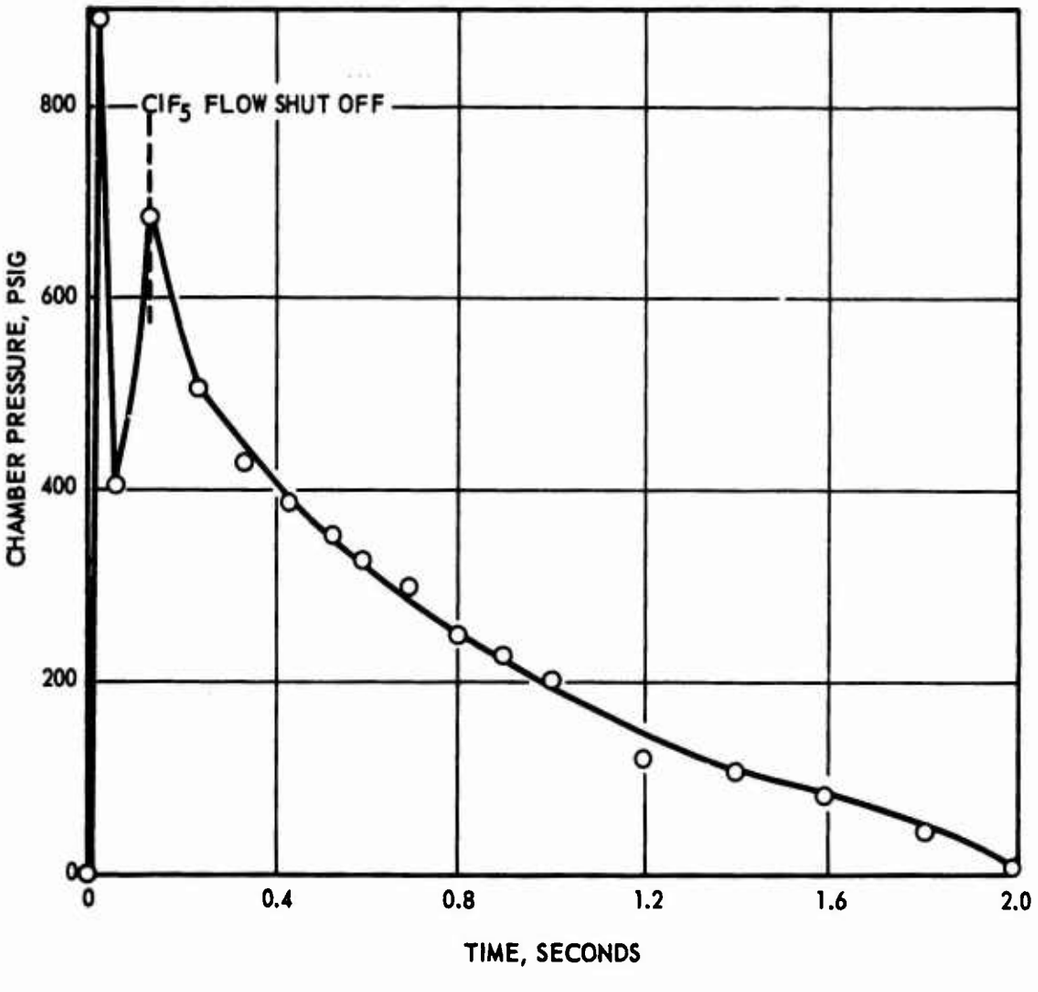


Figure 95. Chamber Pressure vs Time

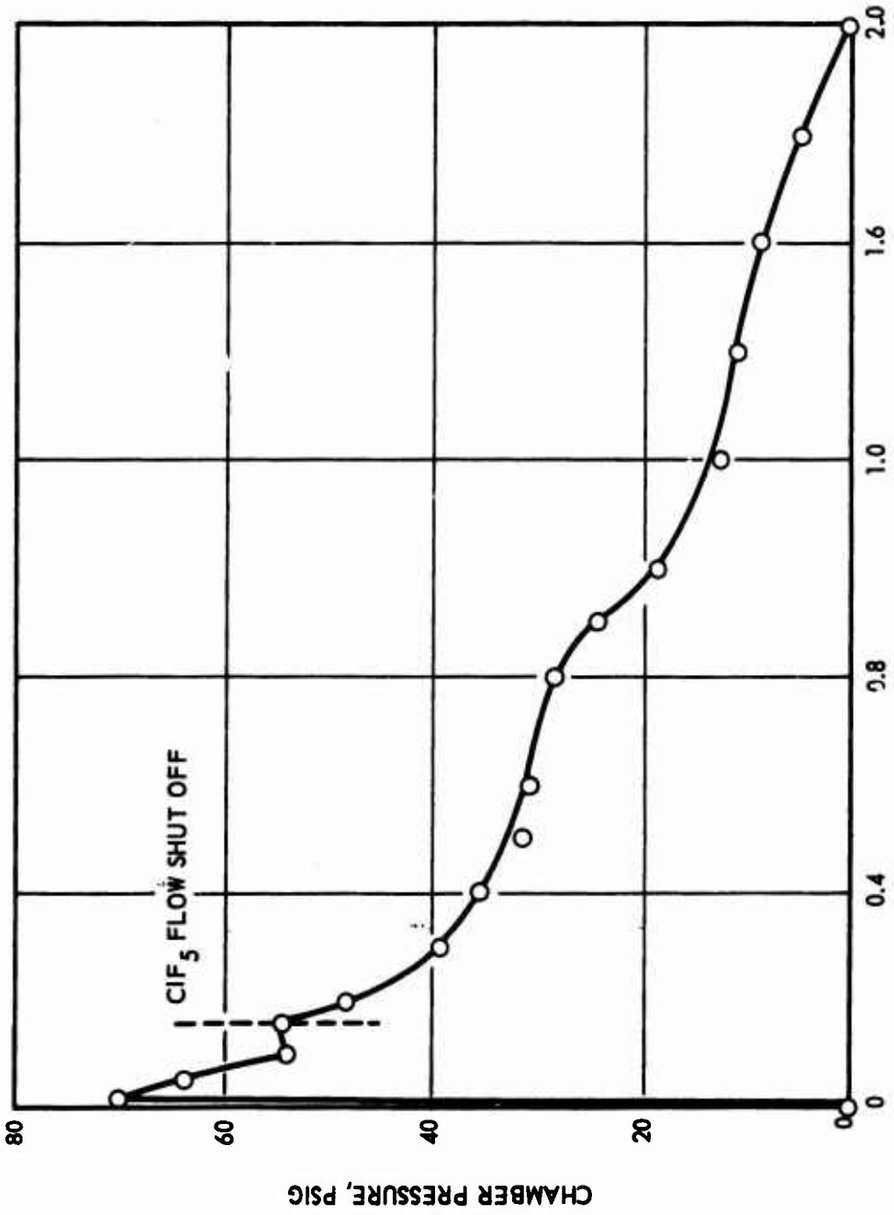


Figure 96. Chamber Pressure vs Time for Test No. 60

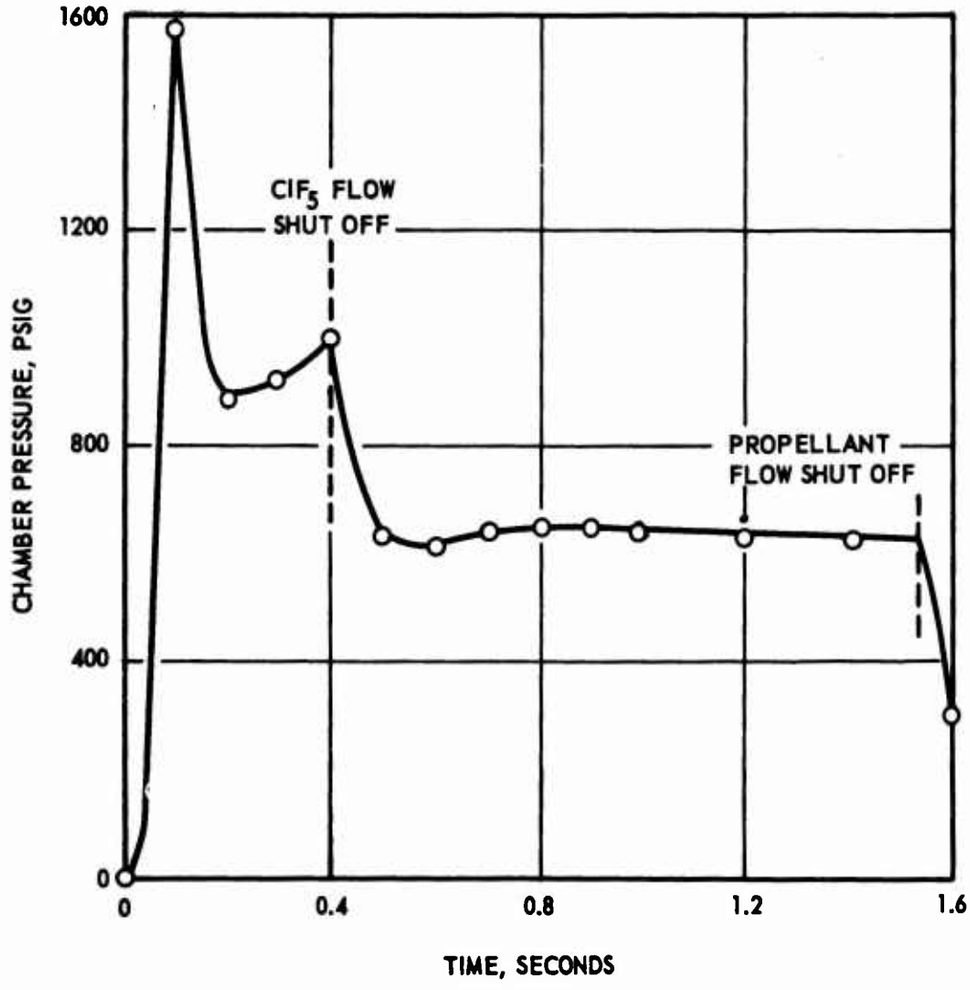


Figure 97. Chamber Pressure vs Time for Test No. 61

tank suddenly froze within the cylinder. All attempts to dislodge it by the application of pressure to either side failed. The entire assembly was then removed and the piston was bored out. The cylinder wall was found to be badly scored, necessitating a complete resurfacing operation, which was accomplished by a vendor. However, to avoid delay in performance testing, the system was rearranged to allow use of the alternate positive-displacement tank for performance testing. This removed the possibility of making concurrent flow measurements. A new piston was fabricated from aluminum to reduce the possibility of freezing in the cylinder as the original stainless-steel piston had done. Before the first cylinder had been returned to the test stand, the piston in the second cylinder also froze. Therefore, this piston was bored out and the cylinder was vended for rework while the original run tank with the new aluminum piston was reinstalled in the system. Performance testing continued with the one tank. However, the aluminum piston in this tank also jammed before the second tank was returned to the stand. Inspection of the cylinder walls again revealed a large score mark requiring a surface regrinding. At this point, a Teflon piston was fabricated and placed in the No. 2 tank when received.

The Teflon piston continued to operate satisfactorily during the remainder of the performance tests. The other cylinder could not be refinished in time to be placed in operation before the end of the test program. As a result, it was impossible to obtain all the flow data originally planned.

Fuel system pressure drops were recorded during all performance tests. Overall system drops are summarized in Fig. 98 and injector pressure drops are summarized in Fig. 99

An operational item of some speculation prior to the start of the experimental program was the tank outage efficiency to be expected with the heterogeneous fuels. It was thought that the heavy consistency of the gels might result in very poor expulsion efficiencies when ordinary

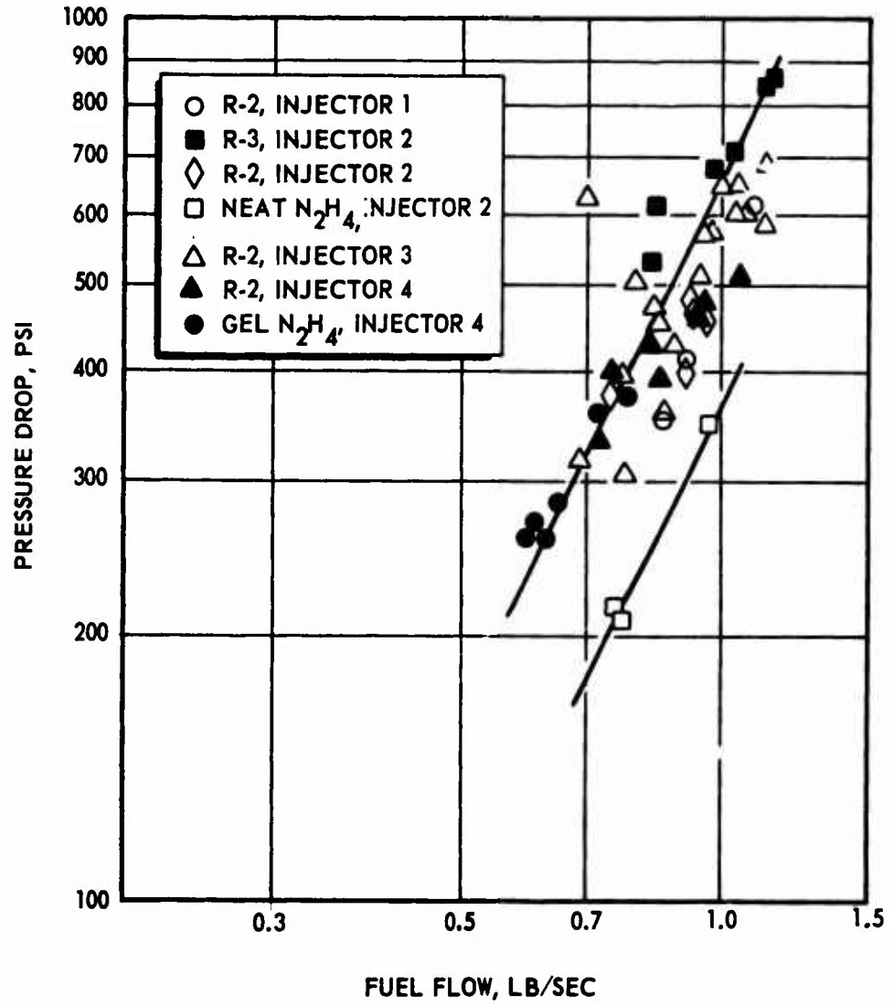


Figure 98. Fuel System Pressure Drops

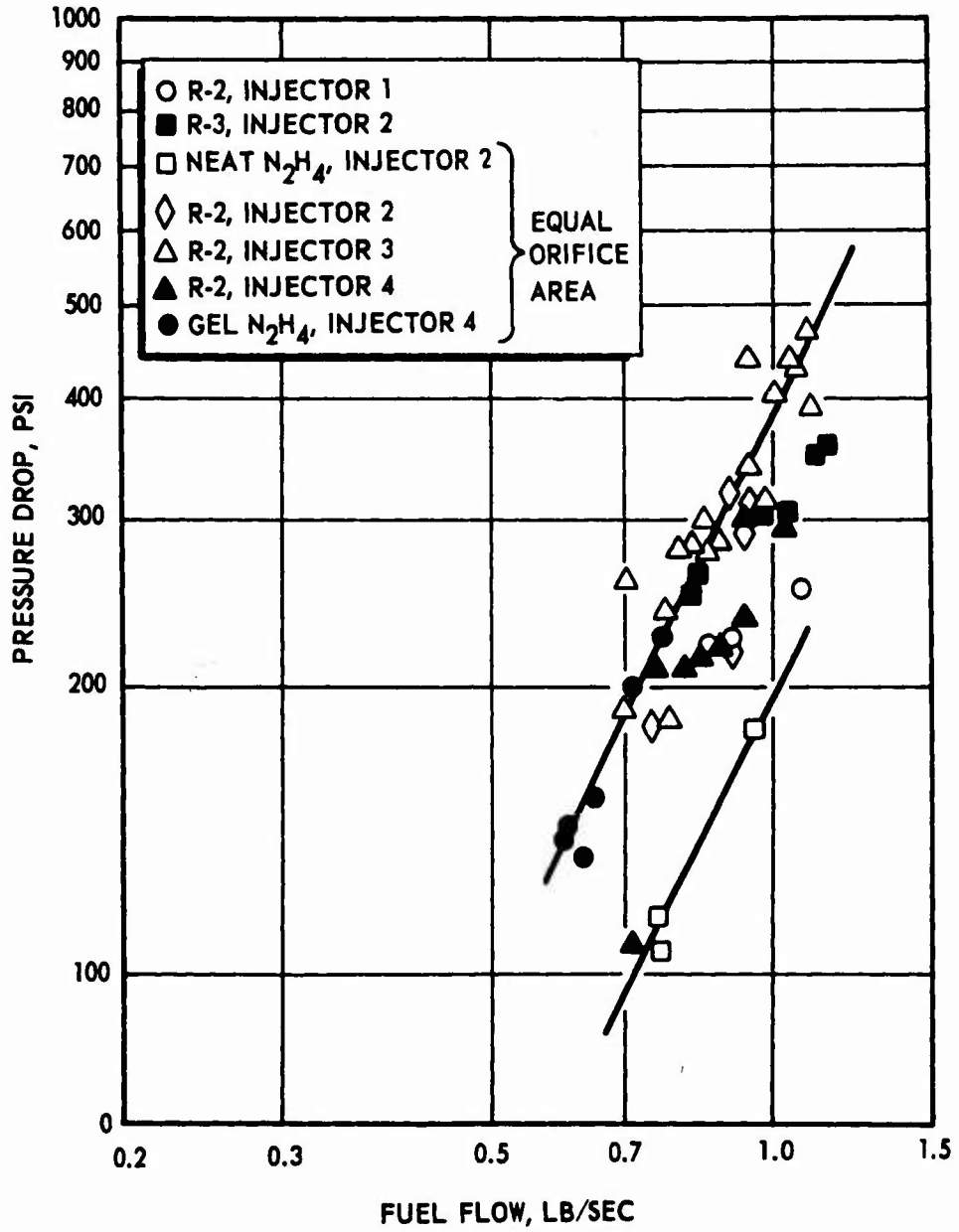


Figure 99. Fuel Injector Pressure Drops

gas pressurization techniques were used for expulsion. The fuel loading technique used for all batches of gel manufactured during this program consisted of using nitrogen pressure to force the gel into the run system, displacing the expulsion piston. Transfer was accomplished either from the glass columns of the mixing facility or from an intermediate steel tank. The diameter of the vessel from which gel was being transferred varied from 4 to 7 inches and the transfer line size varied from 1/4 to 1/2 inch. Because of the very cohesive and elastic nature of the gels produced, transfer efficiency was practically 100 percent in every case.

Once a part of the gel began to flow through the tank outlet, its elasticity tended to "pull" the rest of the gel with it. Tank outage efficiency is, therefore, not a problem with these gels.

ANALYSIS OF PROPELLANT EVALUATION DATA

A complete listing of performance test data is contained in Table 70 The calculated specific impulse efficiencies are based on theoretical values for shifting or equilibrium composition through the expansion nozzle. Because of the nozzle throat plugging phenomenon mentioned previously, calculated values of characteristic velocity could not be used as a valid performance parameter. In many cases, the indicated characteristic velocity efficiency would have been greater than 100 percent. This is illustrated in Fig. 100 for runs No. 13 through 20. Values of characteristic velocity are, therefore, not listed in Table 70.

R-2 Gel With H_2O_2 Oxidizer

Tests with R-2 (71-percent N_2H_4, 29-percent Be)/H_2O_2 system were divided into four categories by hardware variations. These variations are summarized in Table 71.

TABLE 70

THRUST CHAMBER PERFORMANCE

Run No.	Propellant Flowrates, lb/sec								Mixture Ratio, o/f	Chamber Pressure, psia	Thrust, pounds	Specific Impulse, seconds	E
	N_2H_4	H_2O_2	N_2O_4	ClF_5	Al Gel	R-2	R-3	R-5					
1													
2		0.848			1.39				0.61	895	550	245	
3		0.92			1.18				0.78	855	540	257	
4		0.940			1.38				0.68	860	560	241	
5		0.835				0.910			0.92	987	433	248	
6		0.976				0.751			1.30	956	415	241	
7		0.497				1.083			0.46	856	356	226	
8		0.839				0.905			0.93	971	417	239	
9		1.036				0.858			1.21	980	459	243	
10		0.774				0.958			0.81	952	408	236	
11													
12				0.286		0.855				913	383		
13		0.586		0.247		0.800			1.04	976	376	230	
14		0.591		0.208		0.701			1.14	944	376	251	
15		0.484		0.188		1.050			0.64	1007	391	227	
16		0.471		0.221		0.950			0.73	1022	384	234	
17		0.746		0.277		0.696			1.47	1054	415	241	
18		0.659		0.277		0.775			1.21	995	404	236	
19		0.661		0.241		0.850			1.06	1022	413	236	
20		0.538		0.106		1.075			0.60	1050	394	229	
21													
22		0.845				1.000			0.85	963	450	239	
23		0.676				1.1141			0.59	1019	438	241	
24		0.950				0.958			0.99	949	434	228	
25		1.045				0.833			1.25	949	444	236	
26		0.823				0.969			0.85	999	428	239	
27		0.521		0.231		1.068			0.70	1042	421	231	

TABLE 70

T CHAMBER PERFORMANCE DATA

Thrust, pounds	Specific Impulse, seconds	Specific Impulse Efficiency, percent	Injector No.	Nozzle Type	Run Duration, seconds	Comments
			1	Uncooled	0	Explosion in H_2O_2 line on start
550	245	82	1		1.5	
540	257	86	1		3.0	Extensive chamber erosion
560	241	80	2		1.0	
433	248	76.6	2		1.5	Explosion in H_2O_2 manifold on shutdown
415	241	76.2	2		1.5	Extensive nozzle throat erosion
356	226	68.4	1		1.0	Explosion in H_2O_2 manifold on shutdown
417	239	73.7	1		1.0	Extensive nozzle throat erosion
459	243	76.3	1		1.0	Extensive nozzle throat erosion
408	236	72.0	2		1.0	
			3	Cooled	0	Valve failure resulted in no fuel flow
383			3		1.5	Instrumentation failure resulted in loss of flowrate
376	230	70.4	3			
376	251	77.5	3			
391	227	69.0	3			
384	234	71.0	3			
415	241	75.6	3			
404	236	72.9	3			
413	236	73.2	3			
394	229	68.9	3			
			3		0	Instrumentation failure resulted in loss of flowrate
450	239	73.9	3		1.5	
438	241	71.8	3			
434	228	70.0	3			
444	236	74.0	3			
428	239	72.3	3			
421	231	70.0	3	Cooled	3.0	

2

CONFIDENTIAL

TABLE 70

(Continued)

Run No.	Propellant Flowrates, lb/sec								Mixture Ratio, o/f	Chamber Pressure, psia	Thrust, pounds	Specific Impulse, seconds	S I Ef p
	N_2H_4	H_2O_2	N_2O_4	ClF_5	Al Gel	R-2	R-3	R-5					
28		0.699				0.938			0.75	975	408	249	
29		0.744				0.925			0.80	994	415	249	
30			0.914			0.889			1.03	986	455	253	
31			0.724			1.113			0.65	1070	477	260	
32			1.048			0.861			1.22	1026	483	253	
33			1.172			0.786			1.49	1026	488	249	
34		1.101					0.753		1.46	1003	493	265	
35													
36													
37		0.931					0.983		0.95	1034	480	251	
38		0.887					1.134		0.78	974	490	242	
39		0.888					1.158		0.77	964	489	239	
40		1.101					0.827		1.33	1014	490	254	
41		1.084					0.842		1.29	1014	510	265	
42		0.953					1.021		0.93	1024	490	248	
43	0.956	1.110							1.16	1014	497	240	
44	0.765	1.291							1.69	1004	500	243	
45	0.765	1.327							1.74	1014	505	241	
46		0.639				0.943				983	414		
47		0.517		0.179		1.042			0.67	971	401	230	
48		0.665		0.202		0.813			1.07	964	416	248	
49		0.718		0.165		0.850			1.04	943	422	244	
50		0.631		0.169		0.958			0.84	999	432	246	
51		0.798		0.182		0.763			1.28	979	413	237	
52		0.716		0.182		0.893			1.01	1011	451	252	
53		0.817		0.208		0.723			1.42	999	437	250	

TABLE 70

(Continued)

Specific Impulse, seconds	Specific Impulse Efficiency, percent	Injector No.	Nozzle Type	Run Duration, seconds	Comments
249	75.0	2	Uncooled	1.5	
249	75.1	2	Uncooled		
253	80.4	3	Cooled		
260	80.7	3			
253	81.5	3			
249	81.6	3			Water-cooled nozzle destroyed on shutdown
265	81.6	2		0.5	Explosion in H_2O_2 manifold
				1.0	Ignition not achieved
				1.5	Steady-state chamber pressure not achieved
251	74.8	2			
242	72.2	2			
239	71.2	2			
254	77.6	2			
265	80.7	2			
248	74.1	2			
240	86.9	2			Explosion in H_2O_2 manifold
243	85.7	2			
241	84.9	2			Explosion in fuel injector manifold
		4			Instrumentation failure resulted in loss of ClF_5 flowrate
230	69.5	4			
248	76.2	4			
244	75.0	4			
246	74.6	4			
237	73.8	4			
252	77.4	4			
250	78.1	4			

CONFIDENTIAL

TABLE 70
(Concluded)

Run No.	Propellant Flowrates, lb/sec								Mixture Ratio, o/f	Chamber Pressure, psia	Thrust, pounds	Specific Impulse seconds
	N_2H_4	H_2O_2	N_2O_4	ClF_5	Al Gel	R-2	R-3	R-5				
54	0.769	1.028							1.34	896	422	235
55	0.652	1.253							1.92	944	449	236
56	0.598	1.349							2.26	954	453	233
57	0.630	1.278							2.03	954	450	236
58	0.611	1.316							2.15	944	452	235
59	0.722	1.139							1.58	921	440	237
60												
61								1.705		638	293	172

TABLE 70
(Concluded)

Thrust, pounds	Specific Impulse, seconds	Specific Impulse Efficiency, percent	Injector No.	Nozzle Type	Run Duration, seconds	Comments
422	235	85.1	4	Cooled	1.5	
449	236	83.1	4	↓	↓	
453	233	82.5	4			
450	236	82.9	4			
452	235	82.4	4			
440	237	84.5	4			Steady-state chamber pressure not achieved
293	172		4	Uncooled	1.5	

CONFIDENTIAL

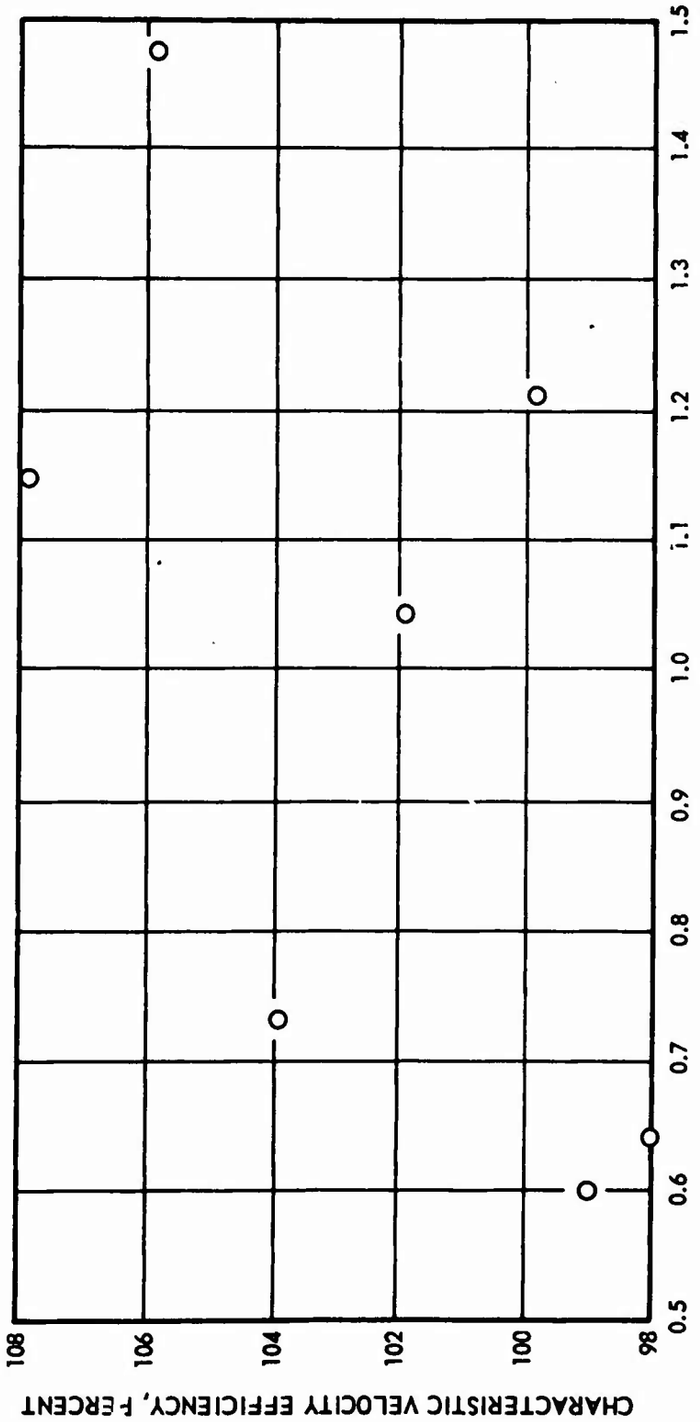


Figure 100. Characteristic Velocity Efficiency
(Runs No. 13 through 20)

TABLE 71

Be-N_2H_4-H_2O_2 SYSTEM

Run No.	Injector No.	Characteristic Length, inches	Nozzle Type
5,6,10	2	170	Uncooled
7,8,9	1	170	Uncooled
22-26	3	170	Water-cooled
28,29	2	308	Uncooled

Delivered specific impulse is plotted as a function of mixture ratio in Fig. 101. No particular trend can be distinguished for the data as a whole. Optimum mixture ratio for this system is 0.55. Therefore, the one run at 0.46 probably should not be considered with the rest of the data, because the low performance may be related more to chemical effects than to the hardware effects being considered. Ignoring this run, there is no apparent difference between injectors No. 1 and 2 with the same chamber hardware. The data for injector No. 3 with the water-cooled nozzle fall slightly below the average. This difference could be ascribed to either a less efficient injector or an increase in heat loss to the nozzle. However, additional data, to be discussed later, also indicate this injector to be less efficient than the No. 2 design, and differences in heat loss to the nozzle do not appear to be significant.

The two tests with injector No. 2 and increased chamber residence time fall some 3 percent above the average value. This may be a significant difference, although it is not outside the scatter of the rest of the data. Further tests would be necessary to define the exact effect.

An increase in specific impulse efficiency with mixture ratio is noted in Fig. 81 and 88. In considering these data, it is essential to be able to distinguish between an increased efficiency caused by increased

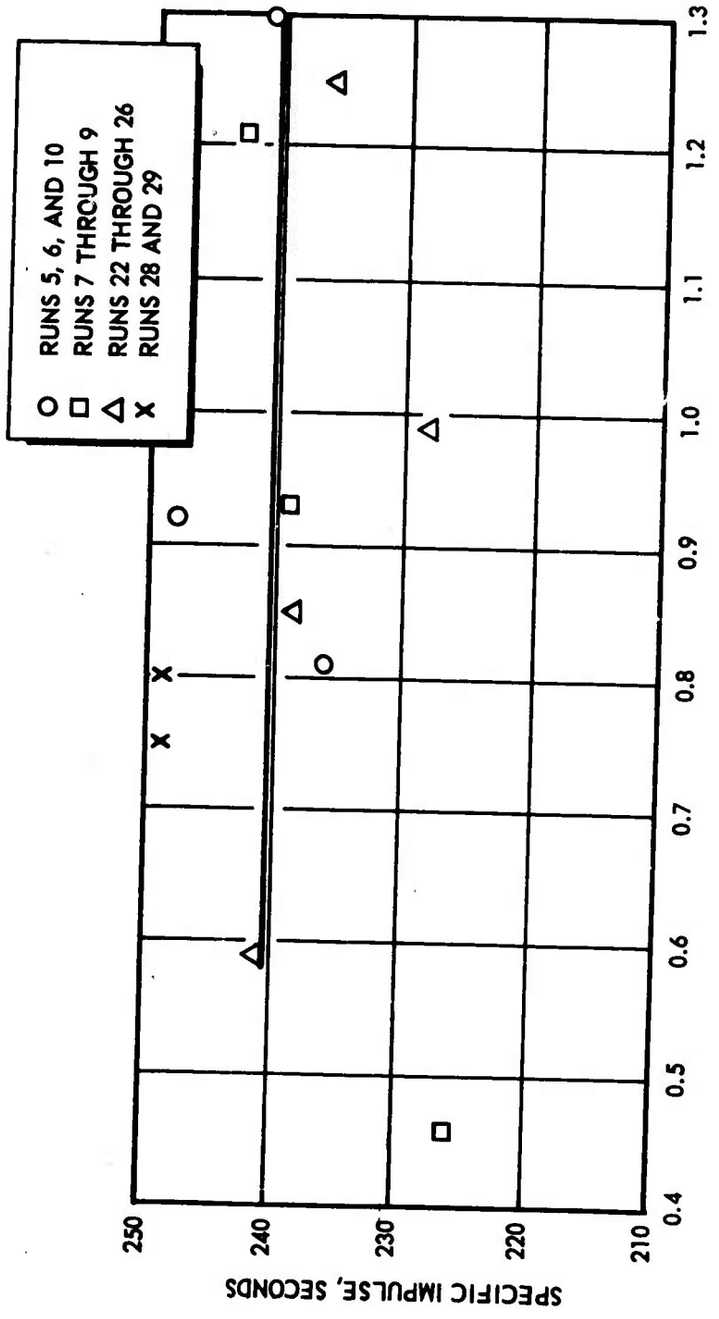


Figure 101. Delivered Specific Impulse With Be-N_2H_4-H_2O_2 System

beryllium combustion and an apparent increase in efficiency caused simply by the fact that beryllium represents a smaller fraction of the total propellant flow at higher mixture ratios. To make this distinction, theoretical calculations were made for performance at various fractions of metal burned. These curves are presented in Fig. 102 along with the experimental curve based on runs No. 5 through 10. The experimental points fall below the theoretical curve for zero-percent beryllium burned. This does not take into account other losses in the motor. If these losses were assumed to be 11 percent, for example, then the 20-percent beryllium combusted curve would coincide closely with the experimental curve. Two assumptions are implied in this comparison: (1) the percentage of beryllium combustion is constant over the experimental mixture ratio range, and (2) the percentage loss caused by other factors is constant over the same range. With regard to the first assumption, it is possible that the percentage of combustion increases as mixture ratio increases; the same average slope as for the 20-percent curve could be obtained if 30 percent of the beryllium burned at a mixture ratio of 0.6 and if the efficiency increased until it reached approximately 36 percent at a mixture ratio of 1.3. To make this curve coincide with the experimental curve, 16 percent would have to be assumed for other losses, compared to 11 percent for constant combustion efficiency of beryllium.

Other motor losses can be estimated by considering the data for hydrazine-peroxide in the same experimental system. These losses ranged from 12 to 18 percent over the range studied (Fig. 92), increasing with mixture ratio. Some difficulties are involved in using these data as a basis for the motor losses. The runs were made at higher mixture ratios than for the metal-loaded fuel. Theoretical calculation of optimum mixture ratio for the N_2H_4-H_2O_2 system is very sensitive to the assumption of either frozen or equilibrium expansion through the nozzle, resulting in values of 1.5 and 2.0, respectively. Injector efficiency is certain to be affected when making a very large change in mixture ratio. However, it seems reasonable to suggest that the data indicate performance losses caused by factors

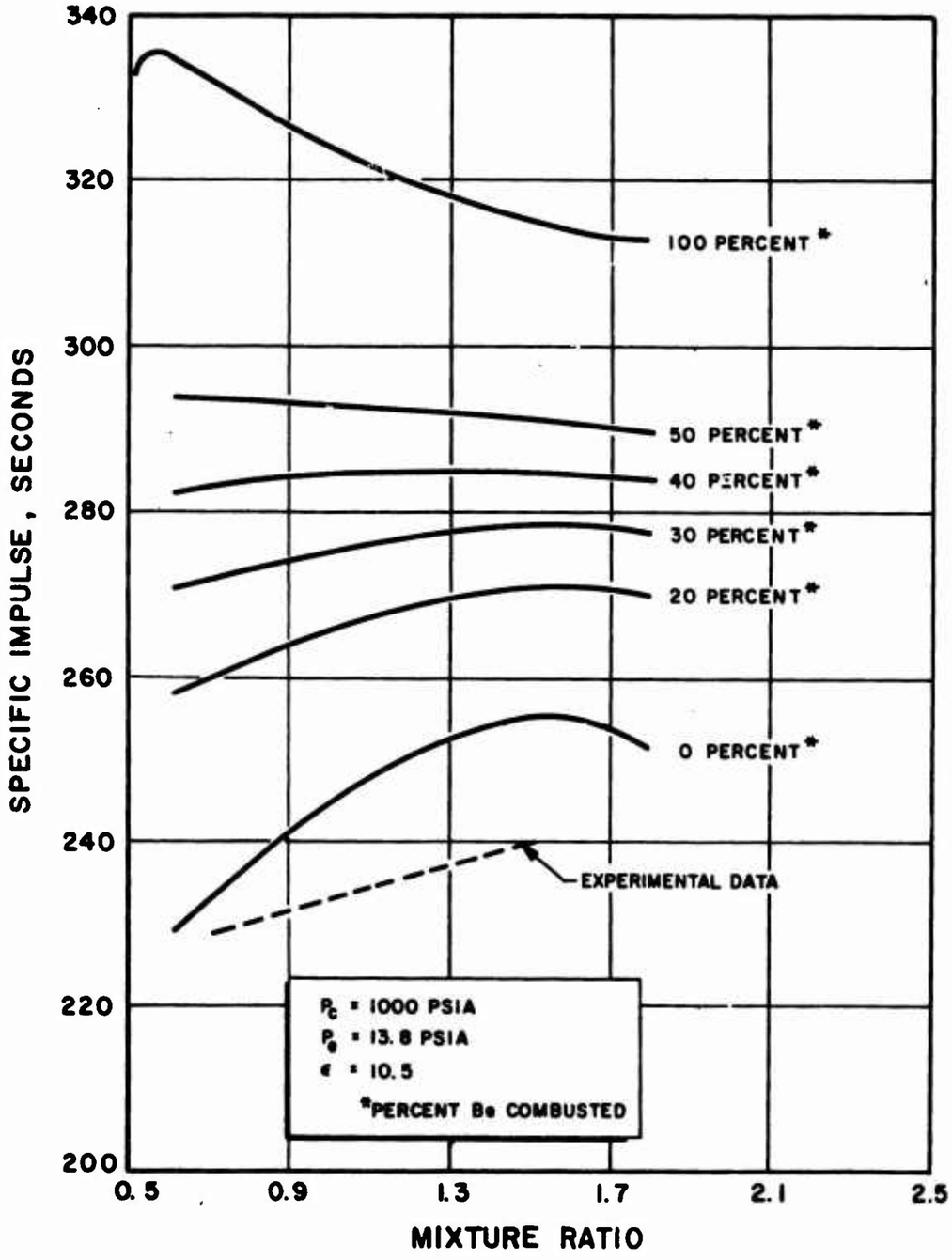


Figure 102. Performance vs Mixture Ratio of 98-Percent H_2O_2/R-2

other than metal combustion of between 10 and 15 percent for the range of mixture ratios studied in the beryllium system. Thus, a beryllium combustion efficiency of between 20 and 30 percent may be estimated.

R-2 Gel With N_2O_4 Oxidizer

Similar theoretical calculations were performed for the R-2/N_2O_4 system, under a company-sponsored program. In Fig.103, the experimental curve is seen to fall above the zero-percent metal combustion curve even if it is assumed that no other motor losses occur, a highly unreasonable assumption. No baseline test data are available for the N_2H_4-N_2O_4 system in the same experimental hardware. It can only be assumed that losses with this system would be comparable to those in the N_2H_4-H_2O_2 system. If 13 percent of other losses are assumed, then the 50-percent curve in Fig.103 would coincide very closely with the experimental data. There is little doubt that the beryllium combustion efficiency with N_2O_4 is considerably higher than with H_2O_2. There are at least two obvious possible reasons for this difference: (1) the R-2/N_2O_4 system has a considerably higher combustion temperature than the R-2/H_2O_2 system, and (2) H_2O_2 may decompose into H_2O and O_2 before reacting with metal and N_2H_4, whereas N_2O_4 may react directly. It is not possible at this time to differentiate between these two mechanisms. It may be that both contribute to the observed difference.

R-2 Gel With H_2O_2-ClF_5 Oxidizer

Uniform Fluorine Distribution Tripropellant Injector. In an effort to improve the combustion efficiency of the Be-N_2H_4-H_2O_2 system, a series of tripropellant test firings was conducted in which the oxidizer consisted of approximately 30-percent ClF_5, 70-percent H_2O_2. Addition of fluorine to the system might be expected to improve combustion in several ways. One hypothesis for the low performance observed is that the metal particles form a protective oxide coating which does not allow combustion to proceed until the chamber temperature reaches the melting point of the

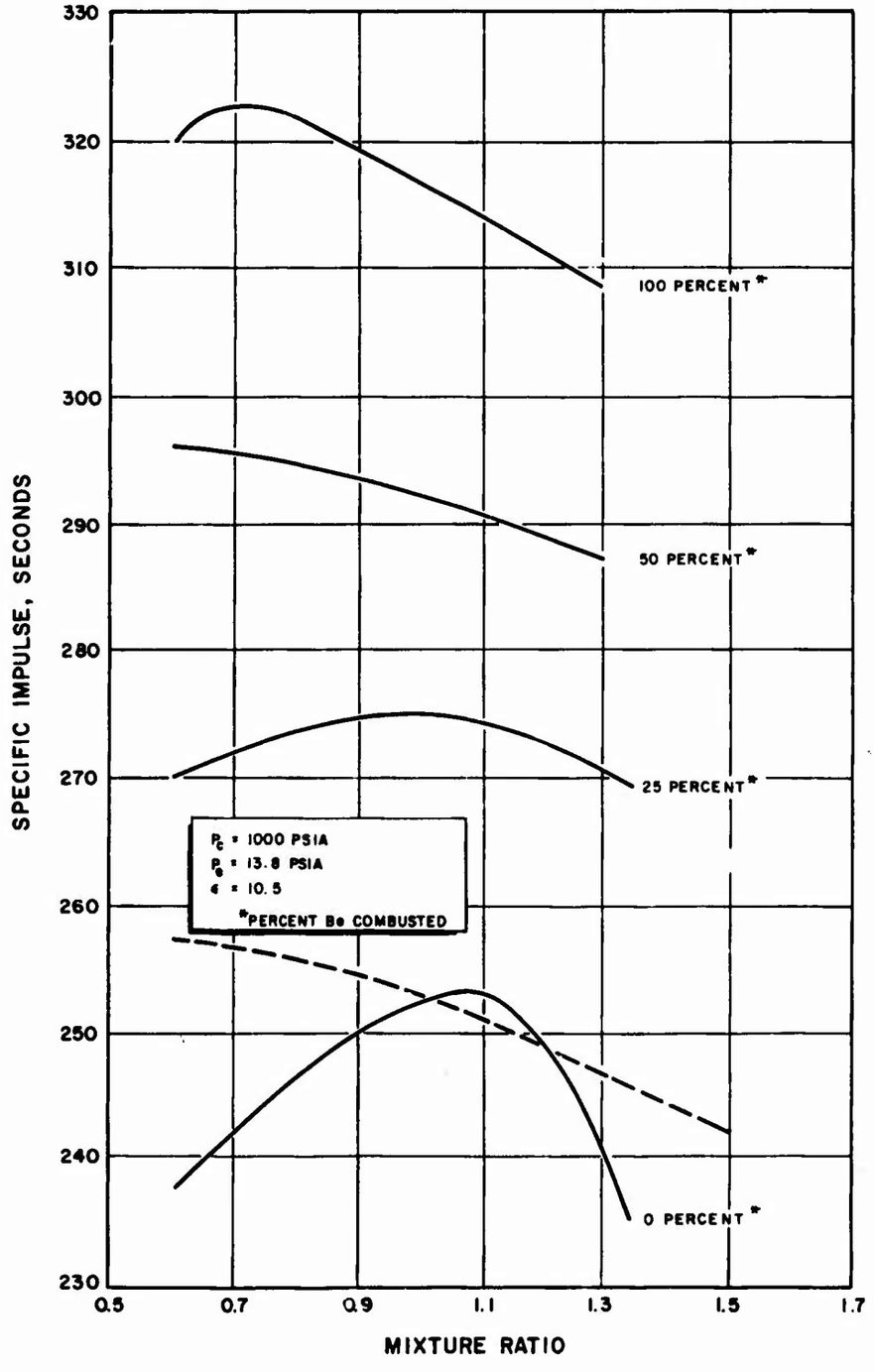


Figure 103. Performance vs Mixture Ratio of N_2O_4/R-2

oxide. The temperature which results if it is assumed that no metal burning takes place is several hundred degrees below the melting point of the oxide. Beryllium fluoride melts at a much lower temperature (800 C) than beryllium oxide (2585 C). Therefore, the reaction of beryllium with fluorine is not as temperature limited. Thus, it was proposed that fluorine in moderate amounts might act as a fluxing agent to remove the protective oxide coating from the metal particles and allow bulk combustion to proceed.

A second possible source of performance losses may be condensation of the combustion products. The velocity and thermal lags between these solid particles and the gas stream reduce the efficiency of the expansion process. Because the condensation temperature of beryllium fluoride is much lower than that of beryllium oxide, losses caused by two-phase flow might be less in a fluoride system. Theoretical calculations of specific impulse, chamber temperature, and percent condensed phase as functions of composition are given in Fig. 104 for the R-2 (71 w/o N_2H_4-29 w/o Be)/H_2O_2/ClF_5 tripropellant system. Test data obtained with this system at an average oxidizer composition of 30-percent ClF_5 showed no significant improvement over the R-2/H_2O_2 system with identical hardware (Fig. 87 vs Fig. 88). The mixture ratio represented in Fig. 35 is based on the sum of the two oxidizer flowrates $(H_2O_2 + ClF_5)/(N_2H_4 + Be)$. In computing performance efficiencies, the addition of ClF_5 lowers the theoretical specific impulse. However, for compositions which are oxidizer rich, the constant specific impulse contours are almost parallel to the constant percent fuel lines, with the result that the theoretical specific impulse is nearly the same at a given overall mixture ratio for either the bipropellant or tripropellant system. Thus, a direct comparison between Fig. 87 and 88 was valid.

A summary of all test data obtained with the uniform fluorine distribution tripropellant injector (No. 3) and water-cooled nozzle is presented in Fig. 105. This graph reiterates the lack of significant difference between the R-2/H_2O_2/ClF_5 systems. It also shows that the performance obtained with N_2O_4 is higher not only on an efficiency basis, but on a delivered impulse basis. This is despite the fact that the theoretical

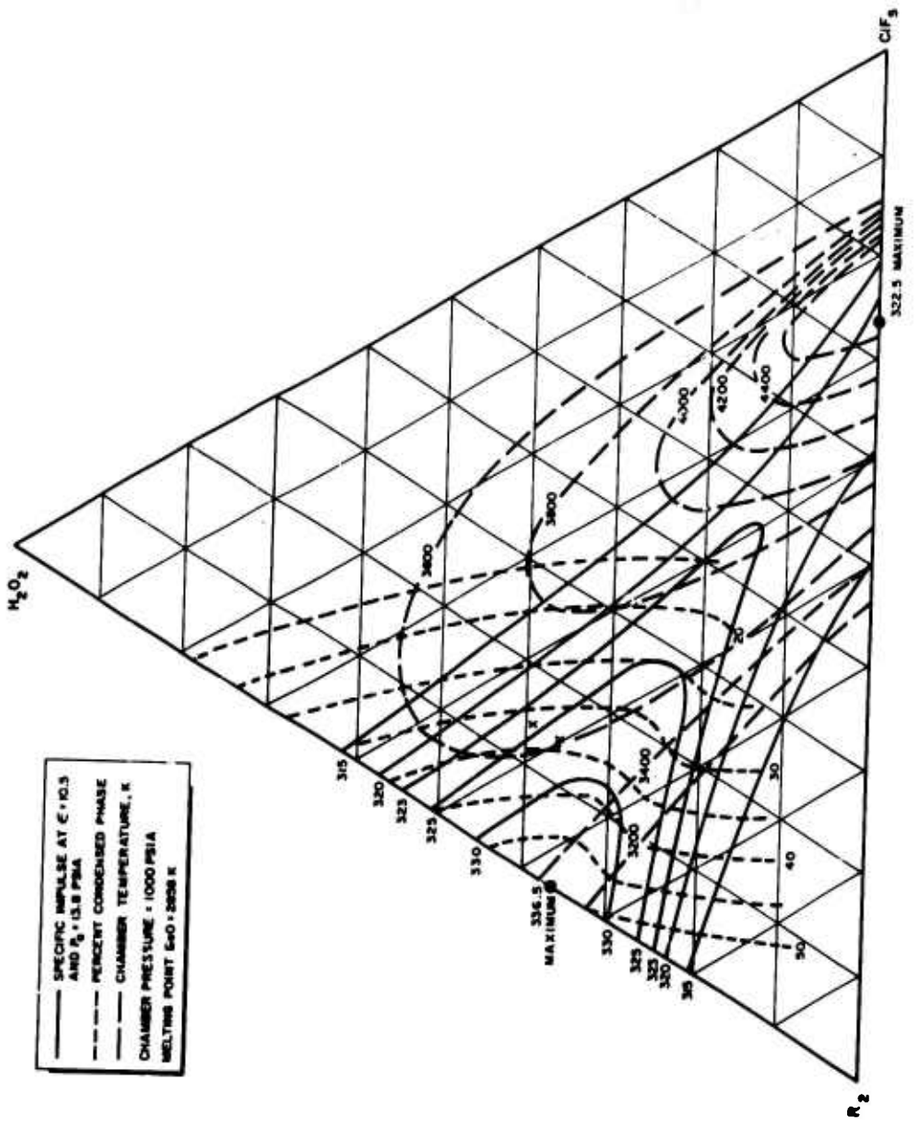


Figure 104. Specific Impulse, Percent Condensed Phase, and Chamber Temperature vs Composition of $H_2O_2/ClF_5/29$-Percent Be in N_2H_4

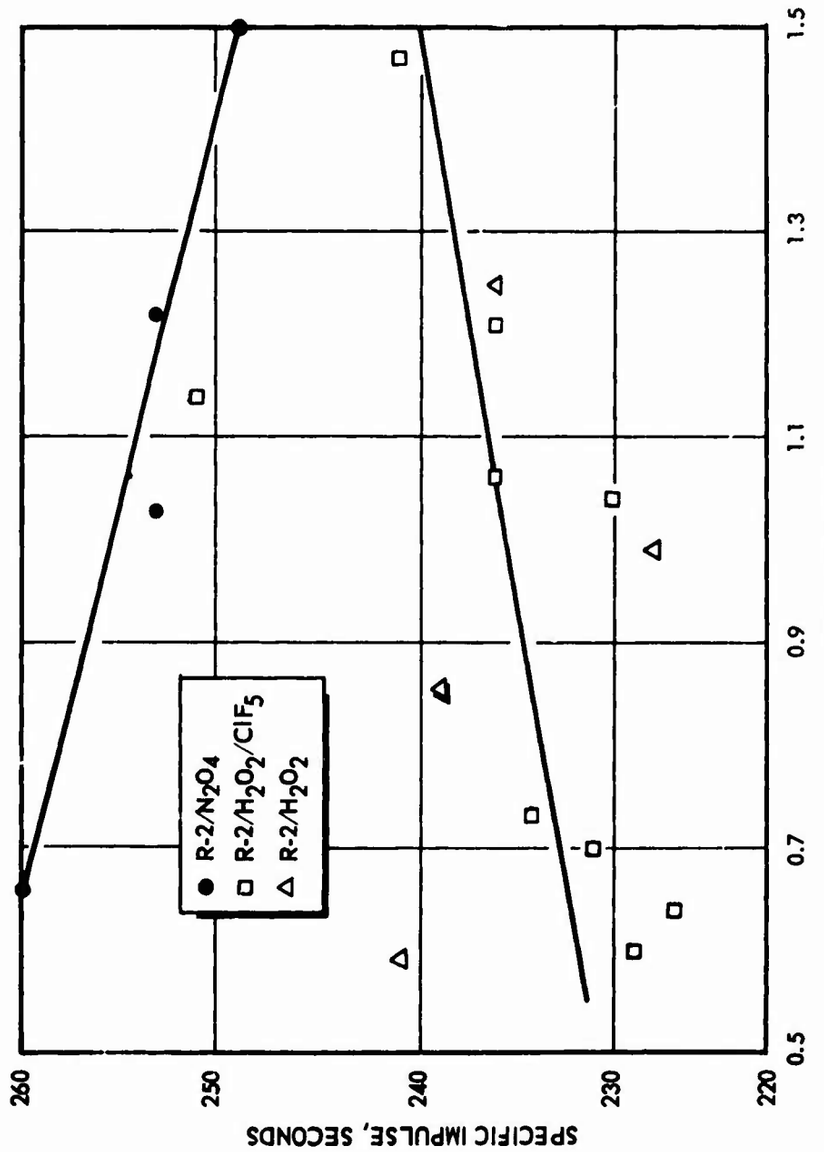


Figure 105. Thrust Chamber Performance With Tripropellant (No. 3) Injector

maximum for the Be-N_2H_4-N_2O_4 system is 7 seconds lower than for Be-N_2H_4-N_2O_4 system is 7 seconds lower than for Be-N_2H_4-H_2O_2 and the R-2 composition is not optimum for use with N_2O_4.

In discussing the difference in combustion efficiency observed between the N_2O_4 and H_2O_2 systems, two possible causes were presented, namely a difference in temperature and a difference in chemical reactivity. The lack of a difference between the H_2O_2 and H_2O_2/ClF_5 systems suggests that temperature may be the decisive factor. If the poor performance of the H_2O_2 system is caused by a slow Be-H_2O reaction, then replacing H_2O_2 with ClF_5, which can react directly, should result in a proportionate increase in the percentage of beryllium burned. On the other hand, if a temperature sufficient to melt the oxide coating is the only important factor, addition of 30-percent ClF_5 may not have increased the temperature above the critical level and, therefore, would have little effect. The maximum increases in system temperature occur only as the oxidizer concentration approaches 100-percent ClF_5. Therefore, these data seem to suggest the greater importance of temperature than chemical composition, per se.

R-2 Gel With Hot-Core Injector. If complete combustion of beryllium can be achieved at any point within the chamber, the heat liberated by this reaction should be sufficient to bring the rest of the propellant flow up to the necessary ignition temperature. This, briefly, is the hot-core injector concept. If, instead of injecting 30-percent ClF_5 uniformly distributed over the chamber, this entire quantity is injected at one point with the appropriate amount of fuel, the maximum temperature indicated in Fig. 104 should be achieved. A comparison of the results obtained with the two methods of introducing ClF_5 is presented in Fig. 106. Although there appears to be an improvement in performance with the hot-core system, the difference is no more than could be attributed to the difference in injector design, regardless of the oxidizer used. Thus, the question of temperature vs chemical limitations is still unanswered.

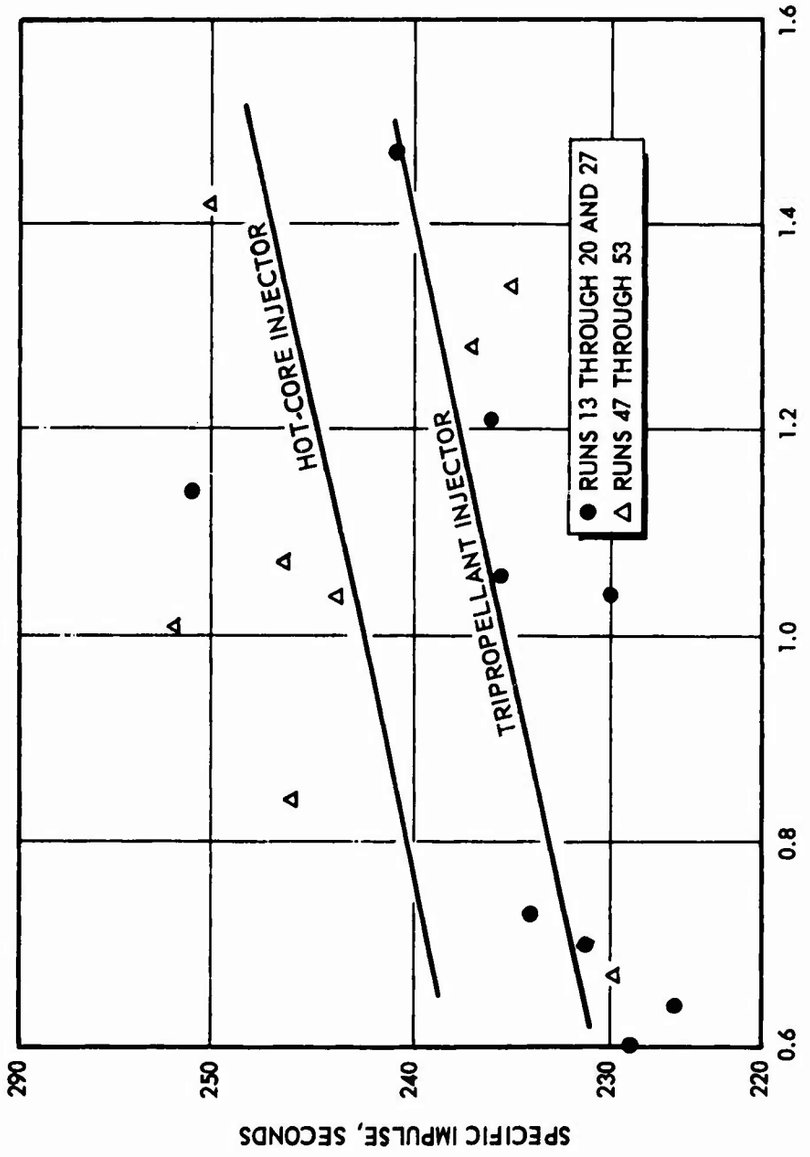


Figure 106. Injector Comparison With Be-N_2H_4-H_2O_2-ClF_5 System

Nonmetallized R-2 Propellant System

The performance of the nonmetallized N_2H_4-H_2O_2 system is also significant (Fig. 93). The most striking difference between these data and the data from the same experimental system with beryllium added is the lack of scatter in the data points. The data fall on a smooth curve as a function of mixture ratio, whereas the metallized system data are all widely scattered. This could be interpreted in various ways. One possible cause would be the presence of nonhomogeneities in the metallized gel. Another possibility might also have been the production of highly nonhomogeneous conditions within the chamber because of poor injection and mixing of the gelled fuel. Although the poor mixing hypothesis in itself did not explain the difference between the behavior of metallized and nonmetallized hydrazine, three points shoud be considered: (1) the theoretical performance of the N_2H_4-H_2O_2 system is affected little by mixture ratio in the region tested, whereas the Be-N_2H_4-H_2O_2 system peaks rather sharply and would be much more affected by local variations in mixture ratio, (2) the data of Fig. 93 clearly indicated a lower performance with gelled N_2H_4 than with neat N_2H_4, (3) the performance obtained with neat N_2H_4 is slightly lower than was expected; losses for this motor hardware had been estimated at approximately 10 percent. It is concluded that significant inefficiencies in atomization and mixing of the gelled fuels may have been present in the experimental system, and that an injector optimization study might lead to appreciably better performance.

R-3 Gel With H_2O_2 Oxidizer

Theoretical calculations of performance as a function of the percentage of beryllium burned were also made for the Be-BeH_2-MMH-H_2O_2 system and are presented in Fig. 107. In this case, as for the R-2/N_2O_4 system, the experimental data are entirely above the curve for zero-percent metal burned. It is assumed that other losses of 10 to 15 percent would place the 50-percent metal burned curve in approximate agreement with the experimental data. A comparison between the specific impulse efficiencies obtained with the R-3 fuel (Fig. 90) and those obtained with the

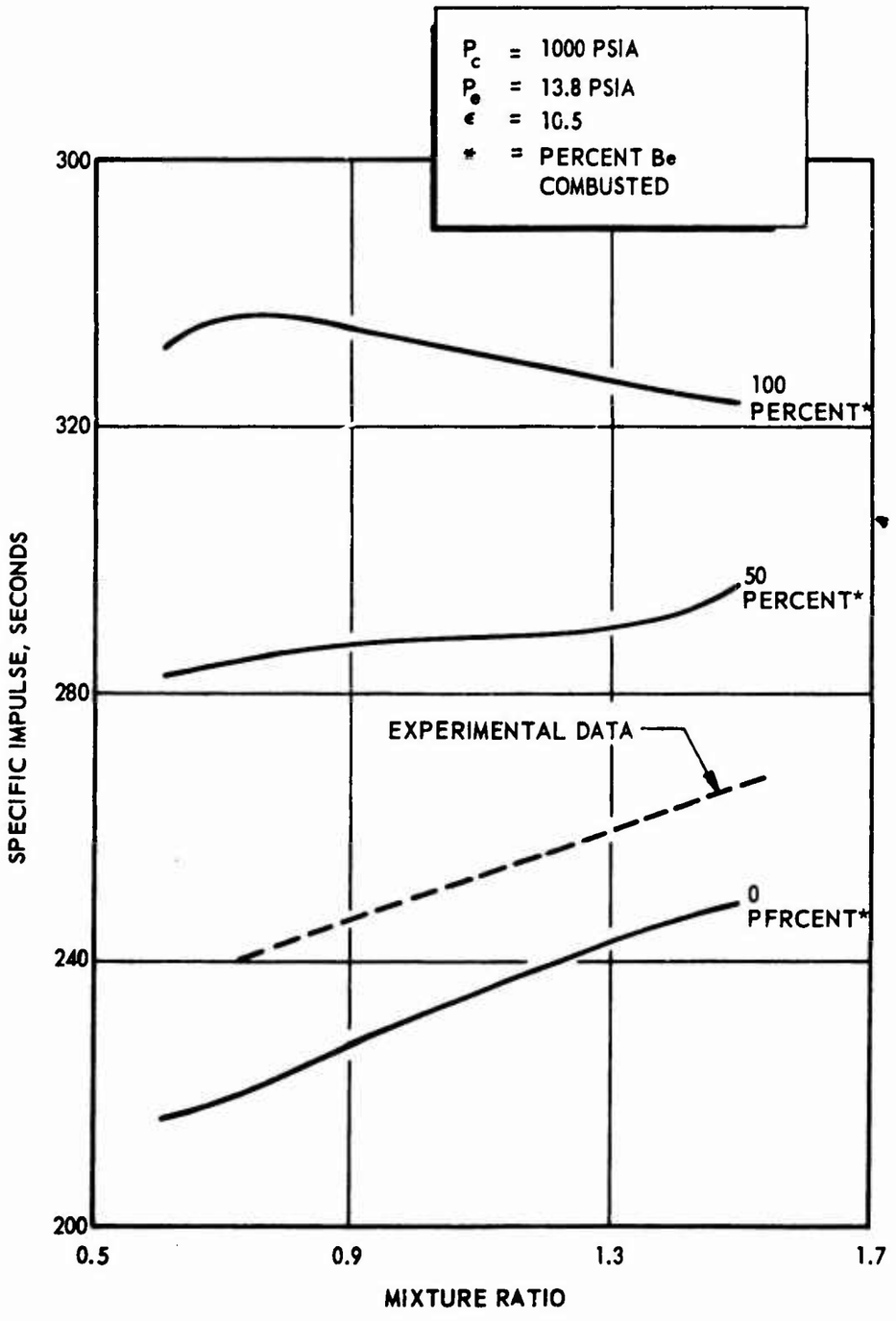


Figure 107. Performance vs Mixture Ratio of R-3/H_2O_2 System

R-2 fuel (Fig. 81 and 88) indicates only a 0- to 6-percent gain for the R-3 system when hydrogen peroxide was used. However, the effect of beryllium combustion on theoretical performance is much greater for the R-3 system. As a result, the small difference in specific impulse efficiency indicates a much greater increase in beryllium combustion efficiency. Although no baseline data are available for the MMH-H_2O_2 system, it seems reasonable to assume that performance losses in this system would be comparable to those in the N_2H_4-H_2O_2 system. It is possible that the difference in performance is caused by rheological properties of the gel rather than chemical factors. The R-3 gel was observed to be highly thixotropic in comparison to the R-2, and shear-thinning was very pronounced. Because of the lower density of R-3 (0.86 as compared to 1.16), much higher pressure drops were required to test R-3 with the same injector (an average system drop of 710 vs 520 psi). These two factors would both work to produce better breakup and atomization of the fuel gel. If, as concluded earlier, fuel atomization and mixing inefficiencies are significant in the experimental hardware used, then the higher performance obtained with R-3 is reasonably explained.

Another reasonable interpretation would be based on the assumption that the decomposition of beryllium hydride would provide a more reactive form of beryllium than the pure metal. If combustion of the pure metal proceeds at the same rate as in the R-2/H_2O_2 system (i.e., 25 percent), then approximately 65 percent of beryllium in the hydride would have to burn to produce the results in Fig. 107

The percentage of metal burned in the R-3/H_2O_2 system is comparable to that in the R-2/N_2O_4 system. One of the reasons postulated for the increased combustion in going from R-2/H_2O_2 to R-2/N_2O_4 was the higher temperature of the N_2H_4/N_2O_4 combination. Although the flame temperature of the MMH/H_2O_2 system is slightly above that for N_2H_4/H_2O_2 (260 F at optimum mixture ratio), the increase is much less than for N_2H_4/N_2O_4 (630 F). The temperature increase in going from R-2 to R-3 with H_2O_2 is comparable to that expected for going from H_2O_2 to H_2O_2, 30-percent ClF_5 with R-2. In other words, the hypothesis of a temperature-limited beryllium combustion cannot accommodate all data presented.

R-5 Monopropellant

The final propellant tested was the R-5 monopropellant mixture. No evidence of monopropellant operation is indicated in Fig.105. After this run, the hydrazine nitrate/water ratio was changed from 40/60 to 50/50. The pressure-time trace in Fig.106, obtained under the same conditions, suggests that monopropellant operation may have begun, but then died out before establishing a steady state. The next run (Fig. 97) was conducted with the same fuel, but in the larger hardware. Steady-state monpropellant operation was clearly established during this run. Several factors may account for the difference in operation achieved (Fig. 96 vs Fig. 97 results): (1) system heat losses would have been higher in the smaller motor, and for a case of marginal operation, the additional heat removed may have been enough to quench the reaction, (2) the targeted chamber pressure in Fig. 97 was twice that in Fig. 96, and monpropellant burning is usually strongly enhanced by increased pressure, (3) ignition in the larger hardware was much more thorough with the bipropellant injector technique used instead of simply injecting the igniter flow into the chamber downstream of the injector as was done with the small motor.

Performance of the R-5 propellant is highly dependent upon combustion of the beryllium. Theoretical specific impulse for the test conditions of run No. 61 (i.e., 650-psia chamber pressure, 10.5 expansion area ratio, 13.8-psia ambient pressure) is presented in Fig.108. The changes in theoretical performance produced by assuming 10- to 15-percent motor losses are also indicated. Because of the lower chamber pressure and operating level, the percentage losses due to causes other than metal combustion are probably smaller than those for the R-2 and R-3 tests. Regardless of what percentage of other losses is assumed in the range of 0 to 15 percent, the experimental specific impulse indicates a beryllium combustion of between 20 and 30 percent. It is highly interesting that this value agrees with the bipropellant test data involving the

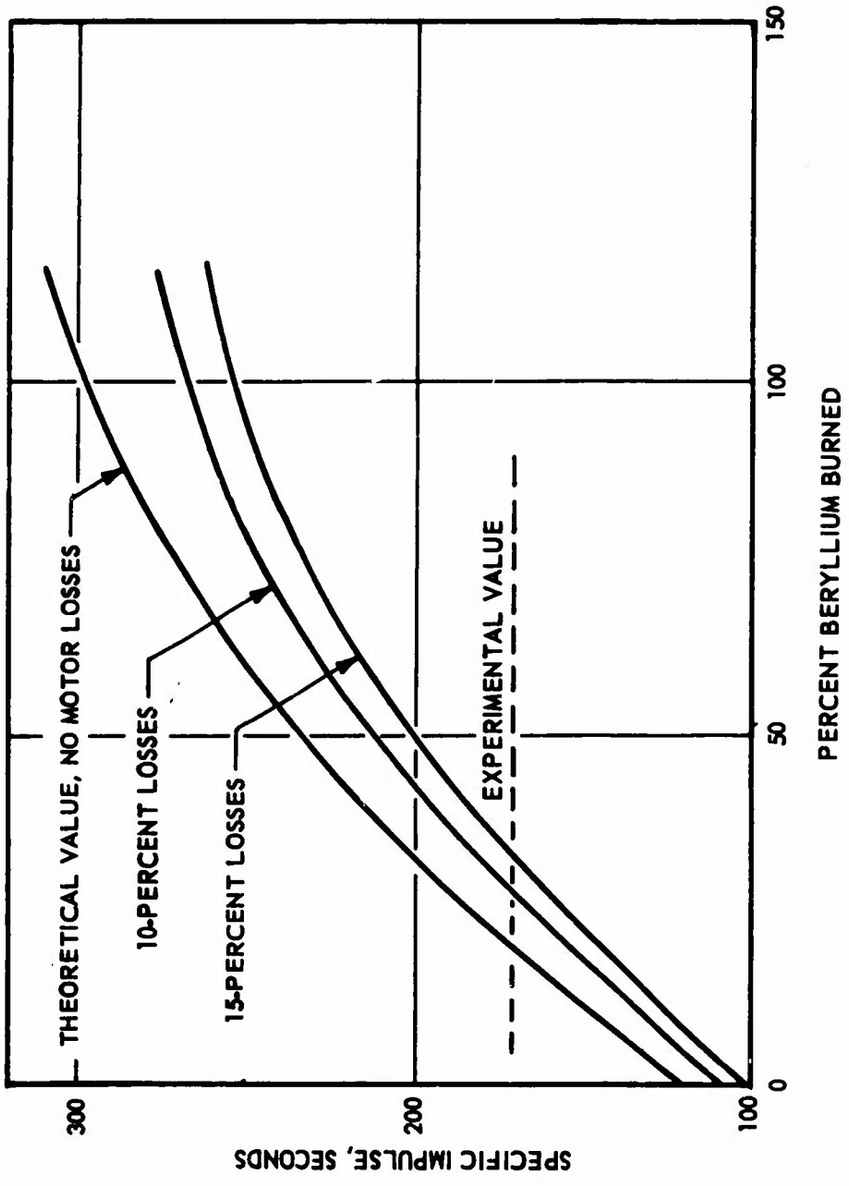


Figure 108. Performance of R-5 Monopropellant

R-2/H_2O_2 system even though the theoretical chamber temperature for zero beryllium burned is more than 2000 F lower in the R-5 system. This strongly reinforces the previous conclusion that system temperature prior to beryllium combustion is not the limiting factor for efficient burning.

System Efficiencies

The experimental program that was conducted for evaluating the performance of heterogeneous propellants was based on making relative comparisons between various propellants in the same motor hardware. No effort was expended in performance optimization by seeking refinements in injector design. It was also recognized that additional performance losses would be incurred by restricting the testing to small-scale motor hardware in place of large-scale firings but it was maintained that the trends indicated in the small motor firings would still be valid in assessing propellant performance. Therefore, discussion and analysis of the test data have been approached on the basis of assessing relative performance with the knowledge that absolute propellant performance can be upgraded both by motor hardware refinements and motor scale up.

Baseline runs for assessment of the small-scale motor hardware used for heterogeneous propellant evaluation were made with neat hydrazine and hydrogen peroxide. The highest measured specific impulse efficiency was 87 percent whereas for a larger optimum motor hardware configuration, 94 percent can be expected. In evaluating the efficiency of the heterogeneous fuels, this reduction in efficiency for the motor hardware must be considered. In assessing the heterogeneous propellant performance, an increase in beryllium combustion may be possible in an optimum system, elevating the beryllium combustion efficiencies from the 20 to 50 percent values demonstrated during this program.

A comparison of performance between beryllium-hydrazine gels and aluminum-hydrazine gels also indicates the possibility of beryllium combustion.

The aluminum-hydrazine performance was only 2 to 3 percent above the efficiency obtained with the R-2/N_2O_4 system in the same mixture ratio range. In terms of delivered specific impulse, the R-2/N_2O_4 system gave higher performance than the aluminum-hydrazine/H_2O_2 ststem, and the R-3/H_2O_2 was only slightly lower. On this basis of comparison, the beryllium system appears relatively favorable even with the attendant low beryllium combustion efficiencies.

CONCLUSIONS

PROPELLANT SENSITIVITY MEASUREMENTS

A summary of the propellant sensitivity measurements is presented in Table 72. Because of the sensitivity of the candidate oxidizer mixtures studied during this program, the effort on these materials was de-emphasized. Only a survey was made on many of the systems rather than a complete investigation of the sensitivity. Several conclusions can be drawn, however.

Both compounds R and T are very sensitive materials. The Wenograd test indicated that Compound T was significantly more sensitive than Compound R as anticipated; however, the U-tube test did not show this difference. One sample of Compound R was more sensitive than the Compound T. In addition, these compounds are capable of propagating an explosion in very-small-diameter charges. The velocity of the propagation was unexpected, being considerably lower than the sonic velocity, but much higher than traditional deflagration propagation rates. These "explosions" did have sufficient energy, however, to fragment very strong tubing; the wall thickness of the capillary tubing being one-half the ID.

Addition of small amounts of oxygen-containing compounds, i.e., N_2O_4 and TNM, to Compounds R and T did not provide any significant desensitization, and in some cases the mixture appeared actually to be more sensitive than Compounds R and T. Mixtures containing up to 25 to 30 w/o Compound R or T in N_2O_4 appear to be safe to handle on the basis of U-tube tests. This may be simply a mass dilution effect, but it does provide a means of safely adding a small amount of a difluoramino oxidizer in N_2O_4 if this is desirable from a performance standpoint. The addition of a low

TABLE 72

SUMMARY OF PROPELLANT SENSITIVITY MEASUREMENTS

Material or System	U-Tube Compression Sensitivity	Wenograd Thermal Sensitivity	JANAF Thermal Stability	Detonation Propagation
Tetranitromethane (TNM)	X	X		
Compound R (R)	X	X		
Compound T (T)	X	X		
N_2F_4		X		
R-N_2O_4	X			
R-N_2F_4-TNM	X			
T-N_2O_4	X			
T-N_2F_4	X			
T-TNM		X		
Hydrazine		X	X*	
Monomethylhydrazine		X		
Hydrazine-Hydrazine Nitrate		X		
R-5 Gel			X*	X

*Reported under Task III

concentration of N_2F_4 to both Compounds R and T does produce a strong desensitization effect. This also may probably be a mass action effect because even at 15 w/o N_2F_4 in the liquid, the vapor is mostly N_2F_4. The addition of TNM to mixtures of Compound R and N_2F_4 appears to have a sensitizing effect.

The tests on the R-5 monopropellant showed that formulations based on liquids containing up to 50 w/o hydrazine nitrate (i.e., R5-A and R5-C) are safe to test fire with feed systems consisting of up to 1-inch OD tubing. As the hydrazine nitrate concentration was raised above this level, the sensitivity increased sharply (the critical diameter decreased rapidly). The R5-D formulation could probably be safely handled in a 1/2-inch-diameter tube feed system if the possibility of loss of water from the propellant could be eliminated. In any formulation, care must be taken to eliminate water loss because of the increase in sensitivity with decreasing water concentration.

HETEROGENEOUS PROPELLANT PERFORMANCE EVALUATION

The test data for beryllium-containing fuels generally indicate an increase in specific impulse efficiency with mixture ratio. However, this appears to be caused only by the fact that beryllium constitutes a smaller fraction of the total propellant flow at higher mixture ratios. An analysis based on the percentage of metal burned correlates with the experimental data when no increase in metal combustion with mixture ratio is assumed.

The estimated percentage of beryllium burned varied from 20 percent for the R-2/H_2O_2, R-2/H_2O_2/ClF_5, and R-5 systems to approximately 50 percent for the R-2/N_2O_4 and R-3/H_2O_2 systems.

If the same fraction of other motor losses is assumed, a comparison of the R-2/H_2O_2 system (20 percent metal burned) with the R-3/H_2O_2 system (50 percent metal burned) suggests that a basic difference may exist

between the efficiency of combustion of beryllium metal and beryllium hydride. This should be ascertained through further experiments.

Differences of 2 to 3 percent in performance were noted between injectors with the same propellants and between gelled and ungelled hydrazine. This, and the increased performance obtained using the R-3 gel, suggested that an optimization of injector design, correlated with gel rheological properties, should produce significant improvements in performance of the fuels studied.

Although the system combustion temperature is probably a contributing factor to performance, a hypothesis that it is the limiting factor cannot be supported by the data of this study.

The results of this investigation indicate that the poor performance obtained with beryllium fuels is caused by a combination of chemical, rheological, and combustion factors. Further work is necessary to define exactly the responsible factors for each system. Sufficient variations in metal combustion efficiency under different conditions have been observed to suggest that substantial improvements should be attainable.

Combustion of the R-5 monopropellant was low in terms of specific impulse efficiency (58 percent), but metal burning was extensive enough at this low level to suggest that much higher performance can be obtained from this system with further work.

REFERENCES

1. R-6147, Final Report, Physico-Chemical Characterization of High-Energy Storable Propellants, Rocketdyne, a Division of North American Aviation, Inc., Canoga Park, California, May 1965, CONFIDENTIAL.

2. AGC-0801-01-6, Evaluation of High-Energy Materials as Liquid Propellants (U), Aerojet-General Corporation, Azusa, California, January 1965, CONFIDENTIAL.

3. Hyman, Herbert H. (Editor): Noble Gas Compounds, The University of Chicago Press, Chicago, Illinois, 276 (1963).

4. Doorenbos, H. E. and B. R. Loy, J. Chem. Phys., 39, 2393 (1953).

5. Classen, H. H., H. Selig, and J. G. Malm, J. Am. Chem. Soc., 84, 3593 (1962).

6. Hyman, Herbert H. (Editor): Noble Gas Compounds, The University of Chicago Press, Chicago, Illinois, 98 (1963).

7. Streng, L. V. and A. G. Streng: J. Inorg. Chem., 4, 1370 (1965).

8. DOW 9958-FR, Sensitivity Studies of NF Compounds, Dow Chemical Company, Midland, Michigan, October 1965.

9. AMCC 0277-C-PR-1, Progress Report No. 1, Rocket Propellant Research and Development, American Cyanamid Company, Stamford, Connecticut, 1 January to 31 March 1965.

10. Sloan, C. K., J. Phys. Chem., 59, 834-40 (1955).

11. Garmon, R. C., et al., Design Criteria for Advanced Propellant Systems, RTD-TDR-63-1062, Texaco Experiment Inc., Richmond, Virginia, 10 June 1963, CONFIDENTIAL.

12. Hanratty, T. J., J. N. Pattison, J. W. Clegg, and A. W. Lemmon, Ind. Eng. Chem., 43, 1113 (1951).

13. Michel, K. W., and H. G. Wagner, Tenth Symposium (International) on Combustion (The Combustion Institute, 1965), p. 353.

14. Eberstein, I. J., and I. Glassman, Tenth Symposium (International) on Combustion (The Combustion Institute, 1965), p. 365.

15. McHale, E. T., B. E. Knox, and H. B. Palmer, Tenth Symposium (International) on Combustion (The Combustion Institute, 1965), p. 341.

16. Moberly, W. H., J. Phys. Chem., 66, 366 (1962).

17. Sawyer, R. F., and I. Glassman, The Homogeneous Gas Phase Kinetics of Reactions in the Hydrazine-Nitrogen Tetroxide Propellant System, Princeton University, AFOSR Scientific Report No. 66-0855, December 1965.

18. Mason, D. M., Symposium on Hydrazine and its Applications, AD-111368, Vol. I, 1953, p. 116, CONFIDENTIAL.

19. Troyan, J. E., Symposium on Hydrazine and its Applications, AD-111368, Vol. I, 1953, p. 203, CONFIDENTIAL.

20. AGC 10783-03, Development of High Energy Metallized Propellant (Table 9), Aerojet-General Corp., Sacramento, Calif., CONFIDENTIAL.

21. AFRPL-TR-66-33, Formulation and Evaluation of Liquid Propellant Dispersions, SRI-66-0291, Annual Summary Report, February 1966, CONFIDENTIAL.

22. Forbes, W. F., and I. R. Leckie, Can. J. Chem., 36, 1371 (1958).

23. Cordes, H. F., J. Phys. Chem., 65, 1473 (1961).

24. R-6475, Final Report, Investigation of Liquid-Metal Hydrides, Rocketdyne, a Division of North American Aviation, Inc., Canoga Park, California, February 1966, CONFIDENTIAL.

25. AFRPL-TR-63-193, Final Report, Preparation of High-Density Light Metal Hydride-2, Rocketdyne, a Division of North American Aviation, Inc., Canoga Park, California, December, 1965, CONFIDENTIAL.

26. RPL-TDR-64-20, Advanced Test Methods for Determining Operational Characteristics of Propellants, Air Reduction Company, 30 June 1963, RE 63-156, CONFIDENTIAL.

27. Verschoyle, P. O., The Ignition of Certain Monopropellants by the Adiabatic Compression of Bubbles: Part I: A Theoretical Analysis of Adiabatic Compression Effects Produced by Sudden Pressurization of a Liquid Column Containing a Vapor Space, Ministry of Supply, E.R.D.E., Report No. 13/R/58.

28. Evaluation of High-Energy Liquid Propellant Rocket Engine Oxidizer and a Pilot Production of Same, 3rd Quarterly Report, Minnesota Mining and Manufacturing Co., Contract AF04(611)-8182, 15 February 1963.

29. AFRPL-TR-65-55, Evaluation of High-Energy Liquid Propellant Rocket Engine Oxidizer and a Pilot Production of Same, Final Report, Minnesota Mining and Manufacturing Co., Contract AF04(611)-8182, December 1964.

30. Verhoek, F. H., and F. Daniels, JACS, 53, 1250 (1931).

31. R-5468-3, Quarterly Progress Report, Physico-Chemical Characterization of High-Energy Storable Propellants, Rocketdyne, a Division of North American Aviation, Inc., Canoga Park, California, 30 June 1964.

32. Wenograd, J., Design and Operation of the Thermal Sensitivity Apparatus, NOLTR 61-98, 15 July 1962.

33. Wenograd, J., "The Behavior of Explosives at Very High Temperatures," Trans. Faraday Soc., 57, 1612 (1962).

34. Wenograd, J., The Thermal Sensitivity of Explosives and Propellants, NOLTR 61-97, 1 September 1961.

35. Wenograd, J., "The Behavior of Explosives at Very High Temperatures," Nav Weps Report (NOL)7328, 15 July 1962.

36. JANAF Liquid Propellant Test Methods, Test No. 6, Thermal Stability Test, Liquid Propellant Information Agency, Applied Physics Laboratory, Johns Hopkins University, Silver Springs, Maryland.

APPENDIX A

PURITY AND PURIFICATION OF PFG

Gas chromatographic analysis of the "as received" sample of PFG indicated a purity of approximately 79 percent. This analysis is not quantitative because the detector was assumed to have an equal sensitivity for all species:

Species	Percent of Peak Area
PFG	79
Air	8
N_2F_4	4
R	2
CF_3NF_2	2
PFF + ? (possibly N_2O)	5

An infrared analysis indicated the presence of N_2O and another impurity which has not been identified.

A portion of the "as received" sample, which had been pressurized with helium, was partially purified by trap-to-trap vacuum distillation. The helium and other noncondensable gases were first removed by passing the impure gaseous mixture through a trap cooled in liquid nitrogen. The compounds remaining in the trap were then fractionated through successive traps held at -78 C (Dry Ice-trichloroethylene bath), -126 C (methylcyclohexane slush), and -196 C. No gases were recovered in the -78 C trap. PFG, Compound R, the unidentified impurity, and traces of PFF were found in the -126 C trap. The -196 C trap contained nitrous oxide,

PFF, and silicon tetrafluoride. The silicon tetrafluoride probably formed from reaction of one of the impurities with the glass traps used in the purification.

The purified sample was found to contain 91-percent PFG. The distribution of impurities is as follows:

Species	Percent of Peak Area
PFF + ?	7
Air	<1
N_2F_4	<1
CF_3NF_2	<1

APPENDIX B

DESIGN OF R-3 FORMULATION EXPERIMENTS

A series of preliminary tests was conducted to select useful gelling agents for the R-3 propellant and a statistically designed experiment was subsequently performed to arrive at a combination of gelling agent and mixing process which would produce a desirable R-3 propellant.

This experimental effort was divided into two parts. During the first of these, powdered Microthene was used instead of the beryllium-beryllium hydride powder mixture. This allowed for the evaluation of experimental variables of secondary interest with considerable saving of time and expense. It was assumed that none of these secondary variables interacted with the simulant because most of them dealt with the manner in which ingredients were processed.

For the second part of the experiment, the type and concentration of gelling agents and cross-linking agents were varied. The beryllium-beryllium hydride mixture was employed and all the other variables were held at the values judged to yield the best results in the evaluation mentioned previously. If the results were not sharply defined, the easiest value to maintain was used. This evaluation was based on several measurements of responses associated with the quality of gel made on each of the sample batches. Linear least-squares regression analysis was employed to implement the analysis.

EXPERIMENTAL VARIABLES

The variables which were thought at the beginning of the experiments to form a most significant casual relationship with gel quality are presented in Table B-1 each with the symbol used to denote the corresponding variable.

TABLE B-1

EXPERIMENTAL VARIABLES

Variable	Symbol
Type of Gelling Agent	T_g
Concentration of Gelling Agent	C_g
Concentration of Cross-Linking Agent	C_c
Purity of MMH	P
Preheating of MMH	H
Order of Addition of Ingredients	O
Presence of Cellulose Acetate	CA
Mixing Intensity	M
Interupted Mixing	IM

Seven gelling agents were evaluated in the experiment: Jaguar 315, Natrosol, Cellosize, SeaTex, Klucel, Jaguar A20-B, and Gelcarin. Each of the other variables was considered at only two levels, although high and low values for concentration of the gelling agent and of the cross-linking agent varied with the type of gelling agent and depended on the results of the preliminary experiments. For Jaguar 315, Natrosol, and SeaTex, no cross-linking agent was used. The following codes are used in Table B-2 . When MMH purity was at the low level (P=-1), it was exposed to air and 2-percent water was added. The high level of purity (P=1) represents MMH which was kept in a nitrogen atmosphere. The high level of H means that the MMH was heated to approximately 170 F. The variable O was at the high level when all solid ingredients were premixed before adding to the liquid ingredients; when O=-1, the solid components were added to the liquid one at a time. A high or low level for cellulose acetate (CA) indicates the presence or absence of this chemical. The high level of mixing (M=1) represents the use of a Polytron, a mixing time of 300 seconds, and a high mixing speed. A Waring Blendor used at a low speed for 150 seconds is represented by

M=-1. The high level of IM corresponds to a process in which mixing was interrupted for two 15-minute intervals to allow the ingredients to interact. When IM was at the low level, the mixing was uninterrupted.

PART 1 OF THE EXPERIMENT

Experimental Design

The design for Part 1 of the experiment is presented in Table B-2 with +1 representing the high level and -1 the low level of each variable. The sample batches were prepared according to the recipes specified in the experimental design and 11 types of responses designed to test the quality of the gels were measured at the time immediately following preparation (Run No. 1) and again 2 weeks later (Run No. 2). At each time, 11 separate step-wise linear regression analyses were performed, where, for each regression, one of the types of response was considered to be the dependent variable and all of the variables of the design were treated as the independent variables. The basic design consisted of three half replicates of a 2^3 factorial design and four half replicates of a 2^4. The variables O, CA, M, and IM were aliased with the positive and negative interactions of P with C_g and P with C_c. Assuming that there is no interaction between P and C_g or C_c, the design allowed for estimation of all main effects and interaction of T_g with any other independent variable.

For the analysis, each type of gelling agent was assigned the value 1 for the batches in which it was used (eight batches of each gelling agent which needed a cross-linking agent were prepared and four were prepared for all other agents) and 0 for the remaining batches. The values of ±1 were used for the remaining variables.

The Response Variables (Gel Properties)

The response variables considered in the analyses are listed in Table B-3 For those variables which were quantitative, the measured value or the negative of it was used, the former if high values were considered more desirable and the latter if low values were preferred. Where the measurement was of a qualitative nature, values were assigned to the qualitative

TABLE B-2

EXPERIMENTAL DESIGN FOR PART I

Test No.	T_g	C_g	P	C_c	H	O	CA	M	IM
11	Jaguar 315	-1	-1		-1	1	1	1	1
12		1	1		-1	1	1	1	1
13		1	-1		1	1	1	1	1
14		-1	1		1	1	1	1	1
21	Natrosol	1	1		1	1	1	1	1
22		-1	-1		1	1	1	1	1
23		-1	1		-1	1	1	1	1
24		1	-1		-1	1	1	1	1
31	Cello-size	-1	-1		-1	1	1	1	1
32		1	1		-1	1	1	1	1
33		1	-1		1	1	1	1	1
34		-1	1		1	1	1	1	1
41	SeaTex HCB	-1	-1	-1	-1	1	1	1	1
42		-1	-1	1	1	1	-1	1	-1
43		-1	1	1	-1	-1	1	-1	1
44		1	-1	1	-1	-1	-1	-1	-1
45		-1	1	-1	1	-1	-1	-1	-1
46		1	-1	-1	1	-1	1	-1	1
47		1	1	-1	-1	1	-1	1	-1
48		1	1	1	1	1	1	1	1
51	Klucel HA	1	1	1	1	-1	-1	1	1
52		1	1	-1	-1	-1	1	1	-1
53		1	-1	-1	1	1	-1	-1	1
54		-1	1	-1	1	1	1	-1	-1
55		-1	-1	1	-1	1	1	-1	-1
56		1	1	1	-1	1	-1	-1	1
57		1	-1	1	1	-1	1	1	-1
58		1	-1	-1	1	-1	-1	1	1
61	Jaguar A20-B	-1	-1	-1	-1	1	1	-1	-1
62		-1	-1	1	1	1	-1	-1	1
63		-1	1	-1	1	-1	1	1	-1
64		1	-1	-1	1	-1	-1	1	1
65		-1	1	1	-1	-1	-1	1	1
66		1	-1	1	-1	-1	1	1	-1
67		1	1	-1	-1	1	-1	-1	1
68		1	1	1	1	1	1	-1	-1
71	Gelcarin SI	1	1	1	1	-1	-1	-1	-1
72		1	1	-1	-1	-1	1	-1	1
73		1	-1	1	-1	1	-1	1	-1
74		-1	1	1	-1	1	1	1	1
75		1	-1	-1	1	1	1	1	1
76		-1	1	-1	1	1	-1	1	-1
77		-1	-1	1	1	-1	1	-1	1
78		-1	-1	-1	-1	-1	-1	-1	-1

TABLE B-3

RESPONSES CONSIDERED

Response	Value
Freedom from Syneresis	2 if no syneresis, 0 if syneresis present
Visible Lumps Absent	2 if absent, 0 if present
Rigidity in Storage Jar	2 if no flow, 1 if slight flow, 0 if flow
Macroscopic Impurities	1 if none, 0 if black specks present
Capillary Plugging	3 if flow, 2 if slight plugging, 1 if erratic flow, 0 if very erratic flow
Incipient Flow Pressure	Actual value in psi
Strand Length	Actual value in inches
Plate Test	Negative of plate area in sq in.
Nonadherence	Negative of weight in grams
Viscosity	Viscosity intercept
Shear Thinning	$10/m\sqrt{\eta}$ x shear thinning number

judgements with the most desirable response assigned the highest value. In the cases where a measurement could not be made on a particular response variable, the batch corresponding to the missing value was eliminated from the analysis for this variable.

The first two responses, relating to the homogeneity of the gel as observed in its storage jar, were qualitative judgements of its degree of syneresis and lumpiness. The rigidity of the gel was judged by tipping the jar. In some samples, black specks were observed, possibly from the mixer seal, or from charring of the Microthene.

The incipient flow pressure was determined by squeezing a sample through a capillary tube of known size. It is a measure of the yield shear stress. The length of a strand of gel which would hand without breaking was measured when extruded downward from the opening of the capillary tube. It is a measure of yield tensile stress. While incipient-flow and strand-length measurements were made, the character of the flow through the capillary (presence or absence of plugging) was observed.

The plate test evaluated the resistance to compressive stress of a sample of the gel as measured by the area over which it spread when squeezed by a predetermined force between two glass plates.

A characterization of the samples by use of a capillary viscometer was also made. From this characterization, apparent viscosity (η) at a shear rate of 100 sec^{-1} was calculated and shear thinning, given by the slope m of a plot of log stress vs log shear rate, was determined. The reciprocal of the shear thinning value multiplied by a constant function of the square root of η was labeled shear thinning number and used as a response variable.

Adherence of the gels was also measured, by expelling a known volume from a metal tube with a standardized volume of compressed nitrogen and weighing the residue adhering to the tube.

Table B-4 and Table B-5 give the values used in the least-squares regression analysis for the various gel properties for Run No. 1 (soon after mixing) and Run No. 2 (after 2 weeks) respectively. Because the macroscopic specks did not tend to appear or disappear after a lapse of time, this response was analyzed only once. Similarly, the adherence measurement was made only once.

Regression Analysis

The technique of stepwise regression was used for each dependent (gel property) variable. In each case, the independent variables were introduced or removed one at a time and a linear least-squares fit was performed after each introduction or removal. The choice was made by considering which variable most improved the quality of the fit by its addition or deletion. The one of these regressions which had the smallest residual variance (or in some cases another regression with slightly larger residual variance but containing one or two more independent variables) was selected as the one best describing the dependent variable in terms of the independent variables.

Table B-6 lists all the processing variables (as opposed to gelling agent type) and gives normalized regression coefficients for each gel property. That is, each coefficient was divided by the standard deviation of the corresponding dependent variable so that all coefficients given are comparable. Where no coefficient is given, the influence of the variable on the response was not judged significant according to the criterion used in the stepwise regression program.

Examination of Table B-6 shows that gels of higher quality tended to result from higher concentrations of gelling agents and lower concentrations of cross-linking agents. It was not possible from this preliminary analysis, however, to determine what constituted an optimum level for any given gelling agent.

TABLE B-4

MEASURED VALUES FOR RESPONSE VARIABLES (RUN NO. 1)

Gel No.	Freedom from Syneresis	Visible Lumps Absent	Rigidity in Storage Jar	Macroscopic Impurities	Capillary Plugging	Incipient Flow Pressure	Strand Length	Plate Test	Viscosity	Shear Thinning
11	1	2		0	1			-1.25	240	0.269
12	0	2	0	1	1			-1.85	245	0.484
13	0	2		0				-1.50	NA	NA
14	1.5	2		0	1			-1.60	NA	NA
21	2	2	2	0	1	5	8	-1.60	3650	1.11
22	2	2	2	1	1		8		2240	0.815
23	1.5	2	2	0	1			-2.25	1430	1.43
24	2	2	2	0	1		12	-1.30	3900	0.925
31	2	2	2	1	1	0	6	-1.35	1970	1.13
32	2	2	2	1	2		8	-2.25	5000	0.655
33	2	2	2	1	0		8	-1.10	4400	0.955
34	1.5	2		1	0			-1.75	NA	NA
41	0	2	1	1			2	-0.85	NA	NA
42	0	2	0	1					NA	NA
43	2	2	0	1	1	-5	1	-1.35	68	1.14
44	1.5	2	0	1	1	-2		-1.90	310	0.598
45	2	1	1	1	2		3	-1.00	318	0.65
46	1.5	2	0	1	1	0	5	-1.90	460	0.795
47	2	2	0	1	1	0	2	-1.50	88	0.96
48	2	0	1	1				-1.10	NA	NA
51	2	2	1	1	0			-4.0	2930	2.30
52	2	2	2	1	0		4	-3.15	3200	NA
53	2	2	2	1	1	0	6	-2.10	2690	1.65
54	2	0	0	1	1	0	2	-4.90	1280	4.53
55	2	2	0	1	1	0	4	-2.75	1220	1.12
56			1	1	1	0	3	-4.40	2040	1.81
57	2	2		0	1	0	4	-2.40	3400	0.60
58	1.5	2	1.5	1	1	0	5	-2.10	2620	1.25
61	2	2	1	1	1	-2	4	-2.25	280	1.06
62	1	2	0	1	1	-5	3	-0.60	21	0.9[illegible]
63	0	0	2	0		-2		-1.00	NA	
64	2	2	2	1	1	0	4	-2.10	458	1.35
65	0	0	2	1		-2		-0.60	NA	
66	2	0	2	1	0				NA	
67	1	2	0	1	1	-2	3	-2.10	146	1.02
68	1	2	0	1	1	-2	3	-1.90	100	0.88
71	2	2	2	1	1	2	5	-1.20	420	0.91
72	2	2	2		1	1	6	-1.10	1050	0.77
73	1.5	2	2	0	0	-2	6	-2.05	1100	0.55
74			2	0	0	0	4	-1.55		
75	1	2	2	1			5	-1.50	770	0.69
76	2	0	2	0		-2		-0.45	NA	
77			1		1	-2	4	-1.75	760	0.83
78	1	2	1	1	1	-2	4	-2.10	440	1.52

CONFIDENTIAL

AFRPL-TR-66-294

TABLE B-5

MEASURED VALUES FOR RESPONSE VARIABLES (RUN NO. 2)

Gel No.	Freedom from Syneresis	Visible Lumps Absent	Rigidity in Storage Jar	Capillary Plugging	Incipient Flow Pressure	Strand Length	Plate Test	Viscosity	Shear Thinning	Nonuniformities
11	2	2	2	3			-0.35	450		-0.[illegible]
12	2	0	2	1		3/4	-1.85	250	0.581	-0.165
13	2	2	2	0			-0.35	NA		-0.120
14	2	2	2	0			-0.80	NA		-0.[illegible]0
21	2	2	2	3	0	1-1/8	-1.75	3850	0.70	-0.130
22	0.5	2	2	3	0		-1.75	2050	0.87	-0.095
23	2	2	2	3	0	3/4	-1.75	1400	1.10	-0.080
24	2	2	2	3	5	1-1/4	-1.30	5360	1.21	-0.140
31	2	2	2	3	0	1-1/16		2100	0.985	-0.200
32	2	2	2	2		1	-2.05	4650	0.54	-0.[illegible]15
33	2	2	2	3	5	1-1/8	-1.20	6800	0.378	-0.095
34	2	2	2	0			-1.30	NA		-0.210
41	0	2	1	0	-2		-1.20	NA		-0.170
42	0	0	2	0	-2		-0.35	NA		-0.140
43	0	2	0	3	-5		-1.50	52	0.56	-0.155
44	0.5	2	2	3	-2		-1.00	540	0.341	-0.140
45	0	2	0	3	-5		-0.95			-0.075
46	0.5	2	2	3	-2		-2.05	580	0.835	-0.230
47	0.5	0	2	2	-2		-1.00	1100	0.155	-0.090
	2	1	2	1	-5			NA		-0.150
51			1	2	0		-4.90	2880	1.24	-0.070
52	2	1.5	1	2	1	5/8	-4.90	3650	0.525	-0.135
53	2	2	2	3	0	1	-1.90	3050	1.81	-0.085
54	2	2	0	3	0	1/8	-4.90	1000	1.25	-0.210
55	2	2	0	3	0-1	3/8	-3.35	1050	1.03	-0.155
56	2	2	0	3	1	1/4	-4.90	2720	0.51	-0.155
57	1	2	2	3		1-1/16	-4.00	6600	0.325	-0.285
58	2	2	2	3	0	3/4	-2.25	2780	1.08	-0.130
61	2	2	2	3	0	3/4	-1.20	565	0.945	-0.160
62	0.5	2	2	3	0		-0.60	63	0.82	-0.185
63	2	0	2	1	0		-0.65	NA		-0.150
64	2	2	2	1	0		-0.75	NA		-0.170
65	0.5	0	2	1			-0.95	NA		-0.[illegible]50
66	2	0	2	2	1-1/2	3/4	-0.75	510	0.32	-0.135
67	2	2	1	3	2	1-1/2	-1.75	475	1.81	-0.[illegible]60
68	0.5	1	2	3	0		-0.35	212	0.675	-0.150
71	2	2	2	3	2	13/16	-0.60	760	0.710	-0.095
72	2	2	2	3	2		-0.80	1520	0.525	-0.095
73	2	2	2	3	0		-1.25	1500	0.61	-0.195
74	0.5	2	2	2	0	1	-1.35	995	0.870	-0.155
75			2	1	0	7/8	-1.60	NA		-0.265
76	2	0	2	1			-0.80	NA		-0.080
77	1.5	2	1	3	0	5/8	-1.75	820	0.725	-0.130
78	1	2	1	3	0	5/8	-1.[illegible]	685	0.97	-0.175

TABLE B-6

COEFFICIENTS OF LINEAR EQUATIONS RELATING GEL PROPERTIES TO PROCESSING VARIABLES

Gel Property	High MMH Purity	High Concentration of Gelling Agent	High Concentration of Cross-Linking Agent	Processing Variable: Cellulose Acetate Added	Processing Variable: Premix all Solids	Preheat MMH	High Shear Mixing	Interrupted Mixing
Freedom from Syneresis (1)		15	26	22				-22
Freedom from Syneresis (2)		27	-27		13			
Visible Lumps Absent (1)	-29	26				-15	-26	29
Visible Lumps Absent (2)	-25						-49	37
Rigidity in Storage Jar (1)					-27		49	
Rigidity in Storage Jar (2)		30	-17			17	38	
Macroscopic Impurities				-20			-20	
Capillary Plugging (1)		14	- 9			-17	-62	13
Capillary Plugging (2)	-17	15	17		-18	-19	-71	
Incipient Flow Pressure (1)	25	39		26				
Incipient Flow Pressure (2)		33	-18		-15			
Strand Length (1)	-25	38	- 9				-13	
Strand Length (2)	-14	42						23
Plate Test (1)	-21				-13	13	14	
Plate Test (2)	-18			-16		11		
Nonadherence	29	-20		-16				
Viscosity (1)	-19	43		13				
Viscosity (2)	-24	50		14				
Shear Thinning (1)	37	-36	-26		-23	26		
Shear Thinning (2)		-20	-33	-36			-27	16

(1) Regression coefficient corresponds to Run No. 1

(2) Regression coefficient corresponds to Run No. 2

AFRPL-TR-66-294

Interrupted mixing appeared to produce gels of higher quality in practically every respect. Cellulose acetate seemed to have very little beneficial effect which could not be enhanced by substituting an equal amount of gelling agent. There seemed to be some indication, too, that presence of CA caused gel deterioration. Heating the MMH did not appear to give conclusive results; so it was decided to eliminate this step of the processing in further experimentation. The more intense mixing appeared to produce firmer gels although there was more lumpiness using this method, probably attributable to the high-shear effect of the Polytron and the heat produced by the higher speed. Because of this phenomenon, a screen for straining the ingredients was subsequently installed in the Polytron and the speed for future mixing was lowered. Maintaining the purity of the MMH did not appear warranted because its deleterious effects were more significant than those that were beneficial. Finally, there appeared to be little difference in the gels as a result of the method used for adding the ingredients. Therefore, the simpler method of premixing all the solid components was selected as the more desirable.

Gelling agent type required a somewhat different analysis from the processing variables because it could not be thought of as occurring at a high or low level. By assigning a value 0 rather than a negative value to the cases where a given type of gelling agent was not used, the average response for each type of agent in the regression was considered in an absolute fashion rather than as the average response for type of agent relative to, for example, a weighted average of all the other types. In either case, the regression coefficients related to gelling agent type are comparable among themselves and are not to be compared with the coefficients obtained for the two-level processing variables. Hence, the standardized coefficients (for the two runs) are listed separately in Table . The results of the two runs actually disagreed only with respect to strand length of the gels made with Klucel. One of the most obvious indications presented in Table B-7 is that Cellosize and probably Natrosol yielded gels of generally high quality. It appears,

TABLE B-7

COEFFICIENTS OF LINEAR EQUATIONS RELATING
GEL PROPERTIES TO PROCESSING VARIABLES

Gel Property	Jaguar 315	Natrosol HHR	Cello-Size	SeaTex	Klucel	Jaguar A20B	Gelcarin
Free from Syneresis (1)	-137	109	109		50	- 57	
Free from Syneresis (2)				-164		- 53	
Strand Length (1)		275	190		32		82
Strand Length (2)	-130	119	117		-128	134	
Capillary Plugging (1)		143			51		
Capillary Plugging (2)		176	83		60		
Visible Lumps Absent (1)						- 73	
Visible Lumps Absent (2)	- 57			- 85		-118	
Rigidity in Storage Jar (1)	-154	78	78	- 89		96	71
Rigidity in Storage Jar (2)				- 59	-132		
Macroscopic Impurities Absent	-104	-104	59				
Nonadherence	168	111	82				
Incipient Flow Pressure (1)		154		-114		-101	- 29
Incipient Flow Pressure (2)		69	126	-142			
Plate Test (1)					-188		
Plate Test (2)	49				-206	30	
Viscosity (1)		181	210		132		44
Viscosity (2)		136	199		128		48
Shear Thinning (1)	- 73				128		- 41
Shear Thinning (2)		-144		- 11			- 46

(1) Regression coefficient corresponds to Run No. 1.

(2) Regression coefficient corresponds to Run No. 2.

also, that the opposite is true of SeaTex. It became evident during later experimentation, however, that the poor results of SeaTex were largely attributable to poor choice in the concentration of this gelling agent used in Part 1. No decisions were made concerning an elimination of contending gelling agents on the basis of results of Part 1, because this was determined during Part 2 of the experiment after the substitution of the simulants. Examination of the residual variances for the various regressions indicated a lack of interaction of gelling agent type with any other independent variable except concentration of the cross-linking and the gelling agent. Thus, it was possible for a fixed combination of all of the processing variables to compare the quality of the seven gelling agents at various combinations of levels of these two variables which were concerned with concentration.

In this analysis, none of the responses seemed to correlate with overall gel quality, i.e., the responses appeared to be relatively independent. This simply represents the results of the data and does not necessarily imply that all responses are truly completely independent.

The responses differed considerably between Run No. 1 and Run No. 2. There was no test made to determine if these differences were significant. In making decisions concerning future actions however, the results of Run No. 2 were in general considered to be more critical, because it was the object of this work to generate storable propellant systems.

PART 2 OF THE EXPERIMENT

The purpose of the second part of the experiment was to determine (1) which of the gelling agents produced the best gelled propellants, and (2) optimum concentrations of both gelling and cross-linking agents in each case. Although the originally specified propellant ingredients were used during this part of the experiment, the results were consistent with Part 2, during which only simulants were used. The samples were

prepared according to the experimental design presented in Table B-8. In Table B-8, the letters A, B, and C indicate different formulas of gelling agent, which were interpreted to mean that formula A for any given gel may differ from formula B (or C) for that gel in concentration of both gelling and cross-linking agent or in concentration of only gelling or only of cross-linking agents. The formula corresponding to any given letter for any particular gel in general differed from the formula identified by the same letter for another gel not only in type of ingredients, but also in concentration of the ingredients. The formulas designated by the letters were determined partially from the results obtained from the first batches mixed for each gelling agent in Part 2.

Results of Part 2

A pressure buildup was noted for Jaguar 315, Jaguar A20-B, and Klucel. Because the other four gelling agents appeared to yield gels at least as good as the three exhibiting pressure-buildup, the latter three were eliminated from consideration. A summary of the results obtained from this part of the experiment is presented in Table B-8. To expedite the work, no observation was made of some of the gel properties which were noted during Part 1. Also, the lumpiness exhibited in Part 1 could no longer be seen and, perhaps because of the dark color of the gels, black macroscopic impurities were not observable during this part of the experiment. Six of the original response variables were therefore eliminated. There was one gel property, in addition to pressure buildup, that was noted during Part 2 to give an additional criterion for evaluation, viz., the visual appearance with respect to fluidity. In some cases, the gel was obviously not sufficiently stiff. In other cases, the gel concentration was too high, causing syneresis.

TABLE B-8

EXPERIMENTAL DESIGN FOR PART 2

Gelling Agent	Formula
Jaguar 315	A B C D
Natrosol	A B C
Cellosize	A B
SeaTex	A B C D
Klucel	A B C
Jaguar A20-B	A B C
Gelcarin	A

APPENDIX C

TOXIC CHEMICALS LABORATORIES
SAFETY STANDING OPERATING PROCEDURE (SSOP)

1. Definition of Area

The Toxic Chemicals Laboratories are defined as Rooms 1525 and 1527 in the Vanowen Building at Canoga Park, and may be expanded to include Room 1523 as required.

2. Nature of Work in Area

a. The Toxic Laboratories are reserved for research and development programs on LIGHT METAL (unclassified designation) and its compounds.

b. Primary control will be based on containment of the material by such means as glove box transferring and use of closed systems.

3. Scope of SSOP

This SSOP is written specifically to define the particulars of work with LIGHT METAL. Amendments and/or revisions are to be issued for any other toxic materials handled in the area.

4. Exposure Limits and Monitoring

Limits for exposure of personnel to LIGHT METAL are as follows:

a. Airborne contamination is not to exceed a concentration of 2.0 micrograms per cubic meter as an average over an eight hour day, and not to exceed 25.0 micrograms per cubic meter for any period of time, however short.

b. Surface dust is not to exceed 2.0 micrograms per 100 square centimeters.

If quantities in excess of these limits are detected, all work in the laboratories will be stopped until the source of the contamination is eliminated, and appropriate clean-up carried out.

Industrial Hygiene and Safety personnel will establish and conduct the environmental monitoring program. All operations will be monitored to insure established tolerance levels are being maintained.

5. Access to the Laboratory

Only those personnel concerned with specific operations or maintenance shall enter the laboratory, unless prior approval has been obtained from those assigned to the laboratory. Transient personnel will also be required to wear protective equipment, if requested by those assigned to the laboratory.

6. Protective Equipment for Personnel

a. Types of Equipment - All personnel conducting experimental operations will wear lab coats, or coveralls plus shoe covers, and respirators. Gloves, as appropriate, may also be necessary. Coveralls and shoe covers will be provided as part of each program. Lab coats, respirators and respirator cartridges (MSA respirator with Type H Ultra Filter Cartridge or other cartridge capable of filtering 200 A particles), and gloves are stock items.

b. Use of Equipment

(1) Coveralls and shoe covers must be worn whenever working with LIGHT METAL in a situation where a spill offers appreciable possibility of contaminating the immediate working area. Lab coats may be worn otherwise. None of these articles of clothing should be worn outside of the laboratory, and clean and used sets of clothing should be kept separated.

(2) Respirators must be around the neck ready for use at all times. They must be worn whenever the possibility of airborne contamination is appreciable. Each individual will draw his own respirator from stock and be responsible for its care and cleanliness. Filter cartridges should be replaced whenever flow resistence interferes with "normal" breathing.

(3) Gloves must be worn during any direct handling, transfer, or manipulation of LIGHT METAL. In addition, any person with cuts or abrasions on the hands, however minor, must wear protective gloves at all times in the laboratory.

7. Personal Hygiene and Safety

a. Medical Program - Medical (Dept. 051) will place all operating personnel on a medical surveillance program as established by the Corporate Standard Medical Control Program. No one may work in the laboratory unless Medical has indicated approval. Any unusual incident in the laboratory, involving known or possible contamination of personnel, must be immediately reported to Medical, and personnel involved in such an incident must adhere strictly to instructions given by Medical in such instances.

b. Specific Laboratory Notes

(1) Personnel are advised to wash their hands and face before leaving the laboratory or immediately thereafter.

(2) Food or beverages will not be permitted in the laboratory.

(3) Any cut, abrasion or skin irritation regardless of severity must be treated by Medical (Dept. 051). All such incidents must also be reported to Industrial Hygiene and Safety (Ext. 2273).

8. Housekeeping

a. General Cleanliness - Vacuuming of floors, walls, and overhead, and mopping of floors will be provided on a regular schedule by D/546. Vacuuming will be done only with the special vacuum cleaner which will remain in the laboratory. D/546 personnel will be allowed to do such general cleaning only when monitoring indicates levels well below limits established in Paragraph 4 (above). In addition, laboratory personnel will clean benches, hoods, and sink areas, and decontaminate used equipment as needed, but in no case at more than 10 working day intervals. Dry dusting is not permissible; the areas must be washed or vacuumed.

b. Cleaning Equipment - Equipment containing toxic residues shall be decontaminated by treating with dilute hydrochloric acid and then washing with copious amounts of water. In the case of air sensitive residues (potentially spontaneously inflammable), the equipment shall be placed in an inert gas-filled heavy polyethylene bag, transferred to a hood, and a few holes punched in the bag to allow slow diffusion of air to the residue. (Bags are stock items). After several days weathering, the equipment can then be removed from the bag, and cleaned by successive treatments with alcohol, dilute hydrochloric acid, and water.

c. Spills - All minor spills must be cleaned immediately by washing the area with dilute HCl and water. In the event of a major spill, or one generating appreciable amounts of airborne material (e.g., spill of small amount of spontaneously inflammable compound), all personnel must be alerted, the lab evacuated, and Industrial Hygiene and Safety, Dept. 051, notified. Work may be resumed in the laboratory only after effecting the required decontamination and the collection of appropriate air and/or wipe samples. Decontamination is to be coordinated with D/051.

Any spill, no matter how small, that results in contamination of clothing, requires a complete change of protective clothing. Any larger spill which requires vacuuming will be taken up by a special vacuum cleaner equipped with tight seals and an ultra-filter.

9. Disposal

Drums will be provided for the disposal of materials that cannot be conveniently decontaminated in the laboratory by acid-water treatment. Such materials will first be placed in heavy polyethylene bags and sealed before loading into the drums. Such drums will be clearly labeled and when filled will be covered, sealed and collected for disposal by a California State approved disposal company. These drums are not meant to be a catch-all for laboratory wastes. Uncontaminated (or decontaminated) paper, broken glassware, and the like, will be discarded in the laboratory waste baskets. The drums will be reserved for such items as large amounts of chemicals, contaminated oils, broken contaminated glassware of such nature that decontamination presents a hazard, and the like.

10. Laboratory Air Filtering and Pressure

Laboratory air is exhausted through hoods with absolute* filters located on the roof of the Vanowen Building. Laboratory personnel will check the differential pressure gauges on the filters at least weekly. Filters will be changed whenever pressure drops across the filters of greater than 2.0 inches water are noted.

All hoods in the laboratories must be kept running during working hours to insure a negative pressure with respect to areas adjacent to the laboratories. At the end of the working day, at least two hoods are to be left running in each room, and the door between rooms closed. Industrial Hygiene and Safety (Dept. 051) will check face velocities of the hoods weekly.

11. Specific Laboratory Operations

a. Control of LIGHT METAL - Once LIGHT METAL or its compounds has been received in the laboratories, it is only to be removed as follows:

(1) Transfer to another LIGHT METAL operation area.

(2) Transfer to analytical or examination areas will be permitted in quantities of less than one (1) gram when packaged according to sub-paragraph c (below). Appropriate controls for the metal in these areas are established and supervised by Industrial Hygiene and Safety (Dept. 051). Unused portions of such samples are to be returned to the Toxic Laboratories, or treated as described in Disposal (9, above).

b. Transport of LIGHT METAL - Any LIGHT METAL material in a glass container that is to be transported beyond the limits of the Toxic Laboratories must be enclosed in either a closed metal can or a sealed plastic bag.

*Absolute filter is defined as one operating at 99.97 efficiency down to 0.3 micron particles.

c. Storage of LIGHT METAL - LIGHT METAL materials may be stored in fume hoods or in laboratory cabinets if specifically identified as well as marked "Caution - Toxic." Materials stored for prolonged periods in glass should be enclosed in a can or sealed plastic bag. Storage in dry boxes is restricted to those materials that are used repeatedly.

d. Working Areas for LIGHT METAL - Open work, (e.g.; opening storage containers, transfers, and the like) must be carried out either in fume hoods or dry boxes. Closed container operations are permitted on unhooded bench tops, but benches in hoods are to be preferred, and unhooded bench top operations should be held to less than one (1) gram of LIGHT METAL.

12. Implementation of SSOP

Enforcement of regulations will be on the basis of working groups, with Principal Scientists each responsible for their areas. In order to have responsible persons in charge who have maximum familiarity with the actual operations, alternates in the laboratory may be appointed at the discretion of the Principal Scientists.

13. Additional Information Sources

All personnel should be familiar with the following reports:

A. ASD-TR-62-7-665 (April, 1962) prepared under Contract AF33(600) 37211 by the Kettering Laboratory. Unclassified.

B. Atlantic Research Corporation, Contract AF33(616)-6623, Report of September 1962 (period July 1, 1961 - June 30, 1962). Unclassified.

APPENDIX D

THEORETICAL ANALYSIS OF WENOGRAD THERMAL SENSITIVITY APPARATUS

Wenograd (Ref. D-1 through D-4) devised a test for the sensitivity of a substance to thermal initiation of explosion under conditions of high heat flux. Because the method appeared to offer a convenient means for sensitivity testing of a number of compounds with hazardous handling characteristics, an experimental apparatus to implement Wenograd's method was built.

In the Wenograd test for thermal sensitivity, a small sample of the substance to be tested is placed inside a short length of capillary tubing. The sample is then heated by suddenly discharging a capacitor by means of a thyratron tube and passing the electric current through the tubing. Temperatures as high as 1000 C can be reached in times of less than 40 microseconds. The two essential pieces of data obtained are the temperature to which the sample is heated and the time required for the sample to explode. To obtain these data, the sample tube is used as one arm of a Wheatstone bridge circuit. Figure D-1 is a schematic of the experimental apparatus. R_s represents the length of capillary tubing containing the sample. The voltage unbalance across the bridge is observed on an oscilloscope. This voltage is used to calculate the electrical resistance of the sample tube. Because the resistance varies with temperature, one can compute the tube temperature from the voltage measurements.

Time measurements are obtained in two ways. For short times, the photograph of the oscilloscope trace is used. When the sample explodes, the resistance of the tube will usually change drastically and this causes a corresponding change in the bridge voltage being displayed on the oscilloscope. The second method of time measurement utilizes an electronic counter and a microphone. The counter is automatically started when the capacitor discharge button is pressed and is stopped by the microphone which picks up the sound of the explosion.

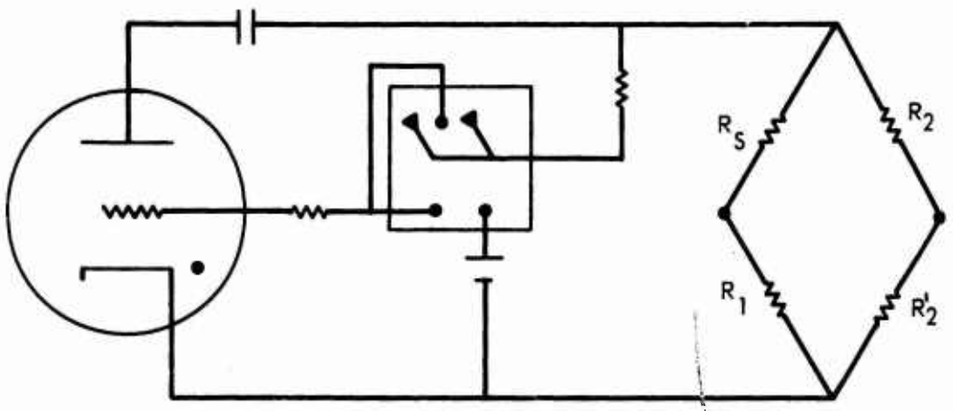


Figure D-1. Wenograd Thermal Sensitivity Apparatus

Test data are plotted as the logarithm of the time delay to explosion vs reciprocal absolute temperature. Different time delays are produced by varying the initial charge on the capacitor. Data for a given substance are usually found to scatter about a straight line. It is not yet possible to attach any absolute value to the line thus obtained for a single substance. The test appears to be a measure of the rate of evolution of heat during the thermal decomposition of a material. However, by running calibration tests on a number of substances with known handling characteristics, it is possible to form a relative scale of sensitivity. Tests on a new substance can then be interpreted on the basis of comparison to known materials.

THEORETICAL ANALYSIS OF EXPERIMENT

A complete theoretical analysis of the Wenograd experiment was conducted by Groetzinger and Clem (Ref. D-5). Their approach and results, however, differ from those of this study.

Referring to Fig. D-1, when the thyratron tube is activat· ·t becomes essentially a short circuit, allowing the capacitor to discharge through the bridge circuit consisting of the sample, represented by R_s, and the three fixed resistors R_1, R_2, and R_2'. Because R_2 and R_2' have much higher resistance values, most of the current flows through the path $R_1 + R_s$. The variation of voltage with time across a discharging capacitor is governed by the differential equation:

$$\frac{dE}{dt} = \frac{-E}{CR_c} \qquad \text{(D-1)}$$

where C is the capacitance of the condenser and R_c is the resistance of the circuit through which the capacitor is discharging. Referring again to Fig. D-1, it is seen that:

$$R_c \cong R_s + R_1 \qquad \text{(D-2)}$$

If R_c remains constant, as assumed by Groetzinger and Clem, Eq. D-1 can be integrated with the initial condition $E = E_o$ at $t = o$ to yield:

$$E = E_o\, e^{-t/R_c C} \qquad \text{(D-3)}$$

The heat generated in the sample because of the resistance heating effect is given by:

$$Q = I^2 R_s \qquad \text{(D-4)}$$

The current I, however, is dependent not upon R_s but the total circuit resistance, R_c:

$$I = E/R_c \qquad \text{(D-5)}$$

Therefore, from Eq. D-3 through D-5:

$$Q = \frac{R_s E_o^{\,2}}{R_c^{\,2}}\, e^{\frac{-2t}{R_c C}} \qquad \text{(D-6)}$$

At the initial temperature, $R_1 = R_s$ and $R_c = 2R_s$. If these resistances are assumed constant, then:

$$Q = \frac{E_c^{\,2}}{4R_s}\, e^{-t/R_s C} \qquad \text{(D-7)}$$

If this equation is compared to Eq. 3 in Ref. D-5, they are seen to be different by the factor 4 in the denominator of Eq. D-7.

The assumption of constant resistance in the above derivation cannot be considered particularly valid. R_s may change by as much as 60 or 70 percent during the discharging and heating-up period. The variation of R_s with temperature can be represented by a second-degree polynomial of the form:

$$R_s = a + bT + cT^2 \qquad \text{(D-8)}$$

R_1, because of its greater mass, is assumed to remain at constant temperature. Equation D-1 now cannot be integrated because T is also a function of E and R. The temperature T is determined by an energy balance between the resistance heating and the heat transferred by radiation, convection, and conduction. The following analysis will be applied to an empty capillary tube, containing no sample. Groetzinger and Clem used a combined radiation and convection heat transfer coefficient to describe the exchange of heat between the outside of the capillary tube and the surroundings. This technique is acceptable at low temperatures where radiation effects are negligible; but at the high temperatures reached by samples in the Wenograd apparatus, thermal radiation becomes the controlling factor in heat transfer. Radiative heat transfer is proportional to the fourth power of temperature instead of the first power as used with the combined radiation-convection coefficient. Radiative heat transfer is governed by:

$$q_r = \epsilon\sigma A \left(T^4 - T_o^4\right) \qquad \text{(D-9)}$$

and convective heat transfer by:

$$q_c = hA \left(T - T_o\right) \qquad \text{(D-10)}$$

A heat balance for the capillary tube results in the differential equation:

$$MC_p \frac{dT}{dt} = \frac{E^2 R_s}{R_c^2} - hA \left(T - T_o\right) - \epsilon\sigma\left(T^4 - T_o^4\right) \qquad \text{(D-11)}$$

This analysis assumes a uniform temperature within the tube wall and no end effects. The Groetzinger-Clem analysis of the radial temperature distribution showed no significant temperature gradient within the tube wall. End effects could be significant but are not easily accounted for. Equations D-1, D-8, and D-11 must be solved simultaneously. The solution was accomplished using numerical techniques and a digital computer. An iterative procedure based on the Clippinger-Dimsdale successive approximation method for differential equations was utilized.

The calculated results show that for a 3000 volt initial capacitor voltage, the capacitor is completely discharged in slightly more than 0.02 millisecond. This compares favorably to the 0.03 ±0.005 millisecond obtained from the increasing temperature portion of the oscilloscope trace. The calculated maximum temperature rise is approximately 400 R. This is several degrees more than the calculated adiabatic temperature rise based on a constant sample resistance equal to one-half the circuit resistance. The actual observed temperature rise in an empty sample tube with a 3000-volt initial charge on the capacitor is lower than the calculated value because part of the current from the discharging capacitor flows through alternate pathways (Fig. D-1). The difference, however, is less than 10 percent. The Groetzinger-Clem analysis predicted a temperature rise of 1600 degrees or more, probably because of their error in deriving an expression comparable to Eq. D-7.

Because the capacitor is completely discharged in 0.02 millisecond, it is reasonable to make further analyses by assuming the temperature rise in the sample tube to be instantaneous. After this instantaneous increase, the temperature will decrease according to:

$$MC \frac{dT}{dt} = -hA\ (T-T_o) - \epsilon\sigma A\ (T^4-T_c^4) \qquad (D-12)$$

Figure D-2 offers a comparison between the calculated cooling rate from Eq. D-12 and the experimentally observed rate from an oscilloscope trace obtained with an empty sample tube. Comparisons between the curves in Fig. D-2 should be limited to the slope and rate of change of each curve. The temperature level, or the exact vertical position of the curves, is somewhat arbitrary because of slight differences in initial sample tube resistance and initial capacitor charge. Almost exact agreement is seen betweeen the two curves for an empty sample tube. Both show a temperature drop of considerably less than 1 percent in 10 milliseconds.

The analysis will now be extended to the case of a sample tube filled with an inert liquid. On the basis of the preceding results, heat transfer from the outside surface of the tube to the surroundings can be considered

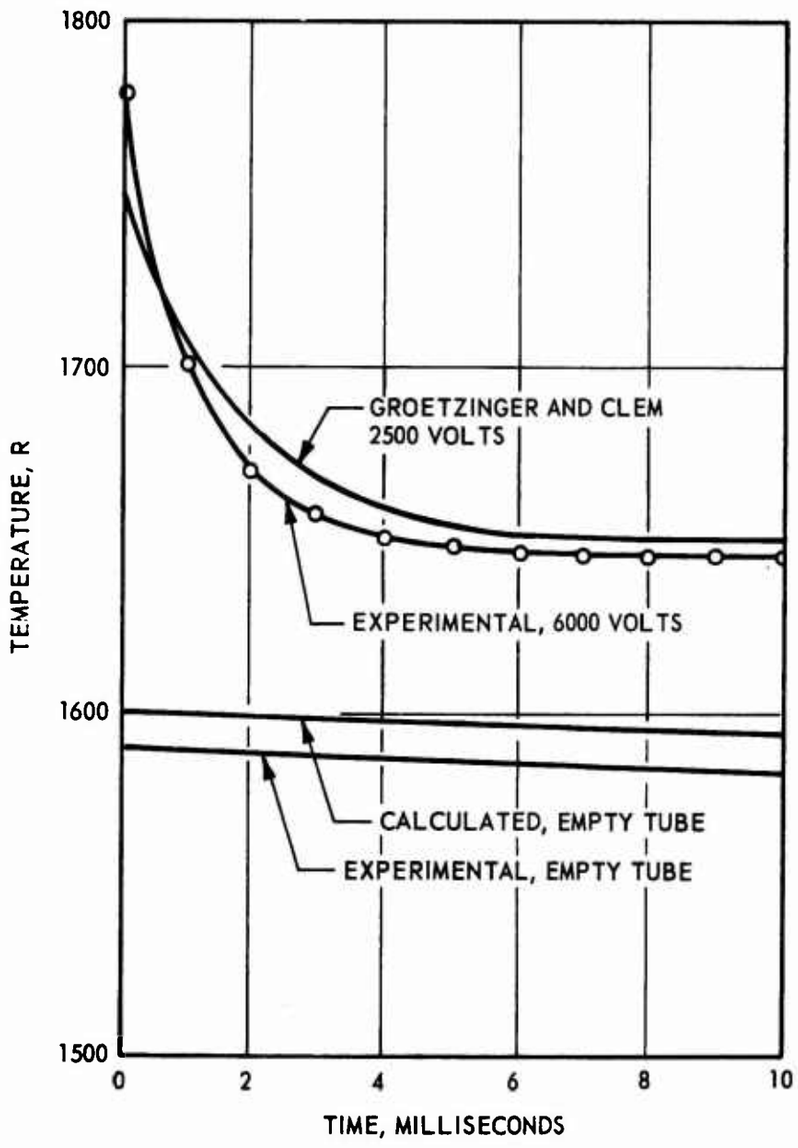


Figure D-2. Experimental vs Calculated Temperatures

negligible. The variation of temperature with time and distance within the sample is expressed by:

$$\rho C_s \frac{\partial T}{\partial t} = k_s \frac{\partial^2 T}{\partial r^2} + \frac{k_s}{r} \frac{\partial T}{\partial r} \qquad \text{(D-13)}$$

where

r = radial distance within the sample cylinder

k = thermal conductivity

C_s = heat capacity of the sample

The heat flux into the sample from the tube wall is:

$$q_h = k_s A_i \frac{\partial T}{\partial r}\Bigg|_{r = a} \qquad \text{(D-14)}$$

where

a = inside radius of the sample tube

A_i = inside surface area

If cooling of the capillary tube is assumed to be due only to heat transfer to the sample, then the temperature of the tube is given by:

$$MC \frac{dT_s}{dt} = kA_i \frac{\partial T}{\partial r}\Bigg|_{r = a} \qquad \text{(D-15)}$$

where

T_s = tube surface temperature

$T = T_s$ at r = a

No direct analytical solution for Eq. D-13 can be obtained because of Eq. D-15 . Groetzinger and Clem obtained a numerical solution through the use of explicit finite difference techniques. In Fig. D-2 , it is

seen that their calculated cooling curve closely approximates the actual experimental curve obtained for water. This confirms the validity of the mathematical model used but does not enable one to use the results for further analytical treatment of the experiment.

If the surface temperature is assumed to remain constant, then an analytical solution of Eq. D-13 exists. It should then be possible to approximate a solution by considering small changes in the temperature. Zinn and Mader (Ref. D-6) used this technique in adjusting for the temperature rise caused by the reaction in a cylinder of explosive being heated at the outer surface. The usual form of the analytical solution of Eq. D-13 is an infinite series of Bessel functions. However, this form is not suitable for very small time intervals. Zinn and Mader, to obtain satisfactory convergence of the series for small time intervals, extended the summation over 500 terms of the infinite series. For very small time intervals, the following solution (Ref. D-7) is valid:

$$T = T_o + \frac{(T_s - T_o)\, a^{1/2}}{r^{1/2}} \operatorname{erfc}\left(\frac{a-r}{2\sqrt{\alpha t}}\right) +$$

$$\frac{(T_s - T_o)(a - r)(\alpha t a)^{1/2}}{4\, a r^{3/2}} \operatorname{ierfc}\left(\frac{a - r}{2\sqrt{\alpha t}}\right) +$$

$$\frac{(T_s - T_o)(9a^2 - 7r^2 - 2ar)\,\alpha t}{32\, a^{3/2}\, r^{5/2}} i^2\operatorname{erfc}\left(\frac{a-r}{2\sqrt{\alpha t}}\right) \qquad \text{(D-15)}$$

where

T_o = initial temperature

T_s = surface temperature after time zero

a = radius of sample

$\alpha = k/\rho C$

The heat flux into the sample, given by Eq. D-14, is found by differentiating Eq. D-16:

$$q_h = k_s A_i (T_s - T_o) \left(\frac{1}{\sqrt{\pi \alpha t}} - \frac{1}{2a} \right) \qquad \text{(D-17)}$$

Assuming that the change in T_s will still be small, Eq. D-15 becomes, for the case of an inert liquid sample:

$$MC \frac{dT_s}{dt} = k_s A_i (T_s - T_o) \left(\frac{1}{\sqrt{\pi \alpha t}} - \frac{1}{2a} \right) \qquad \text{(D-18)}$$

In Fig. D-2 , the cooling curve calculated from Eq. D-16 (calculated curve No. 1) is compared to the experimental curve obtained with water. The range of validity of Eq. D-16 is only about 3 milliseconds because of the extremely small dimensions of the sample. This range, however, is sufficient to cover more than 80 percent of the experimental data. Equation D-18 can then be used with the reservation that the longer time intervals are not to be considered. If the region of interest is further restricted to the time interval covered by the oscilloscope trace, 0.5 millisecond, then Eq. D-17 can be simplified to:

$$q_h = \frac{k_s A_i (T_s - T_o)}{\sqrt{\pi \alpha t}} \qquad \text{(D-19)}$$

Both experimental and calculated results have thus far shown that the surface temperature is not truly constant during the first few milliseconds of the experiment. However, sufficiently accurate analysis of the heat transfer has been made to allow the analysis to be extended to the case of an explosive, rather than an inert sample in the capillary tube. The variation of temperature with time and distance inside an explosive cylinder is expressed by the following equation:

$$\rho C \frac{\partial T}{\partial t} = k \frac{\partial^2 T}{\partial r^2} + \frac{k}{r} \frac{\partial T}{\partial r} + \rho Q \frac{dN}{dt} \qquad \text{(D-20)}$$

where

Q = heat of reaction

dN/dt = the rate of reaction

Again, although the computations are quite lengthy, numerical solutions are possible, and have been worked out by Groetzinger and Clem (Ref. D-5) and by Zinn and Mader (Ref. D-7) for specific cases. This approach, which allows one to predict test data for materials whose physical and kinetic constants are known, provides little insight into methods of interpreting and correlating new test data. Because of the high heat flux and small time interval involved in the Wenograd experiment, chemical initiation and explosion occurs at or near the surface of the explosive. Thus, it should be possible to take a simplified approach, considering only the surface energy flux, along the lines developed by Andersen (Ref. D-8).

The heat generated within the sample by reaction will be very small compared to that transferred through the wall until the reaction is well underway and approaching the ignition point. If the heat generation term is dropped from Eq. D-20 the result is Eq. D-13, the solution of which was given in Eq. D-16.

Andersen, following the criterion derived by Hicks (Ref. D-9), assumed ignition of explosion to occur when the heat flux caused by the reaction becomes equal to the flux through the wall.

Equation D-19 describes the transport of energy into the inert explosive from the hot tube wall. As the temperature of the liquid is increased at the surface, it will begin to decompose. The decomposition reactions of explosives are commonly observed to follow first-order kinetics, in which case:

$$\frac{dN}{dt} = - KN \qquad (D-21)$$

where

N = number of moles of unreacted explosive

and

$$K = Ze^{-E/RT} \tag{D-22}$$

where Z and E are referred to as the frequency factor and activation energy for the decomposition reaction.

The rate of heat liberation by chemical reaction is:

$$q_r = \rho\, QLA_i Ze^{-E/RT_s} \tag{D-23}$$

where

Q = heat of reaction

L = thickness of the layer of explosive undergoing reaction at the temperature T_s

To determine L, the thermal velocity v is defined as the velocity of propagation of a plane wave of magnitude $(T_s - T_o)$ through the liquid so that the heat flux is equal to that given by Eq. D-19.

$$v = \frac{\text{Btu/hr-sq ft transferred at interface}}{\text{Btu/ cu ft required to raise temperature from } T_o \text{ to } T_s} \tag{D-24}$$

$$v = \frac{q_h}{\rho C(T_s - T_o)} = \sqrt{\frac{\alpha}{\pi t}} \tag{D-25}$$

The length L is then given by:

$$L = vt = \sqrt{\frac{\alpha t}{\pi}} \tag{D-26}$$

and

$$q_r = A_i \rho QZ \sqrt{\frac{\alpha t}{\pi}} e^{-E/RT_s} \qquad \text{(D-27)}$$

The criterion of equal heat flux means that ignition occurs when $q_r = q_h$, or from Eq. D-19 and D-27:

$$\frac{kA_i(T_s - T_o)}{\sqrt{\pi \alpha t}} = A_i \rho QZ \sqrt{\frac{\alpha t}{\pi}} e^{-E/RT_s} \qquad \text{(D-28)}$$

Equation D-28 can now be solved for the ignition delay time:

$$t = \frac{C(T_s - T_o) e^{E/RT_s}}{QZ} \qquad \text{(D-29)}$$

This equation differs from Andersen's by a factor $1/\sqrt{\pi}$. Equation D-29 predicts a nonlinear relationship between the logarithm of the delay time and the reciprocal of the absolute temperature. However, the exponential term in temperature will still be the controlling quantity. At present, insufficient data of suitable accuracy are available to determine whether Eq. D-29 describes the test data more adequately than Wenograd's assumption of linear changes in log time with reciprocal temperature. The experimental scatter exhibited by test data obtained to date precludes the use of other than linear regression lines.

REFERENCES

D-1. Wenograd, J., NOLTR61-98, 15 July 1962.

D-2. Wenograd, J., Trans. Faraday Soc., 57, 1612, (1962)

D-3. Wenograd, J., NOLTR61-97, 1 September 1961.

D-4. Wenograd, J., Nav. Weps Report (NOL)7328, 15 July 1962.

D-5. Groetzinger, W. and J. Clem, Report No. 5-44, Rohm & Haas Company, Redstone Arsenal, 3 March 1964.

D-6. Zinn, J. and C. Mader, Journal of Applied Physics, Vol. 31, No. 2, p.323, February 1960.

D-7. Carslaw, H. and J. Jaeger, Conduction of Heat in Solids, Oxford University Press, London, 1959.

D-8. Andersen, W., I&EC Process Design & Development, Vol. 4, No. 3, p. 286, July 1965.

D-9. Hicks, B., Journal of Chemical Physics, Vol. 22, No. 3, p. 414, March 1954.

APPENDIX E

AIR AND WATER POLLUTION CONTROL

Because of the toxicity of beryllium particles in the size ranges encountered during rocket motor testing, it was necessary to monitor all operations for release of hazardous materials. Air samples were taken continuously in a downwind location during all thrust chamber tests. Surface wipe samples were taken periodically in the test pit area to detect any gradual accumulation of beryllium particles.

The maximum concentration of beryllium detected in the air downwind of the scrubber during a test firing was less than 0.05 μ gm/m^3. Since the accepted standard for an exposure of 40 hours per week is 2.0 μ gm/m^3, it is seen that no hazard whatever was produced from exhaust particles in the air during testing.

Surface wipe samples were taken after every day of test operation. Surfaces inside the control center were also sampled occasionally. The standard procedure was to analyze only a random selection of the wipe samples submitted.

If no excessive beryllium concentrations were found, no further analyses would be made. If large concentrations were found, then the rest of the samples in the batch submitted were analyzed to determine the extent of the residue buildup. Any time the wipe samples exceeded 2 μ gm/100 cm^2, cleanup procedures were initiated. Highest readings were usually obtained in the immediate vicinity of the thrust stand and scrubber front and were most likely related to dismantling of the thrust chamber assembly after a test. A listing of individual sample analyses are presented in Appendix G . At no time was a level of surface contamination detected which was considered hazardous to unprotected personnel.

Water from the exhaust scrubber system was pumped through a series of filters and into a holding tank where it was analyzed for beryllium before

being released. The filtration efficiently removed both beryllium and beryllium oxide particles, which are insoluble. Introduction of fluorine into the propellant system created an additional problem in that soluble beryllium fluorides are produced which cannot be filtered. To solve this problem, an intermediate water pressurization tank was added to the scrubber system as indicated in Fig. 76 . This is the upright cylindrical tank in Fig. 75 . Addition of this tank made it possible to maintain a closed recirculation system for the scrubber water. After a test firing, the water is pumped directly back into the pressurization tank for reuse in the next test firing. The volume of water requiring special treatment can thus be limited to the quantity required for a single test firing.

A laboratory investigation of the removal of beryllium from solution in the presence of fluoride ions was undertaken to find an inexpensive way of bringing the beryllium concentration down to less than 10 ppm. Water at this concentration could be dumped safely with adequate dilution. Details of the investigation are presented in Appendix F. The results indicated that the addition of ammonium hydroxide and calcium chloride would produce a filterable precipitate, removing both fluorine and beryllium from the solution. In practice, the reagents were placed directly in the scrubber body, and then the scrubber water was recirculated two or three times before filtering and pumping to the holding tank. This method proved both efficient and economical.

APPENDIX F

REMOVAL OF DISSOLVED BERYLLIUM FROM SOLUTION

The removal of beryllium from solution can be achieved by many precipitating agents. However, the cost of some of these reagents is relatively expensive. Beryllium is known to form an insoluble hydroxide. When Na_2CO_3 is added to a beryllium salt solution, a mixed precipitate of $Be(OH)_2$ and $BeCO_3$ is formed.

Beryllium is known to form the tetrafluoroberyllate ion in a solution containing excess fluoride. This ion is isomorphous with sulphate ion and is precipitated as a double salt with barium. Because calcium sulphate is somewhat insoluble, it was speculated that $CaBeF_4$ might also be insoluble.

Beryllium hydroxide is very insoluble, but somewhat amphoteric and dissolves in highly basic solutions to form the soluble $Be(OH)_4^{=}$ ion. A weak base, such as NH_3 solution, should precipitate $Be(OH)_2$ adequately.

Therefore, three precipitating agents were chosen, each of which was quite inexpensive:

1. Sodium carbonate
2. Calcium oxide
3. Ammonium hydroxide solution

A stock solution of beryllium was made to contain 689 ppm Be^{++}. A four-fold excess of fluoride ion was added as NaF and the solution acidified. Twenty-milliliter aliquots of this solution were taken and the reagents were added in excess. The resulting precipitate was filtered and the filtrate was analyzed quantitatively by emission spectroscopy to determine the remaining beryllium in solution. The results are presented in Table F-1.

TABLE F-1

BERYLLIUM REMOVAL AT HIGH FLUORIDE CONCENTRATIONS

Precipitating Agent	Concentration of Beryllium, ppm	
	Initial	Final
NA_2CO_3	680	> 300
CaO	680	> 300
NH_4OH	680	> 300

The results indicated that at a high fluorine/beryllium ratio, removal of beryllium was not accomplished. Although it was not expected that the fluorine/beryllium ratio would ever be over 2:1 in the scrubber water, the removal of beryllium as the hydroxide was studied at different fluoride concentrations. Aliquots of a stock solution of beryllium were treated with increasing amounts of fluoride ion. Excess NH_4OH solution was added and the precipitate was filtered out. The filtrate was analyzed by cupferron precipitation and, where necessary, by emission spectroscopy. The results are presented in Table F-2.

TABLE F-2

BERYLLIUM REMOVAL AT VARYING FLUORINE/BERYLLIUM RATIOS

Fluorine Beryllium Ratio	Initial Concentration, ppm	Final Concentration	
		Cupferron Precipitation	Emission Spectroscopy, ppm
No Fluoride	651	None	1.5
1:1	651	None	--
2:1	651	None	4.1
3:1	651	Cloudy	15

The results indicated that fluoride ion did not significantly interfere with the precipitation of $Be(OH)_2$ by NH_4OH solution until the fluorine/beryllium ratio was 3 to 1 or higher.

In cases where this was true, the experimental results in Table F-3 showed that prior removal of fluoride ion with calcium chloride would be satisfactory.

TABLE F-3

EFFECT OF CALCIUM CHLORIDE ON BERYLLIUM REMOVAL

Precipitating Agent	Flouride Added	Initial Concentration, ppm	Final Concentration, ppm
Na_2Co_3	None	651	Nil
NH_4OH	None	651	Nil
NH_4OH	4:1	651	330
Na_2CO_3	4:1	651	315
$NH_4OH + CaCl_2$	4:1	651	10.5

APPENDIX G

BERYLLIUM ANALYSES

All wipe samples, air samples, and water samples taken during the motor firing program are presented in the following tabulation. Samples for which no analysis is listed were saved but not analyzed.

Number	Date	Area	Beryllium, micrograms
1	3-17	Scrubber front	2.24
2		Top south wall	28.0
3		Thrust stand top	12.4
4		Cleaning bath	1.48
5		Inside scrubber	192.0
6		Air, 10 minutes at 30 scfm	
7		Inside laboratory	
8	▼	Scrubber water	13 ppb
Area scrubbed down at this time			
9	3-18	Scrubber front	0.6
10		Thrust stand top	0.3
11		Floor between pits 1 and 2	0.2
12		Top south wall	0.3
13		Air, pit front, 10 minutes at 30 cfm	0.1
14	▼	Air, pit back, 10 minutes at 30 cfm	0.1
15	3-23	Scrubber front	1.0
16		South wall	0.7
17		Thrust stand top	1.0
18	▼	Floor between pits 1 and 2	0.5
18A	4-4	Waste barrels	0
18B		Waste barrels	0
18C		Waste barrels	0
18D		Waste barrels	0
19	4-26	Water, after adding $Ca(OH)_2$	19.4 ppm
20	4-28	Top south wall	0.8
21	▼	Scrubber front	12.0

Number	Date	Area	Beryllium, micrograms
22	4-28	Thrust stand front	
23		Floor between pits 1 and 2	
24		Air, 60 minutes at 30 cfm	
New samples taken after run			
25	4-28	Floor between pits 1 and 2	0.4
26		Thrust stand front	
27		South top wall	
28		Scrubber top	
New samples taken after second run			
29	4-28	Scrubber front	4.4
30		South top wall	0.9
31		Floor, pit 2	
Area scrubbed down at this time			
32	5-5	Scrubber front	0.4
33		Floor between pits 1 and 2	0.6
34		South top wall	
35		Air, 90 minutes at 30 scfm	2.0
36	5-10	Air, 60 minutes at 30 scfm	0
37		Scrubber back	0.3
38		Scrubber front	
39		South wall	
40		Air, 30 minutes at 30 scfm	1.4
41	5-12	Scrubber body	0.5
42		Floor, pit 1	
43		Thrust stand	1.0
44	5-16	Scrubber front	
45		Scrubber back	
46		Floor between pits 2 and 3	
47		Air, 120 minutes at 30 cfm	2.0
47A	5-18	Inside laboratory	0.7
47B		Inside laboratory	1.0
47C		Inside laboratory	0.4

Number	Date	Area	Beryllium, micrograms
47D	5-18	Inside laboratory	0.2
47E	↓	Inside laboratory	0.6
47F	↓	Inside laboratory	0.5
47G	5-24	Inside laboratory	0.1
47H	↓	Inside laboratory	0.1
47I	↓	Inside laboratory	0.1
47J	↓	Inside laboratory	0.1
47K	↓	Inside laboratory	0.2
47L	↓	Scrubber front	20.5
47M	↓	Thrust stand	2.4
47N	↓	Inside laboratory	0.2
470	↓	South wall	0.6
47P	↓	Floor, pit 2	0.2
47Q	↓	Inside laboratory	0.5
Area scrubbed down at this time			
47R	5-26	Scrubber water	100 ppm
47S	5-31	Scrubber water after adding NH_4OH	13 ppm
48	6-7	Top south wall	0.3
49	↓	Thrust stand	
50	↓	Scrubber face	1.5
51	↓	Floor, pit 2	0.3
52	↓	Floor, pit 2	
53	↓	Scrubber plate	
54	6-10	Water after filtering	0.1 ppm
Scrubber water dumped at this point			
55	7-13	Pit 2 floor	0.1
56	↓	South wall	0.4
57	↓	Thrust stand	0.2
58	8-1	Pit 1 valve cover	0.8
59	↓	Pit 1 floor	0.9
60	8-4	Air sample	0

Number	Date	Area	Beryllium, micrograms
61	8-5	Air sample	<0.002
62	8-17	Air sample	0
63	8-18	Air sample	0
64	8-19	Air sample	0.02
65	↓	Pit 2 floor	0.1
66	↓	Thrust stand	0.6
67	8-22	Scrubber water	0.6

Scrubber water dumped at this point

CONFIDENTIAL

Security Classification

DOCUMENT CONTROL DATA - R&D

(Security classification of title, body of abstract and indexing annotation must be entered when the overall report is classified)

1. ORIGINATING ACTIVITY (Corporate author) Rocketdyne, a Division of North American Aviation, Inc., 6633 Canoga Avenue, Canoga Park, California	2a. REPORT SECURITY CLASSIFICATION CONFIDENTIAL 2b. GROUP 4

3. REPORT TITLE

PHYSICO-CHEMICAL CHARACTERIZATION OF HIGH-ENERGY STORABLE PROPELLANTS

4. DESCRIPTIVE NOTES (Type of report and inclusive dates)

Final

5. AUTHOR(S) (Last name, first name, initial)

Cain, E. F.; Farrar, J.; Axworthy, A.; Gunderloy, F.; Sinor, J.; Ogimachi, N.

6. REPORT DATE	7a. TOTAL NO. OF PAGES	7b. NO. OF REFS
14 October 1966	404	35

8a. CONTRACT OR GRANT NO.	9a. ORIGINATOR'S REPORT NUMBER(S)
AF04(611)-10544 b. PROJECT NO. 3148 c. Air Force Program Structure d. No. 750G	R-6737 9b. OTHER REPORT NO(S) (Any other numbers that may be assigned this report) AFRPL-TR-66-294

10. AVAILABILITY/LIMITATION NOTICES In addition to security requirements which must be met, this document is subject to special export controls and each transmittal to foreign governments or foreign nationals may be made only with prior approval of AFRPL (RPPR-STINFO), Edwards, California, 93523

11. SUPPLEMENTARY NOTES	12. SPONSORING MILITARY ACTIVITY
	Air Force Rocket Propulsion Laboratory Edwards, California

13. ABSTRACT

Homogeneous oxidizer mixtures based on Compounds R and T were studied and found to be intractable. The kinetics of the decomposition of CNF oxidizers were studied and the results indicated that the additive approach to inhibition did not seem promising. Heterogeneous fuels based on Be/N_2H_4, Be-BeH_2/MMH were formulated and evaluated during small motor firings. A monopropellant containing a Be + BeH_2/H_2O-HN was also prepared and evaluated in a small rocket motor. The mechanisms of gas forming reactions of such heterogeneous propellants were studied. A new family of stable heterogeneous fuels based upon the use of various alane- and borane-terminated beryllium hydride liquids was conceived and studied. A stable gel was formulated. The effect of the addition of up to 25 w/o of a fluorine to the oxidizer in the Be-N_2H_4/H_2O_2 was studied in a small rocket engine system. (C)

DD FORM 1 JAN 64 1473

CONFIDENTIAL

Security Classification

CONFIDENTIAL

Security Classification

14. KEY WORDS	LINK A		LINK B		LINK C	
	ROLE	WT	ROLE	WT	ROLE	WT
Propellants Oxidizers Impact Sensitivity Thermal Stability Combustion Efficiency						

INSTRUCTIONS

1. **ORIGINATING ACTIVITY:** Enter the name and address of the contractor, subcontractor, grantee, Department of Defense activity or other organization *(corporate author)* issuing the report.

2a. **REPORT SECURITY CLASSIFICATION:** Enter the overall security classification of the report. Indicate whether "Restricted Data" is included. Marking is to be in accordance with appropriate security regulations.

2b. **GROUP:** Automatic downgrading is specified in DoD Directive 5200.10 and Armed Forces Industrial Manual. Enter the group number. Also, when applicable, show that optional markings have been used for Group 3 and Group 4 as authorized.

3. **REPORT TITLE:** Enter the complete report title in all capital letters. Titles in all cases should be unclassified. If a meaningful title cannot be selected without classification, show title classification in all capitals in parenthesis immediately following the title.

4. **DESCRIPTIVE NOTES:** If appropriate, enter the type of report, e.g., interim, progress, summary, annual, or final. Give the inclusive dates when a specific reporting period is covered.

5. **AUTHOR(S):** Enter the name(s) of author(s) as shown on or in the report. Enter last name, first name, middle initial. If military, show rank and branch of service. The name of the principal author is an absolute minimum requirement.

6. **REPORT DATE:** Enter the date of the report as day, month, year; or month, year. If more than one date appears on the report, use date of publication.

7a. **TOTAL NUMBER OF PAGES:** The total page count should follow normal pagination procedures, i.e., enter the number of pages containing information.

7b. **NUMBER OF REFERENCES:** Enter the total number of references cited in the report.

8a. **CONTRACT OR GRANT NUMBER:** If appropriate, enter the applicable number of the contract or grant under which the report was written.

8b, 8c, & 8d. **PROJECT NUMBER:** Enter the appropriate military department identification, such as project number, subproject number, system numbers, task number, etc.

9a. **ORIGINATOR'S REPORT NUMBER(S):** Enter the official report number by which the document will be identified and controlled by the originating activity. This number must be unique to this report.

9b. **OTHER REPORT NUMBER(S):** If the report has been assigned any other report numbers *(either by the originator or by the sponsor)*, also enter this number(s).

10. **AVAILABILITY/LIMITATION NOTICES:** Enter any limitations on further dissemination of the report, other than those imposed by security classification, using standard statements such as:

(1) "Qualified requesters may obtain copies of this report from DDC."

(2) "Foreign announcement and dissemination of this report by DDC is not authorized."

(3) "U. S. Government agencies may obtain copies of this report directly from DDC. Other qualified DDC users shall request through _____."

(4) "U. S. military agencies may obtain copies of this report directly from DDC. Other qualified users shall request through _____."

(5) "All distribution of this report is controlled. Qualified DDC users shall request through _____."

If the report has been furnished to the Office of Technical Services, Department of Commerce, for sale to the public, indicate this fact and enter the price, if known.

11. **SUPPLEMENTARY NOTES:** Use for additional explanatory notes.

12. **SPONSORING MILITARY ACTIVITY:** Enter the name of the departmental project office or laboratory sponsoring *(paying for)* the research and development. Include address.

13. **ABSTRACT:** Enter an abstract giving a brief and factual summary of the document indicative of the report, even though it may also appear elsewhere in the body of the technical report. If additional space is required, a continuation sheet shall be attached.

It is highly desirable that the abstract of classified reports be unclassified. Each paragraph of the abstract shall end with an indication of the military security classification of the information in the paragraph, represented as *(TS)*, *(S)*, *(C)*, or *(U)*.

There is no limitation on the length of the abstract. However, the suggested length is from 150 to 225 words.

14. **KEY WORDS:** Key words are technically meaningful terms or short phrases that characterize a report and may be used as index entries for cataloging the report. Key words must be selected so that no security classification is required. Identifiers, such as equipment model designation, trade name, military project code name, geographic location, may be used as key words but will be followed by an indication of technical context. The assignment of links, rules, and weights is optional.

CONFIDENTIAL

Security Classification